



D3.3 Science support report

WP3 – Science Support

Deliverable Lead: ZAMG

Dissemination Level: Public

Deliverable due date: 30/11/2019

Actual submission date: 24/04/2020

Updated: 01/09/2020

Revised according to reviewer comments: 04/02/2021

Version 1.1.1



Document Control Page	
Title	Science support plan and concept
Creator	Robert Goler (ZAMG)
Description	This document provides a report of the work performed in WP3 since the project start (material from D3.2 is included herein) updated with work performed since D3.2 until the project end.
Publisher	CLARITY Consortium
Contributors	Robert Goler (ZAMG), Maja Zuvela-Aloise (ZAMG), Astrid Kainz (ZAMG), Claudia Hahn (ZAMG), Wolfgang Loibl (AIT), Laura Parra (CEDEX), Alberto Compte (CEDEX), Emilio Diego (METEOGRID), Luis Torres (METEOGRID), Lena Strömbäck (SMHI), Jorge H. Amorim (SMHI), Yeshewatesfa Hundecha (SMHI), Mauro Iorio (EUREKA), Giulio Zuccaro (PLINIVS), Mattia Leone (PLINIVS), Jose Cubillo (ACCIONA)
Creation date	30/10/2019
Type	Text
Language	en-GB
Rights	copyright "CLARITY Consortium"
Audience	<input checked="" type="checkbox"/> Public <input type="checkbox"/> Confidential <input type="checkbox"/> Classified
Status	<input type="checkbox"/> In Progress <input type="checkbox"/> For Review <input type="checkbox"/> For Approval <input checked="" type="checkbox"/> Approved

Disclaimer

Disclaimer

The text, figures and tables in this report can be reused under a provision of the Creative Commons Attribution 4.0 International License. Logos and other trademarks are not covered by this license.

The content of the publication herein is the sole responsibility of the publishers and it does not necessarily represent the views expressed by the European Commission or its services.

While the information contained in the documents is believed to be accurate, the authors(s) or any other participant in the CLARITY consortium make no warranty of any kind with regard to this material including, but not limited to the implied warranties of merchantability and fitness for a particular purpose.

Neither the CLARITY Consortium nor any of its members, their officers, employees or agents shall be responsible or liable in negligence or otherwise howsoever in respect of any inaccuracy or omission herein.

Without derogating from the generality of the foregoing neither the CLARITY Consortium nor any of its members, their officers, employees or agents shall be liable for any direct or indirect or consequential loss or damage caused by or arising from any information advice or inaccuracy or omission herein.

Table of Contents

1	Introduction	23
1.1	CLARITY Science Support	23
1.2	CLARITY Methodology	24
1.3	Screening and Expert Studies	25
2	Basic and Advanced Screening Services	26
2.1	Hazard Characterisation	26
2.1.1	Climate Indices.....	26
2.1.2	Local Effect Estimation.....	28
2.2	Evaluation of Exposure	52
2.3	Vulnerability Analysis.....	52
2.4	Impact Scenario Analysis	54
2.4.1	Economic Impact of Heat Waves	55
2.4.2	Economic Impact of Flooding.....	62
2.5	Adaptation Options and their Economic Appraisal	74
2.5.1	Cost/Benefit Analysis of Adaptation Options (CBA).....	85
2.5.2	Cost Estimation of the Adaptation Measures	86
3	Expert Services	90
3.1	DC1	90
3.1.1	Climate change scenarios for the city of Naples	91
3.1.2	Heat waves – local effect	97
3.1.3	Flood – local effect.....	103
3.1.4	Climate adaptation strategies for the city of Naples	108
3.1.5	Summary	109
3.2	DC2	111
3.2.1	Water Hazards and Supply (US-DC2-100)	111
3.2.2	Health and Environment (US-DC2-200)	115
3.2.3	Summary	122
3.3	DC3	123
3.3.1	Regional and Urban Climate Modelling	123
3.3.2	Microclimate Modelling.....	123
3.3.3	Summary	127
3.4	DC4	128
3.4.1	Adaptation elements and its economical appraisal.....	130
3.4.2	Summary	135
4	Conclusions	136
5	Acknowledgement	138
6	References.....	139
7	Annex I: Climate Indices	143
7.1	Data used for the calculation of the indices	144
7.1.1	Ensemble standard deviation	146
7.1.2	Generalized discussion of results.....	147
7.2	Consecutive summer days (CSU)	148
7.3	Heat wave days exceeding 75th percentile of consecutive daily maximum temperature.....	151
7.4	Hot days (HD).....	154
7.5	Summer days (SD).....	157
7.6	Tropical nights (TN).....	160
7.7	Hot days with respect to the 90 th percentile of daily maximum temperature (Tx90p).....	163
7.8	Consecutive frost days (CFD)	166
7.9	Frost days (FD)	169
7.10	Ice days (ID)	172
7.11	Cold days with respect to the 10 th percentile of daily minimum temperature (Tn10p).....	175
7.12	Extreme temperature range (ETR).....	179

7.13	Highest 1-day precipitation amount (RX1day)	182
7.14	Highest 5-day precipitation amount (RX1day)	185
7.15	Snow days	188
7.16	Consecutive wet days (CWD)	191
7.17	Wet days (RR1mm)	194
7.18	Heavy precipitation days (RR20mm)	197
7.19	Wet days with respect to the 90 th percentile of daily precipitation (RR90p)	200
7.20	Maximum wind speed	203
7.21	Wind speed with respect to the 98th percentile of daily wind (Wind98p)	206
7.22	Torro17	209
7.23	Consecutive dry days (CDD).....	212
7.24	River flooding.....	215
7.25	Forest fires	217
7.26	Landslides	220
7.27	Hazard scale maps	220
8	Annex II: Adaptation options	221
9	Annex III: Adaptation Measures Technical Cards.....	223

List of Figures

Figure 1: The 7 steps of the CLARITY methodology	24
Figure 2: Schematic illustrating the basic (left) and advanced (right) screening services.	25
Figure 3: Detailed land use used in DC1, in red the Point of Interest (POIs) used in the calibration.	30
Figure 4: Comparison of Ts values across the different models used in the calibration phase, on 24 test points in 4 different land use categories (in the legend, left, SOLWEIG; middle, ENVI-met; right PLINIVS-DC1 HWLEM).....	32
Figure 5: Difference between PLINIVS-LUPT (lower left panel) and SOLWEIG (lower right panel) outputs for Ts and Tmrt values for “buildings” land use class in the various calibration steps. The top panel shows the locations for the curves in the lower two panels.	33
Figure 6: As in Figure 5 but showing values for the “built open spaces” land use class.....	34
Figure 7: As in Figure 5 but showing values for the “roads” land use class.....	35
Figure 8: As in Figure 5 but showing values for the “vegetated areas” land use class.....	35
Figure 9: Comparison of Tmrt from PLINIVS-DC1 HWLEM (left) and SOLWEIG (right) before the calibration for 56 sample points.....	36
Figure 10: Comparison of Tmrt values (y-axis) from the PLINIVS-DC1 HWLEM and SOLWEIG before the calibration for each of the 56 cells (x-axis) in the analysed sample.....	37
Figure 11: Comparison of Tmrt from PLINIVS-DC1 HWLEM (left) and SOLWEIG (right) after the calibration, for 56 sample cells.....	37
Figure 12: As in Figure 10 but after the calibration steps have been implemented	38
Figure 13: Overlapping of grids used by PLINIVS HWLEM (plinivs_hwlem_grid) and CSIS HWLEM (laea_etr5_500m_grid SAMPLE).	39
Figure 14: Sample cells excluded by the comparison for relevant discrepancy in land use attribution.....	40
Figure 15: Comparison graph, Tmrt and Delta maps for Scenario A. The top left the graph represents the Tmrt difference in the sample cells between PLINIVS HWLEM and CSIS HWLEM. The maps on the left show the difference (Delta) in the results before (CSIS 1) and after (CSIS 2) the calibration of the Surface Temperature parameter in CSIS HWLEM. The maps on the right represent the Tmrt values from PLINIVS HWLEM, and the CSIS HWLEM before (CSIS 1) and after (CSIS 2) the calibration of the Surface Temperature parameter.....	41
Figure 16: As in Figure 15 showing the results from Scenario B.....	42
Figure 17: As in Figure 15 showing the results from Scenario C.....	43
Figure 18: As in Figure 14 showing the results from Scenario D.....	44
Figure 19: Comparison graph, Tmrt and Delta maps for Scenario B, with homogenization of Diffuse and Incoming fraction short-wave solar radiation among CSIS HWLEM and PLINIVS HWLEM. On the left the graph represents the Tmrt difference in the sample cells between PLINIVS HWLEM and CSIS HWLEM. The maps on the left show the difference (Delta) in the results before (CSIS 1) and after (CSIS 2) the calibration of the Surface Temperature parameter in CSIS HWLEM. The maps on the right represent the Tmrt values from PLINIVS HWLEM and the CSIS HWLEM before (CSIS 1) and after (CSIS 2) the calibration of the Surface Temperature parameter.....	45
Figure 20: Land use comparison of sample cells in Naples area (left, CSIS HWLEM; right, PLINIVS HWLEM). The two images above include a railway track area which is more precisely represented by PLINIVS HWLEM land use. The two images below include a portion of water which is not currently included the PLINIVS HWLEM land use.	46
Figure 21: Land use comparison of sample cells in Naples area (left, CSIS HWLEM; right, PLINIVS HWLEM). Land use matching aligns the observed delta around the mean value of 4°C.....	47
Figure 22: Land use comparison of sample cells in Naples area (left, CSIS HWLEM; right, PLINIVS HWLEM). Comparison of cells where the discrepancy in land use concerns the “trees” layers result in almost identical Tmrt values, meaning that the observed underestimation obtained with CSIS HWLEM is reduced here. The reason is that tree shadow is significantly impacting the Tmrt calculation in the SOLWEIG model, and the reduced presence of trees in the CSIS land use increase the value aligning it with PLINIVS HWLEM results.	47

Figure 23: Naples area showing (left) runoff coefficient, and (right) its classification of imperviousness on a scale (1-5).	49
Figure 24: Naples area showing (left) the elevation from the DEM, (centre) urban watersheds, and (right) classification results.....	49
Figure 25: Naples area showing (left) flow accumulation streams, and (right) classification results.....	50
Figure 26: Naples area showing (left) number of emergency calls recorded, and (right) classification results.	50
Figure 27: Classification of the Naples area according to hazard level (dark green = very low; light green = low, orange = medium, red = high).	52
Figure 28: Vulnerability matrices according to flooding value and vulnerability curves for the Direct damage (DD) class.	54
Figure 29: Example of distribution of damage typologies necessary for the calculation of the costs of hospitalization.	58
Figure 30: Calculation of the human health intervention costs.....	59
Figure 31: Calculation of the indirect cost of the deceased.....	60
Figure 32: Calculation of the indirect cost of the local value added due to hospitalization effects (losses in productivity).	61
Figure 33: Schematic showing the process used in [20] to generate depth-damage curves.	64
Figure 34: Damage factor curves for the four vulnerability classes for several EU countries taken from [20].	65
Figure 35: Depth-damage table for the vulnerability class of residential buildings. The example illustrated is explained within the text.....	66
Figure 36: As in Figure 35 but for the case of multiple elements of exposure.	66
Figure 37: The total damage cost can be calculated by multiplying the damage per area by the area of those elements within the grid cell.	67
Figure 38: Example of adaptation strategies integrating multiple adaptation options (e.g. top, a possible adaptation strategy aimed at maximising opportunities for urban agriculture enhancement).....	82
Figure 39: Test of adaptation measures effect on a 250 m × 250 m cell in the urban area of Naples.	83
Figure 40: Cost of adaptation strategy effect on a 250 m × 250 m cell in the urban area of Naples. Note that the modified land use takes into account the adaptation measures included, but these are grouped by category for readability (e.g. a percentage of built open spaces has been converted to green, with trees and agriculture, and a percentage of roads has been converted into bioswale. All these are summarized as “vegetated” in the right diagram).	83
Figure 41: Example of alternative adaptation for specific land use classes (in brackets the percentage of application on the existing land use).....	84
Figure 42: Conceptualisation of Decision Maker (end-user) modelling.....	85
Figure 43: Schematic of the process to calculate the total benefit value of applying an adaptation measure..	86
Figure 44: Example of data collected in Naples area used as input of the models applied to identify the “local effect” hazard conditions.	91
Figure 45: Annual averages in the period 1971-2000 of rainfall and air temperatures for the city of Naples. For the 1971-2000 period, annual cumulative precipitation values (left), average maximum temperature (centre) and average minimum temperature (right) up high for the Capodichino Station; on the 1971-2005 lapse, models are forced through observational datasets (20C3M) while for 2006-2100 lapse are considered the concentration scenarios RCP4.5 (green) and RCP8.5 (red). Source: CMCC – Centro Euro mediterraneo sui Cambiamenti Climatici (in [27]).	92
Figure 46: Mean annual number of summer days (daily maximum temperature > 25°C) derived from the cuboid method and MUKLIMO_3 urban climate model results, based on long-term climate information from EURO-CORDEX regional climate historical scenarios for the period 1971-2000.....	93
Figure 47: Annual average number of hot days (daily maximum temperature > 30 °C) during the period 1971-2000.....	93

Figure 48: Annual average number of tropical nights (daily minimum temperature > 20 °C) during the period 1971-2000.	94
Figure 49: Heat waves lasting 3 days for the period 1971-2100. The data for the period 1971-2011 show the number of events that have actually occurred, while the events that will occur in the period 2018-2100 refer to the RCP4.5 (left) and RCP8.5 (right) emission scenarios. The three curves in each panel represent the threshold temperatures: 34 °C (blue), 36 °C (grey), 38 °C (orange).	95
Figure 50: Heat waves lasting 6 days for the period 1971-2100. The data for the period 1971-2011 show the number of events that have actually occurred, while the events that will occur in the period 2018-2100 refer to the RCP4.5 (left) and RCP8.5 (right) emission scenarios. The three curves in each panel represent the threshold temperatures: 34 °C (blue), 36 °C (grey), 38 °C (orange).	95
Figure 51: Heat waves lasting 9 days for the period 1971-2100. The data for the period 1971-2011 show the number of events that have actually occurred, while the events that will occur in the period 2018-2100 refer to the RCP4.5 (left) and RCP8.5 (right) emission scenarios. The three curves in each panel represent the threshold temperatures: 34 °C (blue), 36 °C (grey), 38 °C (orange).	95
Figure 52: Extreme precipitation events for the period 1971-2100. The data for the 1971-2011 period show the number of events that have actually occurred, while the events that will occur in the period 2018-2100 refer to the RCP4.5 (left) and RCP8.5 (right) emission scenarios.	96
Figure 53: Reworked land use map used by simulation models of the “local effect” for heat waves and floods (Source: Comune di Napoli / PLINIVS-LUPT, CLARITY project).	97
Figure 54: Mean radiant temperature map for a typical day of heat wave with air temperature of 36-37 °C (on grid 250 m × 250 m). (Source: PLINIVS-LUPT, CLARITY project).	98
Figure 55: Detailed analysis of Tmrt in an area of the ancient centre, for a typical heat wave day with an air temperature of 36-37 °C. (Source: PLINIVS-LUPT, CLARITY project).	99
Figure 56: Detailed analysis of Tmrt in the Rione Traiano area, for a typical heat wave day with an air temperature of 36-37 °C. (Source: PLINIVS-LUPT, CLARITY project).	99
Figure 57: Detailed analysis of Tmrt in the Ponticelli area, for a typical day of heat wave with an air temperature of 36-37 °C. (Source: PLINIVS-LUPT, CLARITY project).	100
Figure 58: Universal Thermal Climate Index (UTCI) map for a typical day of heat wave with an air temperature of 36-37 °C (on 250 m × 250 m grid). (Source: PLINIVS-LUPT, CLARITY project).	101
Figure 59: Detailed simulations in the Ponticelli area showing Tmrt which are used as input for the implementation of the Ponticelli Urban Regeneration project.	103
Figure 60: Examples of PLINIVS-LUPT simplified model output. The left panel is the far right segment of the four panels shown on the right side, and shows the flow length coloured.	104
Figure 61: Run-off coefficient in relation to land use. (Source: PLINIVS-LUPT, CLARITY project).	105
Figure 62: Drainage basins and run-off streams in the Municipality of Naples. (Source: PLINIVS-LUPT, CLARITY project).	106
Figure 63: Simulations of the water depth and speed values in the catchment area of Naples east (on the left) and geolocation of emergency calls following extreme precipitation events (on the right). (Source: Civil Protection, PLINIVS-LUPT, CLARITY project).	107
Figure 64: Risk propensity for flooding of urban spaces. Colour scale is: dark green = very low, light green = low, orange = medium, red = high. (Source: PLINIVS-LUPT, CLARITY project).	107
Figure 65: Example of the calculations of the impacts of adaptation measures in terms of cost.	109
Figure 66: General framework of CLARITY climate services support for the Municipality of Naples.	110
Figure 67: Comparison of extreme river flow simulated using bias-corrected hourly precipitation data and the corresponding observed extreme flows at river gauging stations across southern Sweden.	113
Figure 68: Projected percentage change in the 10-year extreme hourly river flow across southern Sweden.	114
Figure 69: Example of the urban heat island over Stockholm visualized on the Urban SIS portal.	117
Figure 70: Example of PM10 concentrations over Stockholm from Urban SIS.	117
Figure 71: Example of heat induced mortality over Stockholm from the Urban SIS portal.	118
Figure 72: Example of combined NO2 and PM2.5 mortality per 100 000 inhabitants over Stockholm.	118

Figure 73: Planning scenarios developed for Stockholm. The construction of 140,000 new homes by 2030 (left) and the regional development plan for 2050 (right).....	119
Figure 74: Monthly average temperature increase for future planning scenarios over Stockholm, 2030 with construction of 140 000 new homes (left), the 2050 regional development plan (middle), and a reference scenario where all urban vegetation is removed from today's city (right).....	120
Figure 75: 3D modelling of a 450 m long street section in central Stockholm to see the effect of trees on air quality.....	121
Figure 76: Effect of trees on street level annual PM10 concentrations along Birger Jarlsgatan in central Stockholm. Left: without trees, right: with trees (black dots). Colours indicate concentration in $\mu\text{g m}^{-3}$ (including only local traffic emissions).....	122
Figure 77: Hypothetical adaptation measure: a) current layout, b) proposed greening of the main square in the city centre.....	124
Figure 78: Simulations of the mean radiant temperature (MRT) averaged over 24 hours, a) with the current layer and b) with the increased greening.....	124
Figure 79: Locations of infrared camera measurements at AIT campus. The numbers in the leftmost column correspond to the numbers on the image at right.....	125
Figure 80: Comparison of measured and simulated values for the locations a) "asphalt sun" and b) "asphalt shadow". The dark blue line represents the measured surface temperature, while the other lines represent values calculated either from ENVI-MET or Rhino/Grasshopper (GH).....	126
Figure 81: Map showing the region of interest.....	129
Figure 82: Side view of slope at <i>pk 72+900 to pk 73+150</i>	133
Figure 83: Aerial view of the slope at <i>pk 72+900 to pk 73+150</i> and surface estimation.....	133
Figure 84: Average daily traffic distribution per hour.....	134
Figure 85: Traffic map (source: https://mapas.fomento.gob.es/mapatrafico/2017/).....	135
Figure 86: Evolution of the forcing agents' atmospheric CO ₂ -equivalent concentrations (in parts-per-million-by-volume (ppmv)) of the four RCPs used by the fifth IPCC Assessment Report to make predictions. (Source: https://en.wikipedia.org/wiki/Representative_Concentration_Pathway).....	144
Figure 87: The effect of quantile mapping <i>s</i> to correct the temperature distribution of the model (blue curve) to that of the observations. (Source: [49]).....	147
Figure 88: Maximum number of consecutive summer days for the baseline period 1971-2000. (a) Ensemble mean and (b) ensemble standard deviation.....	148
Figure 89: Maximum number of consecutive summer days for 2041-2070. (left panels) Ensemble mean and (right panels) ensemble standard deviation. (a, b) RCP2.6, (c, d) RCP4.5, (e, f) RCP8.5.....	149
Figure 90: Maximum number of consecutive summer days for 2071-2100. (left panels) Ensemble mean and (right panels) ensemble standard deviation. (a, b) RCP2.6, (c, d) RCP4.5, (e, f) RCP8.5.....	150
Figure 91: Tx75p maximum consecutive for the baseline period 1971-2000. (a) Ensemble mean and (b) ensemble standard deviation.....	151
Figure 92: Tx75p maximum consecutive for the period 2041-2070. (left panels) Ensemble mean and (right panels) ensemble standard deviation. (a, b) RCP2.6, (c, d) RCP4.5, (e, f) RCP8.5.....	152
Figure 93: Tx75p maximum consecutive for the period 2071-2100. (left panels) Ensemble mean and (right panels) ensemble standard deviation. (a, b) RCP2.6, (c, d) RCP4.5, (e, f) RCP8.5.....	153
Figure 94: Hot days for the baseline period 1971-2000. (a) Ensemble mean and (b) ensemble standard deviation.....	154
Figure 95: Hot days for the period 2041-2070. (left panels) Ensemble mean and (right panels) ensemble standard deviation. (a, b) RCP2.6, (c, d) RCP4.5, (e, f) RCP8.5.....	155
Figure 96: Hot days for the period 2071-2100. (left panels) Ensemble mean and (right panels) ensemble standard deviation. (a, b) RCP2.6, (c, d) RCP4.5, (e, f) RCP8.5.....	156
Figure 97: Summer days for the baseline period 1971-2000. (a) Ensemble mean and (b) ensemble standard deviation.....	157
Figure 98: Summer days for the period 2041-2070. (left panels) Ensemble mean and (right panels) ensemble standard deviation. (a, b) RCP2.6, (c, d) RCP4.5, (e, f) RCP8.5.....	158

Figure 99: Summer days for the period 2071-2100. (left panels) Ensemble mean and (right panels) ensemble standard deviation. (a, b) RCP2.6, (c, d) RCP4.5, (e, f) RCP8.5.	159
Figure 100: Tropical nights for the baseline period 1971-2000. (a) Ensemble mean and (b) ensemble standard deviation.....	160
Figure 101: Tropical nights for the period 2041-2070. (left panels) Ensemble mean and (right panels) ensemble standard deviation. (a, b) RCP2.6, (c, d) RCP4.5, (e, f) RCP8.5.	161
Figure 102: Tropical nights for the period 2071-2100. (left panels) Ensemble mean and (right panels) ensemble standard deviation. (a, b) RCP2.6, (c, d) RCP4.5, (e, f) RCP8.5.	162
Figure 103: Tx90p for the baseline period 1971-2000. (a) Ensemble mean and (b) ensemble standard deviation.....	163
Figure 104: Tx90p for the period 2041-2070. (left panels) Ensemble mean and (right panels) ensemble standard deviation. (a, b) RCP2.6, (c, d) RCP4.5, (e, f) RCP8.5.	164
Figure 105: Tx90p for the period 2071-2100. (left panels) Ensemble mean and (right panels) ensemble standard deviation. (a, b) RCP2.6, (c, d) RCP4.5, (e, f) RCP8.5.	165
Figure 106: Consecutive frost days for the baseline period 1971-2000. (a) Ensemble mean and (b) ensemble standard deviation.....	166
Figure 107: Consecutive frost days for the period 2041-2070. (left panels) Ensemble mean and (right panels) ensemble standard deviation. (a, b) RCP2.6, (c, d) RCP4.5, (e, f) RCP8.5.....	167
Figure 108: Consecutive frost days for the period 2071-2100. (left panels) Ensemble mean and (right panels) ensemble standard deviation. (a, b) RCP2.6, (c, d) RCP4.5, (e, f) RCP8.5.....	168
Figure 109: Frost days for the baseline period 1971-2000. (a) Ensemble mean and (b) ensemble standard deviation.....	169
Figure 110: Frost days for the period 2041-2070. (left panels) Ensemble mean and (right panels) ensemble standard deviation. (a, b) RCP2.6, (c, d) RCP4.5, (e, f) RCP8.5.	170
Figure 111: Frost days for the period 2071-2100. (left panels) Ensemble mean and (right panels) ensemble standard deviation. (a, b) RCP2.6, (c, d) RCP4.5, (e, f) RCP8.5.	171
Figure 112: Ice days for the baseline period 1971-2000. (a) Ensemble mean and (b) ensemble standard deviation.....	172
Figure 113: Ice days for the period 2041-2070. (left panels) Ensemble mean and (right panels) ensemble standard deviation. (a, b) RCP2.6, (c, d) RCP4.5, (e, f) RCP8.5.	173
Figure 114: Ice days for the period 2071-2100. (left panels) Ensemble mean and (right panels) ensemble standard deviation. (a, b) RCP2.6, (c, d) RCP4.5, (e, f) RCP8.5.	174
Figure 115: Tn10p for the baseline period 1971-2000. (a) Ensemble mean and (b) ensemble standard deviation.....	175
Figure 116: Tn10p for the period 2041-2070. (left panels) Ensemble mean and (right panels) ensemble standard deviation. (a, b) RCP2.6, (c, d) RCP4.5, (e, f) RCP8.5.	177
Figure 117: Tn10p for the period 2071-2100. (left panels) Ensemble mean and (right panels) ensemble standard deviation. (a, b) RCP2.6, (c, d) RCP4.5, (e, f) RCP8.5.	178
Figure 118: Extreme temperature range for the baseline period 1971-2000. (a) Ensemble mean and (b) ensemble standard deviation.....	179
Figure 119: Extreme temperature range for the period 2041-2070. (left panels) Ensemble mean and (right panels) ensemble standard deviation. (a, b) RCP2.6, (c, d) RCP4.5, (e, f) RCP8.5.....	180
Figure 120: Extreme temperature range for the period 2071-2100. (left panels) Ensemble mean and (right panels) ensemble standard deviation. (a, b) RCP2.6, (c, d) RCP4.5, (e, f) RCP8.5.....	181
Figure 121: RX1day for the baseline period 1971-2000. (a) Ensemble mean and (b) ensemble standard deviation.....	182
Figure 122: RX1day for the period 2041-2070. (left panels) Ensemble mean and (right panels) ensemble standard deviation. (a, b) RCP2.6, (c, d) RCP4.5, (e, f) RCP8.5.	183
Figure 123: RX1day for the period 2071-2100. (left panels) Ensemble mean and (right panels) ensemble standard deviation. (a, b) RCP2.6, (c, d) RCP4.5, (e, f) RCP8.5.	184
Figure 124: RX5day for the baseline period 1971-2000. (a) Ensemble mean and (b) ensemble standard deviation.....	185

Figure 125: RX5day for the period 2041-2070. (left panels) Ensemble mean and (right panels) ensemble standard deviation. (a, b) RCP2.6, (c, d) RCP4.5, (e, f) RCP8.5.	186
Figure 126: RX5day for the period 2071-2100. (left panels) Ensemble mean and (right panels) ensemble standard deviation. (a, b) RCP2.6, (c, d) RCP4.5, (e, f) RCP8.5.	187
Figure 127: Snow days for the baseline period 1971-2000. (a) Ensemble mean and (b) ensemble standard deviation.	188
Figure 128: Snow days for the period 2041-2070. (left panels) Ensemble mean and (right panels) ensemble standard deviation. (a, b) RCP2.6, (c, d) RCP4.5, (e, f) RCP8.5.	189
Figure 129: Snow days for the period 2071-2100. (left panels) Ensemble mean and (right panels) ensemble standard deviation. (a, b) RCP2.6, (c, d) RCP4.5, (e, f) RCP8.5.	190
Figure 130: Consecutive wet days for the baseline period 1971-2000. (a) Ensemble mean and (b) ensemble standard deviation.	191
Figure 131: Consecutive wet days for the period 2041-2070. (left panels) Ensemble mean and (right panels) ensemble standard deviation. (a, b) RCP2.6, (c, d) RCP4.5, (e, f) RCP8.5.	192
Figure 132: Consecutive wet days for the period 2071-2100. (left panels) Ensemble mean and (right panels) ensemble standard deviation. (a, b) RCP2.6, (c, d) RCP4.5, (e, f) RCP8.5.	193
Figure 133: RR1mm for the baseline period 1971-2000. (a) Ensemble mean and (b) ensemble standard deviation.	194
Figure 134: Wet days for the period 2041-2070. (left panels) Ensemble mean and (right panels) ensemble standard deviation. (a, b) RCP2.6, (c, d) RCP4.5, (e, f) RCP8.5.	195
Figure 135: Wet days for the period 2071-2100. (left panels) Ensemble mean and (right panels) ensemble standard deviation. (a, b) RCP2.6, (c, d) RCP4.5, (e, f) RCP8.5.	196
Figure 136: RR20mm for the baseline period 1971-2000. (a) Ensemble mean and (b) ensemble standard deviation.	197
Figure 137: Very heavy precipitation days for the period 2041-2070. (left panels) Ensemble mean and (right panels) ensemble standard deviation. (a, b) RCP2.6, (c, d) RCP4.5, (e, f) RCP8.5.	198
Figure 138: Very heavy precipitation days for the period 2071-2100. (left panels) Ensemble mean and (right panels) ensemble standard deviation. (a, b) RCP2.6, (c, d) RCP4.5, (e, f) RCP8.5.	199
Figure 139: RR90p for the baseline period 1971-2000. (a) Ensemble mean and (b) ensemble standard deviation.	200
Figure 140: RR90p for the period 2041-2070. (left panels) Ensemble mean and (right panels) ensemble standard deviation. (a, b) RCP2.6, (c, d) RCP4.5, (e, f) RCP8.5.	201
Figure 141: RR90p for the period 2071-2100. (left panels) Ensemble mean and (right panels) ensemble standard deviation. (a, b) RCP2.6, (c, d) RCP4.5, (e, f) RCP8.5.	202
Figure 142: Maximum wind speed for the baseline period 1971-2000. (a) Ensemble mean and (b) ensemble standard deviation.	203
Figure 143: Maximum wind speed for the period 2041-2070. (left panels) Ensemble mean and (right panels) ensemble standard deviation. (a, b) RCP2.6, (c, d) RCP4.5, (e, f) RCP8.5.	204
Figure 144: Maximum wind speed for the period 2071-2100. (left panels) Ensemble mean and (right panels) ensemble standard deviation. (a, b) RCP2.6, (c, d) RCP4.5, (e, f) RCP8.5.	205
Figure 145: Wind98p for the baseline period 1971-2000. (a) Ensemble mean and (b) ensemble standard deviation.	206
Figure 146: Wind98p for the period 2041-2070. (left panels) Ensemble mean and (right panels) ensemble standard deviation. (a, b) RCP2.6, (c, d) RCP4.5, (e, f) RCP8.5.	207
Figure 147: Wind98p for the period 2071-2100. (left panels) Ensemble mean and (right panels) ensemble standard deviation. (a, b) RCP2.6, (c, d) RCP4.5, (e, f) RCP8.5.	208
Figure 148: Torro17 for the baseline period 1971-2000. (a) Ensemble mean and (b) ensemble standard deviation.	209
Figure 149: Torro17 for the period 2041-2070. (left panels) Ensemble mean and (right panels) ensemble standard deviation. (a, b) RCP2.6, (c, d) RCP4.5, (e, f) RCP8.5.	210
Figure 150: Torro17 for the period 2071-2100. (left panels) Ensemble mean and (right panels) ensemble standard deviation. (a, b) RCP2.6, (c, d) RCP4.5, (e, f) RCP8.5.	211

Figure 151: Consecutive dry days for the baseline period 1971-2000. (a) Ensemble mean and (b) ensemble standard deviation.....	212
Figure 152: Consecutive dry days for the period 2041-2070. (left panels) Ensemble mean and (right panels) ensemble standard deviation. (a, b) RCP2.6, (c, d) RCP4.5, (e, f) RCP8.5.	213
Figure 153: Consecutive dry days for the period 2071-2100. (left panels) Ensemble mean and (right panels) ensemble standard deviation. (a, b) RCP2.6, (c, d) RCP4.5, (e, f) RCP8.5.	214
Figure 154: Projected changes in the 10-year river flow relative to the reference period for three future time periods across Europe.	216
Figure 155: Models and workflow used for FWI calculations.	219

List of Tables

Table 1: Summary of the climate indices used for hazard characterisation.	27
Table 2: Heat wave events for a grid point representing Naples from the SMHI, ICHEC GCM. Each heat wave shows the greatest number of consecutive days where the maximum temperature of each day is equal to or exceeds the temperature shown.	29
Table 3: Land use attribute table in DC1.	30
Table 4: Comparison of the Ta/Ts relation in ENVI-met and the HWLEM used in DC1.	31
Table 5: Summary of deltas for the four scenarios before the calibration of Ts parameter in CSIS HWLEM.	46
Table 6: Summary of deltas for the four scenarios after the calibration of Ts parameter in CSIS HWLEM. ...	46
Table 7: Classification scheme for each of the four parameters in the Naples data package.	51
Table 8: Probability of flooding classification level.	51
Table 9: Example of a vulnerability matrix for a specific vulnerability class of a given element at risk under effect of a specific hazard.	52
Table 10: People damage classification.	53
Table 11: Vulnerability classes example definition: $f(D,Q)$. HC: Historical Centre; S: Suburb, C: Countryside. DD: Direct Damage, ID: Indirect Damage.	54
Table 12: Damage typologies for the six levels of damage and the corresponding level of medical care and time of hospital stay.	56
Table 13: Summary of the direct and indirect costs to be calculated for the heat wave hazard and with population as the element at risk.	59
Table 14: Parameters for the calculation of the human health intervention costs.	60
Table 15: Parameters for the calculation of the cost of the deceased.	60
Table 16: Parameters for the calculation of the cost of the local value added due to hospitalization effects (losses in productivity).	61
Table 17: Parameters for the calculation of the decrease in local value added due to diseases of the employed population.	62
Table 18: Elements at risk and the vulnerability classes for the flood hazard.	63
Table 19: Parameters for the calculation of damages related to the residential/industrial buildings.	69
Table 20: Parameters for the calculation of damages related to the agriculture.	70
Table 21: Parameters for the calculation of damages related to the infrastructure, roads.	70
Table 22: Parameters for the calculation of reconstruction costs.	71
Table 23: Parameters for the calculation of rehabilitation costs.	71
Table 24: Parameters for the calculation of evacuation direct costs.	71
Table 25: Parameters for the calculation of evacuation assistance costs.	72
Table 26: Parameters for the calculation of emergency costs.	72
Table 27: Parameters for the calculation of human health intervention costs.	72
Table 28: Parameters for the calculation of back home costs.	72
Table 29: Parameters for the calculation of mud clean-up costs.	73
Table 30: Parameters for the calculation of the local value added due to psychological effects.	73
Table 31: Parameters for the calculation of changes in the Gross Local Product (GLP) or in the Local Value-Added (LVA).	73
Table 32: List of adaptation measures available in CSIS.	75
Table 33: Main modelling parameters attributed to adaptation measures.	76
Table 34: A subset of the analysis of the Ts/Ta relation for the identified adaptation measures (columns) in Table 32 . The first and the last row indicate the correspondence between the PLINIVS-LUPT model layers and ENVI-met presets (source: ENVI-met 4.0 elaboration). The first column shows the hours in a day, followed by the air temperature Ta.	76
Table 35: Overall possible adaptation actions for transport infrastructure. The components of the transport infrastructure are 1 = cut; 2 = embankment; 3 = pavement; 4 = channeling; 5 = drainage; 6 = structure; 7 = traffic condition; 8 = sign posts (Source: ROADADAPT project).	77
Table 36: Parametric cost of adaptation measures (see Annex II for details).	80

Table 37: Co-benefits linked to adaptation measures.	80
Table 38: Parameters necessary to calculate the cost of an AM used in a scenario from the current year until a specific year in the future in order to perform the cost-benefit analysis.	87
Table 39: Parameters necessary to calculate the benefits that arise from an AM deployed in relation to events that could happen in a specific time in the future. The benefits are calculated using the Avoided Costs Method, considering both economic impact with and without the AM or set of AMs.	88
Table 40: Cost Effectiveness Index of AMs.	88
Table 41: Cost Efficiency Index of AMs.	89
Table 42: Overview of the workflow of DC1 and its relation to the EU-GL methodology.	90
Table 43: EURO-CORDEX climate model configurations used as input for the derivation of urban climate indices.	94
Table 44: Classes of damage from thermal stress related to UTCI values, referring to the more vulnerable population groups (children under 15 years and elderly over 65 years) for the Naples climate zone. (Source: PLINIVS-LUPT, CLARITY project).	100
Table 45: Overview of the workflow of DC2 and its relation to the EU-GL methodology.	111
Table 46: Overview of available datasets used for this case study and for which EU-GL step they are mainly useful.	112
Table 47: List of hourly EURO-CORDEX configurations used for climate projections of flooding for DC2. ...	113
Table 48: Overview of the workflow of DC1 and its relation to the EU-GL methodology.	123
Table 49: Comparison between measurements of global radiation and temperature at different locations.	127
Table 50: Overview of the workflow of DC4 and its relation to the EU-GL methodology.	128
Table 51: Overall workflow including the cost parameters for the adaptation measure.	130
Table 52: DC4 Adaptation measures for each element and risk with cost scale and expected efficiency. ...	131
Table 53: Estimation of costs related to closure of lane between <i>PK 72+900 to PK 73+150</i> ,	134
Table 54: Summary of the climate indices used for hazard characterisation.	143
Table 55: List of EURO-CORDEX climate model configurations showing the institute, driving global model (GCM) and regional climate model (RCM). The last three columns show the availability of the emissions scenarios RCP2.6 (early response), RCP4.5 (effective measures), and RCP8.5 (business as usual / worst case). The rows highlighted in green show the model combinations ultimately used after taking into account the EURO-CORDEX errata.	145
Table 56: EURO-CORDEX climate model configurations used for climate impact analysis of river flooding.	215
Table 57: EURO-CORDEX climate model configurations considered in the calculation of the FWI.	218

CLARITY Project Overview

Urban areas and transportation infrastructure are highly vulnerable to climate change. Smart use of existing climate intelligence can increase urban resilience and generate added value for businesses and society at large. Based on the results of FP7 (7th Framework Programme) climate change, future internet and crisis preparedness projects (SUDPLAN, ENVIROFI, CRISMA) with an average Technical Readiness LEVEL (TRL) of 4-5 and following an agile and user-centred design process, end-users, purveyors and providers of climate intelligence CLARITY co-create an integrated Climate Services Information System (CSIS) to integrate resilience into urban infrastructure and look into the way to adjust the CSIS to transport infrastructure.

As a result, CLARITY provides an operational eco-system of cloud-based climate services to calculate and present the expected effects of Climate Change (CC)-induced and -amplified hazards at the level of risk, vulnerability and impact functions. CLARITY offers what-if decision support functions to investigate the effects of adaptation measures and risk reduction options in the specific project context and allow the comparison of alternative strategies. Three demonstration cases showcase CLARITY climate services in different climatic, regional, infrastructure and hazard contexts in Italy, Sweden, and Austria; focusing on the planning and implementation of urban infrastructure development projects. A fourth demonstration case in Spain illustrates how the expected effects of CC hazards and risk can be assessed in the case of road transport infrastructure and the flexibility of the CSIS system to adapt to other sectors.

CLARITY provides the practical means to include the effects of CC hazards and possible adaptation and risk management strategies into planning and implementation of such projects, focusing on increasing CC resilience. Decision makers involved in these projects will be empowered to perform climate proof and adaptive planning of adaptation and risk reduction options.

Abbreviations and Glossary

A common glossary of terms for all CLARITY deliverables, as well as a list of abbreviations, can be found in the public document “CLARITY Glossary” available at CLARITY-H2020.eu.

The following table was generated from http://cat.clarity-h2020.eu/glossary?machine_name%5B%5D=abbreviations_and_acronyms on February 11th, 2019 and contains all the acronyms that are used in the project.

Name	Term description
AAO	Appraisal of Adaptation Options
ADM	Architecture Development Method
AHF	Anthropogenic Heat Flux
AJAX	Asynchronous JavaScript and XML
AR	Assessment Report
AR4	Fourth Assessment Report
AR5	Fifth Assessment Report
BB	Building Block
BC	Bias Correction
C3S	Copernicus Climate Change Services
CA	Consortium Agreement
CBA	Cost-benefit-analysis
CC	Climate Change
CCA	Climate Change Adaptation
CCD	Consecutive Dry Days
CCH	Climate Change Hazards
CDD	Consecutive Dry Days
CERN	Conseil Européen pour la Recherche Nucléaire
CFS	Climate Forecast System
CKAN	Comprehensive Kerbal Archive Network
CLARITY	Integrated Climate Adaptation Service Tools for Improving Resilience Measure
CLC	CORINE Land Cover
Climate-ADAPT	European Climate Adaptation Platform
CMIP	Coupled Model Intercomparison Project
COSMO-CLM	COntortium for Small-scale MOdelling - Climate Local Model
COTS	Commercial Off-The-Shelf
CRISMA	Modelling crisis management for improved action and preparedness
CRM	Continuous Risk Management
CS	Climate Service
CSIS	CLARITY Climate Services Information System
CSS	Cascading Style Sheets
CSV	Comma Separated Values
CSW	Catalogue Service for the Web
CTA	Constructive Technology Assessment
DC	Demonstration Case
DC	Dublin Core
DEM	Digital Elevation Model
DFO	Dartmouth Flood Observatory
DHI	Danish Hydraulic Institute
DM	Decision Maker

DMP	Data Management Plan
DoA	Description of the Actions (Annex 1 to the Grant Agreement)
DOI	Digital Object Identifier
DOM	Document Object Model
DPA	Data Protection Agency
DRM	Disaster Risk Management
DRR	Disaster Risk Reduction
DS	Decision Support
DSM	Digital Surface Model
DV	Dynamic Vulnerability
DWD	Deutscher Wetterdienst
EC	European Commission
ECA&D	ECA&D European Climate Assessment & Dataset
ECMWF	European Centre of Medium-Range Weather Forecasts
ECV	Essential Climate Variable
ECW	Enhanced Compression Wavelet
EE	Evaluation of Exposure
EEA	European Environment Agency
EFFIS	European Forest Fire Information System
EFTA	European Free Trade Association
EGI	European Grid Infrastructure
EM	Exploitation Manager
EM-DAT	Emergency Events Database
EMSC	European-Mediterranean Seismological Centre
EO	Earth Observation
EPS	Ensemble Prediction System
ERA40	ERA 40-year Reanalysis
ERDDAP	Environmental Research Division's Data Access Program
ESD	Empirical Statistical Downscaling
ESDAC	European Soil Data Centre
ESGF	Earth System Grid Federation
ESM	Earth System Model
EU-GL	Non-paper Guidelines for Project Managers: Making vulnerable investments climate resilient (Document)
EU-MACS	European Market for Climate Services
FP7	7th Framework Programme
FRP	Fire Radiative Power
FTY	Forest Type
FUA	Functional Urban Areas
FWI	Fire Weather Index
GA	General Assembly
GCM	Global Climate Model
GDAL	Geospatial Data Abstraction Library
GDP	Gross Domestic Product
GeoJSON	geographical JavaScript Object Notation
GEOSS	Global Earth Observation System of Systems
GeoTIFF	Geographic Tagged Image File Format
GFAS	Global Fire Assimilation System
GFCS	Global Framework for Climate Services
GIS	Geographic Information System

GML	Geography Markup Language
GPM	General Project Manager
GPS	Global Positioning System
GPX	GPS Exchange Format
GUI	Graphical User Interface
H	Human
HC	Hazard Characterisation
HRL	High Resolution Layers
HRU	Hydrological Response Unit
HTML5	Hypertext Markup Language, version 5
HTTP	Hypertext Transfer Protocol
HW	Heat Waves
HWMI	Heat Wave Magnitude Index
IA	Impact Assessment
IAAP	Integration of Adaptation Action Plan
IAO	Identification of Adaptation Options
ICC	Indicators, Criteria and Cost
ICMS	Integrated Crisis Management Middleware
ICT	Information and Communication Technologies
IFS	Integrated Forecast System
IPCC	Intergovernmental Panel on Climate Change
IPR	Intellectual Property Rights
JMA	Japan Meteorological Agency
JRA-25	Japanese 25-year ReAnalysis
JRC	Joint Research Centre
JSON	JavaScript Object Notation
LRI	Large Research Infrastructure
MCDA	Multi-Criteria Decision Analysis
MMU	Minimum Mapping Unit
MRU	Minimum Reference Unit
MUKLIMO_3	Mikroskaliges Urbanes Klimamodell 3D
NaTech	Natural Hazard Triggering Technological Disasters
NCEP	National Centers for Environmental Prediction
NDH	Natural Hazards
NDSM	Normalized Differential Surface Model
NetCDF	Network Common Data Format
NGO	Non-Governmental Organization
NWP	Numerical Weather Prediction
OAI-PMH	Open Archive Initiative – Protocol Metadata Harvesting
OGC	Open Geospatial Consortium
OGR	OpenGIS Simple Features Reference Implementation
OpenAIRE	Open Access Infrastructure for Research in Europe
OpenDAP	Open-source Project for a Network Data Access Protocol
ORFEUS	Observatories & Research Facilities for European Seismology
OSM	Open Street Maps
PDF	Portable Document Format
PDSI	Palmer Drought Severity Index
PHP	PHP Hypertext Preprocessor
POPD	Protection of Personal Data
PPEA	Precipitation Potential Evaporation Anomaly

QA	Quality Assurance
QAP	Quality Assurance Plan
R10mm	Heavy precipitation days (precipitation \geq 10mm)
R20mm	Very heavy precipitation days (precipitation \geq 20mm)
R95p	Very wet days
RA	Risk Assessment
RCM	Regional Climate Model
RCP	Representative Concentration Pathway
RDBMS	Relational Database Management System
REST	Representational State Transfer
RIA	Rich Internet Application
RS	Reference Scenario
S2D	Subseasonal-to-Decadal
SD	Statistical Downscaling
SME	Small and Medium Enterprise
SMS	Scenario Management System
SOS	Sensor Observation Service
SPA	Single Page Application
SPBS	Stochastic back-scatter scheme
SPI	Standardized Precipitation Index
SPPT	Stochastically perturbed parameterized tendency
SPS	Sensor Planning Service
SQA	Software Quality Assurance
SQAP	Software Quality Assurance Plan
SQL	Structured Query Language
SSR	Seasonal Severity Rating
STL	Street Tree Layer
SU	Number of summer days
SUDPLAN	Sustainable Urban Development Planner for Climate Change Adaptation
SWD	Staff Working Document
SWICCA	Service for Water Indicators in Climate Change Adaptation
TC	Test Case
TCD	Tree Cover Density
TL	Task Leader
TM	Scientific & Technical Manager
TOC	Table of Content
TOGAF	The Open Group Architecture Framework
TR	Number of tropical nights
TRL	Technology Readiness Level
UN	United Nations
uncertML	Uncertainty Markup Language
UNGA	United Nations General Assembly
UNISDR	United Nations Office for Disaster Risk Reduction
UrbanSIS	Climate Information for European Cities
US	User Story
VA	Vulnerability Analysis
VC	Vulnerability Curve
VEI	Volcanic Explosivity Index
WFS	Web Feature Service
WHO	World Health Organization

WMO	World Meteorological Organization
WMS	Web Map Service
WMTS	Web Map Tile Service
WP	Work Package
WPL	Work Package Leader

The following table contains EU-GL Methodology terms used in the CLARITY project. Complete description can be found in the “CLARITY Glossary” available at http://cat.clarity-h2020.eu/glossary?machine_name%5B%5D=eu_gl_methodology_terms.

Name	Term description
Hazard	The potential occurrence of a natural or human-induced physical <i>event</i> or trend or physical <i>impact</i> that may cause loss of life, injury, or other health impacts, as well as damage and loss to property, infrastructure, livelihoods, <i>service</i> provision, ecosystems, and environmental resources (IPCC, 2014). In the IPCC context, the term <i>hazard</i> usually refers to climate-related physical events or trends or their physical impacts. (IPCC, 2014).
Exposure	The presence of people, infrastructure, housing, production capacities and other tangible human assets in hazard-prone areas.
Vulnerability	The probability of a given element at risk, classified as part of a specific Vulnerability class, to be affected by a level of damage, according to a prefixed scale of damages, under a given hazard intensity (Glossary of the CLARITY Proposal).
Risk Analysis	Risk is the potential for consequences where something of value is at stake and where the outcome is uncertain, recognizing the diversity of values. Risk is often represented as probability of occurrence of hazardous events or trends multiplied by the impacts if these events or trends occur. Risk results from the interaction of vulnerability, exposure, and hazard. (IPCC, 2014). Risk Analysis is a systematic use of available information to determine how often specified events may occur and the magnitude of their likely consequences (CRISMA Project glossary).
Impact Scenario Analysis	In probabilistic terms choosing in a deterministic way one or more significant events, among actually occurred past events or as a result of numerical hazard simulation models, shall be obtained as damage evaluation following a specific event.
Adaptation Options	The array of strategies and measures that are available and appropriate for addressing adaptation needs. They include a wide range of actions that can be categorized as structural, institutional, or social (IPCC, 2014).
Decision Support	Functions that help in evaluating the data and deciding what to do.
Action Plan	Functions that help in establishing the report / implementation plan / guideline.
Integration	Integration of adaptation plan into the project.

Executive Summary

This document is deliverable D3.3 “Science support report” of the CLARITY project (H2020, Contract number 730355). It presents a report on the work performed and results obtained in WP3 since the deliverable D3.2, and thus concludes the Science Support part of CLARITY.

The CLARITY project follows the seven steps¹ of the EU-GL methodology described in detail in the D3.1. Consequently, the work and results presented here will follow this workflow. The association of the original Tasks 3.2, 3.3, 3.4, and 3.5 of this work package with the EU-GL workflow is presented in the Introduction (Chapter 1).

CLARITY produces data and climate, risk and impact assessments at two different levels of detail. Consequently, this deliverable separates the work in these areas into two chapters. Chapter 2 shows the work and results for the pan-European Screening Level following the EU-GL structure. Climate indices which characterise the hazards have been calculated for a majority of the global climate model/regional climate model combinations. Focus is on the heat and flooding hazards. Methods to downscale the coarse pan-European data to urban scales have been developed. This local effect calculation relies on high-resolution data layers of the urban environment to characterise the effect that buildings, parks, roads, etc. have on the climate. These local effect calculations for heat waves and flooding employ physical principles which must be appropriately represented for calculations, such that they can be run and produce results in real-time on spatial resolutions of 500 m × 500 m over an entire urban area.

The local effect is vital for the subsequent calculations of the impact that hazards have, here in terms of health and mortality for population when considering heat waves, or in terms of financial costs for buildings and infrastructure when considering floods. Methods for these impact calculations have been developed herein. One significant outcome of this is that the assessment of the hazard impact allows one to evaluate the benefits of implementing certain adaptation options or measures. Such adaptation measures are vital, as they provide a way of mitigating the damage that hazards will produce in an environment warming through climate change. A number of relevant adaptation options are presented and their impact on the urban environment can be modelled within the CSIS.

Chapter 3 focuses on the four demonstration cases, which, owing to their different aims, are structured independent from each other. They address some, but not necessarily all, of the steps of the EU-GL methodology.

DC1 (Naples, Italy) examines the hazards of heat waves, floods, and to a lesser extent, landslides. The employment of local effect models, developed by PLINIVS, downscale pan-European data to a spatial resolution of 250 m × 250 m. This enables the calculation of impact from heat waves and floods at the urban scale, and these results are still under analysis. Relevant adaptation measures have been investigated with the aim of reducing the impacts of heat waves and floods. Preliminary tests of the proposed calculation methodology to assess their benefits have been conducted for various adaptation measures, and the results are still under analysis.

DC2 (southern Sweden) examines the hazards of pluvial flooding from intense precipitation, and heat waves. In the case of flooding, the hazard was characterised from climate index data as well as through the development and implementation of a flow model for southern Sweden. Existing adaptation measures were evaluated in terms of their effect mitigating climate change for Jönköping, Sweden. Furthermore, the case of land use modification was addressed by investigating the change to the flooding hazard in Jönköping by the replacement of forest and farmland with increased paved areas upstream. In the case of heat waves, Urban SIS climate data and impact indicators as well as the SURFEX model were employed to capture the small-scale elements of the urban environment (building density, vegetation fraction) at 1×1 km² resolution.

¹ Hazard Characterisation, Evaluation of Exposure, Vulnerability Analysis, Risk & Impact Assessment, Identification of Adaptation Options, Appraisal of Adaptation Options, Integration of Adaptation Action Plan.

Impact indicators relating to the vulnerability of the population concerning heat (e.g. heat-induced mortality) and air quality were investigated. Relevant adaptation options of how the city develops in the future in terms of the amount of vegetation and density of buildings were assessed in terms of the changes in air temperature and pollution.

DC3 (Linz, Austria) examines the hazard of heat at three different spatial scales through climate modelling. The calculation of several heat indices from climate models for the baseline (historical) period and future periods showed how the heat load for Linz changed. Interest was on an assessment of possible adaptation options in mitigating the heat hazard. This analysis was performed on both the urban scale (changes to roof albedo, roof greening, reduction of soil sealing) affecting the entire urban area, and at the city-block/suburb scale (increased greening) affecting only certain streets, and showed how such changes can lead to a reduction in the heat load in the affected areas.

DC4 (Spain) examines the hazards of heat and cold waves, and floods, with the element of exposure being road infrastructure, and indirectly people which are dependent on such transport routes and the maintenance thereof. The road infrastructure was most vulnerable to damage during extended periods of extreme heat or cold. The impacts on the road included surface damage and deformities during extreme heat, and the build-up of snow and ice on elevated and exposed road sections during extreme cold. A number of adaptation options were proposed, including changes in road orientation or shadowing to minimise solar radiation in the case of heat, or changes to routes to lower elevations in the case of cold. For the flooding hazard caused by heavy precipitation in short periods of time, a necessary adaptation measure would be to increase the size of drainage channels to accommodate the water. The calculations are still ongoing.

1 Introduction

This deliverable presents a report on the work performed in WP3 since the last deliverable D3.2 and represents the conclusion of the “Science Support” contribution to the CLARITY project. It includes inputs from all WP3 “Science Support” tasks and is partly related to the co-creation process in WP1 “CO-Creation”, as well as the data collection process in WP2 “Demonstration and Validation”. As the science was not finished in time for the actual delivery date of this deliverable, it has meant that the final version of this document has been delayed. Consequently, the version which is being submitted now is an incomplete version which will be updated at the conclusion of the project.

As this document builds on the work and results and methodologies presented already in the previous deliverables D3.1 and D3.2, where possible, references are made to these deliverables in order to avoid repetition herein.

Section 1 presents the structure of this deliverable and summarizes the main objectives of WP3 “Science Support”. Section 2 presents work which has been performed for the Screening Services. Section 3 presents work which has been performed for Expert Services on the four Demonstration Cases (DCs). Section 4 presents the conclusions.

1.1 CLARITY Science Support

The main objectives of WP3 (Science Support), manifested through the work package (WP) Tasks T3.1 – T3.5, are described in the following.

Task 3.1 (Scientific Background) contributes to the initial WP activities in terms of providing the scientific base (literature overview, models, datasets, and algorithms) needed for the realization of the CLARITY climate services, while continually referring to the EU-GL methodology. The main outcome of T3.1 is reflected in the previous deliverable (D3.1 “Science Support Plan and Concept”).

Task 3.2 (Climate Intelligence) provides climate and environmental data for reference scenarios in accordance with end-user requirements. Downscaled climate projections, based on IPCC scenarios, are used to perform impact assessment. To improve the projections of environmental variables, customized models and algorithms are used for applying the downscaling procedures and bias-correction methods. T3.2 integrates available local data and aims to determine the environmental response to CC forcing (with and without adaptation measures). The main output from T3.2 will be used for Risk Assessment and Impact Scenario Analysis in T3.3 “Risk Assessment and Impact Scenario Analysis”.

Task 3.3 (Risk Assessment and Impact Scenario Analysis) discusses and applies indicators for risk and impact assessment, manifested through an interplay of the three variables Hazards, Exposure and Vulnerability, based on the output from the previous tasks and referring to the EU-GL methodology. This includes the quantification and evaluation of risk under the consideration of CC, characteristics of the most relevant climate hazards (e.g. based on statistical parameters) and the assessment of exposure and vulnerability parameters likely to be affected by the considered hazards (e.g. by using a number of climate models and vulnerability functions). For this purpose, concepts and methods from previous European and national projects will be included. The former name of this task (Vulnerability and Risk Assessment) has been changed due to an updated version of the EU-GL steps.

Task 3.4 (Adaptation Strategies and Decision Support) provides models and algorithms to evaluate adaptation strategies, based on the information from Risk Assessment and Impact Scenario Analysis. The implementation of the adaptation measures leads to a modified impact scenario assessment due to the modification of input parameters.

Task 3.5 (Economic and Societal Impact) appraises economic and societal consequences of the implementation of different adaptation strategies with the aim of identifying the most efficient options

(e.g. by applying cost-benefit analyses). This enables an evaluation and comparison of alternative adaptation scenarios and allows for an ‘optimal’ selection of mitigation/adaptation options.

As the CLARITY project has adopted the EU-GL methodology (i. Hazard Characterisation, ii. Evaluation of Exposure, iii. Vulnerability Analysis, iv. Risk & Impact Assessment, v. Identification of Adaptation Options, vi. Appraisal of Adaptation Options, vii. Integration of Adaptation Action Plan), which was presented in detail in deliverable “D3.1 Science Support Plan and Concept” and is summarised in section 1.2, the work and results will primarily follow this workflow. How this workflow is associated with the original tasks are as follows:

Task 3.2 – i. Hazard Characterisation, ii. Evaluation of Exposure

Task 3.3 – iii. Vulnerability Analysis, iv. Risk & Impact Assessment

Task 3.4 – v. Identification of Adaptation Options

Task 3.5 – vi. Appraisal of Adaptation Options, vii. Integration of Adaptation Action Plan.

1.2 CLARITY Methodology

The CLARITY workflow is based on the methodology of the “Non-paper Guidelines for Project Managers: Making vulnerable investments climate resilient” [1]. The Climate Resilience Toolkit as presented in this document was updated to also comply with the Fifth Assessment Report (AR5) of the Intergovernmental Panel on Climate Change (IPCC) in order to promote an integrated modelling approach of Disaster Risk Reduction (DRR) and Climate Change Adaptation (CCA). The 7 steps of the updated EU-GL methodology are illustrated in **Figure 1**. These steps should be considered in climate resilient planning of any kind. The methodology, including a detailed description for each of the 7 EU-GL steps is presented in the deliverable “D3.1 Science Support Plan and Concept”.



Figure 1: The 7 steps of the CLARITY methodology

1.3 Screening and Expert Studies

The CLARITY CSIS will provide services at three levels of detail:

- 1) Basic screening level which aims to provide freely available data and climate evaluations for all of Europe limited to the spatial scale of 0.11° (12 km),
- 2) Advanced screening level which employs the local-scale models, currently only for heat waves and floods, to downscale these climate evaluations to scales useful for the urban environment (500m) and performs an impact assessment on the fly, and
- 3) Expert level service which will supplement the advanced screening level study which additional, high resolution data and climate analyses based on user needs at a cost to the user.

The basic screening (**Figure 2**) provides a screening service to perform a hazard characterization (at ≈12km resolution) and exposure analysis to roughly estimate the impact of climate hazards in a qualitative way. It enables the user to explore their study region, to overlay climate data with additional datasets (e.g. land-use data sets available from Copernicus) and to get information about different adaptation options. For regions available in Urban Atlas, European Settlement Map, and Street Tree layer, these land-use data sets were combined and processed and thus refined land use information is provided.

The advanced screening service (**Figure 2**) provides a screening service to estimate the impact of heat and pluvial flooding on the fly, at 500m x 500m resolution. It merges information about climate change derived from climate models (temperature or precipitation changes) with other openly available data (land use, topography, population) to obtain information about the hazard at the urban scale and to derive impact estimates for certain elements at risk using vulnerability and impact functions. Estimations of the hazard at local scale and of the impact are based on models, which have been simplified so that on the fly calculations for any location within Europe can be provided. Accordingly, these results represent a first approximation and should be used as guidance for the situation.

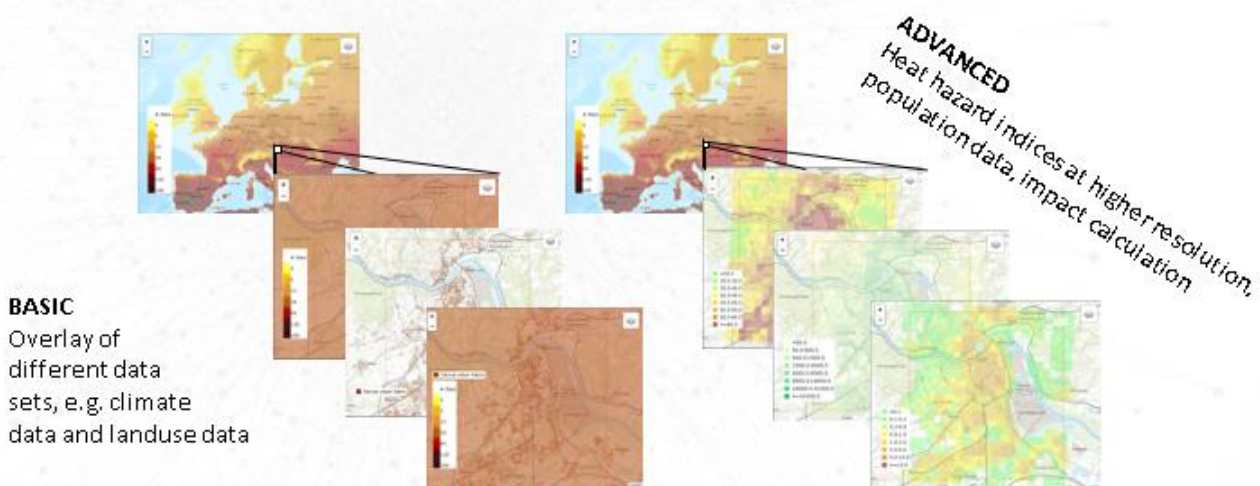


Figure 2: Schematic illustrating the basic (left) and advanced (right) screening services.

The difference between the advanced screening level and the expert level study is that the expert level will provide a higher data resolution, additional datasets, more sophisticated models and thus an analysis better tailored to the urban area or infrastructure project investigated by the user. Depending on the user needs, the expert analysis can focus on certain steps of the CLARITY methodology, such as hazard characterisation and adaptation option assessment only. In this case, the CLARITY framework and CSIS screening study help to ensure that the remaining steps will at least be considered in a qualitative way.

This deliverable will present results of the work which has been performed on both the screening levels (basic in Section 2.1.1, advanced in Sections 2.1.2-2.5) and the expert level (Chapter 3).

2 Basic and Advanced Screening Services

The Screening Level services proposed in CLARITY aims at making data and climate analyses for all of Europe freely accessible for users who wish to perform assessments on the risk and impact of various climate hazards in their region of interest. These services will be provided at two levels:

- 1) Basic screening level which aims to provide freely available data and climate evaluations for all of Europe limited to the spatial scale of 0.11° (12 km),
- 2) Advanced screening level which employs the local-scale models, currently only for heat waves and floods, to downscale these climate evaluations to scales useful for the urban environment (500m),

The structure of this chapter is based on the EU-GL [1] workflow on which CLARITY is based (**Figure 1**).

The provision of a pan-European service on-the-fly requires that the spatial resolution of the data be kept low – here around 0.11° - such that calculations can be performed within a reasonable time for the user. However, in cases where additional data is locally available (data packages), or alternatively, an algorithm exists to downscale the coarse climate data to urban scales with the assistance of urban-landscape data, climate analyses on smaller spatial scales can be achieved. This will be described in more detail in Section 2.1.2.

2.1 Hazard Characterisation

2.1.1 Climate Indices

Climate hazards can be identified by using a range of climate variables and indices. When calculated for a baseline/observed climate period as well as a future period calculated from climate prediction models, one can assess the change of each climate variable or hazard in the future.

The hazards which CLARITY will consider include: temperature related hazards such as extreme heat or cold, precipitation related hazards such as floods, wind storms, droughts, forest fires and landslides. Each hazard will be characterised using climate indices which are commonly used in the climate community or have been specifically designed for risk assessment (e.g. ECA&D², Urban SIS³, ETCCDI⁴). These indices are summarised in **Table 1**.

All climate indices were calculated for a baseline period (1971-2000) and three future time-periods (2011-2040, 2041-2070, 2071-2100) using bias corrected EURO-CORDEX data⁵ [2]. For the future time periods, three different greenhouse gas emissions scenarios (Representative Concentration Pathways), which were also used in the AR5 of the IPCC, are used: RCP2.6 (early response), RCP4.5 (effective measures) and RCP8.5 (business as usual / worst case scenario) [3]. A comparison of the climate indices calculated for the baseline and future periods indicates how the climate will change under different RCP scenarios until the end of the 21st century. To account for the uncertainty in model predictions, the climate indices were calculated using several climate models and the ensemble mean and ensemble standard deviation was calculated. More information regarding the indices, their definition and results, as well as the data and models used to derive the climate indices is provided in **Annex I: Climate Indices**.

Additionally, for each climate index, a *synthetic index* was defined to represent each hazard on a 3-level intensity scale (low, medium, high). It was intended to integrate this synthetic index into the CSIS tool in the form of a table, indicating the severity of each hazard for current and future climate periods under the

² <https://www.ecad.eu/indicesextremes/>

³ <http://urbansis.climate.copernicus.eu/>

⁴ http://etccdi.pacificclimate.org/list_27_indices.shtml

⁵ <http://www.euro-cordex.net/>

three different greenhouse gas emissions scenarios. However, its implementation within the CSIS was not as straightforward as planned, and so it was decided to omit this for the moment. Owing to page-restrictions, further information on this index, along with the other calculated hazard indices have been summarised in **Annex I: Climate Indices**.

Table 1: Summary of the climate indices used for hazard characterisation.

Hazard	Index
HEAT: Heat waves	Consecutive summer days
	Consecutive hot days $\geq 75^{\text{th}}$ percentile
HEAT: Extreme heat	Hot days
	Summer days
	Tropical nights
	Maximum temperature $\geq 75^{\text{th}}$ percentile
COLD: Cold waves	Consecutive frost days
COLD: Extreme cold	Frost days
	Ice days
	Minimum temperature $\leq 10^{\text{th}}$ percentile
Thermal stress	Extreme temperature range
FLOODS: Extreme precipitation	Maximum 1-day precipitation
	Maximum 5-day precipitation
	Snow days
FLOODS: Wet periods	Consecutive wet days
	Wet days
	Heavy precipitation days
	Days where daily precipitation $\geq 90^{\text{th}}$ percentile
FLOODS: River flooding	Flood recurrence
	River flow
FLOODS: Pluvial flood	Water runoff
STORMS: Extreme wind speed	98 th percentile wind speed
	Maximum wind speed
	Days with wind speed ≥ 17 m/s
DROUGHTS	Consecutive dry days
FOREST FIRES	Fire weather index

As the focus in the development of the CSIS was on heat-related hazards and flooding, only some of the indices originally planned were calculated. Additional information about heat needed to be provided to enable the “local effect” calculation. Currently, this information is made available in CSIS under the hazard characterisation step in form of a table, while the other climate indices are displayed in the map component.

2.1.2 Local Effect Estimation

The EURO-CORDEX data at 0.11° resolution as it stands is too coarse to analyse the impacts of climate change at the urban/city scale. Therefore, there is a need to provide information on finer spatial scales through the application of downscaling techniques. Section 2.2.1 of Deliverable 3.2 outlined the physical principles behind the downscaling methods to be used to calculate the local effect for heat waves and flooding. What is presented in the following concerns refinements to the heat model in its calibration and validation (Sections 2.1.2.1 – 2.1.2.2). The flood model was simplified using a similar approach to that used within DC1, and is still under development (Section 2.1.2.3).

2.1.2.1 Heat wave events as input for local effect calculation

Although several definitions of heat waves exist in the literature ([4], [5], [6]), including those calculated in the list of climate indices shown in **Table 1**, a suitable definition of heat waves had to be used to relate them to the excess mortality rate for the local effect calculation, e.g. [7]. Accordingly, a heat wave which has a detrimental effect on health is defined as *a period of at least two consecutive days and to have maximum daily temperatures equal to or exceeding the 95th percentile of the daily maximum temperature during the warm season (April – September) of the baseline period*. The rate of occurrence of a heat wave is classified as occurring either:

- Once per year (frequent event; probability of occurrence in a year = 1.0),
- Once in 5 years (occasional event; probability of occurrence = 0.2), or
- Once in 20 years (rare event; probability of occurrence = 0.05).

Heat wave events of the three rates of occurrences have been calculated for each EURO-CORDEX grid point in Europe. As an aside it should be noted, that the definition of such events is not unique – it is possible that a heat wave of longer duration with a lower maximum daily temperature has similar probability of occurrence as a heat wave of a shorter duration but with a higher maximum daily temperature. In such cases, the latter type of (intense) heat wave event with the greater maximum daily temperature is used, with the idea being that heat wave intensity *may* be more of a major driver of heat wave associated mortality compared with duration.

Table 2 shows an example of the most intense heat wave events for a grid point representative of Naples (DC1) for each of the three future time periods and the three emissions scenarios. For the mortality calculation (e.g. Section 3.1.2), all days of such heat waves are summed over the 30-year period and averaged to produce yearly-averaged values.

Table 2: Heat wave events for a grid point representing Naples from the SMHI, ICHEC GCM. Each heat wave shows the greatest number of consecutive days where the maximum temperature of each day is equal to or exceeds the temperature shown.

Period	Emissions Scenario	Frequent	Occasional	Rare
2011-2040	RCP26	36.0 °C, 5 days	37.0 °C, 2 days	39.5 °C, 2 days
	RCP45	35.5 °C, 11 days	37.5 °C, 2 days	40.0 °C, 2 days
	RCP85	36.0 °C, 8 days	40.5 °C 2 days	41.0 °C, 2 days
2041-2070	RCP26	36.5 °C, 5 days	38.0 °C, 2 days	39.5 °C, 2 days
	RCP45	37.5 °C, 8 days	39.0 °C, 4 days	40.0 °C, 2 days
	RCP85	37.5 °C, 7 days	39.5 °C, 4 days	40.5 °C, 3 days
2071-2100	RCP26	36.0 °C, 6 days	37.5 °C, 2 days	39.0 °C, 2 days
	RCP45	37.0 °C, 4 days	38.5 °C, 2 days	39.5 °C, 2 days
	RCP85	39.0 °C, 3 days	39.5 °C, 2 days	40.0 °C, 3 days

2.1.2.2 Heat wave local effect at the advanced screening level

The accuracy of the heat wave local effect model (HWLEM) developed by PLINIVS-LUPT has been evaluated by comparing its results against those from the validated SOLWEIG tool [8] in two ways:

- 1) By running the HWLEM from within the Demonstration Case of Naples (DC1), and
- 2) By running the HWLEM within the CSIS as an advanced screening level study.

From the outset it is to be expected that the margin of error will be lower using the first comparison than for the second. This is because the land use data currently available within CSIS is of lower resolution than that available within DC1, and that the georeferencing method is different.

A calibration of the parameters used in the model has been performed on the DC1 version of the HWLEM, following the comparison on sample areas characterized by different land uses distributions (see following section). The adjusted parameters are then transferred to the CSIS version of the model.

2.1.2.2.1 Calibration of the Heat wave local effect model

The DC1 version of the heat wave local effect model is based on a specific land use classification (**Figure 3**). The calculation of the Mean Radiant Temperature (T_{mrt}), which is an important variable used for the thermal comfort (see Section 2.2.1 of D3.2 for more information), requires as input albedo, emissivity, sky view factor, vegetation shadow, surface temperature, among others. Values of these quantities have been specified for each land use class for Naples and are shown in **Table 3**.

A series of preliminary tests were conducted by varying one of the key parameters mentioned previously on sample areas in Naples. It was found that the major discrepancies in the results concern the value of surface temperature (T_s). To better calculate this parameter, the HWLEM uses a table that correlates, for each land use class, T_s to the air temperature (T_a) and the solar radiation for each land use class. The correction of this value, originally attributed through literature, has been performed using another validated model, ENVI-met⁶ v4.0, which is able to parameterize that relationship for relevant land use classes (**Table 4**). This refinement step allows T_s to be calibrated in the DC1 version of the HWLEM, the results of which are shown in Figure 4. Here values obtained through SOLWEIG, ENVI-met and the PLINIVS-DC1 HWLEM are shown for 24 test points (x-axis) corresponding to four different land use classes.

⁶ <https://www.envi-met.com/>



Figure 3: Detailed land use used in DC1, in red the Point of Interest (POIs) used in the calibration.

Table 3: Land use attribute table in DC1.

class	albedo	emissivity	tau (transmissivity)	psi_v (hillshade_gf)
AGRICULTURAL AREAS	0,16	0,94	1	0,97
BARE SOIL	0,11	0,95	1	0,97
BUILDINGS	0,18	0,95	1	0,97
BUILT OPEN SPACES	0,25	0,9	1	0,97
RAILWAYS	0,2	0,85	1	0,97
ROADS	0,18	0,95	1	0,97
SPORTS FACILITIES	0,21	0,96	1	0,97
TREES	0,13	0,97	0,25	0,37
VEGETATED AREAS	0,21	0,94	0,25	0,97
WATER	0,07	0,96	1	0,97

class	psi_b (hillshade_b)	density	
BUILT OPEN SPACES	1	0	very low building density
BUILT OPEN SPACES	0,9	1	low building density
BUILT OPEN SPACES	0,8	2	medium building density
BUILT OPEN SPACES	0,6	3	high building density
ROADS	1	0	very low building density
ROADS	0,9	1	low building density
ROADS	0,8	2	medium building density
ROADS	0,6	3	high building density

Table 4: Comparison of the Ta/Ts relation in ENVI-met and the HWLEM used in DC1.

layer PLINIVS MODEL		agricultural areas		bare soil		building		built open spaces		railways		roads		sport		vegetated areas		water	
hours	Ta (Envimet)	Ts Envimet	Ta/Ts variation	Ts Envimet	Ta/Ts variation	Ts Envimet	Ta/Ts variation	Ts Envimet	Ta/Ts variation	Ts Envimet	Ta/Ts variation	Ts Envimet	Ta/Ts variation	Ts Envimet	Ta/Ts variation	Ts Envimet	Ta/Ts variation	Ts Envimet	Ta/Ts variation
0	21,9	17,5	-20%	17,2	-21%	24,4	12%	25	15%	20,9	-4%	24,3	11%	17,7	-18%	17,7	-18%	18,8	-15%
1	21,1	17,2	-18%	17	-19%	24	12%	24,4	14%	20,8	-5%	23,8	11%	17,6	-19%	17,6	-19%	18,6	-14%
2	20,4	19,5	-4%	19,2	-6%	19,8	14%	19,8	16%	19,4	-1%	19,8	13%	19,3	-17%	19,3	-17%	19,2	-12%
3	19,8	17,3	-13%	16,7	-16%	19,2	-3%	19,4	-3%	17,9	-5%	19,2	-3%	16,9	-5%	16,9	-5%	17,4	-6%
4	19,2	16,4	-15%	15,8	-18%	18,8	-3%	19	-2%	17,3	-10%	18,7	-3%	16,1	-15%	16,1	-15%	16,6	-12%
5	18,8	16	-15%	15,4	-18%	18,6	-2%	18,8	-1%	17,2	-10%	18,5	-3%	15,7	-16%	15,7	-16%	16,2	-14%
6	19,6	15,9	-19%	15,4	-21%	18,8	-1%	19	0%	17,6	-9%	18,8	-2%	15,9	-16%	15,9	-16%	16,2	-14%
7	21	17,8	-15%	17,8	-15%	20,8	-4%	20,6	-3%	19,9	-10%	20,9	-4%	18	-19%	18	-19%	17,3	-17%
8	23	23,9	4%	23,9	4%	26,8	-1%	26,1	-2%	24,6	-5%	27,3	0%	23,6	-14%	23,6	-14%	20,6	-18%
9	24,7	27,2	10%	27,6	12%	33,2	17%	32,6	13%	28,6	7%	34,1	19%	27,2	3%	27,2	3%	24,4	-10%
10	26,5	29,9	13%	31	17%	39,3	35%	38,8	32%	32,9	16%	40,5	38%	30,1	10%	30,1	10%	27,3	-1%
11	28,4	32,3	14%	33,9	19%	44,3	48%	44,1	46%	37,9	24%	45,6	53%	32,8	14%	32,8	14%	29,2	3%
12	29,6	34,4	16%	36,9	25%	48,0	56%	48,2	55%	43,6	33%	49,5	61%	35,3	15%	35,3	15%	30,4	3%
13	30,4	36,3	19%	39,8	31%	50,4	62%	50,9	63%	48,8	47%	51,9	67%	37,6	19%	37,6	19%	31,1	3%
14	31	38	23%	43,1	39%	51,5	66%	52,3	67%	50,6	61%	53	71%	40	24%	40	24%	31,5	2%
15	31,6	39,1	24%	45,6	44%	51,4	66%	52,3	69%	49,8	63%	52,8	71%	42	29%	42	29%	31,5	2%
16	32	39,3	23%	45,9	43%	49,9	63%	51,1	66%	47,8	58%	51,2	67%	42,5	33%	42,5	33%	31,1	0%
17	32,2	38,5	20%	43,6	35%	47,2	56%	48,5	60%	44,8	49%	48,3	60%	41,2	33%	41,2	33%	30,1	-3%
18	31,4	35,8	14%	38,8	24%	43,0	47%	44,4	51%	40,1	39%	43,9	50%	37,4	28%	37,4	28%	28,4	-7%
19	30	30,6	2%	32,4	8%	37,7	37%	39,1	41%	34,2	28%	38,2	40%	31,5	19%	31,5	19%	25,9	-10%
20	28	24,6	-12%	24,9	-11%	32	26%	33,4	30%	27,7	14%	32,1	27%	24,9	5%	24,9	5%	23,2	-14%
21	26,4	22	-17%	22	-17%	29,2	14%	30,3	19%	25,4	-1%	29,2	15%	22,3	-11%	22,3	-11%	21,8	-17%
22	24,8	20,1	-19%	20	-19%	27,2	11%	28,1	15%	23,6	-4%	27,1	11%	20,4	-16%	20,4	-16%	20,6	-17%
23	23	18,6	-19%	18,4	-20%	25,6	10%	26,4	13%	22,1	-5%	25,5	9%	18,8	-18%	18,8	-18%	19,6	-17%
layer ENVIMET		Soja 63 cm		Lomy soil		Asphalt / red stones		Concrete pavement dark		Smashed brick		Asphalt roads		Grass 50 cm aver. dense		Grass 50 cm aver. dense		Deep water	

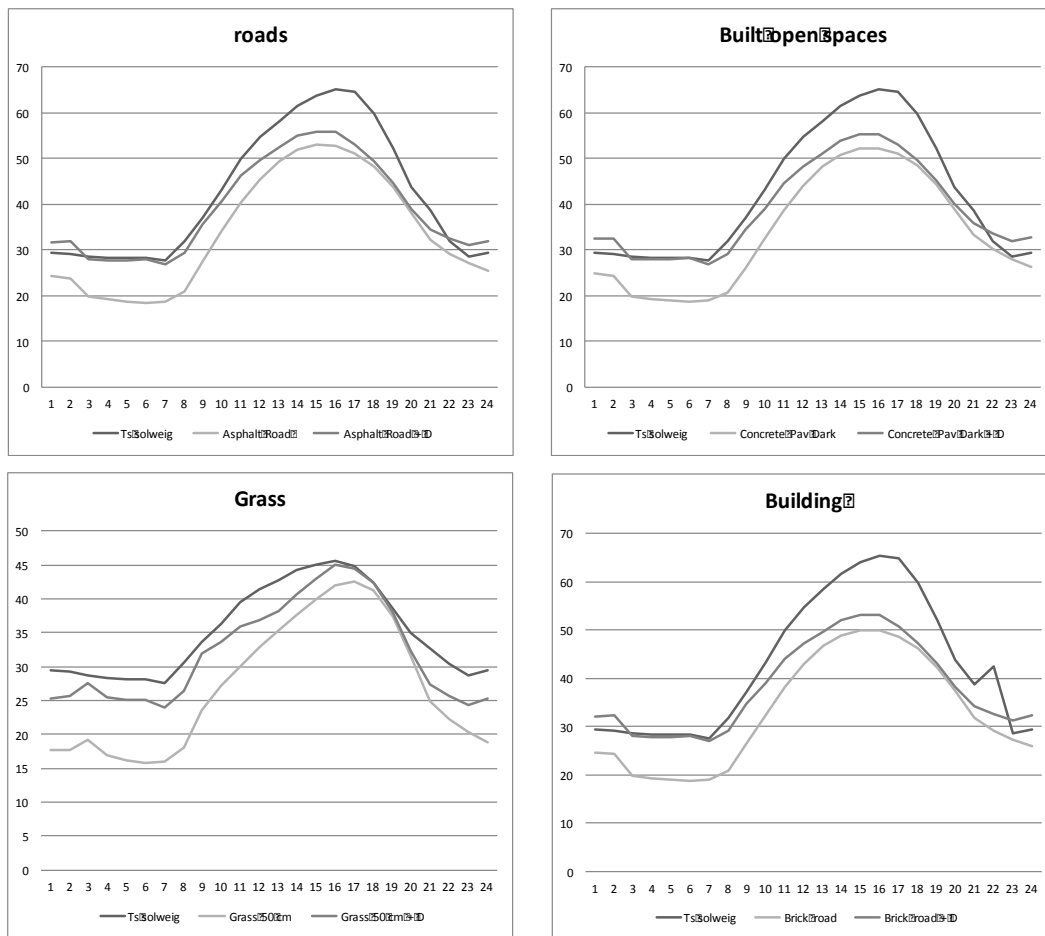


Figure 4: Comparison of Ts values across the different models used in the calibration phase, on 24 test points in 4 different land use categories (in the legend, left, SOLWEIG; middle, ENVI-met; right PLINIVS-DC1 HWLEM).

The new run of the HWLEM following this first calibration step (“Tmrt PLINIVS 2” in the graphs shown in the following pages) produced values of Tmrt values in better agreement with SOLWEIG in the cases of sunny areas. To improve the HWLEM in shaded areas, the values of the transmissivity parameter Ts were further calibrated. The result of this can be seen in **Figure 5 – Figure 8** for the point labelled “Tmrt PLINIVS 3”. The other three points in the figures illustrate the calibration results for each land use class located in “sunny” conditions. In each figure, the top panel shows the locations where the data for the curves in the lower two panels were measured.

Buildings

Despite the differences and approximations that exist between the HWLEM from PLINIVS-LUPT and the SOLWEIG model, the buildings class show a very similar output result for both the Tmrt and Ts (**Figure 5**).

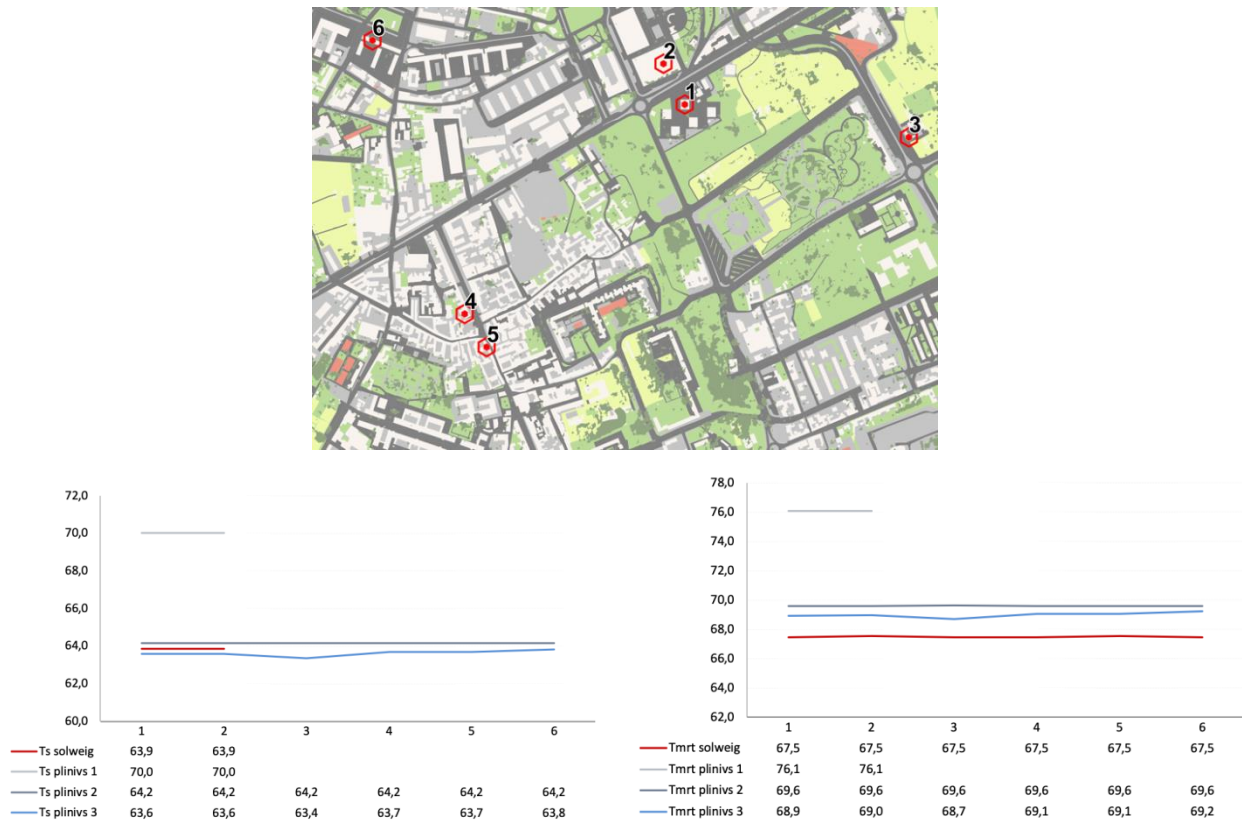


Figure 5: Difference between PLINIVS-LUPT (lower left panel) and SOLWEIG (lower right panel) outputs for Ts and Tmrt values for “buildings” land use class in the various calibration steps. The top panel shows the locations for the curves in the lower two panels.

Built open spaces

For the “built open spaces” class the Tmrt from the PLINIVS-LUPT HWLEM is slightly lower than that from SOLWEIG (**Figure 6**). This is due to the different albedo and emissivity parameters used by the two models - SOLWEIG uses an average albedo value for all surface land use types, whereas the PLINIVS-LUPT HWLEM specifies it for each land use. In contrast though, Ts is similar for both models.

It is important to highlight that SOLWEIG uses a single land use class (“paved” areas) for both the built open spaces and the roads. However, these two are considered different land use categories in the PLINIVS-LUPT HWLEM. This is done to better distinguish the difference of asphalt, which often characterizes roads as surface material, from the grey or lighter coloured stones usually used for sidewalks and squares. The result of this will be emphasised for the following class.

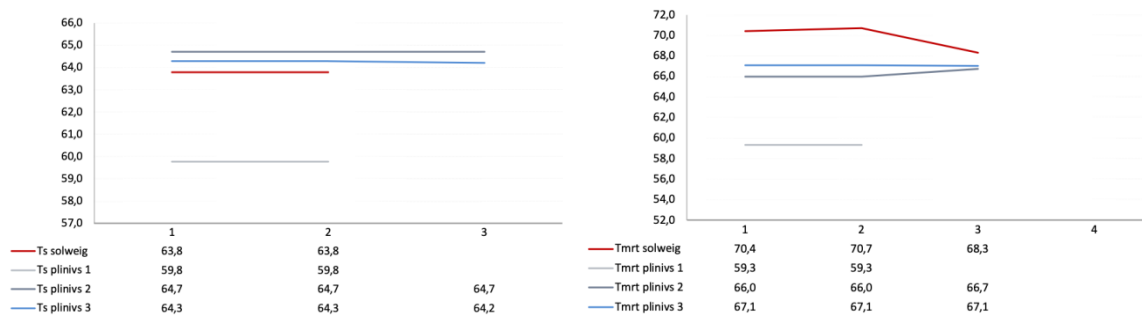


Figure 6: As in **Figure 5** but showing values for the “built open spaces” land use class.

Roads

The “roads” class of the PLINIVS-LUPT model also corresponds to the “paved” class in SOLWEIG. Unlike for SOLWEIG, it differs from the “built open spaces” class with different values of albedo and emissivity, such that a slightly higher Tmrt value is expected than for the Built open spaces class. The output results confirm this with the PLINIVS-LUPT HWLEM slightly overestimating Tmrt and Ts with respect to SOLWEIG (**Figure 7**). Comparing the values in the “roads” and “built open spaces” classes from the PLINIVS-LUPT HWLEM, and those from the “paved” class from SOLWEIG, shows that discrepancies in these values arises because SOLWEIG groups these two categories together. This is shown by the overestimation of Tmrt values on “roads” being compensated by the underestimation on “built open spaces”, and may suggest the hypothesis that results from the PLINIVS-LUPT model may be more precise for these land use classes.

Vegetated areas

The “vegetated areas” class of PLINIVS-LUPT HWLEM corresponds to the “grass” class in SOLWEIG. The output results of Tmrt and Ts from the PLINIVS-LUPT HWLEM are lower compared to the SOLWEIG model despite the surface temperature being slightly overestimated (**Figure 8**).

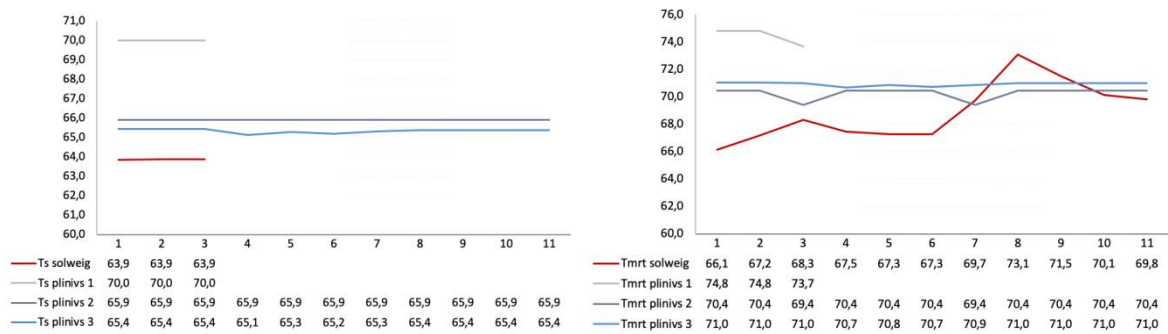
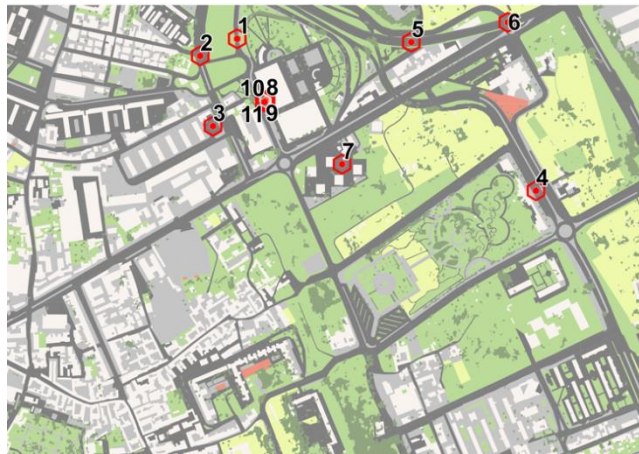


Figure 7: As in Figure 5 but showing values for the “roads” land use class.

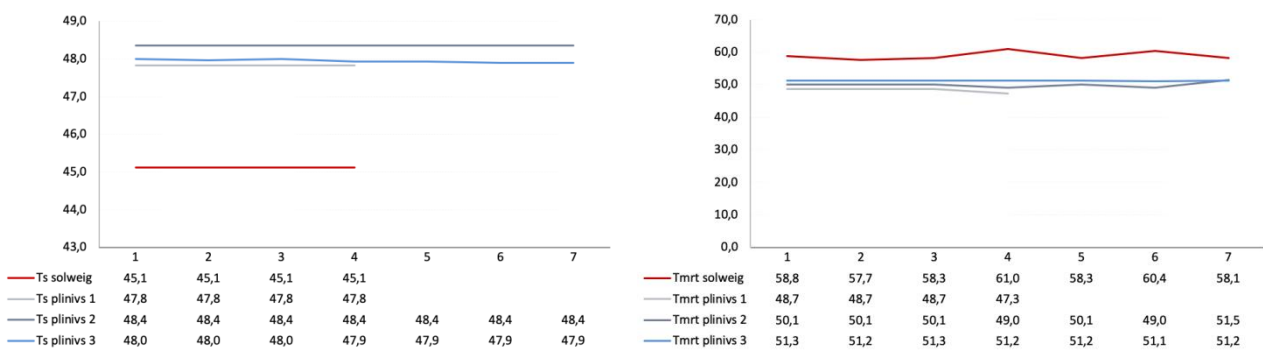
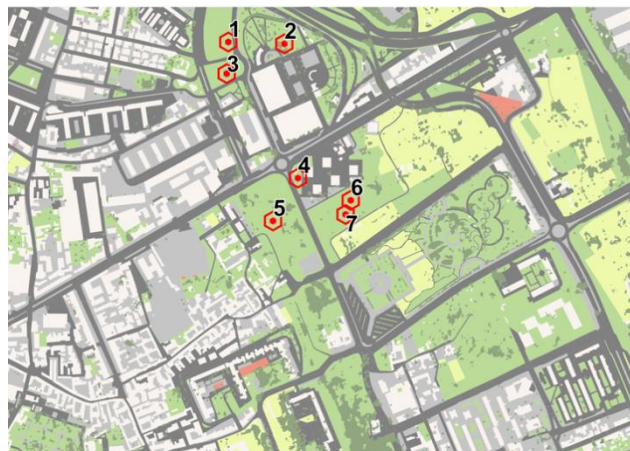


Figure 8: As in Figure 5 but showing values for the “vegetated areas” land use class.

The calibration steps above have been performed by comparing points for each land use class common to the two models. However, further calibration was needed to resolve the problem of the discrepancy of the results in shaded areas. It is important to highlight that the PLINIVS-LUPT HWLEM is designed to produce results on a mesh overlapped on the territory with a minimum size of 250 m × 250 m (500 m × 500 m in the CSIS). Here the calibration has been performed by looking at discrepancies for several individual points representing the diverse land use distributions. It can be expected that the differences could be reduced when, instead, the values within all cells of a particular land use class are averaged and used in the comparison. This was not performed owing to time constraints.

In order to further align the results from the PLINIVS-LUPT HWLEM with those from SOLWEIG, a final calibration step has been performed regarding the input data of the model related to building and vegetation shadow, which are only calculated as an average value for each cell. The results of this step, which came about through the validation of the model, are discussed in the following section.

2.1.2.2.2 Validation of results

This section illustrates the steps performed first to validate the PLINIVS-DC1 version of the Heat Wave Local Effect Model (HWLEM) against the results obtained with SOLWEIG, which is a model well regarded in the literature as a validated model, and then discusses the validation of the CSIS version of the HWLEM.

PLINIVS-DC1 Heat Wave Local Effect Model Validation

The SOLWEIG and PLINIVS-LUPT models measure outdoor thermal comfort using Tmrt as a main indicator. The difference between the two models is that the PLINIVS-LUPT HWLEM uses vector input data and produces output data on a 250 m × 250 m grid, while the SOLWEIG model uses raster data both as input and output. This allows a 3D analysis of radiation flux through the use of a DSM (Digital Surface Model) of the urban environment and to dynamically simulate local microclimate conditions based on regional climate data and urban morphology information. To allow a comparison, the results of the respective models have been homogenized by computing SOLWEIG results on the same grid 250 m × 250 m as for the PLINIVS-LUPT HWLEM (**Figure 9**).

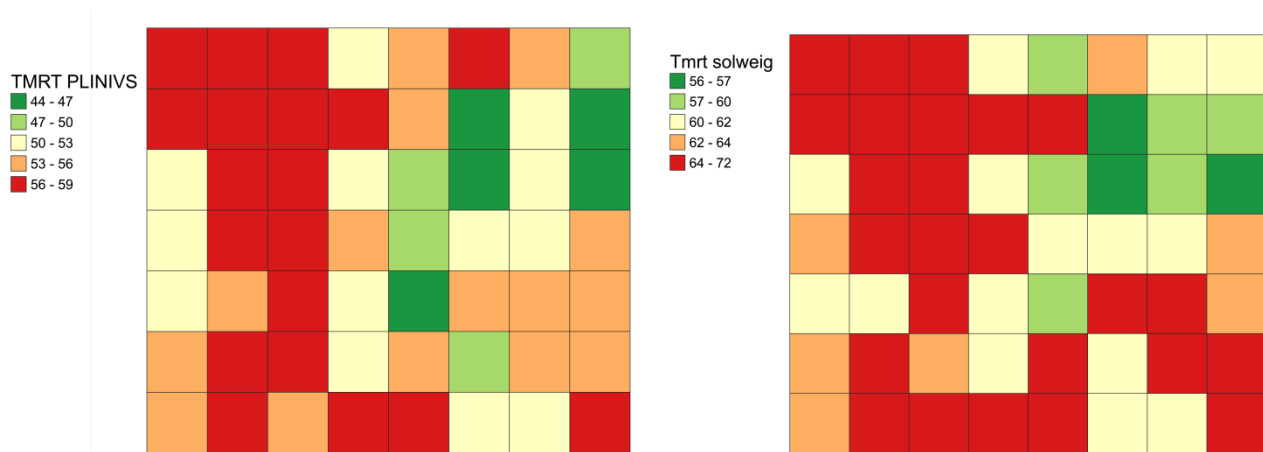


Figure 9: Comparison of Tmrt from PLINIVS-DC1 HWLEM (left) and SOLWEIG (right) before the calibration for 56 sample points.

Before the calibration, a comparison of the models shows that the values of Tmrt from the PLINIVS-LUPT HWLEM are lower than those from SOLWEIG for all sample points analysed (**Figure 10**).

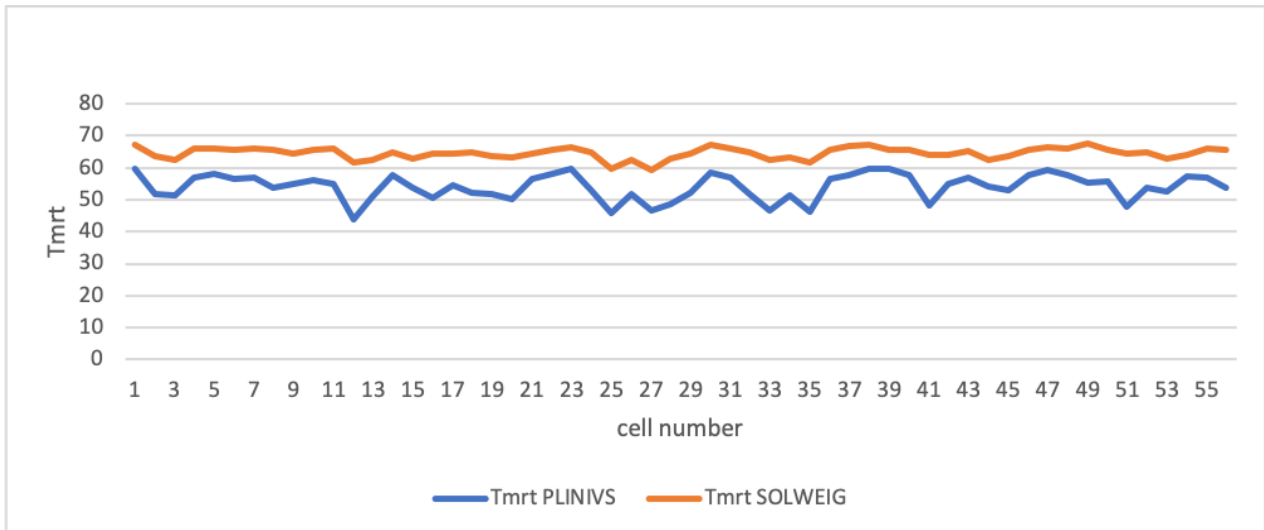


Figure 10: Comparison of Tmrt values (y-axis) from the PLINIVS-DC1 HWLEM and SOLWEIG before the calibration for each of the 56 cells (x-axis) in the analysed sample.

Implementing the calibration process described in Section 2.1.2.2.1 along with the further calibration of parameters related to the influence of buildings and trees shadow on Tmrt values within the HWLEM produced results much more aligned to those from SOLWEIG (**Figure 11** and **Figure 12**).

Through the calibration, the Tmrt results from the PLINIVS-LUPT HWLEM show about 46% of the analysed cells deviate by less than ± 2.5 °C from SOLWEIG, 25% between ± 2.5 - 5 °C and 18% between ± 5 – 7.5 °C. For the samples cells analysed, on average, the Tmrt from the PLINIVS-LUPT HWLEM is approximately 3.6 °C lower than SOLWEIG. In general, the most marked differences are found in cells that with a prevalence of trees and vegetated areas land uses. In the next developments of the model further calibration will be conducted to improve the matching of PLINIVS HWLEM results with the reference SOLWEIG model.

These results are considered satisfactory for the purpose of highlighting the areas for which the urban context conditions determines an aggravation of the heat wave hazard, and as such the PLINIVS-HWLEM is considered appropriate for its use within CLARITY. The validation and calibration process will be in any case continued in the next months adding further sample cells in the database and analysing the results to determine possible further refinement of the values adopted for the model parameters.

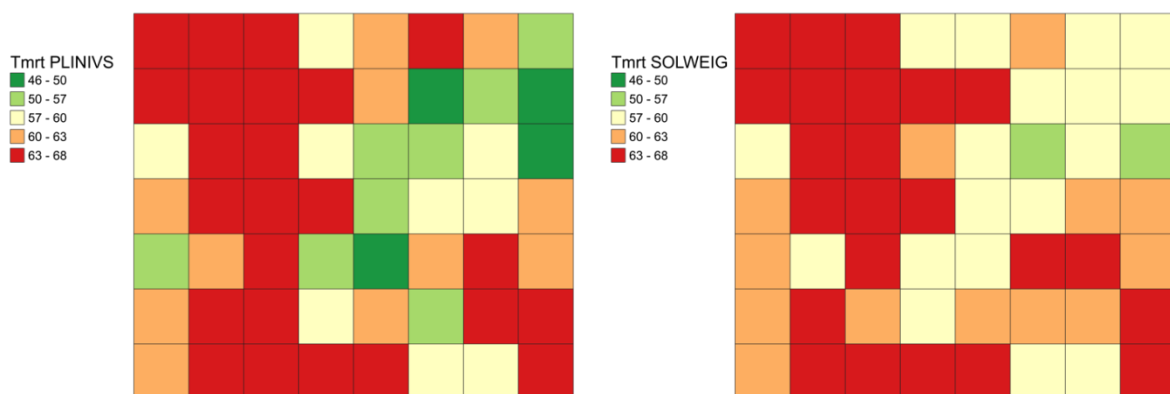


Figure 11: Comparison of Tmrt from PLINIVS-DC1 HWLEM (left) and SOLWEIG (right) after the calibration, for 56 sample cells.

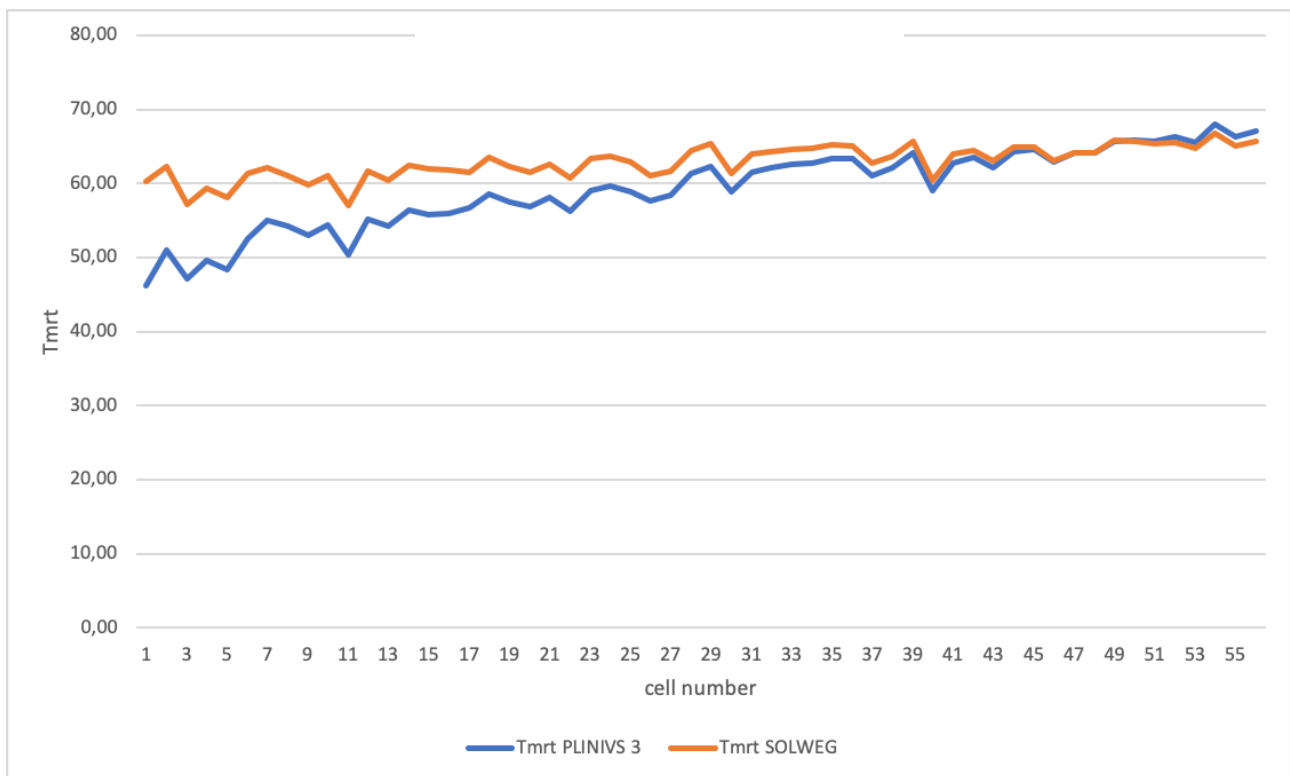


Figure 12: As in **Figure 10** but after the calibration steps have been implemented

2.1.2.2.3 CSIS Heat Wave Local Effect Model Validation – Post Calibration

The CSIS HWLEM validation can be performed using the CSIS for any given European city included in the CSIS database with the results obtained for the same urban area, both through on site measurements (provided that key input parameters such as global radiation, air temperature, air humidity, etc. are the same used for the CSIS calculation) and/or by applying a validated model able to calculate the Tmrt values depending on meteorological and land use data. In this section, the comparison between the CSIS HWLEM and PLINIVS HWLEM for the Naples area is illustrated.

The two models display the results on different grid systems, since CSIS adopts a 500 m × 500 m grid on the EPSG:3035 - ETRS89 / LAEA Europe coordinate system, while the PLINIVS HWLEM model works on a 250 m × 250 m grid drawn on the EPSG:32633 - WGS 84 / UTM zone 33N coordinate system, upon specific request of DC1 end users, motivated by the fact that this grid is used also for hazard and impact assessment of other types of natural hazards, such as earthquakes and volcanic eruptions. As shown in **Figure 13**, the two grids do not match, so a specific processing step has been implemented to compare the results.

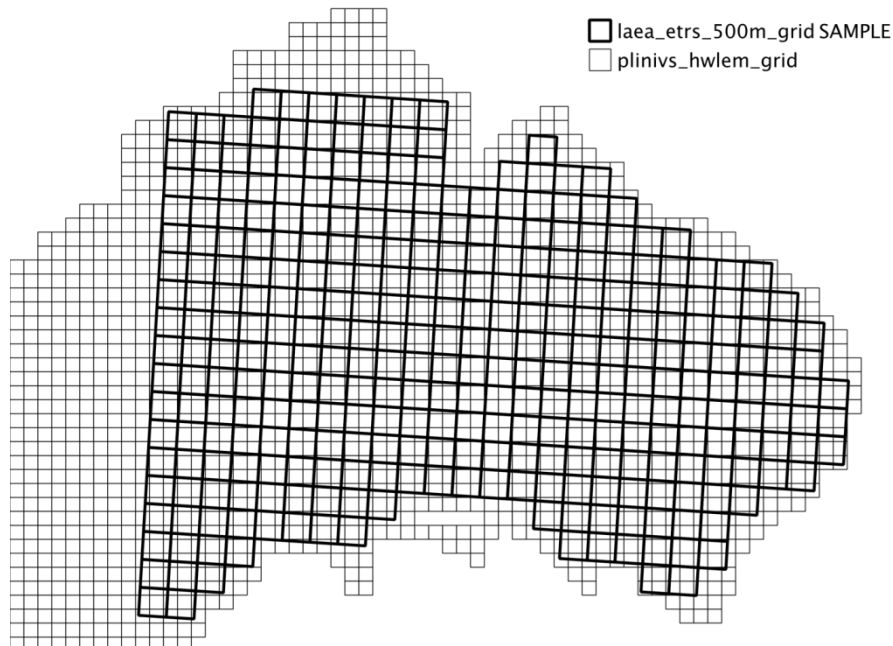


Figure 13: Overlapping of grids used by PLINIVS HWLEM (plinivs_hwlem_grid) and CSIS HWLEM (laea_etrs_500m_grid SAMPLE).

A number of reference heat wave events (i.e. combination of time period, RCP scenario and frequency) have been randomly selected on the CSIS to perform the comparison, namely:

- A. Historical, frequent;
- B. 2011-2040, RCP4.5, occasional;
- C. 2011-2040, RCP8.5, frequent;
- D. 2041-2070, RCP8.5, rare.

The results of the CSIS HWLEM for the above scenarios have been downloaded from csis.myclimateservice.eu and the data tables uploaded in a GIS environment. The data are consequently displayed on a 500 m × 500 m grid with the WGS84 UTM 33 N coordinate system.

The PLINIVS HWLEM is then applied to four scenarios with the following data characterizing a timestamp of the reference heat wave event:

- A. GG/MM 21/06; Hours 14:00; Tair 33.5 °C; eta angle 72.57°; theta angle 176.34°; Global radiation 1068.57 W/m²; Wind Speed 2.50 m/s; Rh 56%.
- B. GG/MM 21/06; Hours 14:00; Tair 39 °C; eta angle 72.57°; theta angle 176.34°; Global radiation 1068.57 W/m²; Wind Speed 2.50 m/s; Rh 56%.
- C. GG/MM 21/06; Hours 14:00; Tair 34 °C; eta angle 72.57°; theta angle 176.34°; Global radiation 1068.57 W/m²; Wind Speed 2.50 m/s; Rh 56%.
- D. GG/MM 21/06; Hours 14:00; Tair 41 °C; eta angle 72.57°; theta angle 176.34°; Global radiation 1068.57 W/m²; Wind Speed 2.50 m/s; Rh 56%.

Results are then extracted for each scenario, and displayed on the same a 500 m × 500 m grid in the WGS84 UTM 33 N coordinate system. Before comparing the results from the two models, a small number of cells that do not perfectly overlap between the two grids were excluded from the selection.

Although the CSIS HWLEM and PLINIVS HWLEM use the same logical model (i.e. the Solar LongWave Environmental Irradiance Geometry model - SOLWEIG) to estimate the heat wave hazard including spatial variations due to relevant microclimate variables, the algorithms implemented to calculate Tmrt, which are

based on pan-European open data in the case of CSIS HWLEM and on detailed land use information in the case of PLINIVS HWLEM, do show some differences that are reflected in the models' results. This directly affects the specific attribution of land-use-dependent parameters (e.g. emissivity, albedo, T_s/T_a , etc.) in each cell. Another difference is associated with CSIS HWLEM considering building shadow ratios dependent on built-up densities, while PLINIVS HWLEM calculates shadow masks depending on actual building heights (which is information currently not available for all cities in Europe through reliable open data sources). The third, and perhaps most important, difference is that for the CSIS HWLEM and PLINIVS HWLEM use different coefficients in the calculation of Incoming Short-Wave Solar Radiation fraction and Diffuse Short-Wave Solar Radiation fraction – $0.27 \times G$ for Diffuse and $0.77 \times G$ for Incoming in CSIS, while PLINIVS use $0.30 \times G$ for Diffuse and $0.70 \times G$ for Incoming (where G is the global solar radiation, fixed at noon of 21th June in both models).

When the results from the CSIS HWLEM and PLINIVS HWLEM were compared, discrepancies were found in some sample cells where the difference in land use attribution between the two models is more marked. In the sample area used for the comparison, these cells are located south of the study area, on the coastline, where the CSIS HWLEM model attributes to a large portion of these cells ($> 10\%$) the land use "water", which is currently not included in the PLINIVS HWLEM classification (**Figure 14**).

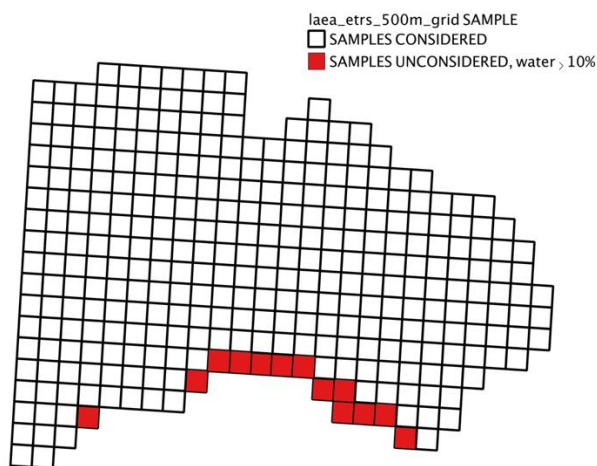


Figure 14: Sample cells excluded by the comparison for relevant discrepancy in land use attribution.

The comparison between CSIS HWLEM and PLINIVS HWLEM was performed twice, before and after the calibration of the T_s parameter (see Section 2.1.2.2.1). In the following paragraphs these two CSIS results are indicated as T_{mrt} CSIS 1 / DELTA 1 and T_{mrt} CSIS 2 / DELTA 2. "DELTA" indicates the differences in T_{mrt} resulting from the CSIS HWLEM and PLINIVS HWLEM calculations. The following figures show the results of the comparison for the 310 cells examined for the 4 Scenarios (A, B, C, D).

Tmrt PLINIVS mean	Tmrt CSIS 1 mean	Tmrt CSIS 2 mean	DELTA 1 mean	DELTA 2 mean
59.5 °C	50.0 °C	54.6 °C	-9.5 °C	-4.9 °C

Scenario A: historical, frequent (Tair 33.5 °C)

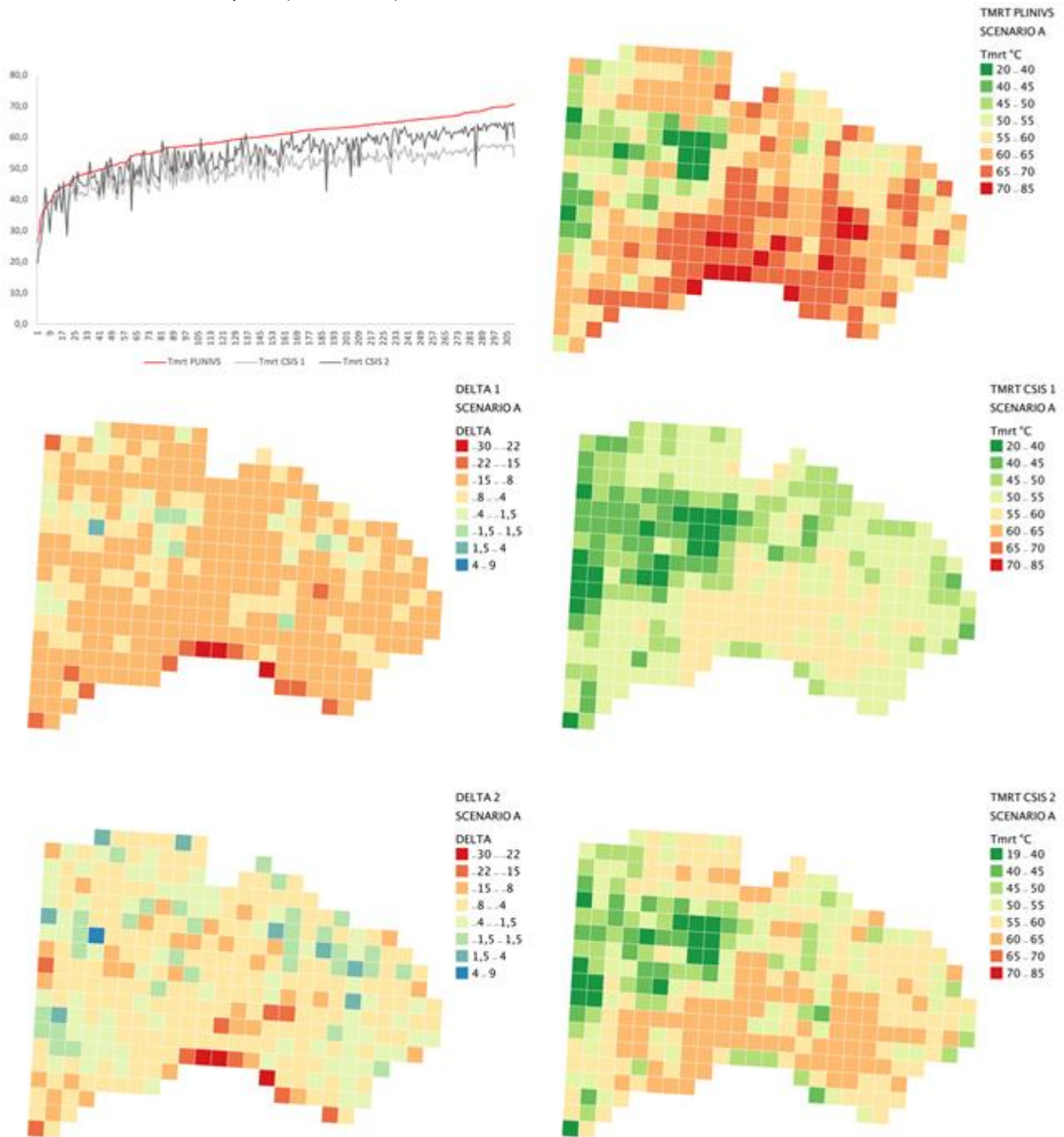


Figure 15: Comparison graph, Tmrt and Delta maps for Scenario A. The top left the graph represents the Tmrt difference in the sample cells between PLINIVS HWLEM and CSIS HWLEM. The maps on the left show the difference (Delta) in the results before (CSIS 1) and after (CSIS 2) the calibration of the Surface Temperature parameter in CSIS HWLEM. The maps on the right represent the Tmrt values from PLINIVS HWLEM, and the CSIS HWLEM before (CSIS 1) and after (CSIS 2) the calibration of the Surface Temperature parameter.

Tmrt PLINIVS mean	Tmrt CSIS 1 mean	Tmrt CSIS 2 mean	DELTA B 1 mean	DELTA B 2 mean
67.1 °C	57.6 °C	63.1 °C	-9.5 °C	-3.9 °C

Scenario B: 2011-2040, RCP4.5, occasional. (Tair 39 °C)

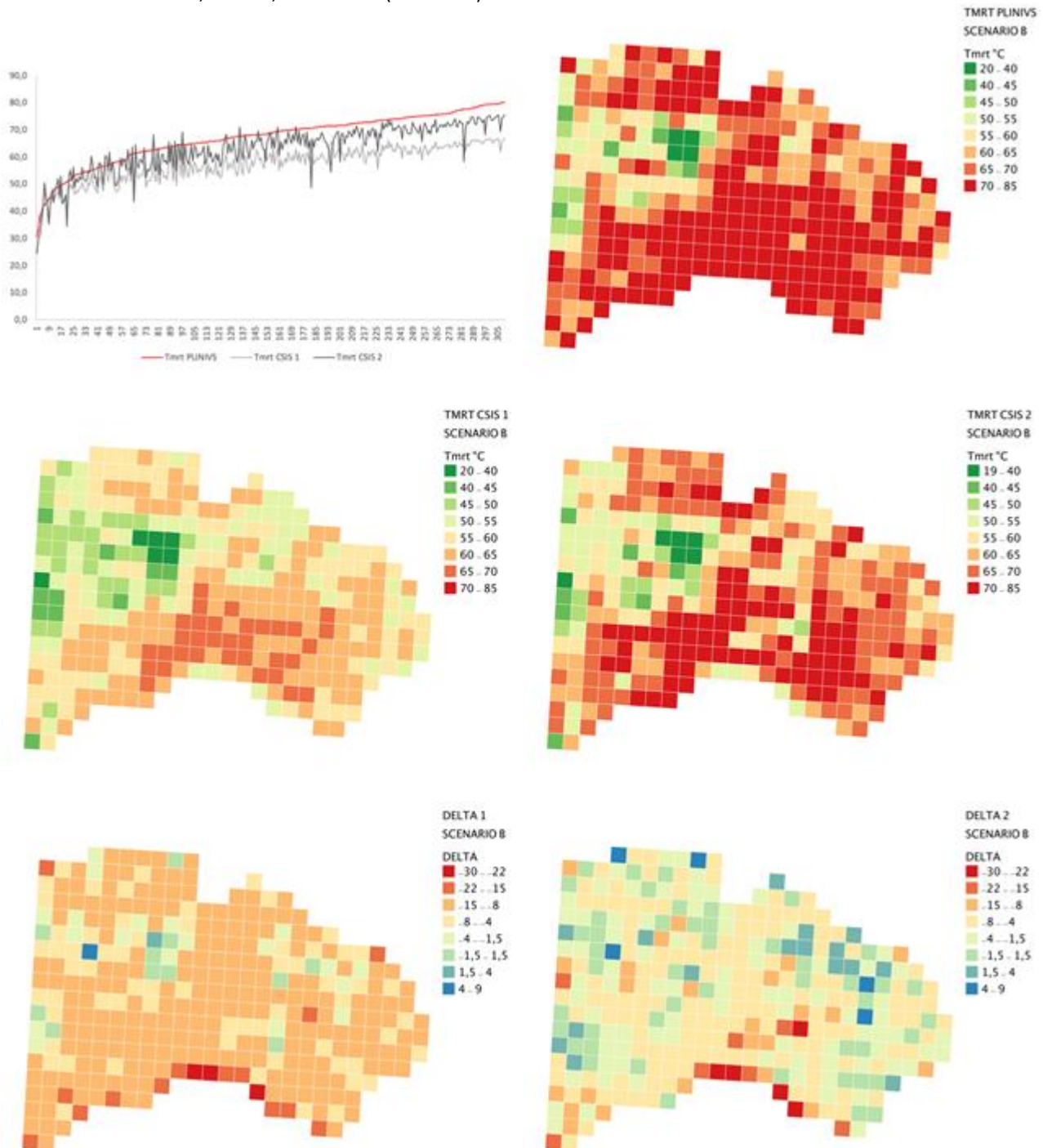


Figure 16: As in Figure 15 showing the results from Scenario B.

Tmrt PLINIVS mean	Tmrt CSIS 1 mean	Tmrt CSIS 2 mean	DELTA C 1 mean	DELTA C 2 mean
60.2 °C	50.7 °C	55.4 °C	-9.5 °C	-4.8 °C

Scenario C: 2011-2040, RCP8.5, frequent. (Tair 34 °C)

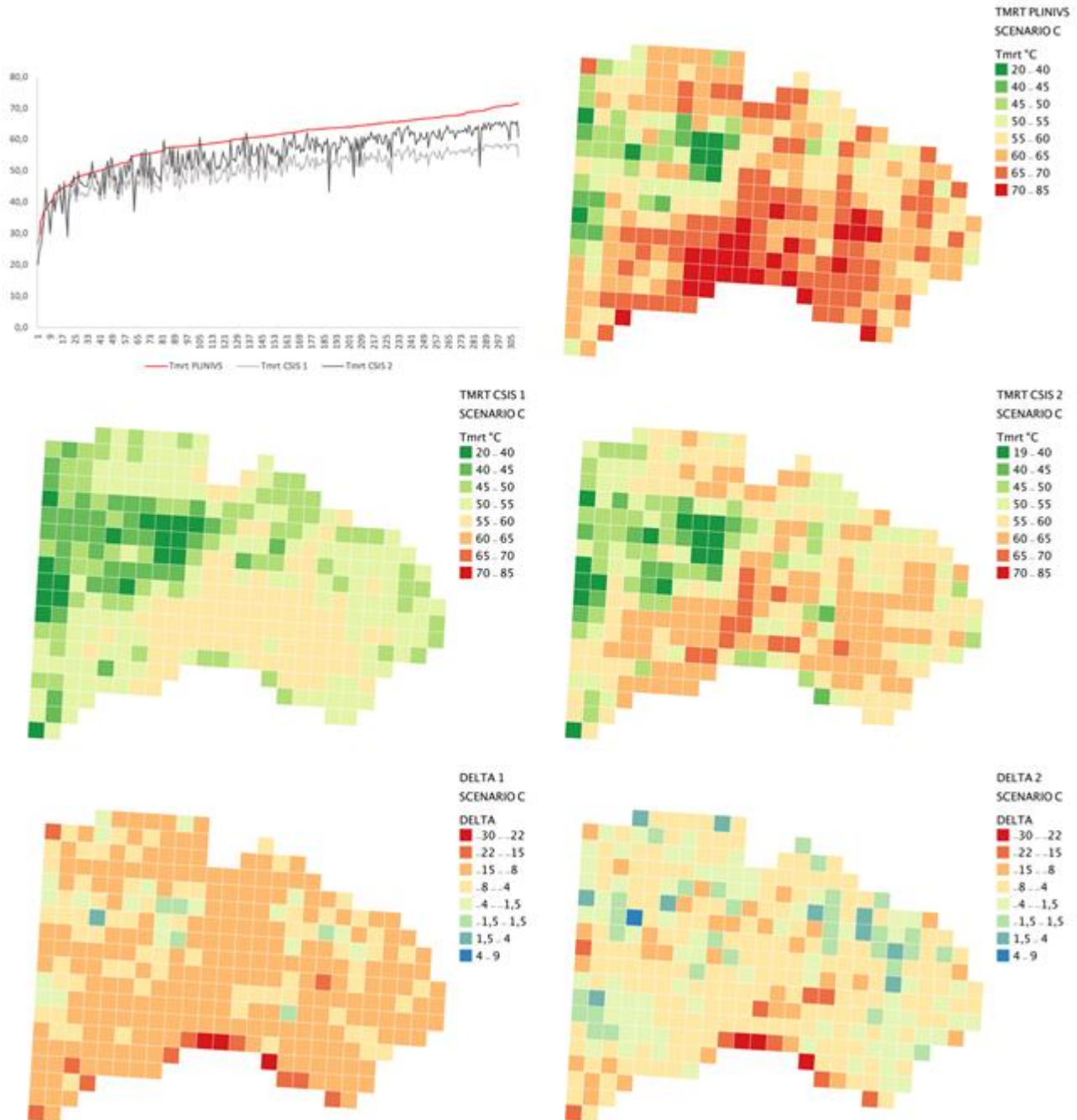


Figure 17: As in **Figure 15** showing the results from Scenario C.

Tmrt PLINIVS mean	Tmrt CSIS 1 mean	Tmrt CSIS 2 mean	DELTA D 1 mean	DELTA D 2 mean
70.3 °C	60.6 °C	66.7 °C	-9.6 °C	-3.6 °C

Scenario D: 2041-2070, RCP8.5, rare. (Tair 41 °C)

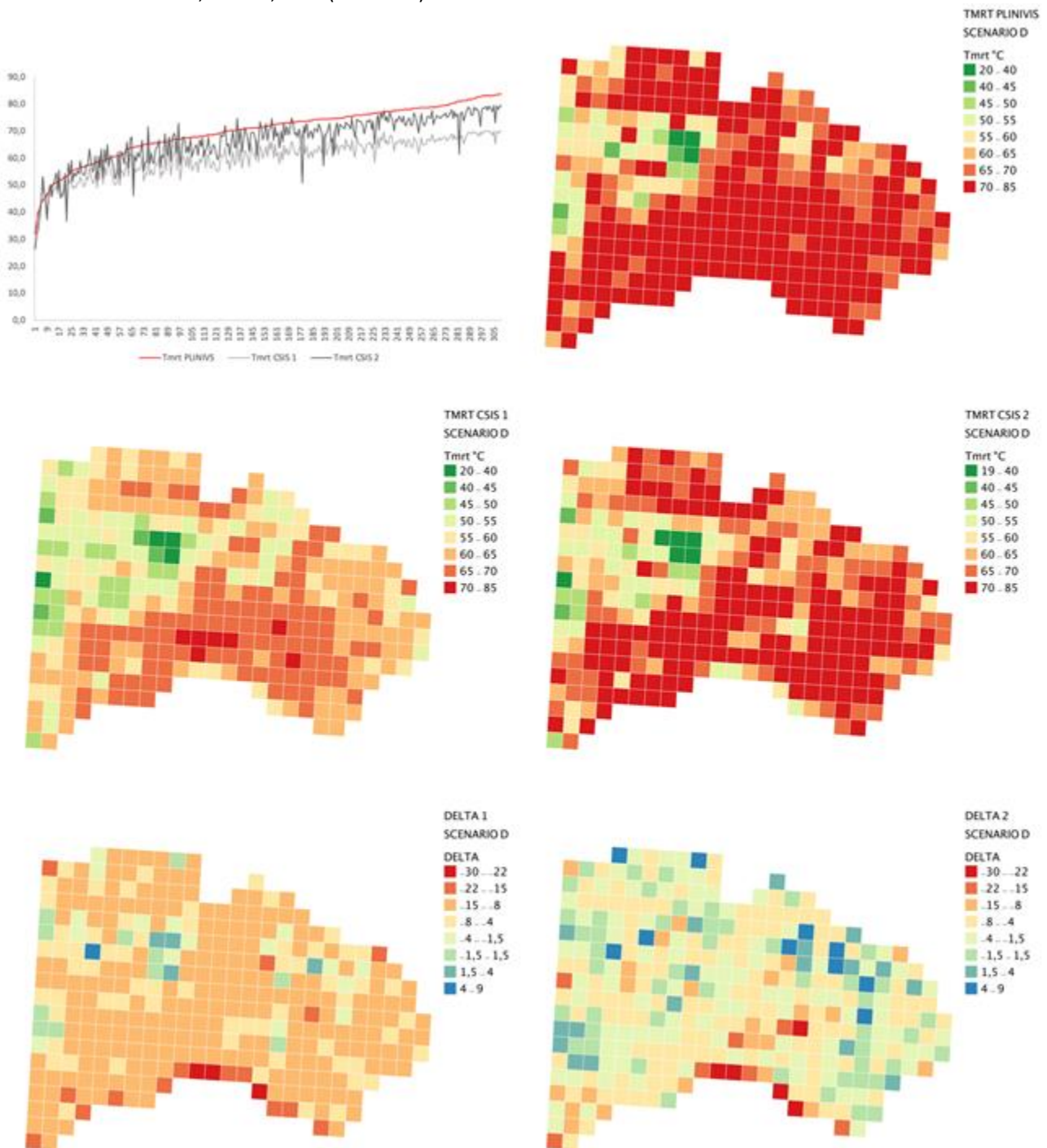


Figure 18: As in Figure 14 showing the results from Scenario D.

The results obtained following the calibration of Ts parameter in the CSIS HWLEM are considered acceptable, with a mean underestimation of the Tmrt always below 5 °C for all scenarios. As explained above, this is mainly due to a different value of the Incoming/Diffuse Short-Wave Solar Radiation fraction. In fact, when performing the comparison applying the same Diffuse and Incoming short-wave fraction solar radiation values, the Delta (mean) is 0.2 °C (**Figure 19**).

Tmrt PLINIVS 2	Tmrt CSIS 2	DELTA 3
62.9 °C	63.1 °C	0.2 °C

Scenario: 2011-2040, RCP4.5, occasional. (Tair 39 °C)

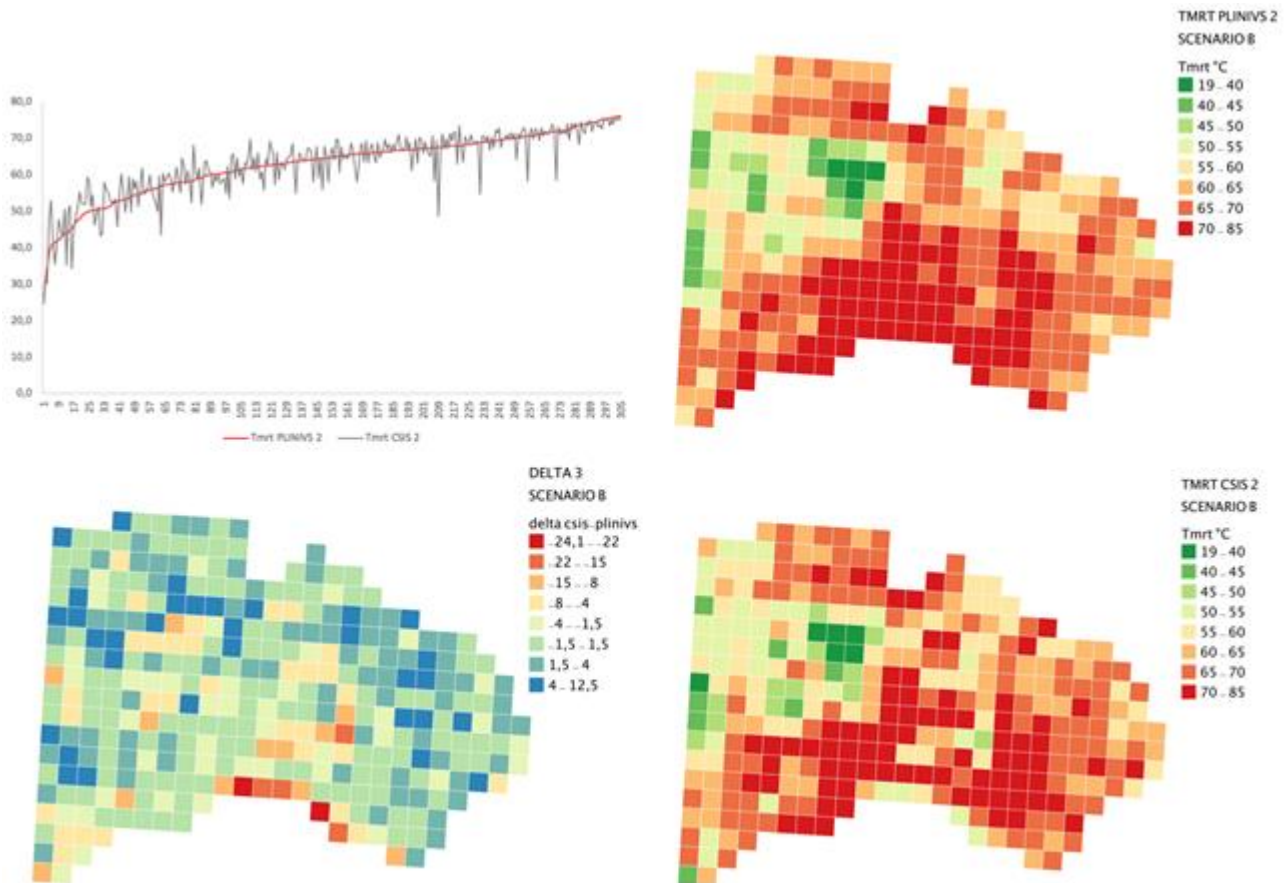


Figure 19: Comparison graph, Tmrt and Delta maps for Scenario B, with homogenization of Diffuse and Incoming fraction short-wave solar radiation among CSIS HWLEM and PLINIVS HWLEM. On the left the graph represents the Tmrt difference in the sample cells between PLINIVS HWLEM and CSIS HWLEM. The maps on the left show the difference (Delta) in the results before (CSIS 1) and after (CSIS 2) the calibration of the Surface Temperature parameter in CSIS HWLEM. The maps on the right represent the Tmrt values from PLINIVS HWLEM and the CSIS HWLEM before (CSIS 1) and after (CSIS 2) the calibration of the Surface Temperature parameter.

Further calibration of CSIS HWLEM parameters should allow a better alignment with PLINIVS HWLEM results (which have been validated against SOLWEIG in the native UMEP software environment). A major achievement, considering the above mentioned difference in the algorithms implemented for the two models within CLARITY, is that the difference in the results is always constant. This consistency is demonstrated by the standard deviation between the deltas of each cell in the various scenarios, which is close to zero both for the first (**Table 5**) and the second (**Table 6**) iteration.

Table 5: Summary of deltas for the four scenarios before the calibration of Ts parameter in CSIS HWLEM.

DELTA A 1 mean	DELTA B 1 mean	DELTA C 1 mean	DELTA D 1 mean	STANDARD DEVIATION mean
-9.4 °C	-9.5 °C	-9.4 °C	-9.6 °C	0.4 °C

Table 6: Summary of deltas for the four scenarios after the calibration of Ts parameter in CSIS HWLEM.

DELTA A 2 mean	DELTA B 2 mean	DELTA C 2 mean	DELTA D 2 mean	STANDARD DEVIATION mean
-4.9 °C	-3.9 °C	-4.8 °C	-3.6 °C	0.7 °C

A spatial analysis of the results was performed to better understand the differences emerging from the models' results. The images below show the land uses used by the CSIS HWLEM and PLINIVS HWLEM, aligned on the same 500 m × 500 m grid used by the CSIS HWLEM. The number displayed in the cell is value of delta among the models for Scenario B. This analysis shows that more marked deltas correspond to substantial differences in land use with further calibration still continuing. However, the results obtained so far already validate the modelling approach implemented in the CSIS HWLEM against the SOLWEIG model approach.

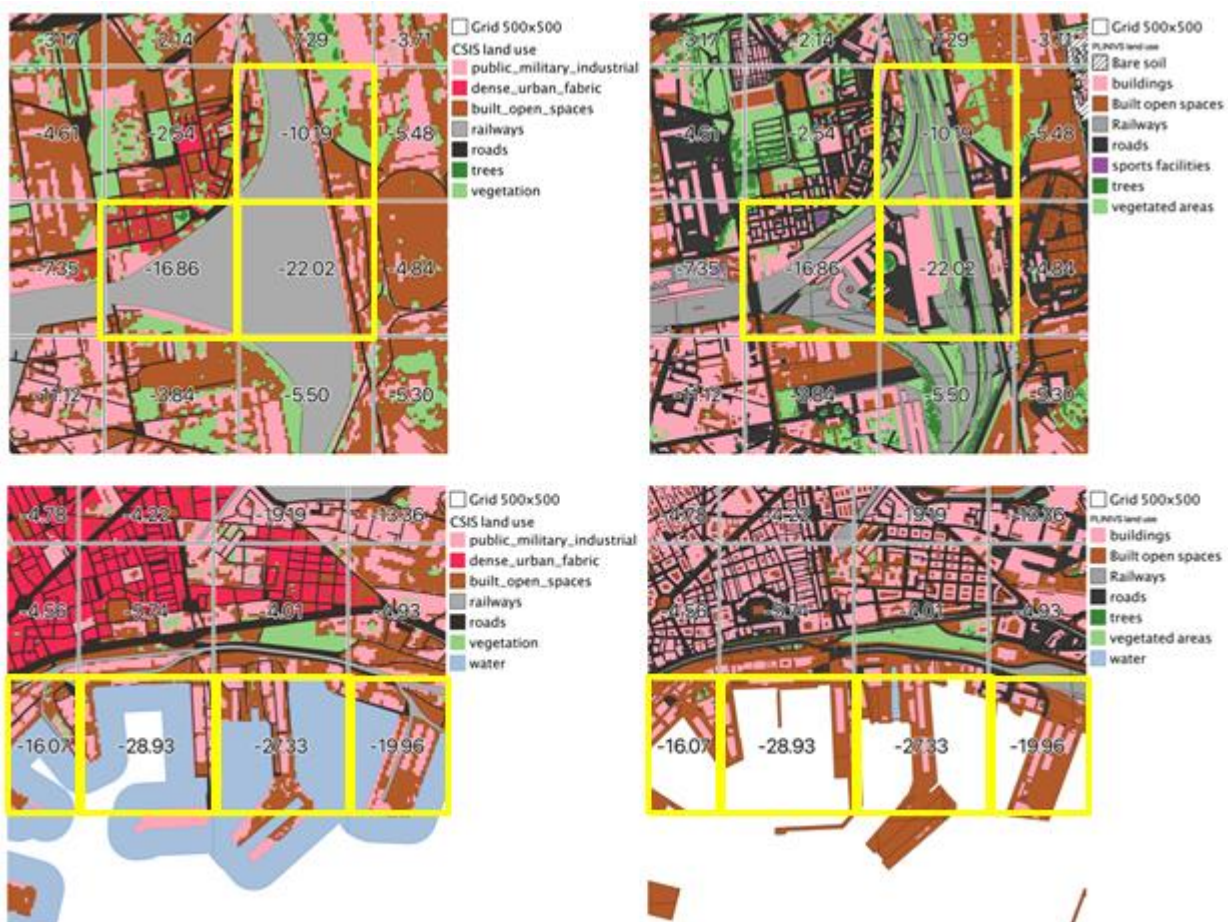


Figure 20: Land use comparison of sample cells in Naples area (left, CSIS HWLEM; right, PLINIVS HWLEM). The two images above include a railway track area which is more precisely represented by PLINIVS HWLEM land use. The two images below include a portion of water which is not currently included the PLINIVS HWLEM land use.

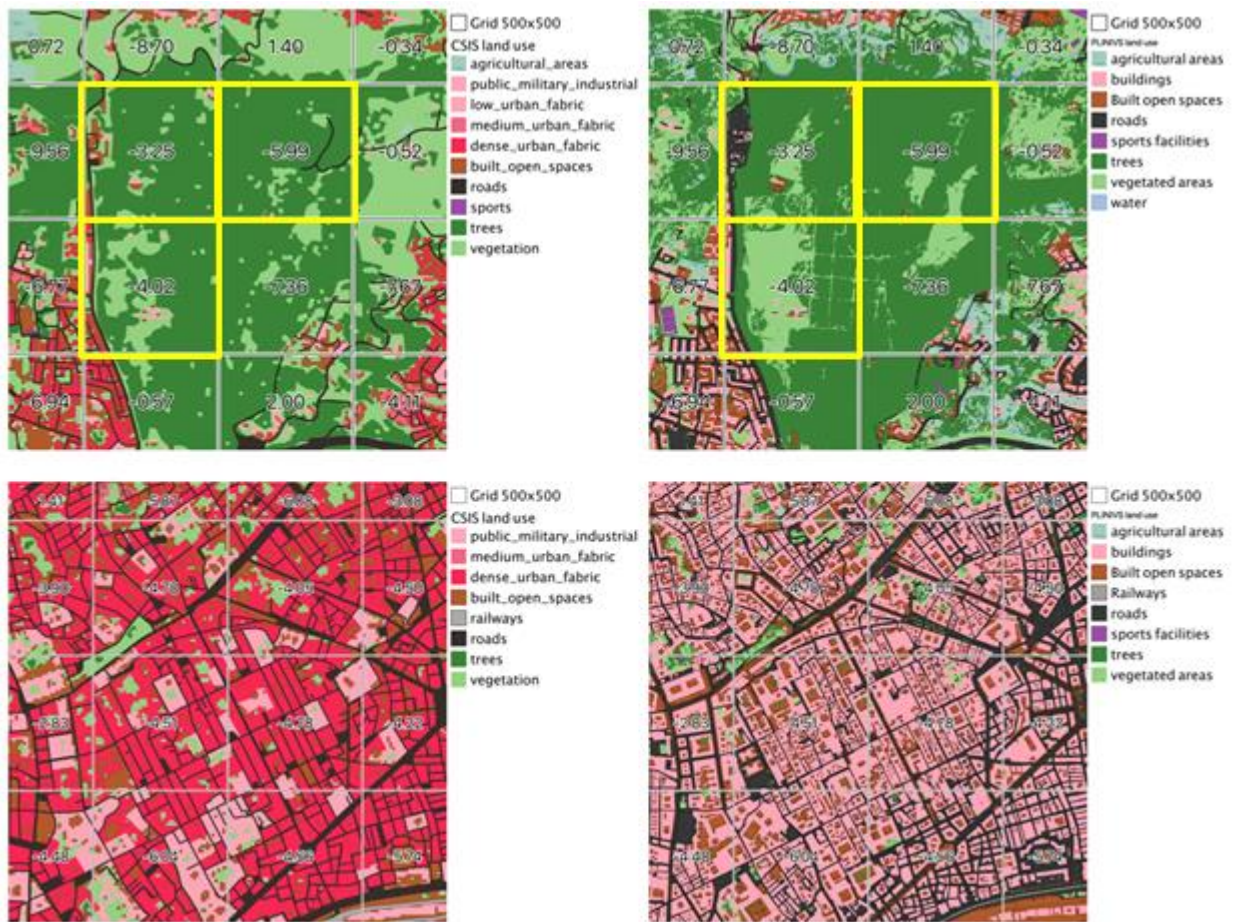


Figure 21: Land use comparison of sample cells in Naples area (left, CSIS HWLEM; right, PLINIVS HWLEM). Land use matching aligns the observed delta around the mean value of 4°C.

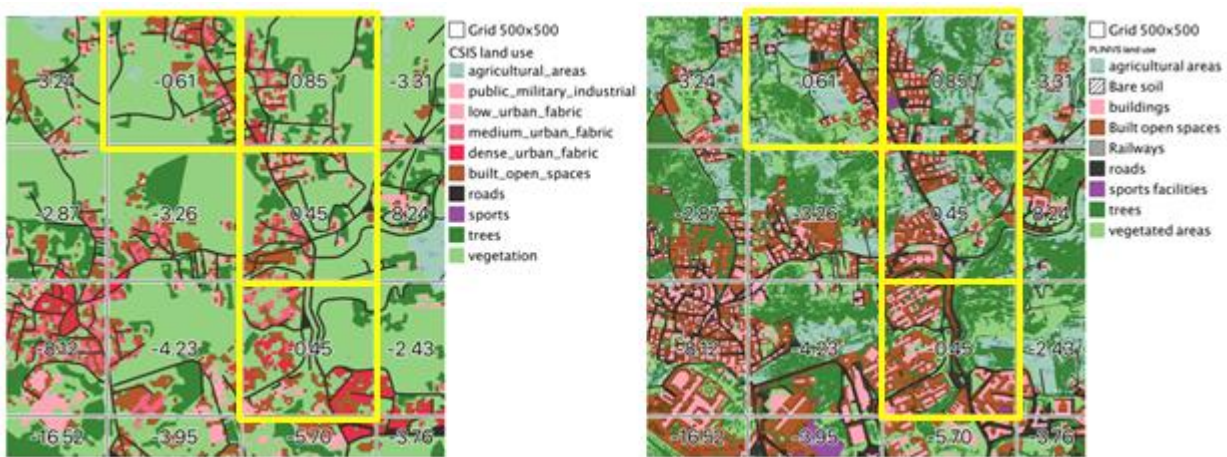


Figure 22: Land use comparison of sample cells in Naples area (left, CSIS HWLEM; right, PLINIVS HWLEM). Comparison of cells where the discrepancy in land use concerns the “trees” layers result in almost identical Tmrt values, meaning that the observed underestimation obtained with CSIS HWLEM is reduced here. The reason is that tree shadow is significantly impacting the Tmrt calculation in the SOLWEIG model, and the reduced presence of trees in the CSIS land use increase the value aligning it with PLINIVS HWLEM results.

2.1.2.3 Urban pluvial flooding local effect at the advanced screening level

In the context of the CLARITY CSIS, the flooding hazard is considered in relation to the effect of intense and/or prolonged rainfall which generates a runoff volume greater than the capacity of existing drainage system. This phenomenon predominately occurs in urban areas, inducing extensive damages. Although the general definition of urban pluvial flooding is pretty clear, there is still an open debate regarding its particular characteristics and how it relates to other types of flooding, such as surface water, minor watercourses and sewer flooding. Currently, it can be defined only referring to direct runoff flow before it enters a natural or man-made drainage system or water course [9], [10] and [11], or as proposed by [12] and [13] by considering, in addition to direct runoff, floodwater coming from surcharged sewers and/or urban minor watercourses, the flow capacity of which has been exceeded as a result of heavy rainfall. Although the second definition is more accurate, it is much too broad and complex to be implemented at the European level and, for that reason, in this context, we only refer to the direct runoff flow, as a proxy for the ability of urban areas to absorb and/or divert rainwater during extreme precipitation events.

Runoff flow modelling aims to evaluate which part of the total rainfall amount is converted to flow over the urban surface. Therefore, soil type and land use/land cover acquire an essential role in all the possible models that could be applied.

In order to reduce the operational time and to exploit the data provided at a European level, basins and streams provided by Copernicus and USGS-HydroSHEDS have been applied. They were used as input for the rational method developed in United States by Emil Kuichling in 1889. It was adopted since it is a simplified approach able to model the run-off in both urban and rural watersheds [14] [15]

$$Q = \frac{C \times F_t \times A_b \times h}{\frac{4 \times \sqrt{A_b} + 1.5 \times L \times 60}{0.8 \times \sqrt{z}}}$$

where, Q is the peak discharge, A_b is the area of the basin, L is the length of the flow accumulation streams, h is rain intensity, z is the difference between the maximum and the minimum altitude of the flow direction streams, C is the runoff coefficient and F_t is a building density coefficient. This latter parameter has been added to the original equation to describe the potential increase in water depth and velocity that occurs during the “channelling” effect occurring in urban areas in presence of narrow streets surrounded by buildings or other “hard” barriers. The concentration time was estimated through the equation proposed by Giandotti in [16]. The runoff coefficient, C, is a key parameter for the rational method since it is able to convert the rainfall amount into runoff. Although it can be estimated through various methods, it has been set according to the values reported, for each land use class, in the German DIN 4095.

Given the complexity of running an advanced screening level study based on such a simplified model at a pan-European level, tests which were performed showed the method to be computationally intensive. Accordingly, an alternative approach has been proposed for the CSIS flood local effect model (FLEM), which produces as output a preliminary proxy of the probability for urban areas to get flooded in case of heavy rain. This alternative model is based on the following data, to be collected and classified for each European city present in the CSIS.

- Runoff coefficient for each land use type
- Urban watersheds
- Digital Elevation Model
- Digital Surface Model
- Flow accumulation streams for each watershed
- Emergency calls for flooding (optional)

The procedure aims at identifying four main parameters for each cell of the analysis grid that contribute to the flooding probability due to land use, urban orography and hydrology:

1. Runoff coefficient
2. Relative elevation in the watershed

3. Presence of flow accumulation streams
4. Sewage system efficiency (optional)

The runoff value is attributed to each land use surface, and an average is calculated for each cell of the analysis grid, assigning a value (1 to 5) based on the level of imperviousness of the cell, where 1 corresponds to an area with a high infiltration and 5 to an area with a low local drainage capacity. **Figure 23** shows an example of this classification performed in the case of Naples, on a 250×250 m² grid (left, runoff coefficient and right, classification results).

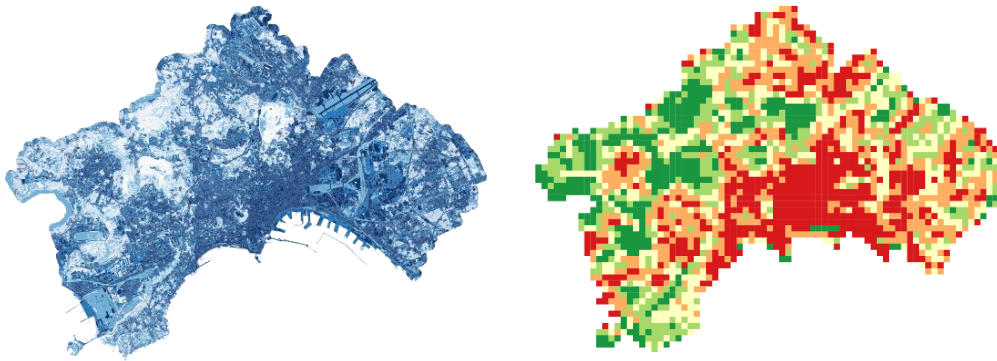


Figure 23: Naples area showing (left) runoff coefficient, and (right) its classification of imperviousness on a scale (1-5).

The second relevant factor is represented by the relative elevation of the cell within the watershed, with the assumption that downstream cells have a higher probability of flooding compared to those upstream. Accordingly, the average elevation of the terrain in relation to the watershed to which the cell belongs has to be assigned. The elevation value of the minimum point of the corresponding watershed is then subtracted from this value. The GIS procedure adopted to implement this step for each 250×250 m² grid cell can be summarized as follows:

1. Perform a zonal statistic from DEM on the grid to identify the mean value.
2. Assign a watershed to each cell of the grid.
3. Calculate the minimum point of each watershed.
4. Subtract the minimum point from the mean elevation for each cell belonging to each watershed.
5. Classify cells by assigning a value from 1 to 5.

Figure 24 shows an example of this classification performed on a 250×250 m² grid for the Naples area.

A measure of the flow accumulation by streams is obtained by assigning to each cell of the grid the number of streams present. **Figure 25** shows an example of this classification performed on a 250×250 m² grid for the Naples area.



Figure 24: Naples area showing (left) the elevation from the DEM, (centre) urban watersheds, and (right) classification results.

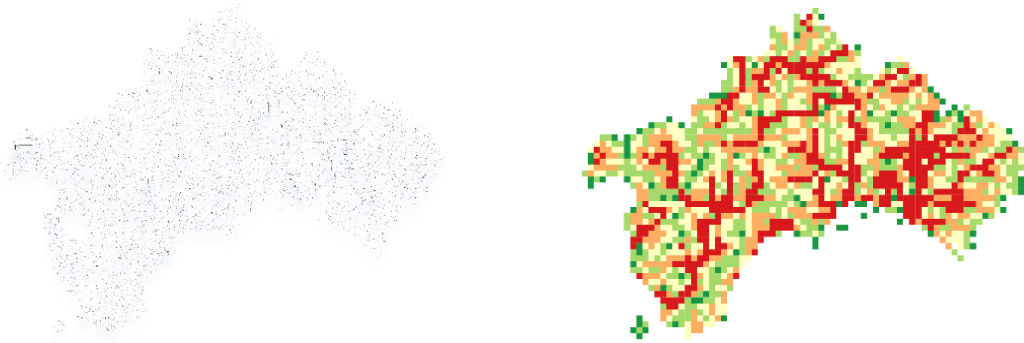


Figure 25: Naples area showing (left) flow accumulation streams, and (right) classification results.

The sewage system efficiency is a crucial condition determining the urban flooding in the case of heavy rain. Several studies (e.g. H2020 RESCCUE project) have shown that, not only is the capacity of the sewer itself important, but also its maintenance condition of manholes in urban areas. This information is almost impossible to acquire without performing local surveys for data collection and detailed flood hazard 2D-analyses. A possible approach to include this parameter, although in an approximate way, has been experimented for the Naples area, showing good results when included with the other three parameters considered above. This consists of the geolocalization of emergency calls received during and/or following a recorded extreme precipitation event. As this information is not available at a pan-European level, this step is considered optional in the CSIS calculation with the EU data package. However, the inclusion of this dataset within the local data packages is recommended if the proxy-based flood model proposed here is to be performed.

The implementation of this step involves counting the number of emergency calls recorded for each cell of the analysis grid. **Figure 26** show an example of this classification performed on a 250×250 m² for the Naples area.

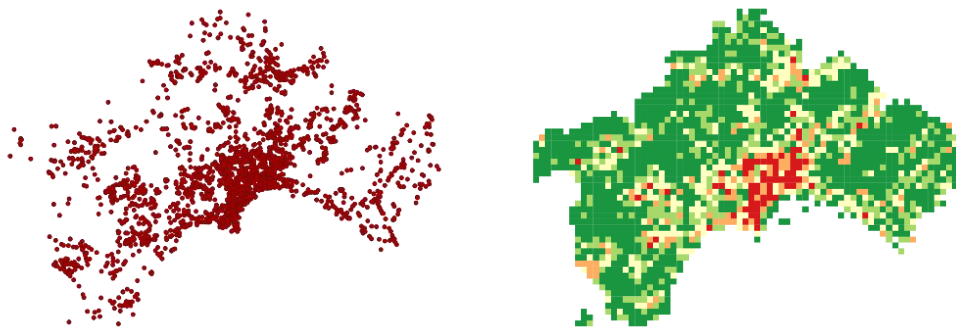


Figure 26: Naples area showing (left) number of emergency calls recorded, and (right) classification results.

Table 7 shows the classification scheme adopted for each parameter in the Naples data package. The data for each parameter is then normalized by categorizing each parameter with a 6-class scale (0-5), where 0 represents the lowest probability of flooding in the case of extreme precipitation events. Once the data are normalized, the local effect flood map is obtained by accumulating the values of each single parameter:

$$\text{Total} = [(p_1 \times 0.25) + (p_2 \times 0.25) + (p_3 \times 0.25) + (p_4 \times 0.25)] ,$$

and thus obtain values in the range 0 to 5 which are classified according to the ranges shown in **Table 8**.

Table 7: Classification scheme for each of the four parameters in the Naples data package.

class	runoff coefficient		relative elevation		flow accumulation streams		emergency calls	
	from	to	from	to	from	to	from	to
0	0	0,05		> 441	0	0	0	0
1	0,06	0,229	440	143,5	1	8200600	1	1
2	0,23	0,396	143,4	73,7	8200601	23866704	2	3
3	0,397	0,564	73,6	27,8	23866705	55028923	4	6
4	0,565	0,732	27,7	11,8	55028924	168006422	7	12
5	0,733	1	11,7	0	168006423	9598931471	13	24

Table 8: Probability of flooding classification level.

Range	Description of hazard level
0.00 – 1.49	Very low
1.50 – 2.24	Low
2.25 – 3.49	Medium
3.50 – 5.00	High

Figure 27 shows an example of the final result obtained for the Naples area. The map has been validated by the Municipality of Naples, following a comparative analysis of urban areas included as having a high risk of flooding in the official plan of the local river basin authority, available at the following link <http://www.difesa.suolo.regione.campania.it/content/view/130/110/>.

For the CSIS advanced screening at the European-scale, the classification scheme as listed in **Table 7** needs to be adjusted using relative thresholds, and the following data sources will be used for the analysis:

- EU-DEM (Copernicus)
- EU basins
- EU streams

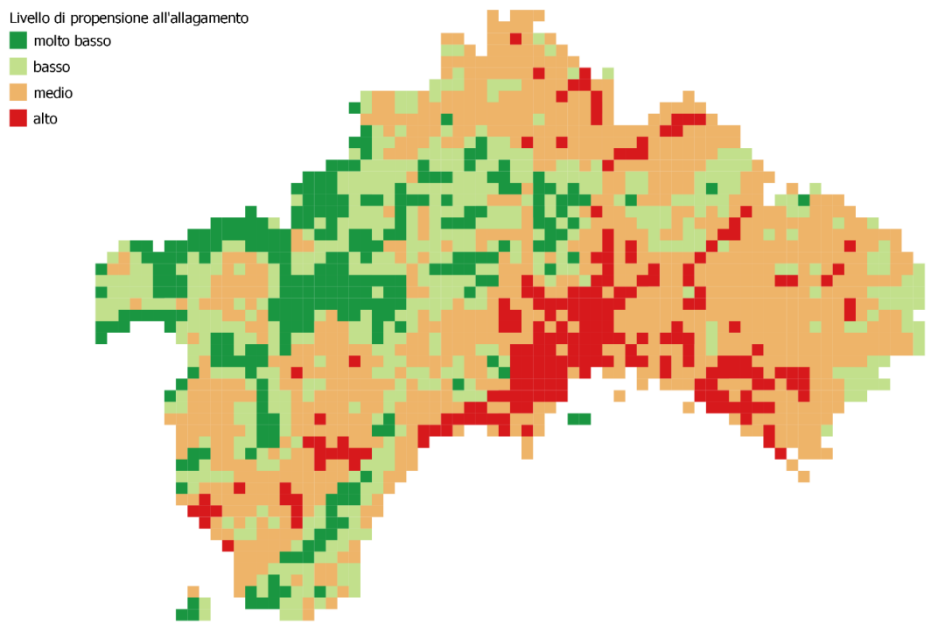


Figure 27: Classification of the Naples area according to hazard level (dark green = very low; light green = low, orange = medium, red = high).

2.2 Evaluation of Exposure

Once the hazard has been established and the local effect characterised, the elements at risk (e.g. population, buildings, infrastructure, etc.) and, consequently, their exposure to the climatic risks can be evaluated. As this was already described in Section 2.4 of D3.2, it will not be repeated here. However, aspects of the exposure which are relevant for the following steps of the EU-GL will be described in those sections.

2.3 Vulnerability Analysis

The vulnerability is defined as the probability that an element at risk, belonging a vulnerability class, experiences a level of damage, according a predefined damage scale, as a response to a hazard event of given intensity. It is expressed in terms of a vulnerability matrix that indicates the percentage of a certain type of element at risk belongs to each vulnerability class for the investigated local effect in the considered area. Table 9 shows an example of such a matrix for a generic element at risk category.

Table 9: Example of a vulnerability matrix for a specific vulnerability class of a given element at risk under effect of a specific hazard.

VULNERABILITY CLASS i				
Level of Damage	Hazard Intensity			
	HI 1	HI 2	HI 3	...
Low	5 %	20 %	50 %	...
Medium	10 %	30 %	70 %	...
High	20 %	50 %	80 %	...

The vulnerability classes for the relevant elements at risk have been defined both for heat wave and flooding, defining also the different levels of damage for those elements. For instance, population as a risk element in the case of heat waves, and was initially distinguished by age in three classes (under 14, 15 – 64 and over 65), spatially distributed on each cell of the grid and, then, ordered according to their ability to be damaged by the hazard from A to C (A: over 65; B: under 14; C: 15 – 64). **Table 10** shows an example of a damage classification of people’s health for heat waves. More information can be found in Section 2.5 of D3.2.

Table 10: People damage classification.

Level of damage	Description
D0	No damage
D1	Fatigue, discomfort
D2	Heat cramps, heat exhaustion
D3	Heat cramps, heatstroke
D4	Heatstroke, sunstroke
D5	Death

The possibility of using the age-class related vulnerability curves depends strictly on the availability of exposure data (i.e. the geolocalization of population in the cities according to age groups). At the moment this information is not present in any EU database, so it has been excluded from the CSIS European data package. Accordingly, the calculation of impact at the advanced screening level is performed with a single vulnerability class for all population groups. However, the use of age classes could be implemented at the expert level, provided that the corresponding local data package includes exposure data related to the different age groups.

Although it was not possible to generate vulnerability curves for the different population age groups, it was possible to produce two versions of this vulnerability curve to reflect the population of Southern Europe and for central and Northern Europe.

A similar classification has been carried out also for the elements at risk in the case of flooding. In that context, two typologies of damages, namely direct and indirect costs, have been taken into account. The former is related to the restoration cost, while the latter is due to the loss of production. Five levels of damages have been identified for both typologies.

Figure 28 shows the vulnerability curves in the case of pluvial flooding for the category Direct Damage (DD) on the basis of the hazard input. Indeed, for N defined classes of vulnerability, N vulnerability functions exist, each with M damage probability functions for M classes of damage. **Table 11** shows the vulnerability matrix for buildings in the case of flooding, where buildings and roads are classified according to their geographically location: Historical centre (HC), Suburb (S), Countryside (C). A deeper focus on flood-related vulnerability curves is included in Section 2.4.1.

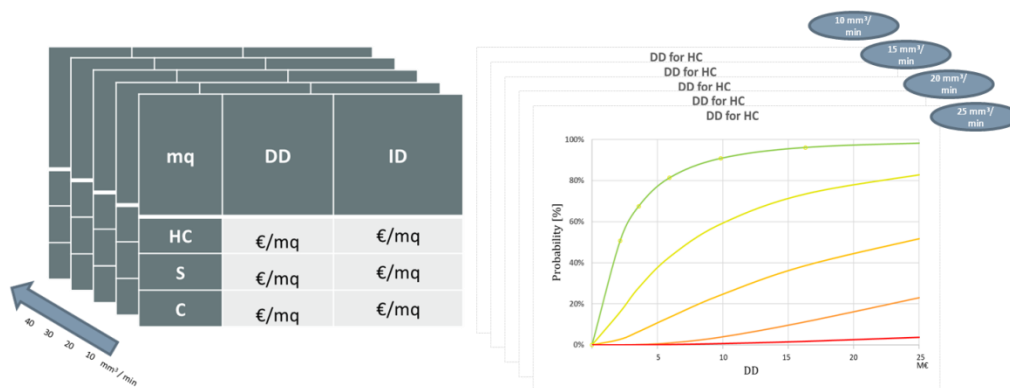


Figure 28: Vulnerability matrices according to flooding value and vulnerability curves for the Direct damage (DD) class.

Table 11: Vulnerability classes example definition: $f(D,Q)$. HC: Historical Centre; S: Suburb, C: Countryside. DD: Direct Damage, ID: Indirect Damage.

mq	DD	ID
HC	€	€
S	€	€
C	€	€

In the case of road transport infrastructures it has not been possible to define vulnerability curves due to the lack of sufficient data and reliable statistics. Therefore, the vulnerability assessment has to be done by a technician with a deep knowledge of the different elements of the road. This approach has been already been successfully implemented in the study "Sections of the state land transport network potentially more exposed due to climate variability and change"; CEDEX June 2018. This document provides a guide for the technician to assess the vulnerability of the elements at risk. It is explained in more detail in Section 3.4 DC4.

2.4 Impact Scenario Analysis

When one or more reference events are selected in a "deterministic" way, the corresponding "impact scenario analyses" shall be carried out by applying numerical impact models, suitable to provide detailed damage estimation on selected elements at risk as a result of specific events. Thus, the impact scenario analysis is intended to simulate the expected impacts of a specific hazard, in terms of intensity, location, etc., derived from the application of an impact model able to correlate hazard, exposure and vulnerability characteristics to produce a detailed quantification of damage on elements at risk considered. As this was described in detail in Section 2.6 of D3.2, it will not be repeated here. Instead, aspects of this will be repeated, where relevant, within the following sections.

In the case of road transport infrastructures, a robust and reliable model that correlates hazard, exposure and vulnerability could unfortunately not be identified. Therefore, for the road section analysis carried out under DC4, the risk assessment has been done on the basis of an "informed decision", which means that an expert, who knows the road section from the point of view of exposure and vulnerability and, with the help of the hazard information produced under CSIS, is able to assess the impact and the risk.

2.4.1 Economic Impact of Heat Waves

The main element at risk (direct or indirect) to heat waves is people. The methods adopted in CLARITY to assess the economic impact of heat waves on the health of people are outlined here. Considerations are to be made on the loss of productivity due to the failing health of people and on the impact on energy consumption from the high temperatures.

Heat waves can cause several health problems/diseases. An increase in body temperature alone does not define the type of heat-related problem but does so in combination with the associated symptoms and signs. This usually comes about as a result of conditions of:

- high ambient temperature,
- high relative humidity,
- physical exertion.

Because heat-related disease is largely avoidable, the most crucial point of intervention concerns the use of appropriate prevention strategies by susceptible individuals. Knowledge of effective prevention and first-aid treatment, besides an awareness of potential side-effects of prescription drugs during hot weather, is crucial for physicians and pharmacists. Body heat loss is controlled by peripheral centres in the skin and organs and the central nervous system via the hypothalamus, with a greater cooling response to temperature elevation via central sensors. A temperature gradient exists between the body core and skin, which promotes heat dissipation when the core is higher than the surface. When the core temperature increases during exercise and the skin temperature also rises as a result of the environment or internal heat production, heat dissipation is reduced. Likewise, when the body's metabolic heat production is greater than what can be transferred outward, the core temperature rises and heat-related problems/diseases can occur. Heat waves, or periods of anomalous warmth, do not affect everyone equally; it is the vulnerable individuals or sectors of society that will most experience their effects. In particular the follow factors are recognised:

Corporeal risk factors

- age > 70;
- reduced autonomy (infirm or wheelchair users) and a person's inability to adapt his behaviour to temperature;
- neurodegenerative diseases such as Parkinson's disease;
- dementias such as Alzheimer's disease;
- cardiovascular diseases and sequelae of cerebrovascular accidents;
- obesity;
- malnutrition;
- taking medicines that can interfere with the body's adaptation to heat;

Environmental factors

- great heat lasts without interruption for several days or continues both day and night;
- prolonged and intense exposure to the sun;
- humidity is high and there is not much wind;
- presence of atmospheric pollution (ozone, sulphur dioxide)
- in a big city, far from the sea, in a strongly urbanized (asphalted) environment, in an old house;
- habitat difficult to refresh (unprotected southern exposure, top floor of a building, attic apartment, flat roofed property, large glass surfaces, bad insulation, etc.);
- lack of trees around the house;
- absence of air conditioning;
- lack of habitation;
- lack of access to fresh areas during the day.

Special living or working conditions

- social isolation (people who live alone, etc.);
- participation in intense sporting activities (cycling, running, etc.);
- heavy physical work (outdoor manual work, buildings, etc.);
- works in sectors with sources of heat (foundry, bakeries, etc.);
- work conditions that require warm or waterproof clothing.

Depending on the above specified factors and temperature increase level, there is a spectrum of heat-related disease hospitalization causes, ranging from low impact heat stress disease to high impact heat stress disease:

It includes the following diagnoses:

- Dehydration
- Electrolyte, acid-base abnormality
- Acute renal failure
- Urinary tract infection
- Syncope
- Rhabdomyolysis
- Atrial fibrillation
- Respiratory failure
- Altered mental status

Since a European database of cost categories and cost parameters/indicators usable in the economic models does not exist, an analytical approach is adopted. The elements at risk considered and the damage analysed are highlighted in **Table 12**. For each specific level of damage, it is necessary to establish the distribution of the damage typologies among the injured people. According with the most relevant literature on the hospitalization costs connected with heat waves [17] [18], it is possible to connect the following intensity of care and the related cost to each level of damage (**Table 12**). The average stay in hospital as a consequence of a heat wave is 3.2 days. Around 80% of people hospitalized for heat wave access the hospital through the emergency department. Based on the report of New York Hospitals from 1991 to 2004 [19], the length of hospital stay in days can be estimated, depending on the severity of disease, and is defined as shown in **Table 12**.

Table 12: Damage typologies for the six levels of damage and the corresponding level of medical care and time of hospital stay.

Level of Damage		Damage Typology	Level of medical care	Avg. hospital stay (days)
D0	No Damage		Not needed	0
D1	Caution	Fatigue, Possible discomfort	Few visits to doctors, generally no hospitalization needed	0.5
D2	Extreme caution	Sunstroke, heat cramps, heat exhaustion possible	Hospitalization needed	4.5
D3	Danger	Sunstroke, heat cramps, heat exhaustion likely, heatstroke possible	Hospitalization needed	7.0
D4	Extreme danger	Sunstroke and heatstroke highly likely	Hospitalization needed	10.5
D5	V. extreme danger	Death	-	-

It is possible that the duration for hospitalization may depend on the geographical location of people affected by a heat wave. This trend has been observed in a study on a huge database of hospitalization from heat wave cases [19]. Each day of hospital admission and hospitalization for treatment of heat-related diseases cost on average around 1,000 USD (US based research - 2004). Assuming an exchange rate of 0.9 Euro per USD [Exchange rate USD/€ January 2020], the assumed cost per each hospitalization day is 900 €. Further adjustment could be done by considering the European average cost of hospitalization for heat waves. Unfortunately, at the moment the poor literature on the topic does not allow this adjustment. Since European focused data are not available in literature, this parameter is adopted in the model. That is, for all damages classes D1-D4 shown in **Table 12**, the average cost per hospitalization stay is 900 € per day.

For each specific level of damage, in the absence of statistical data, it is necessary to establish the distribution of the damage typologies between the injured people in order that the subsequent cost calculations can be made (e.g. hospitalization etc.). An example of such a distribution is shown in **Figure 29**.

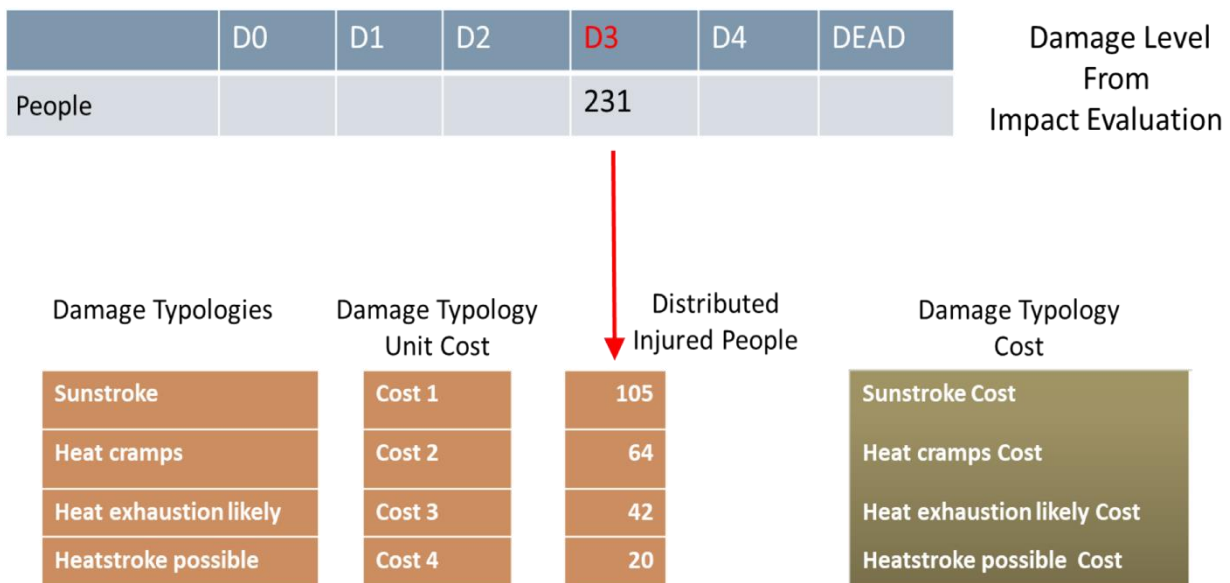
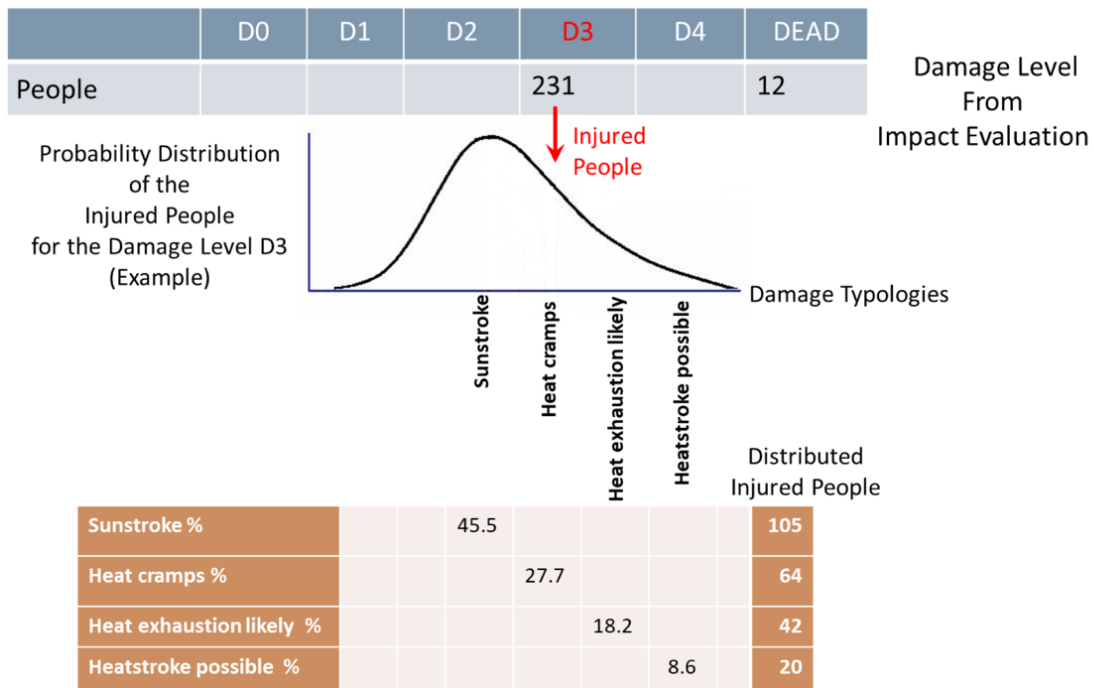


Figure 29: Example of distribution of damage typologies necessary for the calculation of the costs of hospitalization.

2.4.1.1 Impact Evaluation

Before the specific costs for each damage type are addressed, **Table 13** summarizes the direct and indirect cost categories and parameters for the heat wave hazard and for population as the element at risk. Calculations of the costs for these elements will be presented herein.

Table 13: Summary of the direct and indirect costs to be calculated for the heat wave hazard and with population as the element at risk.

Damage type	Cost Categories	Parameters / Indicators
Direct Disease due to hyperthermal effects deriving from heat wave event: <ul style="list-style-type: none"> • Dehydration • Electrolyte, acid-base abnormality • Acute renal failure • Urinary tract infection • Syncope • Rhabdomyolysis • Atrial fibrillation • Respiratory failure • Altered mental status One or more of those direct effects may affect persons exposed to hazard The damage is ranked from D0 to D4	<ul style="list-style-type: none"> • Human Health Intervention Costs (Hospital Treatment x specific Diseases) 	<ul style="list-style-type: none"> • Injured People (Number of person suffering during/after a Heat wave event) • Average days of hospitalization for each damage level • Average cost per hospitalization stay
Indirect: Economic value of loss for dead people due to heat wave event	<ul style="list-style-type: none"> • Value of statistical life of the deceased 	<ul style="list-style-type: none"> • Number of human lives lost • Average cost of a human life
Indirect: Economic value of GDP loss for people hospitalized due to the heat wave event	<ul style="list-style-type: none"> • Decrease in local value added due to hospitalization effects (losses in productivity) 	<ul style="list-style-type: none"> • Number of persons hospitalized • Average hourly GDP product by each worker in the specific country • Average rate of unemployment • Average hour per each work day • Average days of hospitalization stay

In terms of the direction costs, the following scheme illustrates the calculation of the Human Health Intervention Costs, which is an extension of the method outlined previously, with the final step being to multiply the number of people in a particular damage category by the average hospital stay and the cost of such a stay per day (**Figure 30**). The parameters that are needed for this calculation within CSIS are shown in **Table 14**. These costs are related to the health care management concerning the access to the emergency department, chemical analysis, visits, hospitalization, etc.

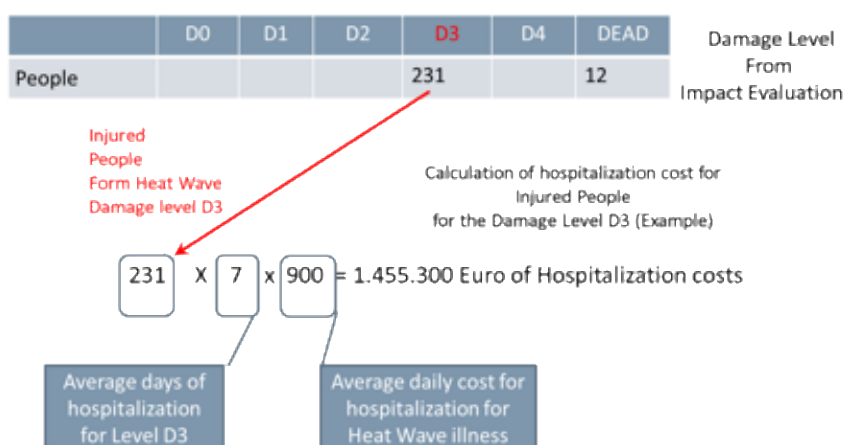


Figure 30: Calculation of the human health intervention costs.

Table 14: Parameters for the calculation of the human health intervention costs.

Parameters / Acronyms	Description	Data Source
NPERSON _D	Number of persons affected by heat wave event in the specific damage category (D)	CLARITY processing
AVGSTAY _D	Average days of hospitalization for the specific damage category (D)	Literature
AVGSTAYCOST	Average hospital stay cost per day	Literature
HHIC	Human Health Intervention Costs: NPERSON _D x AVGSTAY _D x AVGSTAYCOST	Processing

For the very extreme damage class of death, the value of a statistical life of the deceased, which is an indirect cost, is calculated as shown in **Figure 31**, and the relevant parameters are shown in **Table 15**.

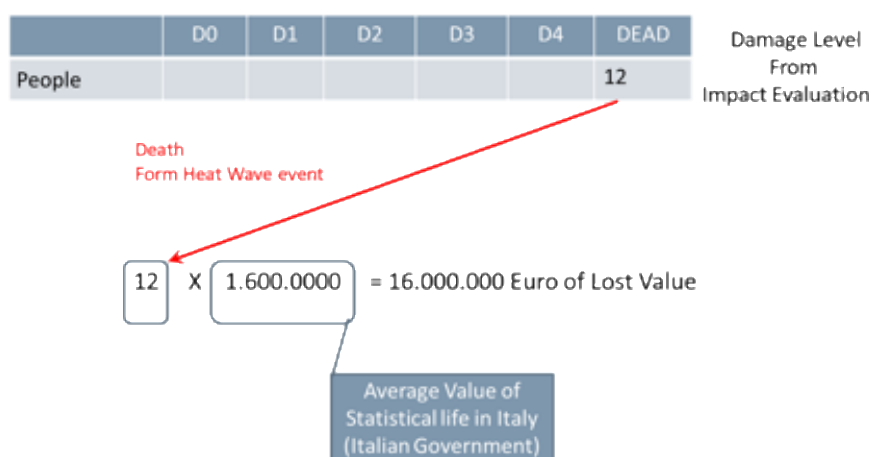


Figure 31: Calculation of the indirect cost of the deceased.

Table 15: Parameters for the calculation of the cost of the deceased.

Parameters / Acronyms	Description	Data Source
VSL _C	Value of statistical life in specific country	Literature
NPERSONDEAD	Number of persons dead	CLARITY processing
VSL	Value of Statistical Life of People Dead: VSL _C X NPERSONDEAD	Processing

The second indirect cost from **Table 13** concerns the calculation of the decrease in local value added due to hospitalization, which is shown in **Figure 32** and whose parameters are summarized in **Table 16**. This cost is estimated by the value of the production lost as the effect caused by emergency and hospitalization of part of resident population and, consequently, human labour production lost.

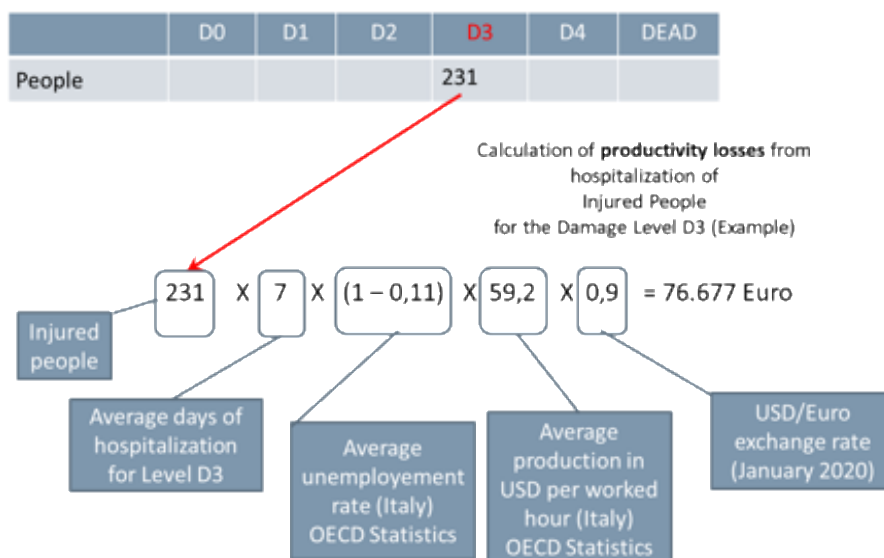


Figure 32: Calculation of the indirect cost of the local value added due to hospitalization effects (losses in productivity).

Table 16: Parameters for the calculation of the cost of the local value added due to hospitalization effects (losses in productivity).

Parameters / Acronyms	Description	Data Source
HPROD _C	Human labour Hourly production in Euro in the specific country (C)	OCSE
AVGSTAY _D	Average days of hospitalization for the specific damage category (D)	Literature
LABDAYH	Labour day average hour	CLARITY assumption
NPERSON _D	Number of persons affected by heat wave event in the specific damage category (D)	CLARITY processing
UNEMPL _C	Rate of Unemployment	OCSE
USDXCHRATE	Exchange rate USD/€	Financial Market
DLAV	Decrease in local value added due to hospitalization effects: (AVGSTAY _D X LABDAYH) X HPROD _C X NPERSON _D X UNEMP _C X USDXCHRATE	Processing

The parameters necessary to calculate the decrease in the local value added due to diseases of the employed population is shown in **Table 17**. This cost is estimated by comparing the value of production at two different times to explore the effects of the diseases of the population which is employed.

Table 17: Parameters for the calculation of the decrease in local value added due to diseases of the employed population.

Parameters / Acronyms	Description	Data Source
$PrVt_0 / PrVt_1$	Production value in t_0 / t_1	CLARITY processing
RP	Resident population	Statistical Data
EPV_{RP}	Resident population	Statistical Data
PI	Productivity Index	Statistical Data
$PSPV_{RP}$	Percentage value of resident disease population	CLARITY processing
	Decrease in local value added due to disease employed: $PrVt_0 - PrVt_1$ $PrVt_0 = RP \times EPV_{RP} \times PI$ $PrVt_1 = PrVt_0 \times (1 - PSPV_{RP})$	Processing

2.4.2 Economic Impact of Flooding

The economic impact assessment for the hazard of flooding is based on the following two elements:

- The depth–damage curves, at the European Level, calculated as described in [20] and [21].
- The maximum damage values (GDP) for the year 2010, associated with each vulnerability class, are reported in the MS-Excel file attached to [20].

Table 18 shows the elements at risk and the vulnerability classes under analysis. The vulnerability classes are defined as:

Residential Buildings (e.g. houses and apartments and their contents):

- Weighted averages based on studies of building stock are used, i.e. taking account of different sizes and quality standards of houses and apartments.
- Damage to assets in residential areas which are not residential buildings (i.e. in the public area and gardens) is not included.

Industrial Buildings (e.g. warehouses, distribution centres, factories, laboratories, and their contents):

- Weighted averages of the various building types are used based on building stock studies.
- Damage to assets in industrial areas (i.e. in the public area and vehicles) is not included.

Infrastructure, Roads, Railroads:

- Direct damage to roads and railroads as a result of contact with (fast flowing) water.

Agriculture:

- Based on damage resulting from flooded agricultural lands only (i.e. does not include farms, sheds, farming material, etc.).
- Value added used as a proxy in this study.

Table 18: Elements at risk and the vulnerability classes for the flood hazard.

Elements at Risk	Vulnerability Classes	Damage Estimation	Hazard Characterization
Residential Buildings	Residential Buildings	€/m ²	Depth (m)
Industrial Buildings	Industrial Buildings	€/m ²	Depth (m)
Agriculture	Agriculture	€/m ²	Depth (m)
Infrastructure, Roads	Roads	€/m ²	Depth (m)

NOTE: The element at risk “*Infrastructure, Roads*” and the vulnerability functions for this element proposed in this chapter are calculated for an urban environment with population density. In the special case described in DC4 for highways between urban areas, these vulnerability functions will not be taken into consideration. As mentioned previously, instead of following this procedure, the vulnerability assessment carried out for flooding (or any other hazard evaluated) has been carried out with an “expert criteria” methodology (as described later in DC4).

2.4.2.1 Calculation concept

In order to assess the damage produced by floods of a given depth, depth-damage curves are produced according to the process outlined in [20] which is schematically illustrated in **Figure 33**. This process involves the following elements:

Data collection:

- A review of literature on flood damage data (damage functions and maximum damage values).
- Obtaining country-specific quantitative data.

Maximum damage values:

- Harmonization of the damage values to the 2010 price level and to Euros.
- Adjustment of the maximum damage values where the damage functions were normalized.
- Harmonization of the construction costs based on regression analysis to extend the data to countries without known maximum damage values for residential, commercial and industrial buildings.
- Computation of the maximum damage values based on value added (agriculture) and European data (infrastructure, roads).

Flood depth-damage functions:

- Normalization (when necessary) to fit the full 0-1 range of the damage factor.
- Derivation of continental damage functions per land-use class.
- Construction of generic global damage curves for agriculture and roads from limited data.

Uncertainty and validation:

- Estimated for the damage functions and for the maximum damage values for residential, commercial and industrial buildings.
- Compared the registered damage to damage calculated using the methods described in this report for flood events in New York City (USA) and Jakarta (Indonesia).

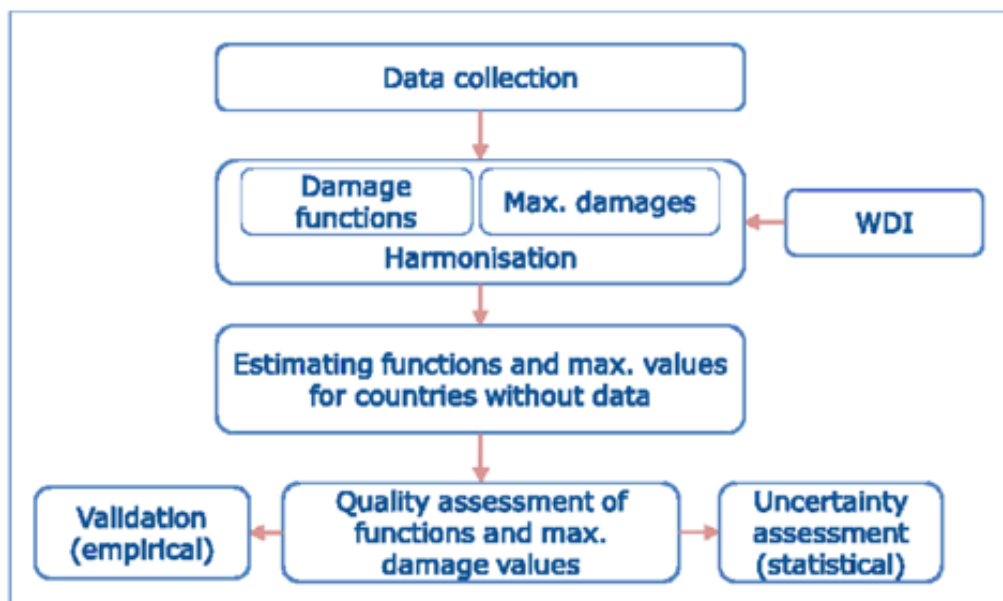


Figure 33: Schematic showing the process used in [20] to generate depth-damage curves.

2.4.2.2 Maximum Damage Calculation for each Vulnerability Class

The maximum damage values from floods for each EU-country are calculated for each vulnerability class outlined in **Table 18** using the values reported in [20].

Damage to buildings (residential and industrial) is expressed as three different measures of damage: building based (structure, content and total), land-use based, and object based. The values were given in Euros/m² except of object-based measure which was in Euros per object. For simplicity, the building-based data is adopted here. The maximum damage-data (construction cost) computes the maximum damage values (before adjustment) for the damage to buildings based on the regression analysis documented in the report.

The maximum damage values for the two types of buildings (residential and industrial) have been further adjusted to suit characteristics of the site considered, manipulating relevant assumptions regarding:

- Calculation of the depreciated value as a share of construction cost.
- Calculation of value of content.
- Size of the building footprint.
- Proportion of the un-damageable part.
- Adjustment for the material used.

There is also additional information provided which can be used to calculate, for example, confidence intervals or make additional adjustment with respect to, e.g. material used. These additional manipulations, however, would need to be undertaken manually by a user.

For the vulnerability class agriculture, the maximum damage value is given as the agricultural value added in Euros per hectare [20]. Additionally, the agricultural area (km²) for each country is provided.

For vulnerability class of infrastructure and roads, the damage is calculated based on continent-specific maximum damage values scaled by the country-to-continent per capital GDP level.

All the values used in these calculations, expressed originally in terms of the 2010 price level, have been actualized to the 2018 using the CPIs (Consumer Price Index⁷) provided by the World Bank.

⁷ The CPI reflects changes in the cost to the average consumer of acquiring a basket of goods and services that may be fixed or changed at specified intervals, such as yearly.

2.4.2.3 Damage Factor Curves and Tables

Damage factor curves define a coefficient of damage in the range 0-1 expected for a given flood depth and are defined for each vulnerability class. Such curves are typically used for housing and other structures where the depth refers to depth of water inside a building and the damage refers to the damage expected from that depth of water. They may be thought of more generally as representing the relationship between hazard magnitude and loss.

The damage factor curves for a set of EU countries are provided by [20] and are shown in **Figure 34**. These damage factor curves, based on samples at specific levels of depth, have been converted into tables. The damage factors related to the other EU countries have been estimated by using countries with similar characteristics based on the closest maximum damage values.

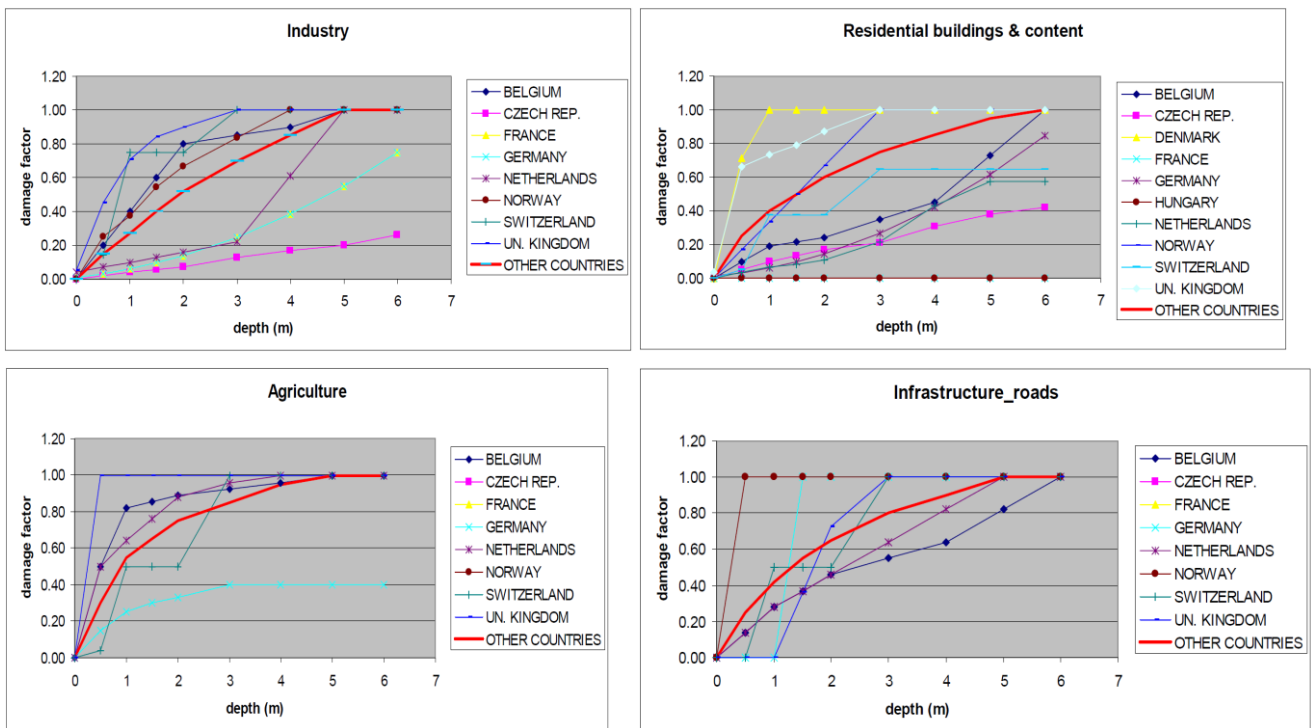


Figure 34: Damage factor curves for the four vulnerability classes for several EU countries taken from [20].

2.4.2.4 Depth-Damage Tables

Depth-damage tables can be used to calculate the economic impact assessment for each vulnerability class. They provide information on the losses expected to result at a specified depth of flood water. These tables have been calculated for each country by spreading the maximum damage value over the damage factor samples. The economic impact assessment provides the loss of GDP (Gross Domestic Product) and therefore includes direct and indirect costs. As an illustration of how such depth-damage tables are used to calculate the economic impact assessment, the vulnerability class of residential buildings in Austria is considered (**Figure 35**). The flooding depth used as input comes from the local scale flooding model, and in this case for a depth of 2m, damages are expected to be 104.38 €/m². If a flooding depth falls between values shown in the table, intermediate damage costs are obtained through linear interpolation.

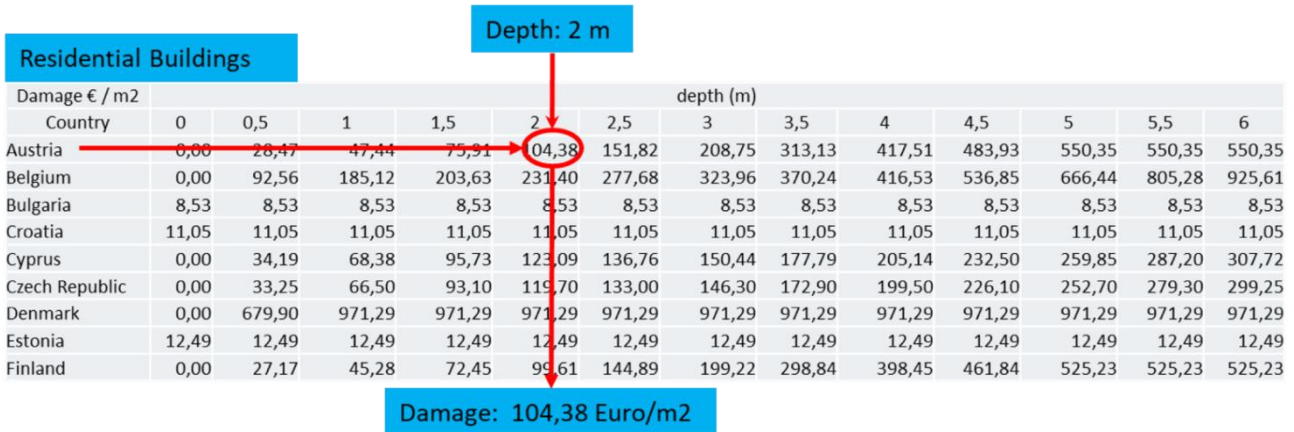


Figure 35: Depth-damage table for the vulnerability class of residential buildings. The example illustrated is explained within the text.

In the case that there are a number of different elements exposed to the hazard, then the appropriate vulnerability class for those elements is used for each cell of the grid, as indicated in **Figure 36**. By multiplying by the total area of those elements within the grid cell, a final damage cost can be obtained (**Figure 37**).

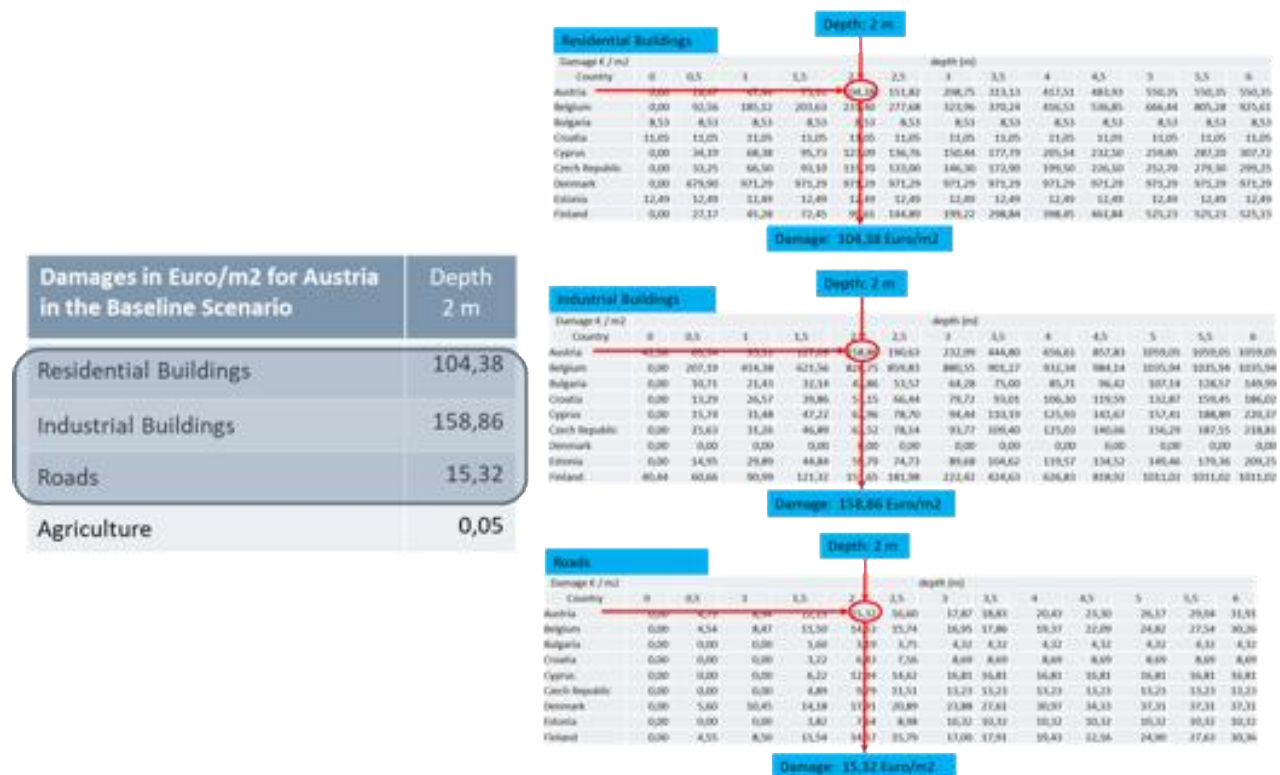


Figure 36: As in **Figure 35** but for the case of multiple elements of exposure.

Damage Evaluation in a single Cell of the Grid Baseline scenario located in Austria		Each Damage value refers to the m2 of the elements at risk (m2 of elements at risk) located in each cell of the grid.	
Elements at Risk	Damage (Euro/m ²)	m ² of the Elements at Risk in the cell	Damage (Euro)
Residential Buildings	104,38	100	10.438,00
Industrial Buildings	158,86	200	31.772,00
Roads	15,32	300	4.596,00
Agriculture	0,05	0	0,00
			Total Damage in the cell 46.806,00 Euro

Figure 37: The total damage cost can be calculated by multiplying the damage per area by the area of those elements within the grid cell.

2.4.2.5 Impact Evaluation

The damage impact evaluation is provided using the depth–damage curves/tables (vulnerability curves). The depth of water comes from the characterization of the flooding in the baseline scenario (grid analysis). An economic impact assessment can be performed to evaluate the direct (including emergency costs) and indirect costs. The economic impact assessment related to the flooding in a specific baseline for each vulnerability class will be provided in terms of €/m².

The elements at risks will be subject to:

- **Direct Damages (Costs)** which are related to direct loss caused by the excess of water (cost/m²), immediate damage (damage of objects, actions for water drainage, actions for mud removal, etc.):
 - Reconstruction Costs
 - Rehabilitation Costs
 - Evacuation Direct Costs
 - Evacuation Assistance Costs
 - Emergency Costs
 - Human Health Intervention Costs
 - Back Home Costs
 - Mud Cleaning-Up Costs
- **Indirect Damages (Costs)** which are related to loss deriving from the forced stop of the business activities for a certain period of time due to persistent water level:
 - Decrease in local value added due to psychological effects
 - Changes in Gross Local Product (GLP) or in Local Value-Added (LVA)

In the tables that follow, each cost category for the flooding hazard is addressed and its method of calculation for the economic impact assessment outlined. The calculations are to be done for a grid cell in a specified country. The categories of costs shown are:

- Damages related to the residential/industrial buildings (**Table 19**),
- Damages related to agriculture (**Table 20**),
- Damages related to infrastructure and roads (**Table 21**)
- Reconstruction / Rehabilitation costs (**Table 22 & Table 23**) – activities provided for removing the physical damage to capital assets, including buildings, infrastructure and industrial plants by the “in place” reconstruction / rehabilitation of assets which are lost / damaged.
- Evacuation direct costs (**Table 24**) – activities provided for the evacuation of the population from the emergency area according to the specific claims induced in the individual municipal plans.

- Evacuation assistance costs (**Table 25**) – activities provided for giving continuous assistance to the population evacuated from the emergency area.
- Emergency costs (**Table 26**) – activities and units engaged in the emergency as operating structures, means, workers, etc⁸.
- Human health intervention costs (**Table 27**) – health care management as the implementation of advanced medical structures, the strengthening of the existing local health structures, the identification of poor people (elderly and disabled), the psychological and social assistance, etc.
- Back home costs (**Table 28**) – activities provided for the “back home” of the population evacuated from the emergency area.
- Mud clean-up costs (**Table 29**) – removal and disposal of mud from roads and railroads.
- Decrease in local value added due to psychological effects (**Table 30**) – estimated by the comparison of the value of the production in two different moments in order to explore the psychological effects caused by emergency on resident population and, consequently, human labour.
- Changes in Gross Local Product (GLP) or in Local Value-Added (LVA) (**Table 31**) – refers to the damage to the flows of goods and services which can be bought and sold in markets. They can include, e.g. lower output from damaged or destroyed assets and infrastructure, loss of income due to damage to marketing infrastructure such as roads and the costs associated with the necessary utilization of more expensive inputs following the uselessness of cheaper normal sources of supply. Indirect cost can be estimated by analysing the temporal changes in gross local product (GLP) or in local value-added, according to the availability of official data.

The input data necessary for the cost calculations may not exist for every EU country. In those cases estimates based on countries which have similar characteristics may be used as a first approximation.

⁸ For example, costs related to the number of people committed in each operating structure to manage the emergency (Protection Civil Department, police, “corpo forestale”, etc) and the organization of equipped area can be included in this group.

Table 19: Parameters for the calculation of damages related to the residential/industrial buildings.

Parameters/Acronyms	Description	Data source
Depth	Depth of flooding (m) comes from the flooding characterization in a cell of the grid related to the baseline or adapted scenario.	CLARITY processing
MaxDamage-Data-Residential/Industrial (Country)	Maximum Damage Data (Construction Cost per capita) computes the maximum damage values for the damage to residential/industrial buildings in Euro in a specific EU Country at 2010.	Literature
MaxDamage Adjustment Coefficients	The following adjustment parameters are useful to suit specificities of the scenario considered: COI1. Construction Cost vs. Depreciated Value: Conversion factor (multiply with CC to get DV) [0 - 1] Default 0.6. COI2. Undamageable part: Percentage that is regarded never to be damaged by a flood [0 - 1] default 0.4. COI3. Material used: In case of less expensive material (multiply with maximum damage building) [0 - 1] Default 1. COI4. Max Damage Content/Inventory. Conversion factor (multiply with maximum damage building) [0 - 3] Default 0.5.	Literature
CPI (Country, Year)	Consumer price index of WDI - World Development Indicators.	World Bank
MaxDamage-Residential/Industrial (Country)	Calculated with a building-based approach (structure plus content) by Country in €/m ² : $\text{MaxDamage-Data-Residential/Industrial (Country)} \times \text{COR1} \times (1-\text{COR2}) \times \text{COR3} \times (1+\text{COR4}) \times [\text{CPI (Country, 2018)} / \text{CPI (Country, 2010)}]$	CLARITY processing
Damage-Factor-Residential/Industrial (Country, Depth)	Damage factor is based on samples of the damage-factor curves at specific levels of depth.	Literature
Damage-Residential/Industrial (Country, Depth)	The Damage-Residential/Industrial is: $\text{MaxDamage-Residential/Industrial (Country)} \times \text{Damage-Factor-Residential/Industrial (Country, Depth)}$	CLARITY processing

Table 20: Parameters for the calculation of damages related to the agriculture.

Parameters/Acronyms	Description	Data source
Depth	Depth of flooding (m) comes from the flooding characterization in a cell of the grid related to the baseline or adapted scenario.	CLARITY processing
MaxDamage-Data-Agriculture (Country)	Agricultural value added at 2010 (avg. 2008-2012) in Euros per hectare converted in Euros per m ² (1 ha = 10000 m ²).	Literature
CPI (Country, Year)	Consumer price index of WDI - World Development Indicators.	World Bank
MaxDamage-Agriculture (Country)	Calculated with a building-based approach (structure plus content) by Country in €/m ² : MaxDamage-Data-Agriculture (Country) x [CPI (Country, 2018) / CPI (Country, 2010)]	CLARITY processing
Damage-Factor-Agriculture (Country, Depth)	Damage factor is based on samples of the damage factor curves at specific levels of depth.	Literature
Damage-Agriculture (Country, Depth)	The Damage-Agriculture is: MaxDamage-Agriculture (Country) x Damage-Factor-Agriculture (Country, Depth)	CLARITY processing

Table 21: Parameters for the calculation of damages related to the infrastructure, roads.

Parameters/Acronyms	Description	Data source
Depth	Depth of flooding (m) comes from the flooding characterization in a cell of the grid related to the baseline or adapted scenario.	CLARITY processing
GDP (Country)	GDP per capita at 2010 by country in US\$	Literature
MaxDamage-Data-Infrastructure_Roads (Country)	It is calculated based on continent-specific maximum damage values scaled by the country-to-continent per capital GDP level. MaxDamage-Data-Infrastructure_Roads (Country) = european_average_max_damage * GDP (Country) / GDP (Europe) where: european_average_max_damage = 751 €/m ² GDP (Europe) = 43097 at 2010 in US\$	CLARITY processing
CPI (Country, Year)	Consumer price index of WDI - World Development Indicators.	World Bank
MaxDamage-Infrastructure_Roads (Country)	The maximum damage to Infrastructure_Roads by country in €/m ² : MaxDamage-Data-Infrastructure_Roads (Country) x [CPI (Country, 2018) / CPI (Country, 2010)]	CLARITY processing
Damage-Factor-Infrastructure_Roads (Country, Depth)	Damage factor for Infrastructure_Roads is based on samples of the damage factor curves at specific levels of depth.	Literature
Damage-Infrastructure_Roads (Country, Depth)	The Damage-Infrastructure_Roads is: MaxDamage-Infrastructure_Roads (Country) x Damage-Factor-Infrastructure_Roads (Country, Depth)	CLARITY processing

Table 22: Parameters for the calculation of reconstruction costs.

Parameters/ Acronyms	Description	Data source
RB / PB / IP	Residential / Public / Industrial buildings surface	CLARITY processing
PL _{RB} / PL _{PB} / PL _{IP}	Percentage of residential / public / industrial buildings surface subject to in place reconstruction interventions	CLARITY processing
ReC _{RB} / ReC _{PB} / ReC _{IP}	Average “in place” reconstruction cost for residential / public / industrial buildings (€/m ²)	CLARITY processing
I	Infrastructure surface	CLARITY processing
PL _I	Percentage of the infrastructure surface subject to in place reconstruction interventions	CLARITY processing
ReC _I	Average “in place” reconstruction cost for the infrastructure (€/mq)	CLARITY processing
	Reconstruction Costs: RB x PL _{RB} x ReC _{RB} + PB x PL _{PB} x ReC _{PB} + IP x PL _{IP} x ReC _{IP} + I x PL _I x ReC _I	Processing

Table 23: Parameters for the calculation of rehabilitation costs.

Parameters/ Acronyms	Description	Data source
RB / PB / IP	Residential / Public / Industrial buildings surface	CLARITY processing
PVD _{RB} / PVD _{PB} / PVD _{IP}	Percentage of residential / public / industrial buildings surface subject to rehabilitation interventions	CLARITY processing
RiC _{RB} / RiC _{PB} / RiC _{IP}	Average rehabilitation cost for residential / public / industrial buildings (€/m ²)	CLARITY processing
I	Infrastructure surface	CLARITY processing
PL _I	Percentage of the infrastructure surface subject to rehabilitation interventions	CLARITY processing
ReC _I	Average rehabilitation cost for the infrastructure (€/mq)	CLARITY processing
	Rehabilitation Costs: RB x PVD _{RB} x RiC _{RB} + PB x PVD _{PB} x RiC _{PB} + IP x PVD _{IP} x RiC _{IP} + I x PVD _I x RiC _I	Processing

Table 24: Parameters for the calculation of evacuation direct costs.

Parameters/ Acronyms	Description	Data source
RP	Resident population	Statistical data
E _V PV _{RP}	Percentage of resident population which is evacuated	CLARITY processing
EC _U	Evacuation Unit Cost (per person)	CLARITY processing
	Evacuation Direct Costs: RP x E _V PV _{RP} X EC _U	Processing

Table 25: Parameters for the calculation of evacuation assistance costs.

Parameters/ Acronyms	Description	Data source
RP	Resident population	Statistical data
E_VPV_{RP}	Percentage of resident population which is evacuated	CLARITY processing
EAC_{U_t}	Evacuation Assistance Unit Cost (per person) in a “t” time unit (to be defined)	CLARITY processing
T	$\sum t$ = Total of the time units included in the emergency period	CLARITY processing
	Evacuation Assistance Costs: $RP \times E_VPV_{RP} \times EAC_{U_t} \times T$	Processing

Table 26: Parameters for the calculation of emergency costs.

Parameters/ Acronyms	Description	Data source
EC_t	Emergency costs in a “t” time unit (to be defined)	CLARITY processing
T	$\sum t$ = Total of the time units included in the emergency period	CLARITY processing
OEC	Other Emergency Costs (one-time costs) caused by emergency in that area	CLARITY processing
	Emergency Costs: $EC_t \times T + OEC$	Processing

Table 27: Parameters for the calculation of human health intervention costs.

Parameters / Acronyms	Description	Data source
$FAMAC_U$	First aid & medical assistance unit cost (per person)	CLARITY processing
RP	Resident population	Statistical data
$FMPV_{RP}$	Percentage of resident population which needs first aid and medical assistance	CLARITY processing
PHIC	Public Health Intervention costs	CLARITY processing
$PSAC_U$	Psychological and social assistance unit cost (per person)	CLARITY processing
$PSPV_{RP}$	Percentage of resident population which needs psychological and social assistance	CLARITY processing
	Human Health intervention costs: $FAMAC_U \times RP \times FMPV_{RP} + PHIC + PSAC_U \times RP \times PSPV_{RP}$	Processing

Table 28: Parameters for the calculation of back home costs.

Parameters / Acronyms	Description	Data source
RP	Resident population	Statistical data
E_VPV_{RP}	Percentage value of resident population which is evacuated	CLARITY processing
BHC_U	Back Home Unit Cost (per person)	CLARITY processing
	Back Home Costs: $RP \times E_VPV_{RP} \times BHC_U$	Processing

Table 29: Parameters for the calculation of mud clean-up costs.

Parameters / Acronyms	Description	Data source
A	Thickness of mud accumulation	CLARITY processing
S_R / S_{RR}	Roads / Railroads surface	CLARITY processing
CCA_R / CCA_{RR}	Average clean-up unit cost (€/mq) connected with a specific thickness for roads / railroads	CLARITY processing
AA	$\sum AA$ = Total mud accumulation (to be defined – in kg/m ² ?)	CLARITY processing
TC_U / DC_U	Mud Transportation / Disposal unit cost	CLARITY processing
	Mud Cleaning-Up Costs: $S_R \times CCA_R + S_{RR} \times CCA_{RR} + AA \times TC_U + AA \times DC_U$	Processing

Table 30: Parameters for the calculation of the local value added due to psychological effects.

Parameters / Acronyms	Description	Data source
$PrVt_0 / PrVt_1$	Production Value at time t_0 / t_1	CLARITY processing
RP	Resident population	Statistical Data
EPV_{RP}	Percentage value of resident population which is employed	Statistical Data
PI	Productivity Index	Statistical Data
$PSPV_{RP}$	Percentage value of resident population with psychological problems because of emergency situation	CLARITY processing
	Decrease in local value added due to psychological effects: $PrVt_0 - Prvt_1$, where $PrVt_0 = RP \times EPV_{RP} \times PI$, and $PrVt_1 = PrVt_0 \times (1 - PSPV_{RP})$	Processing

Table 31: Parameters for the calculation of changes in the Gross Local Product (GLP) or in the Local Value-Added (LVA).

Parameters / Acronyms	Description	Data source
$GLPt_0 / GLPt_1$	Gross Local Product at time t_0 / t_1	CLARITY processing
$LVAt_0 / LVAt_1$	Local Value-Added at time t_0 / t_1	CLARITY processing
	Changes in Gross Local Product (GLP): $GLPt_0 - GLPt_1$ Changes in Local Value-Added (LVA): $LVAt_0 - LVAt_1$	Processing

2.5 Adaptation Options and their Economic Appraisal

The Risk Assessment and Impact Scenario Analysis is a crucial step since it provides a sound information base useful for selecting adaptation strategies to be adopted to tackle the local effect, and consequently, the hazards, identified in the first phase of the EU-GL modelling procedure. Therefore, adaptation options should be strongly connected to the impact model because they are able to reduce local effect intensity, decreasing the damages to which the elements at risk are subjected to, and to change the exposure, proposing a new geographic position of an element at risk towards a location with lower hazard intensity.

The most recurring urban climate adaptation measures have been identified taking into account the most recent literature [22] [23] and classified in relation to their ability to influence the urban microclimate conditions (i.e. the “local effect” of heat wave and flood hazards). In particular, they have been listed and grouped into representative classes and characterized according the most relevant parameters descriptive of local effect and used in the CSIS simplified model, such as, for instance, albedo, emissivity and runoff. These have been made available in a dedicated section of the CSIS⁹, indicating the type of land use to which each option can be assigned. This approach provides a simpler selection of adaptation measures to respond to identified climate-related hazards (**Table 32**) for the end user.

Once applied in a given urban area, the adaptation measure induces a “climate-benefit” variation of the model parameters (**Table 33**). The values have been attributed based on the literature review carried out. A further parameter, relevant for the heat wave hazard, has been introduced, related to the ability of the adaptation measure to influence the surface temperature (Ts) in relation to the air temperature (Ta). This is defined as:

$$T_s = T_a \times (1 + T_{a_{\text{increase}}}) \times CF,$$

where CF is the calibration factor and $T_{a_{\text{increase}}}$ is a ratio relating Ts to Ta in ENVI-met as

$$T_{a_{\text{increase}}} = \left(1 - \frac{T_{s_{\text{env}}}}{T_{a_{\text{env}}}}\right) \times 100 .$$

The latter has been attributed through simulations conducted with the ENVI-met 4.0 model for all adaptation measures presented in **Table 32**. A subset of these calculations is shown in **Table 34**.

⁹ <https://csis.myclimateservice.eu/adaptation-options>

Table 32: List of adaptation measures available in CSIS.

Category	Type	Example measure
GREEN SURFACES	Type A	Rain garden / Bioswale
	Type B	Agriculture
	Type C	Meadow
TREES	Type A	Small trees
	Type B	Average trees
	Type C	Tall trees
PERMEABLE FLOORING	Permeability > 90%	Grassy gravel
	21% < Permeability < 89%	Grassy joint flooring
	Permeability < 20%	Permeable concrete
REFLECTIVE SURFACES	High	Cool flooring / paint (SRI > 0.9)
	Medium	Cool flooring / paint (0.75 < SRI < 0.90)
	Low	Cool flooring / paint (SRI < 0.75)
GREEN ROOFS	Intensive	Roof garden vegetated / semi-vegetated
	Extensive	Sedum vegetated / semi-vegetated
COOL ROOFS	High (SRI > 0.90)	Mineral membrane coated white reflex ultra
	Medium (0.75 < SRI < 0.90)	Mineral membrane reflex white
	Low (SRI < 0.75)	Waterproof aluminium coated membrane
WALLS INSULATION	Type A	Ventilated facades
	Type B	Green wall
	Type C	External insulation
ROOF INSULATION	Type A	Ventilated roof
	Type B	Warm roof
	Type C	Overlapping inclined roof
SHADING SYSTEMS (BUILDINGS)	Type A	Blinds
	Type B	Fixtures with selective glasses
SHADING SYSTEMS (OPEN SPACES)	Type A	Fixed canopy
	Type B	Removable canopy
	Type C	Green pergolas
WATER CHANNELING AND RETENTION	Type A	Retention area
	Type B	Water squares
	Type C	Basins and fountains
	Type D	Gutter
	Type E	Rainwater harvesting and reuse
OTHER	-	Permeable ground floor

Table 33: Main modelling parameters attributed to adaptation measures.

Performance parameter	Description	Range
Albedo	Fraction of incident solar radiation that is reflected. It indicates the reflectivity of a surface. High values correspond to high reflectivity.	0 – 1
Emissivity	Ability of a material to emit thermal radiation. Surfaces with high emissivity factors remain cooler due to their rapid heat release ability.	0.8 – 0.99
Runoff	Correlates the amount of rain with surface run-off. This value is higher for areas with low infiltration and lower for permeable and well-vegetated areas.	0 – 1
Transmissivity	Portion of transmitted solar radiation (measured e.g. under the canopy of trees) with respect to the actual values of the global radiation measured at the nearby open site. Low values represent a high amount of shading.	0 – 1
Sky view factor	The ratio at a point in space between the visible sky and a hemisphere centred over the analysed location. Low values correspond to high building density.	0 - 1

Table 34: A subset of the analysis of the Ts/Ta relation for the identified adaptation measures (columns) in **Table 32**. The first and the last row indicate the correspondence between the PLINIVS-LUPT model layers and ENVI-met presets (source: ENVI-met 4.0 elaboration). The first column shows the hours in a day, followed by the air temperature Ta.

layer PLINIVS		green surface A		trees A		permeable flooring A		reflective surface A		green roofs A	
hours	air T (envimet)	Ts envimet	increase	Ts envimet	increase	Ts envimet	increase	Ts envimet	increase	Ts envimet	increase
0	21.9	18.3	-0.16	17.7	-0.18	23.6	0.07	24.1	0.09	17.86	-0.18
1	21.1	18.15	-0.16	17.6	-0.19	23.1	0.08	23.5	0.10	17.76	-0.18
2	20.4	19.45	-0.14	19.3	-0.17	19.8	0.09	19.8	0.11	19.37	-0.16
3	19.8	17.4	-0.05	16.9	-0.05	19.5	-0.03	19.7	-0.03	17.14	-0.05
4	19.2	16.65	-0.12	16.1	-0.15	19.2	-0.02	19.5	-0.01	16.34	-0.13
5	18.8	16.25	-0.13	15.7	-0.16	19	0.00	19.3	0.02	15.97	-0.15
6	19.6	16.35	-0.14	15.9	-0.16	19.1	0.01	19.4	0.03	16.06	-0.15
7	21	18.05	-0.17	18	-0.19	19.8	-0.03	19.8	-0.01	17.99	-0.18
8	23	23.15	-0.14	23.6	-0.14	21.6	-0.06	21.1	-0.06	23.50	-0.14
9	24.7	26.7	0.01	27.2	0.03	24.1	-0.06	23.1	-0.08	27.00	0.02
10	26.5	29.2	0.08	30.1	0.10	26.9	-0.02	25.5	-0.06	29.77	0.09
11	28.4	31.45	0.10	32.8	0.14	29.6	0.02	28.1	-0.04	32.27	0.12
12	29.6	33.45	0.11	35.3	0.15	31.9	0.04	30.4	-0.01	34.57	0.14
13	30.4	35.15	0.13	37.6	0.19	33.6	0.08	32.3	0.03	36.69	0.17
14	31	36.75	0.16	40	0.24	34.7	0.11	33.6	0.06	38.80	0.21
15	31.6	37.85	0.19	42	0.29	35.2	0.12	34.4	0.08	40.34	0.25
16	32	37.75	0.20	42.5	0.33	35.2	0.11	34.6	0.09	40.51	0.28
17	32.2	36.6	0.18	41.2	0.33	34.5	0.10	34.2	0.08	39.16	0.27
18	31.4	33.9	0.14	37.4	0.28	33	0.07	33.1	0.06	35.86	0.22
19	30	29.45	0.08	31.5	0.19	31	0.05	31.4	0.05	30.57	0.14
20	28	24.35	-0.02	24.9	0.05	28.6	0.03	29.3	0.05	24.59	0.02
21	26.4	22.25	-0.13	22.3	-0.11	27	0.02	27.7	0.05	22.19	-0.12
22	24.8	20.65	-0.16	20.4	-0.16	25.7	0.02	26.3	0.05	20.41	-0.16
23	23	19.3	-0.17	18.8	-0.18	24.5	0.04	25.1	0.06	18.96	-0.18
layer ENVIMET		(grass 50 cm + edge dense 2 m) /2		Grass 50 cm aver. dense		basalt brick road		granite shining		(grass 50 cm + edge dense 2 m + funkia + fern + leuzerne 18 cm + ivy + soja 63 cm)/7	

Transport infrastructure climate adaptation measures have also been identified taking into account the most recent literature [24]. A detailed list of possible adaptation measures to possible extreme weather induced impacts obtained within the ROADADAPT project [24] is given in **Table 35**. For different hazards, several adaptation options have been listed, together with the component of the transport infrastructure that is benefitted from the measure.

Table 35: Overall possible adaptation actions for transport infrastructure. The components of the transport infrastructure are 1 = cut; 2 = embankment; 3 = pavement; 4 = channeling; 5 = drainage; 6 = structure; 7 = traffic condition; 8 = sign posts (Source: ROADADAPT project).

Hazard	Adaptation Options	Component of the Transport Infrastructure							
		1	2	3	4	5	6	7	8
Affectation to the circulation by ice	De-icing agents that cause less damage to pavements and the environment			x					
	Deployment of de-icing agents			x					
	Improving the asphalt specification to increase its failure strain			x					
	Install flexible revetment as artificial armouring			x					
	Allow alternative routes in case of road closure							x	
	Increase surveillance of vulnerable roads in order to prevent disasters							x	
Affectation to the circulation by fog	Increasing the reflectivity (albedo) of dark surfaces			x					
	Allow alternative routes in case of road closure							x	
	Increase surveillance of vulnerable roads in order to prevent disasters							x	
Affectation to the circulation by fire	Increasing the reflectivity (albedo) of dark surfaces			x					
	Install erosion barriers soon after the wildfire			x					
	Allow alternative routes in case of road closure							x	
	Increase surveillance of vulnerable roads in order to prevent disasters							x	
Affectation to the circulation by snow	De-icing agents that cause less damage to pavements and the environment			x					
	Deployment of de-icing agents			x					
	Improving the asphalt specification to increase its failure strain			x					
	Install flexible revetment as artificial armorings			x					
	Allow alternative routes in case of road closure							x	
	Increase surveillance of vulnerable roads in order to prevent disasters							x	
Landslide, material fall and slope erosion	Afforestation of slopes with drought-resistant species	x							
	Implementation of erosion control blankets or granular protection	x							
	Improvement of road maintenance resources	x							
	Reduce the slope of the cut or embankment	x							

	Ensure the selection of materials with high resistance to dry conditions	x							
	Mulching	x							
	Increase water holding capacity and slow infiltration through environmental measures and bio-retention systems to recharge aquifers and reduce surface flow runoff.	x							
	Avoid deforestation in the catchment area	x							
	Avoid deforestation on slopes	x							
	Build channels or deflection walls to direct the flow	x							
	Build flood walls to protect the road from flooding	x							
	Construct a catch ditch at the toe of the slope	x							
	Cover road embankment with geotextile	x							
	Cover slope with vegetation	x							
	Cutting back the slope to a shallower angle	x							
	Extend the footing to support the slope or protect it from erosion	x							
	Install a bulkhead to support the slope and protect it from erosion	x							
	Install active protection systems to prevent rock detachments.	x							
Rutting	Anti-oxidation additives			x					
	Cold mill and overlay, thin surface patches			x					
	Harvesting of heat energy from the pavement			x					
	Heat resistant concrete fixings			x					
	High albedo pavements, heat shield pavements, water retention pavements			x					
	Modify the concrete mixture to ensure adequate workability and curing time			x					
	Use of water capture and storage systems				x	x			
	Readjustment of natural water courses (formation of rivers)				x	x			
	Enclosure materials for flood protection (i.e. waterproof linings)				x	x			
	Increase water holding capacity and slow infiltration through natural or bioengineered systems				x				
Drainage Insufficient capacity	Lifting the pavement with additional drainage capacity - safety factor			x					
	Alternative mixtures for bituminous pavements and surface courses			x					
	Apply porous asphalt surface course			x					
	Avoid deforestation in the catchment area				x				
	Avoid deforestation on slopes				x	x			
	Build channels or deflection walls to direct the flow				x	x			
	Build dams, reservoirs and retaining ponds to buffer the water				x				

	Build flood walls to protect the road from flooding					x	x			
	Cleaning out watercourses and structures of flood prone areas ahead of predicted heavy rainfall					x	x			
	Clear natural blockages such as shrubs and weeds					x	x			
	Cover road embankment with geotextile					x				
	Cover slope with vegetation					x				
	Dredge the channel to increase the width and/or depth					x				
	Dredge to increase depths and/or straighten the stream					x				
	Install barriers to catch material in debris flows					x				
	Increase number and size of drainage infrastructures						x			
	Adapt drainage system to control ground water table						x			
	Drainage of road embankment for fast lowering of groundwater table after flood retreats						x			
	Ensure efficient drainage systems						x			
	Install barriers to catch material in debris flows						x			
Structural Movements	In situ strengthening of granular (sub)bases and subgrade soils, using artificial or natural cements							x		
	Increase the thickness of structural layers							x		
	Increase the thickness of structural layers, using a more compact wearing course layer (SMA for example)							x		

Once adaptation measures are applied in a transport infrastructure the impact due to climate hazards is significantly reduced. No parameters related to the quantification of the impact reduction are given because calculations are done based on expert judgement.

For the adaptation measures excluding transport infrastructure, a parametric cost has been assigned to each of them, based on a detailed analysis carried out for the Italian market, then expanded to other EU countries based on econometric indicators to shift the average costs (see **Table 36** and **Annex II: Adaptation options**).

Social, economic and environmental “co-benefits” (**Table 37**) have also been assigned. This allows cost-benefit assessments not focused only on financial variables to encompass a wider range of potential urban quality improvements linked to climate change adaptation, which will be used in the multi-criteria analyses.

The report "Co-benefits of urban climate action: A framework for cities", published in 2015 by the Economics of Green Cities program highlights how identifying and communicating the co-benefits of climate adaptation is a priority for urban decision-makers. It broadens the consensus regarding resilient urban transformation strategies by local communities, often bearers of urban redevelopment needs not directly related to the improvement of microclimatic conditions (for example better quality of housing, greater provision of equipped public spaces and green areas, better accessibility to transport systems, etc.). It motivates climate action among various stakeholders across multiple sectors and triggers a virtuous circuit supporting the public initiative in the implementation of the interventions.

It should be noted that the CLARITY focus on climate adaptation has to consider as a co-benefit also the contribution of a specific measure to climate change mitigation, defined as a local contribution to the reduction of global greenhouse gas emissions.

Table 36: Parametric cost of adaptation measures (see Annex II for details).

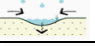





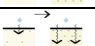







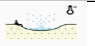



ADAPTATION MEASURES			Parameter	Min.Cost	Max.Cost	Average.Cost	Average.Min.Cost	Average.Max.Cost	Fonte	
GREEN SURFACES	TYPE A		Rain garden/Bioswale	€/mq	50	460	255	152,5	357,5	http://nemo.uconn.edu/raingardens/calculator.htm
	TYPE B		Agriculture	€/mq	30	40	35	32,5	37,5	Catalogo DE 2012 (Genio Civile Milano)
	TYPE C		Meadow	€/mq	30	40	35	32,5	37,5	Catalogo DE 2012 (Genio Civile Milano)
TREES	TYPE A		Small trees	€/Unit	55	220	137,5	96,25	178,75	Prezzario Regione Campania 2016
	TYPE B		Average trees	€/Unit	220	390	305	262,5	347,5	Prezzario Regione Campania 2017
	TYPE C		Tall trees	€/Unit	390	565	477,5	433,75	521,25	Prezzario Regione Campania 2018
PERMEABLE FLOORING	Permeability >= 90%		Grassy gravel	€/mq	50	130	90	70	110	Prezzario Provinciale Provinciale autonoma Trento 2012
	21% <= Permeability <= 9%		Grassy joint flooring	€/mq	30	50	40	35	45	Prezzario Ssoverde 2013-2014 / Prezzario Dpere Civili di provincia autonoma Bolzano Alto
	Permeability <= 0%		Permeable concrete	€/mq	2	4	3	2,5	3,5	Catalogo DE 2012 (Genio Civile Milano)
REFLECTIVE SURFACES	HIGH		Cool flooring (SR1 >= 0,9)	€/mq	10	30	30	20	30	globalcoolcities.org
	MEDIUM		Cool flooring (SR1 >= 0,75 <= 0,9)	€/mq	10	30	20	15	25	globalcoolcities.org
	LOW		Cool flooring (SR1 <= 0,75)	€/mq	10	30	10	10	20	globalcoolcities.org
SHADING SYSTEMS	TYPE A		Fixed canopy	€/mq	150	450	300	225	375	Prezzario Regione Campania 2018
	TYPE B		Removable canopy	€/mq	5	330	167,5	86,25	248,75	Prezzario Regionale della Provincia di Venezia Giulia 2015
	TYPE C		Green pergolas	€/mq	70	140	105	87,5	122,5	Prezzario Opere Pubbliche del Comune di Venezia 2014
WATER CHANNELLING AND RETENTION	TYPE A		Retention area	€/mq	120	400	260	190	330	Prezzario Regione Basilicata 2010
	TYPE B		Water squares	€/mq	200	500	350	275	425	http://www.publicspace.org
	TYPE C		Basins and fountains	€/mq	30	60	45	37,5	52,5	Catalogo DE 2012 (Genio Civile Milano)
	TYPE D		Gutter	€/mq	15	38	26,5	20,75	32,25	globalcoolcities.org
	TYPE E		Rainwater harvesting and reuse	€/Unit	4000	6500	5250	4625	5875	globalcoolcities.org

Table 37: Co-benefits linked to adaptation measures.

Co-benefit category	Co-benefit
Environmental Co-Benefits	<ul style="list-style-type: none"> - Better air quality - Reduction of greenhouse effect gas emissions - Better water collection and safety - Better water quality - Greater biodiversity - Greater control of erosion
Economic Co-Benefits	<ul style="list-style-type: none"> - Employment generation - Operating and maintenance costs savings - Contribution to innovation of local supply chains - Greater value of real estate
Social Co-Benefits	<ul style="list-style-type: none"> - Health and mortality impacts reduced - Greater accessibility of public spaces and services - Greater aesthetic value - Greater cohesion and inclusion of local communities

The adaptation measures have been collected in technical sheets (see **Annex II: Adaptation options**), including a description of climate-benefits and co-benefits, with the aim of providing end-users with a synthetic technical information to be included in the reports. These technical sheets can be also effectively used within co-design workshops, to support the collaborative appraisal of relevant adaptation measures in a given urban context.

In order to maximize the impacts of adaptation measures in terms of climate benefits and associated co-benefits, it is appropriate to develop more complex "adaptation strategies" (**Figure 38**) in the context of urban plans and urban projects. These represent the integration of different measures in relation to urban transformation / regeneration objectives identified, since only a widespread application of the measures in the urban area can guarantee the effectiveness of the adaptation action.

The integration of measures within adaptation strategies can simplify the process of assessing their potential cost and the effect compared to the baseline situation. Considering the existing land use mix of a given urban area (e.g. a 500 m × 500 m cell of the CSIS model analysis grid), the adaptation measures cannot of course be implemented on the entire surface, both for economic reasons, both because the hazard reduction effect is visible already when the measures are applied only for a percentage of the total surface of the land use.

Tests carried out show that for a cell characterized by a critical hazard value (**Figure 39**), an average application of a set of adaptation measures on 50% of the corresponding land use mix is adequate to reduce the local effect conditions. Accordingly, the adaptation strategies can be designed, in relation to the existing land use mix, the end-user objectives in terms of urban infrastructure project, and the potential implementation cost.

Figure 41 shows some examples of adaptation strategies in relation to different land use types. With the CSIS it is possible to evaluate the effects of each selected strategy on urban microclimate, carrying out simulations that combine the different adaptation measures foreseen for all land uses present in each cell, thus allowing the expected costs to reach the set adaptation benchmarks (**Figure 40**).

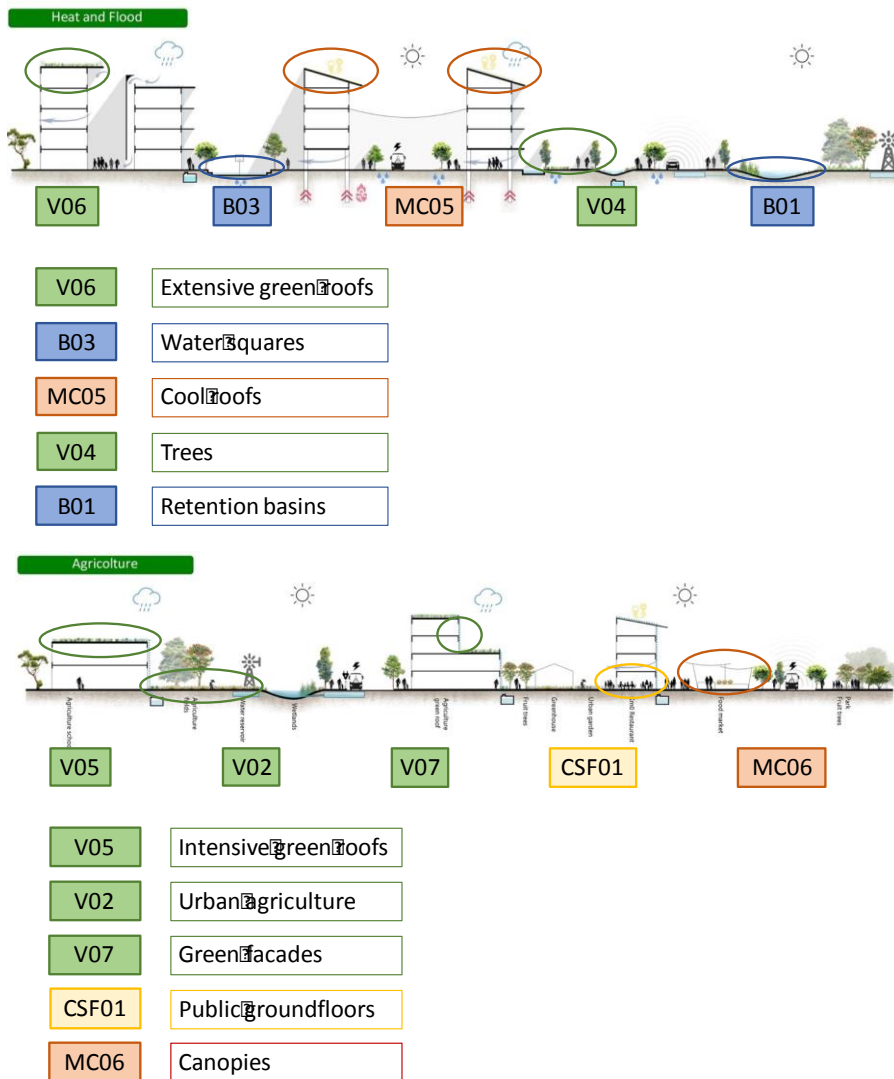
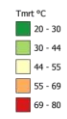


Figure 38: Example of adaptation strategies integrating multiple adaptation options (e.g. top, a possible adaptation strategy aimed at maximising opportunities for urban agriculture enhancement).

Simulazione ondata di calore stato di fatto

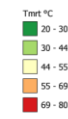


giorno 07-ago-15 gg-mm-aa
 ora 14:00 24h
 air temperature 37 °C
 sun altitude 65,14 °
 sun azimuth 192,35 °
 global radiation 808,8 Wh/m²
 wind speed 3,6 m/s
 relative humidity 36 %



Simulazione ondata di calore ripostata su grilla 250 x 250 stato di fatto

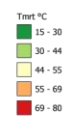
Tmrt 73,1 °C



giorno 07-ago-15 gg-mm-aa
 ora 14:00 24h
 air temperature 37 °C
 sun altitude 65,14 °
 sun azimuth 192,35 °
 global radiation 808,8 Wh/m²
 wind speed 3,6 m/s
 relative humidity 36 %



Simulazione ondata di calore post - adattamento

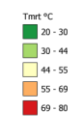


giorno 07-ago-15 gg-mm-aa
 ora 14:00 24h
 air temperature 37 °C
 sun altitude 65,14 °
 sun azimuth 192,35 °
 global radiation 808,8 Wh/m²
 wind speed 3,6 m/s
 relative humidity 36 %



Simulazione ondata di calore ripostata su grilla 250 x 250 post - adattamento

Tmrt 54,9 °C



giorno 07-ago-15 gg-mm-aa
 ora 14:00 24h
 air temperature 37 °C
 sun altitude 65,14 °
 sun azimuth 192,35 °
 global radiation 808,8 Wh/m²
 wind speed 3,6 m/s
 relative humidity 36 %

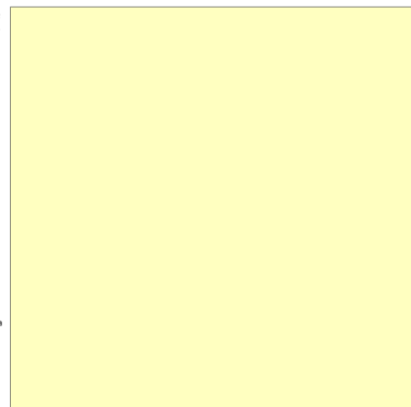
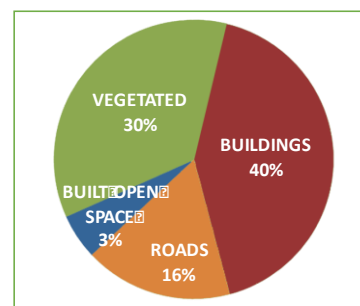
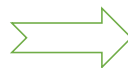
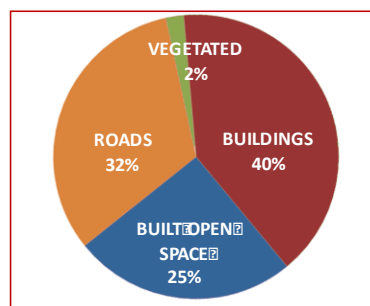
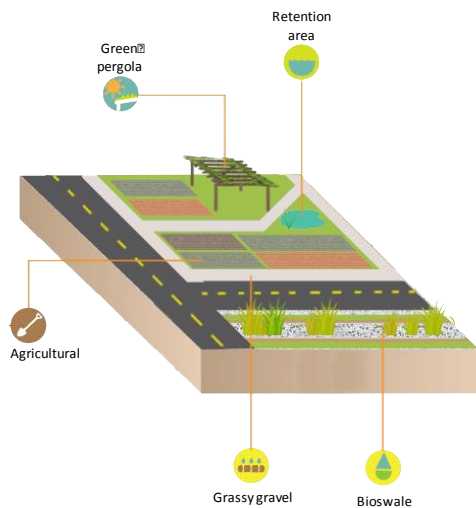


Figure 39: Test of adaptation measures effect on a 250 m × 250 m cell in the urban area of Naples.



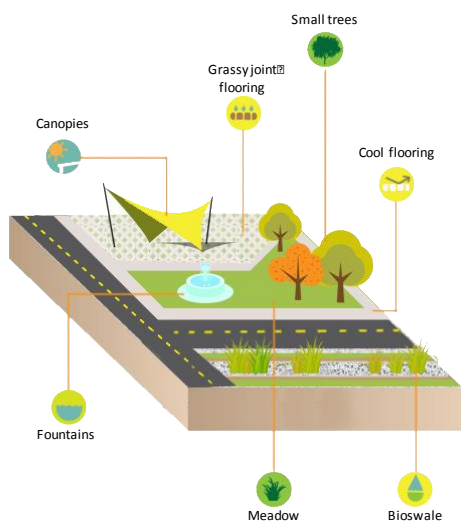
adaptation cost	€ 2.153.138,13
€/m ²	€ 34,45

Figure 40: Cost of adaptation strategy effect on a 250 m × 250 m cell in the urban area of Naples. Note that the modified land use takes into account the adaptation measures included, but these are grouped by category for readability (e.g. a percentage of built open spaces has been converted to green, with trees and agriculture, and a percentage of roads has been converted into bioswale. All these are summarized as “vegetated” in the right diagram).



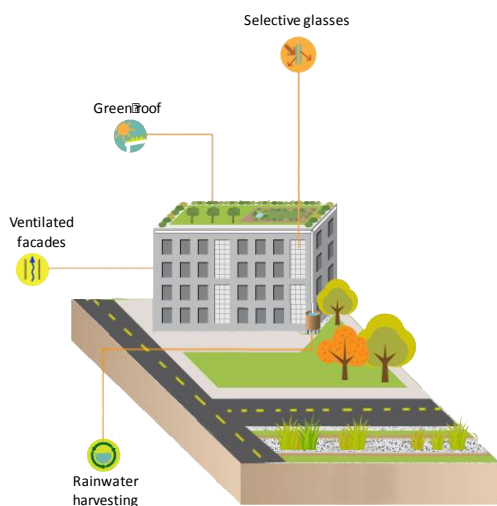
Bare soil example

- A. Agricultural Park:**
 Bioswale (16%), Agricultural (64%), Grassy gravel (10%), Green pergolas (10%), Retention areas (3%)
 € 4.001.562,00 / Area TOT 2500mq; € 64,03/mq
- B. Standard Park:**
 Bioswale (16%), Meadow (64%), Average trees (5%), Grassy joint flooring (10%), Fixed canopies (10%)
 € 3.856.250,00 / Area TOT 2500mq; € 61,70/mq
- C. Water Park:**
 Meadow (5%), Small trees (5%), Grassy joint flooring (10%), Permeable concrete (5%), Fixed canopies (10%), Retention area (10%), Water square (50%)
 € 18.614.844,00 / Area TOT 2500mq; € 297,84/mq



Paved open spaces example

- A. Meadow (15%), Bioswale (16%), Small trees (10%), Grassy joint flooring (30%), Cool flooring (10%), Canopies (15%), Basins and fountains (4%)**
 € 3.745.312,50 / Area TOT 2500mq; € 59,93/mq
- B. Bioswale (16%), Small trees (10%), Permeable concrete (30%), Cool flooring-HIGH (10%), Fixed canopies (10%), Basins and fountains (9%), Gutters (5%)**
 € 4.863.281,25 / Area TOT 2500mq; € 77,81/mq
- C. Medium trees (10%), Grassy joint flooring (10%), Permeable concrete (15%), Fixed canopies (10%), Water square (50%), Gutters (5%)**
 € 35.142.187,50 / Area TOT 2500mq; € 562,28,84/mq



Buildings example

- A. Green roof (extensive vegetated/semi-vegetated), ventilated facades, fixtures with selective glasses, rainwater harvesting and reuse system**
 € 227.070,00 / Area TOT 1050mq; € 216,26/mq
- B. Green roof (intensive vegetated/semi-vegetated), coat insulation, blinds, rainwater harvesting and reuse system**
 € 248.662,50 / Area TOT 1050mq; € 236,82/mq
- C. Cool roof (medium, mineral membrane reflex white), green walls, blinds, rainwater harvesting and reuse system**
 € 471.397,50 / Area TOT 1050mq; € 448,95/mq

Figure 41: Example of alternative adaptation for specific land use classes (in brackets the percentage of application on the existing land use).

The use of adaptation strategies together with the CSIS model allows one to create adaptation scenarios. This can be carried out through the collaboration between local end-users and experts from the CLARITY team. To assist end-users as they navigate among a complex set of scenarios to identify the best option to be adopted, the main information related to adaptation strategies (climate-benefits, implementation costs and co-benefits) have been captured and aggregated in so called (key) performance indicators. This approach has been widely employed in several application fields [25]. These key indicators are able to quantify specific characteristics but not the overall performance of the adaptation strategies and, consequently, they provide a simplistic assessment for the user's choice. Therefore, Multi-Criteria Decision Analysis (MCDA) [26] offers a proper compromise to solve the problem.

This procedure can be schematised as follows (**Figure 42**):

1. Various Impact Scenarios generation (#1);
2. Comparison of all the generated scenarios through synthetic indicators able to describe the scenarios to quickly assess and compare them (#2-3);
3. Definition of a decision strategy by mapping performance indicators to decision criteria, by assigning weights to indicators in order to enhance the priorities, by assessing the level of "Andness" and "Orness" to be considered (#4-5);
4. Application of the multi-criteria decision approach application in order to obtain a ranking of scenarios with respect to the selected decision strategy (#6-7).

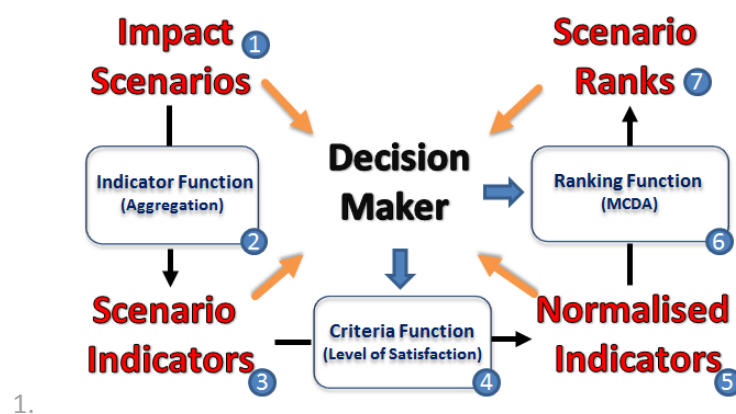


Figure 42: Conceptualisation of Decision Maker (end-user) modelling.

2.5.1 Cost/Benefit Analysis of Adaptation Options (CBA)

The economic impact assessment involves performing a Cost-Benefit Analysis (CBA) on a specific scenario of interest. In order to find the most effect adaptation option or measure (AM), one must do a CBA of all the feasible AMs, including for the case where no AM is undertaken, over a time-frame which is relevant for the project. The AM that shows the most benefits, according to how they are defined, is that which should be favoured. It is necessary to determine which benefits are considered important for the project, e.g. financial in terms of dividing the costs of an investment (e.g. adaptation measures costs) by units of effectiveness, or perhaps in terms of the number of lives saved would be an obvious unit of effectiveness.

The cost efficiency is the act of saving money by performing an activity in a better way. The cost efficiency of an AM is largely based on the avoidance or reduction of the damage costs. The co-benefits generated by an AM are only estimated in qualitative terms, based on the calculation of co-benefits connected to each of them.

Figure 43 summarizes the process to calculate the total benefit value, at the present time, for an adapted scenario, i.e. a baseline scenario with adaptation measures, in relation to events in the future:

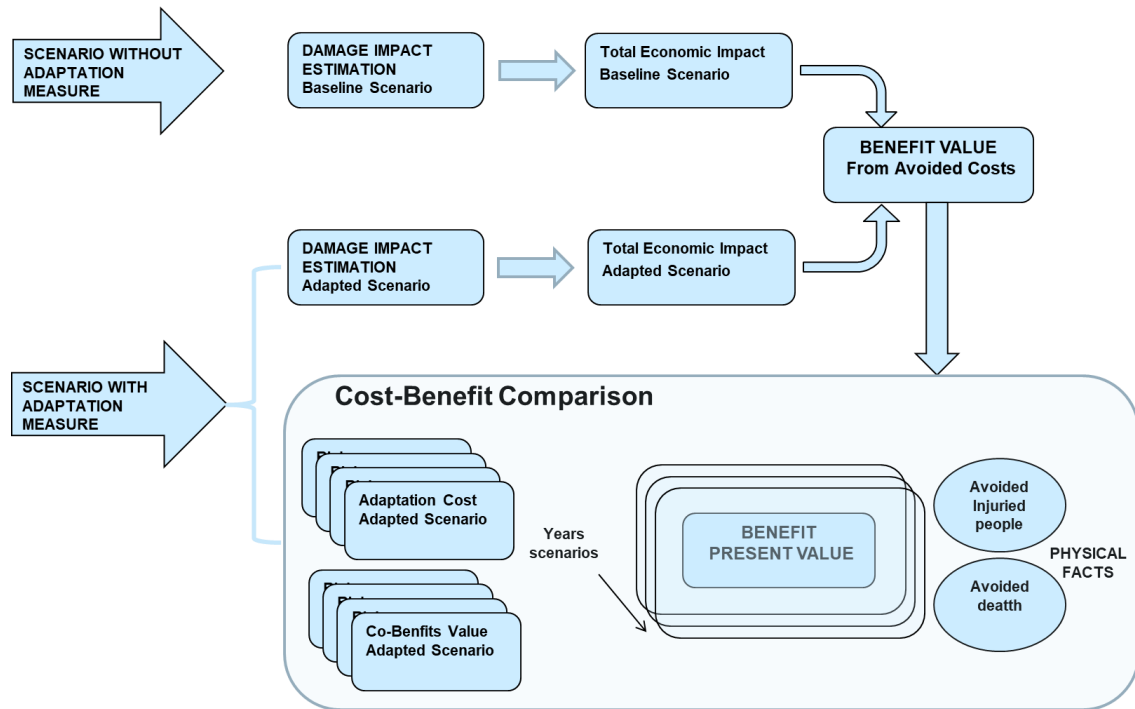


Figure 43: Schematic of the process to calculate the total benefit value of applying an adaptation measure..

2.5.2 Cost Estimation of the Adaptation Measures

To perform the cost estimation, it is necessary to gather the following information for each adaptation measure (AM) that could be implemented:

- Capital costs for new development
- Capital costs for retrofitting
- Operating costs
- Maintenance costs
- New installation duration
- Retrofitting duration

The following tables present the parameters necessary to calculate various aspects of the costs of the AM.

Table 38 shows the parameters concerned with the costs of new development or retrofitting of the selected AM. With this come recurring costs such as the operating and maintenance costs necessary to keep the AM functioning.

Table 39 shows parameters concerned with estimating the benefits of an AM. This is calculated based on the costs avoided when such an AM is implemented, considering the economic impact on both the scenario with and without the AM or set of AMs. In case the event happens each year from t_0+1 to t_f , the Total Benefit Value collects all the “Benefit Value from Avoided Cost in the Adapted Scenario (AS) at t_0 time” calculated year by year from t_0+1 to t_f :

$$TBV_{AS-H-EAR}(t_0) = \sum_{t_j=t_0+1}^{t_f} BV_{AS-H-EAR}(t_j)[1 + I(t_j - t_0)] - C_{AM}(t_0)$$

Table 38: Parameters necessary to calculate the cost of an AM used in a scenario from the current year until a specific year in the future in order to perform the cost-benefit analysis.

Parameters / Acronyms	Description	Data Source
Q_{AM}	Depending on the physical characteristics of the AM, the “Quantity” of the selected adaptation measure can be one of: <ul style="list-style-type: none"> • Number of units (units), or • Number of linear metres (m), or • Number of square meters (m^2), or • Number of cubic meters (m^3). 	CLARITY processing
CCN	Capital Costs for New development: one-off costs incurred on the purchase and installation of the selected AM for new development only.	CLARITY processing
CCR	Capital Costs for Retrofitting: one-off costs incurred on the purchase and installation of the selected AM and to prepare the existing development. These cost calculations are based on the “Quantity” of the selected AM in terms of €/unit, €/m, €/m ² or €/m ³ .	
OC	The Operating Costs are recurring costs (i.e. direct material costs, direct labour, utility costs etc.) required to allow the AM to function.	CLARITY processing
MC	The Maintenance Costs are the costs incurred to keep an item in good condition or good working order (i.e. repairs, replacements, etc.). These are yearly costs and the cost calculation is based on the physical characteristics of the selected AM in terms of €/unit/year, €/m/year, €/m ² /year or €/m ³ /year.	
ND	New Installation Duration is the working duration of the AM in number of years (i.e. the working life of the AM).	CLARITY processing
RD	Retrofitting Duration is the working duration of the AM in number of years (i.e. the working life of the AM).	CLARITY processing
I	Annual Interest Discount Rate 7%	FEMA Discounted Rate
t_0 / t_f	Present year / Future year	System / User input
$CAM(t_0)$	AM Cost Estimation in case of new installation: $C_{AM}(t_0) = \sum_{j=0}^{TRUNC\left[\frac{t_f-t_0}{ND}\right]} CCN \cdot Q_{AM} \cdot [1 + I \cdot j \cdot ND] + (OC + MC) \cdot Q_{AM} \cdot (t_f - t_0)$ AM Cost Estimation in case of retrofitting: $C_{AM}(t_0) = \sum_{j=0}^{TRUNC\left[\frac{t_f-t_0}{RD}\right]} CCN \cdot Q_{AM} \cdot [1 + I \cdot j \cdot RD] + (OC + MC) \cdot Q_{AM} \cdot (t_f - t_0)$ where the TRUNC (x) function removes the fractional part of the number x	Processing

Table 39: Parameters necessary to calculate the benefits that arise from an AM deployed in relation to events that could happen in a specific time in the future. The benefits are calculated using the Avoided Costs Method, considering both economic impact with and without the AM or set of AMs.

Parameters / Acronyms	Description	Data Source
t_0 / t_f	Present year / Future year	System / User input
BS	Baseline Scenario	User input
H	Specific Hazard	User input
EAR	Specific Element at Risk	User input
$C_{AM}(t_0)$	Cost of Specific Adaptation Measure at t_0	CLARITY processing
AS	Specific Adapted Scenario: Baseline Scenario modified with a Specific Adaptation Measure	CLARITY processing
$TEI_{BS-H-EAR}(t_f)$	Total Economic Impact on the Baseline Scenario at t_f	CLARITY processing
$TEI_{AS-H-EAR}(t_f)$	Total Economic Impact on the Adapted Scenario at t_f	CLARITY processing
$BV_{AS-H-EAR}(t_f)$	Benefit Value from Avoided Cost in the Adapted Scenario (AS) at t_f : $TEI_{BS-H-EAR}(t_f) - TEI_{AS-H-EAR}(t_f)$	Processing
I	Annual Interest Discount Rate: 7%	FEMA Discounted Rate
$BV_{AS-H-EAR}(t_0)$	Benefit Value from Avoided Cost in the Adapted Scenario (AS) at t_0 : $BV_{AS-H-EAR}(t_f) \times [1+I \times (t_f - t_0)]$	Processing
$TBV_{AS-H-EAR}(t_0)$	Total Benefit Value in the Adapted Scenario (AS) at t_0 time: $BV_{AS-H-EAR}(t_0) - C_{AM}(t_0)$	Processing

The Cost-Effectiveness Index of AMs, presented in **Table 40**, is calculated by dividing the costs of an investment (e.g. AM cost) by units of effectiveness. As a unit of effectiveness one could use the number of saved lives or the number of injured people. In order to properly compare the effectiveness of the applicable AMs (on the same baseline scenario, with specific hazard and specific element at risk), it is necessary to fix the “cost” (and not the quantity) for the AMs and then count e.g. the number of injured people or saved lives in order to determine the Cost Effectiveness Index. The index is a function of the costs of the applicable AMs, and a year t_f in the future.

Table 40: Cost Effectiveness Index of AMs.

Parameters / Acronyms	Description	Data Source
t_0 / t_f	Present year / Future year	System / User input
BS	Baseline Scenario	User input
H	Specific Hazard	User input
EAR	Specific Element at Risk	User input
$C_{AM}(t_0)$	Cost of Specific Adaptation Measure (fixed value)	CLARITY processing
AS	Specific Adapted Scenario: Baseline Scenario modified with a Specific Adaptation Measure	CLARITY processing
$IP_{AS-H-EAR}$	Number of Injured People in the Specific Adapted Scenario	CLARITY processing
$CE_{S AS-H-EAR}$	Cost Effectiveness Index of a specific AM: $CE_{S AS-H-EAR} = C_{AM}(t_0) / IP_{AS-H-EAR}(t_0)$	Processing

The Cost-Efficiency Index of AMs, presented in Table 41, is the act of saving money by performing an activity in a better way. The cost efficiency of an AM is largely based on the avoidance or reduction of the damage costs. In order to properly compare the efficiency of the applicable AMs (on the same baseline scenario, with a specific hazard and a specific element at risk), it is necessary to fix the “cost” (and not the quantity) for the applicable AMs and then calculate the “Benefit Value from Avoided Costs” in order to determine the Cost Efficiency Index values. The Index is a function of the costs of the applicable AMs, and a year t_f , in the future.

Table 41: Cost Efficiency Index of AMs.

Parameters / Acronyms	Description	Data Source
t_0 / t_f	Present year / Future year	System / User input
BS	Baseline Scenario	User input
H	Specific Hazard	User input
EAR	Specific Element at Risk	User input
$C_{AM}(t_0)$	Cost of Specific Adaptation Measure (fixed value)	CLARITY processing
AS	Specific Adapted Scenario: Baseline Scenario modified with a Specific Adaptation Measure	CLARITY processing
$BV_{AS-H-EAR}(t_0)$	Benefit Value from Avoided Cost in the Adapted Scenario (AS) at t_0 time.	CLARITY processing
$CE_{y AS-H-EAR}$	Cost Efficiency Index of a specific Adaptation Measure: $CE_{y AS-H-EAR} = BV_{AS-H-EAR}(t_0) / C_{AM}(t_0)$	Processing

3 Expert Services

The work done on the four demonstration cases is presented here.

While in deliverable D2.3 the work done in each demonstration case is described following the steps of the EU-GL methodology, the focus here is about the scientific background and the models/ tools used to get high resolution information at the local scale and to assess adaptation options. Tables at the beginning of each DC section provide an overview of the whole workflow in relation to the EU-GL methodology.

3.1 DC1

DC1 implementation aims to demonstrate the outcomes of CLARITY Expert Services in assessing the benefit of integrating adaptation measures in urban redevelopment/retrofitting projects, with a specific focus on heat waves, pluvial flooding and landslide hazards. The implications related to multi-risk conditions related to geophysical hazards, in particular earthquake and volcanic eruptions, will be considered at a later stage of the DC implementation, based on the previous studies already conducted on the Naples area by PLINIVS-LUPT Study Centre, as centre of competence of the Italian Department of National Civil Protection.

The workflow of DC1 according to the EU-GL methodology described in D3.1 is summarized in **Table 42**.

Table 42: Overview of the workflow of DC1 and its relation to the EU-GL methodology.

Hazard Characterisation	Element at risk	Vulnerability	Impact	Adaptation Options
Heat waves	People	High for very young/old age groups	Excess heat mortality Productivity loss	Green roofs Air-conditioned public transport
Pluvial Flooding	Buildings Infrastructure	High for objects in poor drainage areas.	Damage Economic costs for repair / resource unavailability	Increased green areas
Landslides	Buildings Infrastructure	High for objects in mountainous/hilly terrains.	Damage Economic costs for repair / resource unavailability	Increased number of trees / green areas

As outlined in D3.1, the key objectives for the implementation are outlined by the DC1 "high-level" user stories:

- US-DC1-100 Climate Adaptive Planning;
- US-DC1-200 Adaptive Climate Design Guidelines and Construction Regulations.

The science support has concerned itself with the characterization of hazards at the local scale, so to identify reference event(s) to be considered in the impact scenario analyses object of the Expert Service, in relation to which the opportunity of integrating adaptation measures in the urban infrastructure projects identified by the local end-user partner, the Municipality of Naples (see D2.2).

The Municipality of Naples has officially included in January 2020 CLARITY results in the "Preliminary Environmental Report of the City Plan (Rapporto Ambientale Preliminare del PUC del Comune di Napoli,

<http://www.comune.napoli.it/flex/cm/pages/ServeAttachment.php/L/IT/D/1%252F9%252F2%252FD.e7456b9ad07748ac7a95/P/BLOB%3AID%3D37912/E/pdf>, from p. 186)

The study of the “local effect” determined by the feature of urbanized areas and geomorphology of the territory has implied the collection and transformation of relevant datasets used as input of MUKLIMO_3 model (heat waves), PLINIVS-LUPT Flood simplified model (flooding) and PLINIVS-LUPT Landslide model (Figure 44). The following sections synthetically illustrate the work carried out for the three identified hazards.

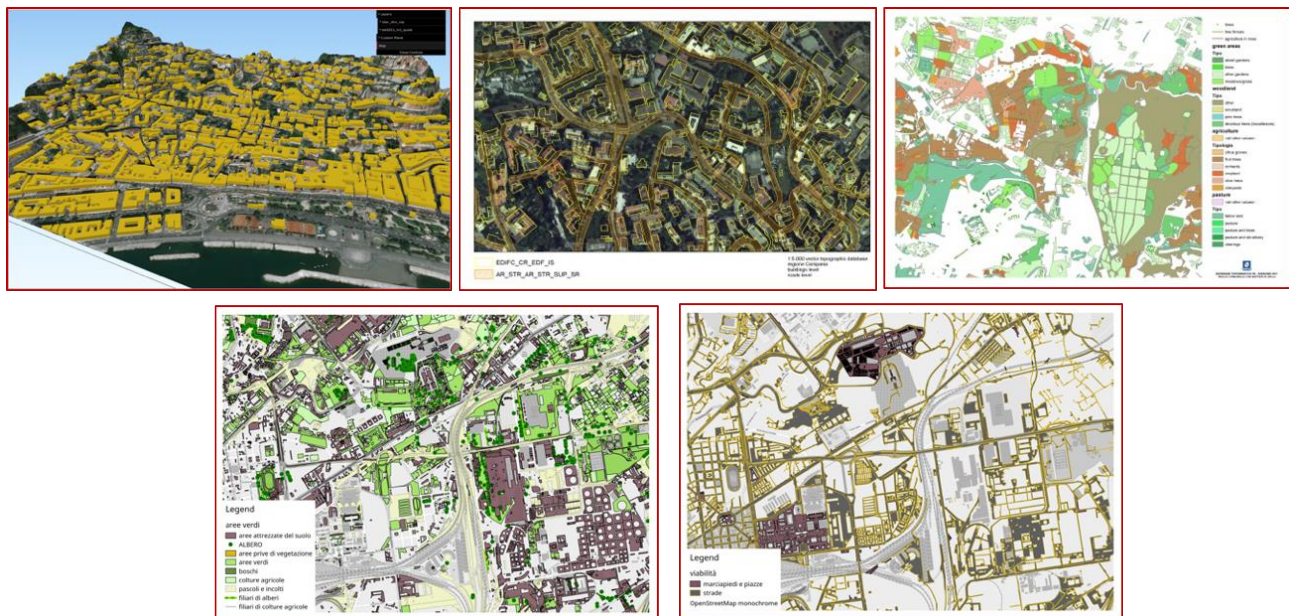


Figure 44: Example of data collected in Naples area used as input of the models applied to identify the “local effect” hazard conditions.

3.1.1 Climate change scenarios for the city of Naples

Naples, as many urban areas in the Mediterranean Europe, has already been facing in recent years a significant climatic variation compared to the 1971-2001 “historical” reference period. The last few years have shown a constant increase in the minimum and maximum temperatures (to which more frequent episodes of heat waves are associated), while seasonal precipitation patterns have seen an increasingly marked alternation between periods of drought and extreme events characterized by high rainfall concentrated in a few hours (which cause episodes of superficial flooding, even critical ones)¹⁰.

The available simulations referring to future scenarios (until 2100), confirm these trends, with uncertainties related to the intensity of the expected climate change related to different of GHG emission scenarios on a global scale.

¹⁰ In the recent publication of OMS-UNFCCC “Climate and Health Country Profile - Italy (2018)”, developed in collaboration with the Health Department, the climate models for Italy produced by “Centro Euro Mediterraneo per I Cambiamenti Climatici (CMCC)” they estimate an increase in temperatures for the end of the century between + 5.1 ° C and + 1.6 ° C depending on the emission scenarios. The climate models predict an increase in the numbers of heat wave days and days of heavy rain, and an increase in the duration of drought periods (Source: Health Department, National Prevention Plan for the effects of heat on health, guidelines for prevention, heat waves and air pollution, July 2019).

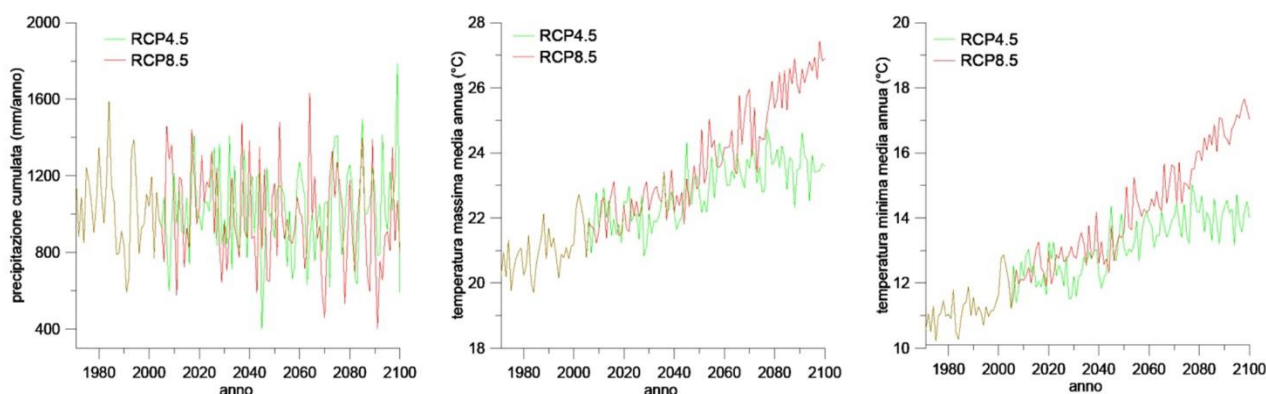


Figure 45: Annual averages in the period 1971-2000 of rainfall and air temperatures for the city of Naples. For the 1971-2000 period, annual cumulative precipitation values (left), average maximum temperature (centre) and average minimum temperature (right) up high for the Capodichino Station; on the 1971-2005 lapse, models are forced through observational datasets (20C3M) while for 2006-2100 lapse are considered the concentration scenarios RCP4.5 (green) and RCP8.5 (red). Source: CMCC – Centro Euro mediterraneo sui Cambiamenti Climatici (in [27]).

Annual average values elaborated with statistical methods from observations on single weather stations (**Figure 45**), however, do not allow the representation of the critical issues that cities face regarding climate change. It is necessary to have more precise information about the frequency of extreme temperatures and precipitation events (often concentrated in limited periods of the year and therefore not represented by annually averaged values) and to consider how the impacts of these extreme events can be aggravated by specific urban characteristics, such as the urban heat island effect and surface run-off conditions.

The CLARITY project has therefore focused on defining these aspects, identifying in detail the increase in frequency of heat waves and heavy rainfall until 2100, and by elaborating an accurate modelling of urban morphology and land use to capture the effect of built environment features on the urban microclimate.

The processing of the different datasets through the simulation models developed by the PLINIVS-LUPT Study Center for CLARITY allows the identification of the expected levels of hazard related to heat waves and surface flooding. This information forms the basis of the corresponding impact models, currently being calibrated, which will allow one to identify the effects of heat waves on the population (in terms of impacts on human health, including the increase in mortality), and the effects of flooding on buildings (in terms of interruption of road networks and economic damage to property or production activities).

3.1.1.1 Heat waves

Heat waves occur when high temperatures are recorded for several consecutive days, often associated with high humidity, strong solar radiation and absence of ventilation. These weather-climatic conditions can represent a risk to the health of the population (Source: Italian Ministry of Health, 2019).

Figure 46, **Figure 47** and **Figure 48** show the first results for the mean annual number of summer days, hot days and tropical nights, respectively, for the baseline period 1971-2000. These are based on urban climate simulations at 250 m resolution and an ensemble of historical (uncorrected) EURO-CORDEX simulations listed in **Table 43**. Urban Atlas land use data¹¹ complemented with CORINE land cover data¹² and standardized representative parameters regarding building structure, percentage of soil sealing and vegetation information were used as input for the urban climate simulations.

¹¹ <https://land.copernicus.eu/local/urban-atlas/urban-atlas-2012>

¹² <https://land.copernicus.eu/pan-european/corine-land-cover/clc-2012>

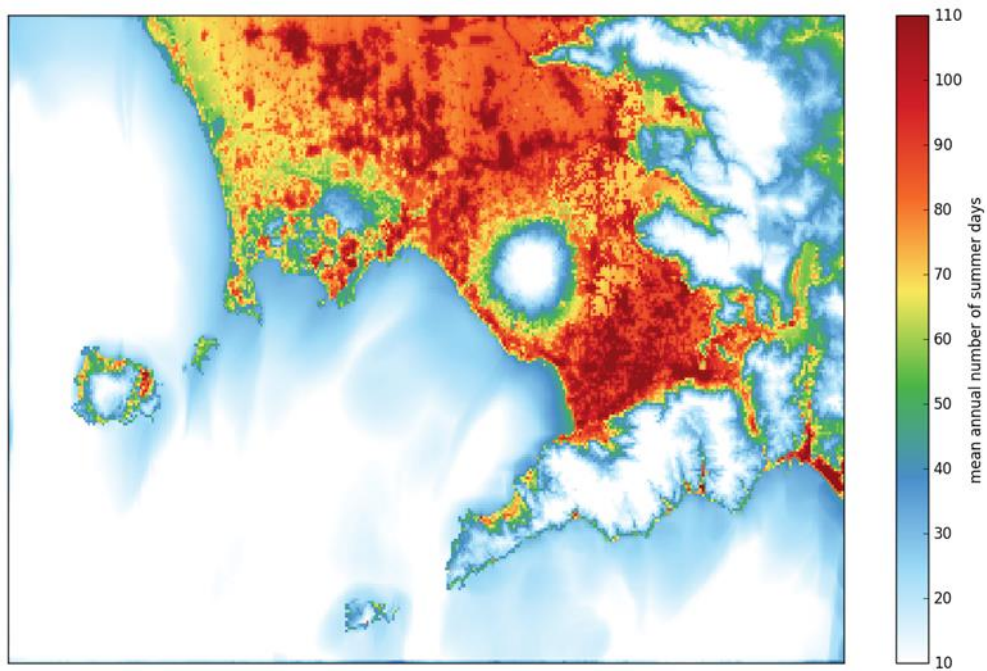


Figure 46: Mean annual number of summer days (daily maximum temperature > 25°C) derived from the cuboid method and MUKLIMO_3 urban climate model results, based on long-term climate information from EURO-CORDEX regional climate historical scenarios for the period 1971-2000.

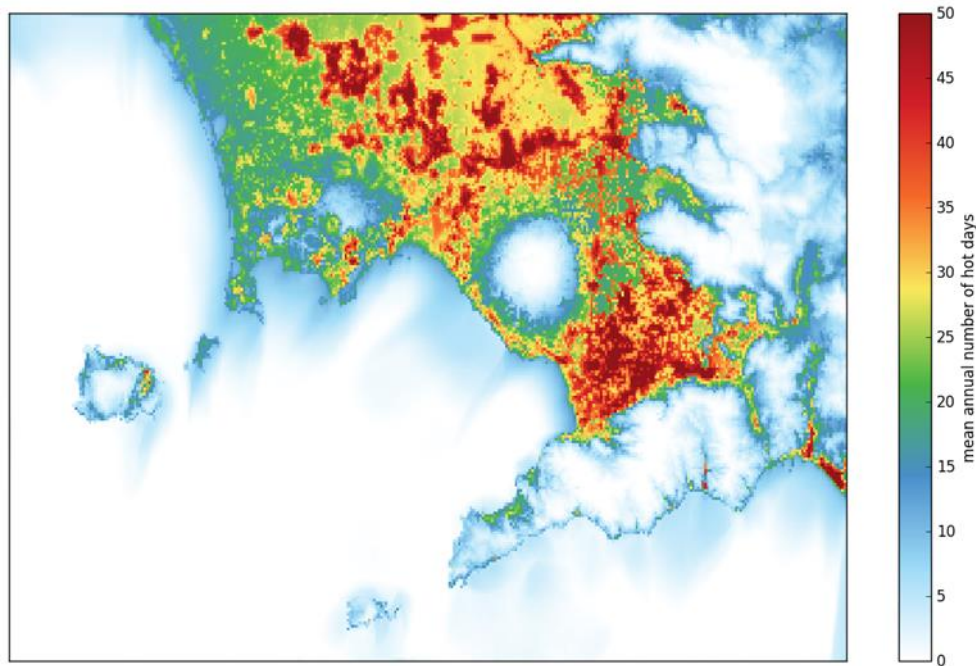


Figure 47: Annual average number of hot days (daily maximum temperature > 30 °C) during the period 1971-2000.

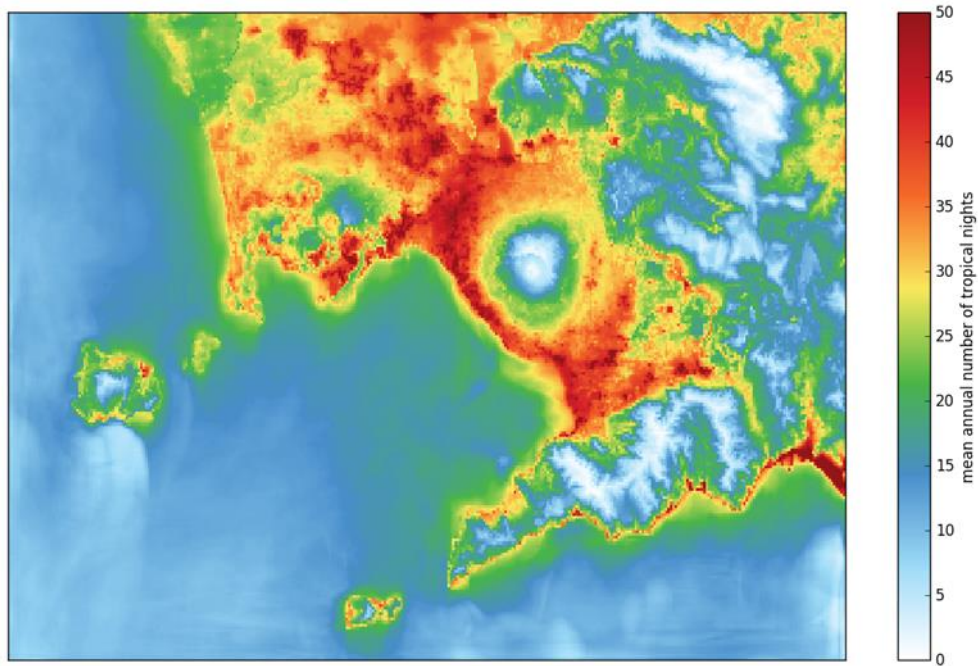


Figure 48: Annual average number of tropical nights (daily minimum temperature > 20 °C) during the period 1971-2000.

Table 43: EURO-CORDEX climate model configurations used as input for the derivation of urban climate indices.

Institute	Driving GCM	RCM
DMI	ICHEC-EC-EARTH	HIRHAM5
	NCC-NorESM1-M	HIRHAM5
KNMI	ICHEC-EC-EARTH	RACMO22E
SMHI	CNRM-CERFACS-CNRM-CM5	RCA4
	ICHEC-EC-EARTH	RCA4
	IPSL-IPSL-CM5A-MR	RCA4
	MOHC-HadGEM2-ES	RCA4
	MPI-M-MPI-ESM-LR	RCA4

Analysis of EURO-CORDEX data produced estimates of the number of events expected in the period 2011-2100, starting from the historical series referring to the period 1971-2011. The projections were made with reference to the emission scenarios formulated by IPCC - Intergovernmental Panel on Climate Change of ONU: RCP8.5 (which reflects the current global warming trend) and RCP4.5 (which reflects a scenario of gradual reduction of emissions on a global scale). The graphs (**Figure 49**, **Figure 50**, **Figure 51**) show the summary of some extreme events as significant for the Naples area, being similar to recorded thresholds in the last 5 years, and the most likely in the future, i.e. heat waves lasting 3, 6, and 9 days, with temperatures of 34-38°C.

The analysis of the data shows that similar events recorded in recent years (36 °C for periods even longer than 6 consecutive days) will increase significantly in terms of frequency and intensity in the next thirty years, up to the second half of the century at intensity levels so far not occurred (over 9 consecutive days with temperatures above 38 °C).

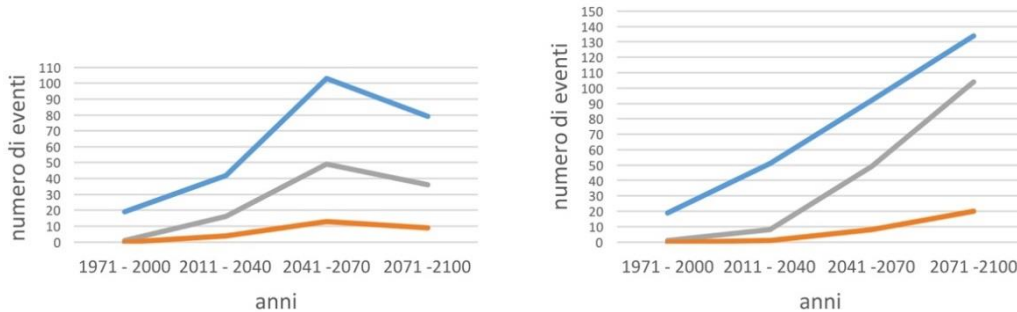


Figure 49: Heat waves lasting 3 days for the period 1971-2100. The data for the period 1971-2011 show the number of events that have actually occurred, while the events that will occur in the period 2018-2100 refer to the RCP4.5 (left) and RCP8.5 (right) emission scenarios. The three curves in each panel represent the threshold temperatures: 34 °C (blue), 36 °C (grey), 38 °C (orange).

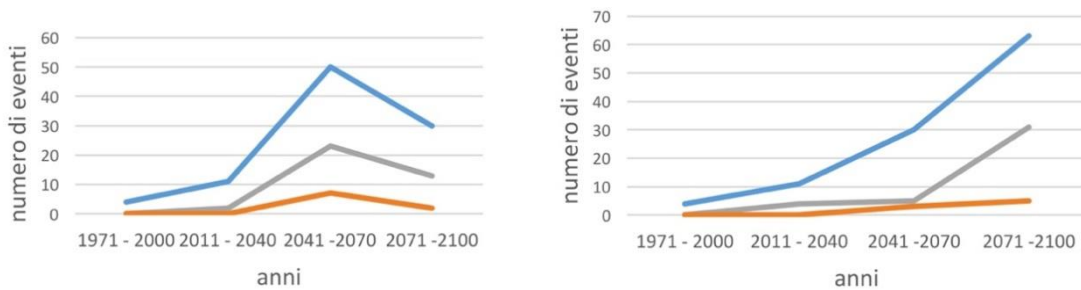


Figure 50: Heat waves lasting 6 days for the period 1971-2100. The data for the period 1971-2011 show the number of events that have actually occurred, while the events that will occur in the period 2018-2100 refer to the RCP4.5 (left) and RCP8.5 (right) emission scenarios. The three curves in each panel represent the threshold temperatures: 34 °C (blue), 36 °C (grey), 38 °C (orange).

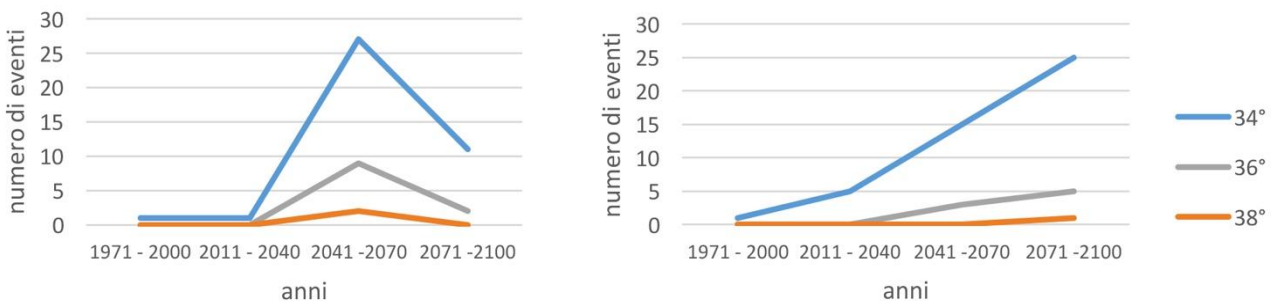


Figure 51: Heat waves lasting 9 days for the period 1971-2100. The data for the period 1971-2011 show the number of events that have actually occurred, while the events that will occur in the period 2018-2100 refer to the RCP4.5 (left) and RCP8.5 (right) emission scenarios. The three curves in each panel represent the threshold temperatures: 34 °C (blue), 36 °C (grey), 38 °C (orange).

3.1.1.2 Heavy rainfall

As for the heat waves, the increased extreme precipitation events represent a signal of the ongoing climate change. Similar events will be more frequent and more intense in the future, with high amounts of rain in limited periods of time, which indicate the transition towards sub-tropical and tropical climatic conditions. The projection of sub-daily precipitation is scientifically complex and accordingly observations of the daily trends are assimilated into time periods of less than 6 hours, which is a recurring characteristic in the case of Naples. **Figure 52** shows the number of expected events in which the amount of rain exceeds the minimum threshold observed in recent storms in Naples (all above 30 mm / day, but concentrated in a few hours). The analysis of the data shows that events similar to those recorded in recent years will increase significantly in terms of frequency and intensity in the next thirty years, up to, in the second half of the century, levels of intensity which have not yet occurred (100 mm / day).

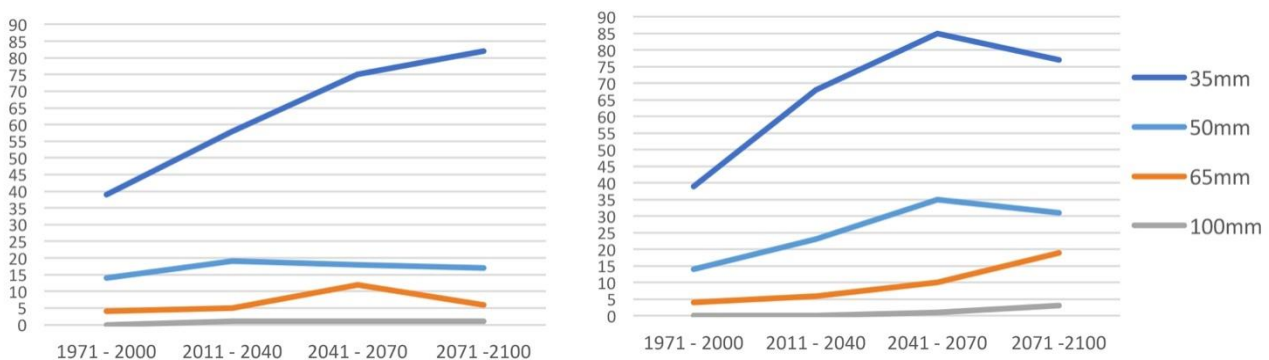


Figure 52: Extreme precipitation events for the period 1971-2100. The data for the 1971-2011 period show the number of events that have actually occurred, while the events that will occur in the period 2018-2100 refer to the RCP4.5 (left) and RCP8.5 (right) emission scenarios.

Analysis of the "local effect" and supporting data for municipal urban planning

As mentioned, the sole analysis of data derived from the observation of past events recorded by local weather stations and projected in the future through statistical "downscaling" of Regional Climate Models (RCM) cannot capture the microclimatic variability linked to the settlement characteristics of the urban environment. The urban morphology and the land cover greatly influence the thermal stress conditions and the ability to absorb rainwater, resulting in a significant diversification of the main hazard parameters.

In order to provide a support for urban planning, specific models have been developed that are able to capture the "local effect" (Section 2.2 of D3.2 and Section 2.1.2), and therefore to provide more precise information on the climate adaptation strategies to be implemented in different parts of the city. The first essential element of information is the creation of a GIS database of land use that contains all parameters necessary for the "local effect" simulations. The datasets shared by the City of Naples (currently used for planning purposes at various levels) have been verified and corrected (in terms of geometries and intended uses) through comparisons with recent high-resolution satellite images (Pleiades 2018 data), and integrated with the input parameters required by the models.

The resulting land use map (**Figure 53**) is extremely detailed, and adds to the geometric and morphological data of buildings and open spaces, also essential elements not present in ordinary cartographies, such as the presence of trees and the characteristics of albedo, emissivity and run-off of the different urban surfaces.

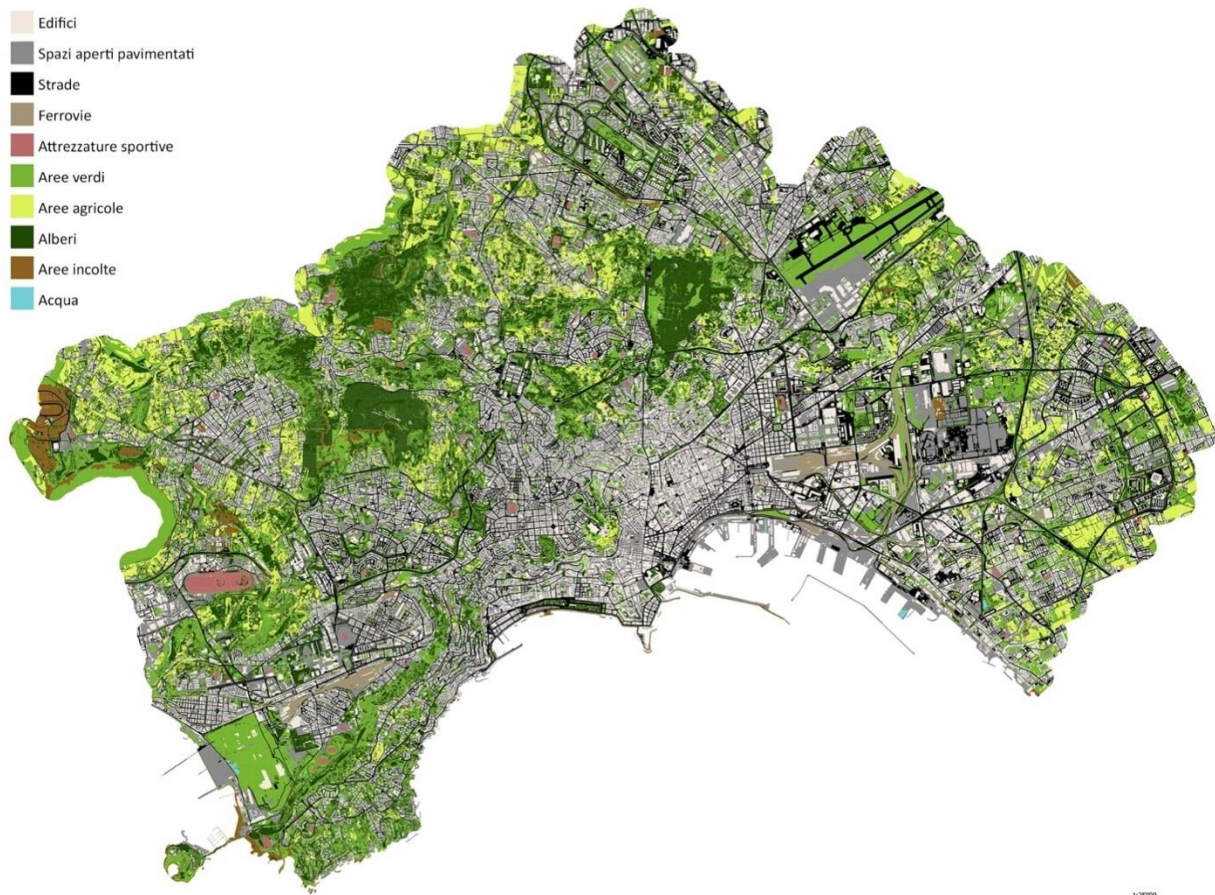


Figure 53: Reworked land use map used by simulation models of the “local effect” for heat waves and floods (Source: Comune di Napoli / PLINIVS-LUPT, CLARITY project).

3.1.2 Heat waves – local effect

The thermal stress variation in the different city areas is simulated through the mean radiant temperature (Tmrt) indicator, which is widely validated in the literature as representative of the perceived outdoor comfort (see e.g. [28], [29]). This is essentially derived from (1) air temperature; (2) surface temperature; (3) urban morphology and surface characteristics of buildings and open spaces. Although Tmrt does not consider wind as a parameter, normally extremely low wind speeds are recorded during heat waves, and therefore the simplification adopted, widely recognized in the scientific literature (e.g. [30], [31]), it is suitable in relation to the objectives of the simulation. **Figure 54** shows Tmrt for the Naples region.

In addition to the data processed by ZAMG and PLINIVS-LUPT related to climate observations and projections, and to the new GIS database developed by the City of Naples and PLINIVS-LUPT, it was necessary to acquire data on surface temperatures in heat wave conditions. During the calibration of the model, the information developed was reworked starting from Landsat satellite data, as part of the Metropolis project [27], referring to the day of 19 July 2015, corresponding to a 3-day heat wave with maximum temperatures of about 36-37 °C.

The choice of such conditions is motivated by the goal to identify, during the calibration phase, heat wave conditions that already currently occur in the city of Naples, and which certainly will occur again, with a high probability of aggravation both in terms of number of consecutive days and temperature thresholds.

Processing of the model's input parameters has allowed a first simulation of a "typical" heat wave to be performed, which has a high probability of occurring considerably more often in the coming years. Once

the model calibration phase has been completed, similar simulations will be developed for heat waves with higher temperature thresholds.

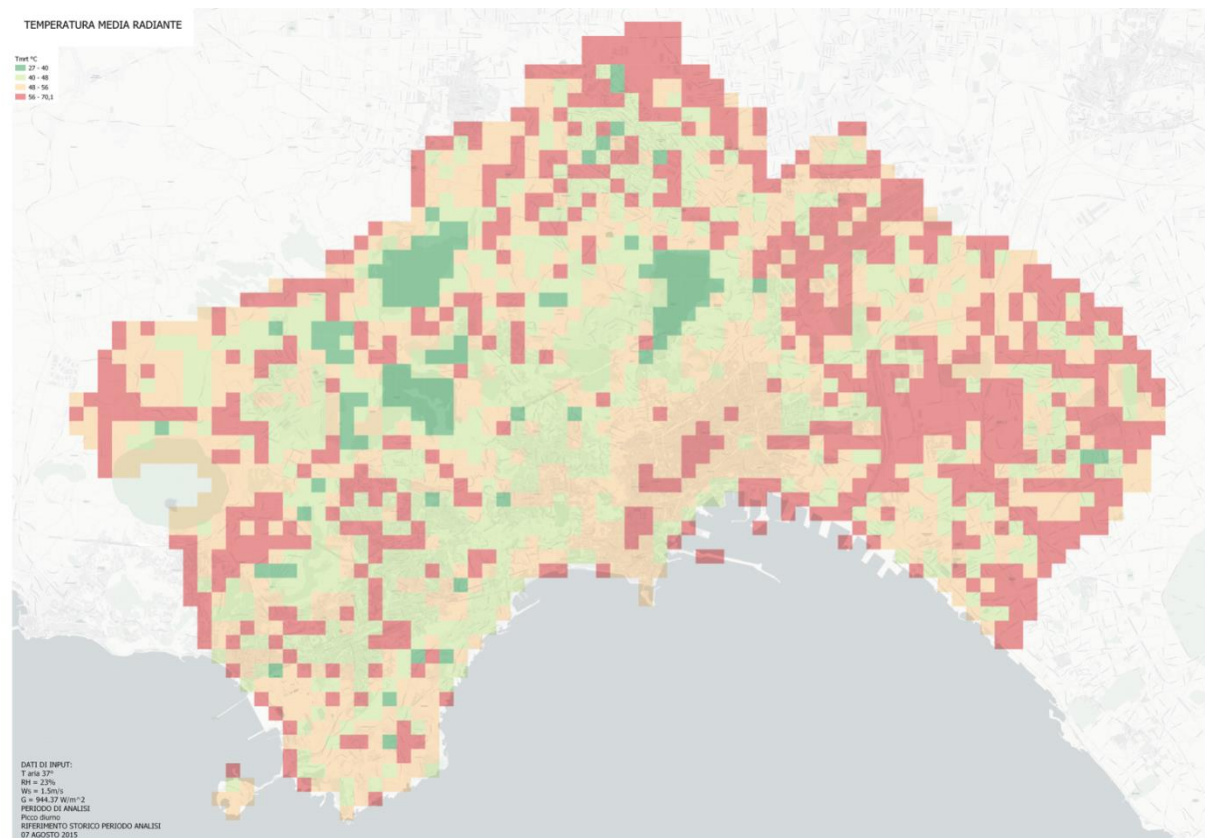


Figure 54: Mean radiant temperature map for a typical day of heat wave with air temperature of 36-37 °C (on grid 250 m × 250 m). (Source: PLINIVS-LUPT, CLARITY project).

Each cell of the grid can be analysed more in detail, so to determine in which extent the specific land uses and the building-open space configurations contribute to higher Tmrt values and therefore higher heat outdoor discomfort and associated health risks.

Figure 55, **Figure 56** and **Figure 57** show some results related to urban areas in the ancient city centre, in the west (Rione Traiano) and east (Ponticelli) areas of Naples. Such detailed analyses highlight some aspects that link urban morphology and land use to microclimatic conditions. In the ancient centre area (**Figure 55**), the building density determines shading conditions that reduce thermal stress. In bigger squares, differences between cooler green areas and overheated asphalt roads can be noticed. Within the courtyards of historic buildings differences can be observed whereby smaller courtyards are cooler due to greater shading. The presence of green areas and trees represents a thermal stress reduction factor in the larger courtyards. In the Rione Traiano (**Figure 56**) and Ponticelli (**Figure 57**) areas, the greater separation between the buildings and the fewer trees result in high Tmrt, especially in the case of Ponticelli.

The model also allows further simulations of the perceived discomfort conditions through the UTCI indicator (Universal Thermal Climate Index, [32]), as well as simulations on the expected impacts on human health, including the increase in mortality (currently being calibrated). The UTCI represents the main indicator of thermal stress in urban open spaces, and can be referred to a scale of discomfort linked to the different ranges observed (**Table 44**). The damage classes are calibrated with reference to the more vulnerable population groups (children under 15 and seniors over 65) for the Naples climate zone. An example of the UTCI for Naples is shown in **Figure 58**.



Figure 55: Detailed analysis of Tmrt in an area of the ancient centre, for a typical heat wave day with an air temperature of 36-37 °C. (Source: PLINIVS-LUPT, CLARITY project).

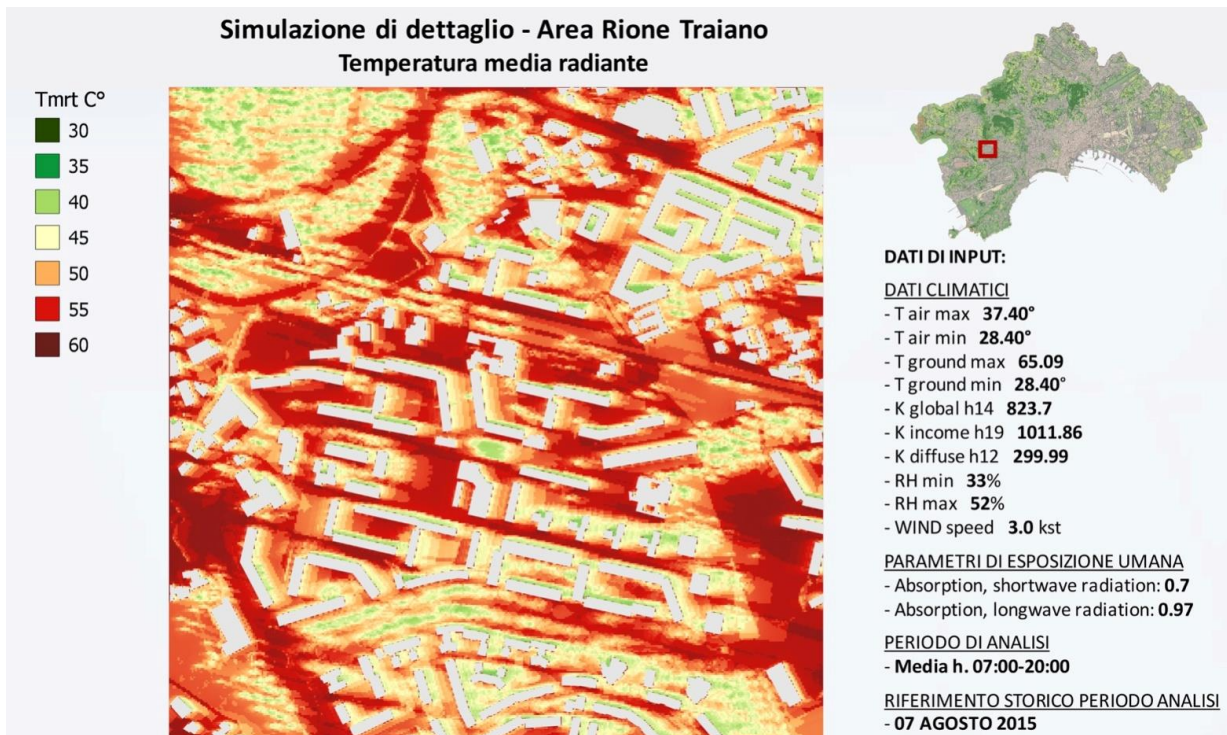


Figure 56: Detailed analysis of Tmrt in the Rione Traiano area, for a typical heat wave day with an air temperature of 36-37 °C. (Source: PLINIVS-LUPT, CLARITY project).

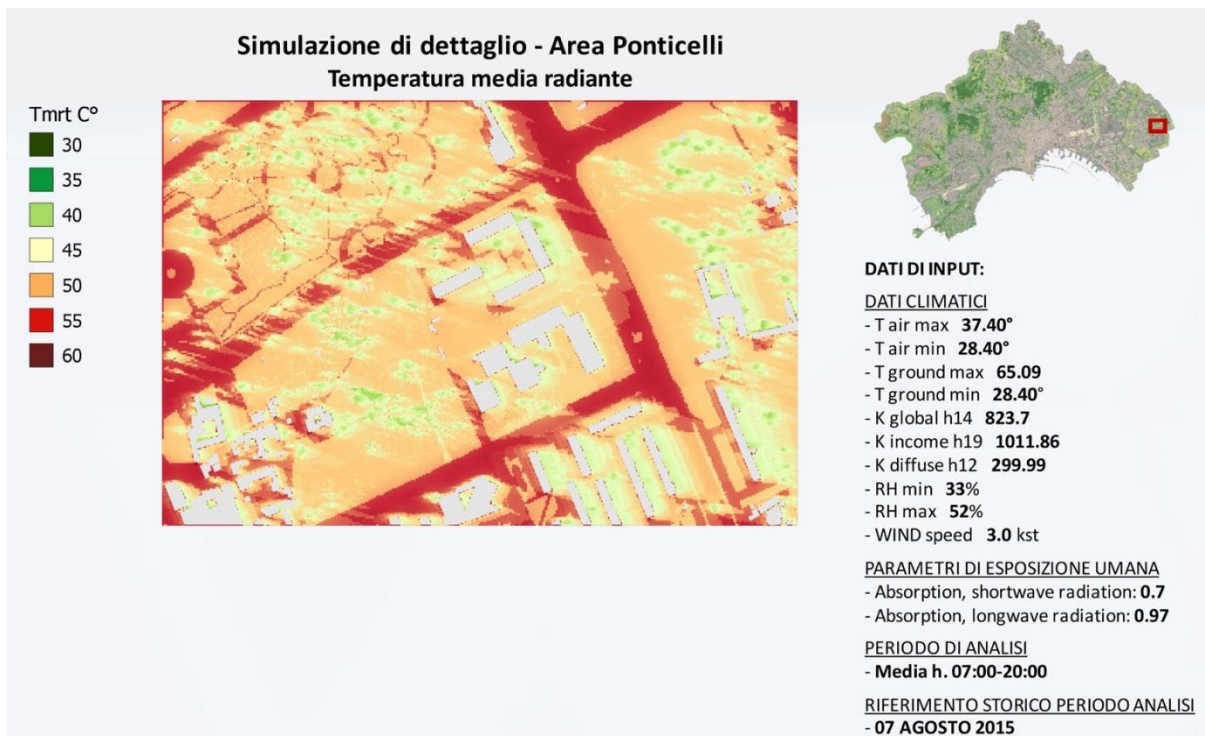


Figure 57: Detailed analysis of Tmrt in the Ponticelli area, for a typical day of heat wave with an air temperature of 36-37 °C. (Source: PLINIVS-LUPT, CLARITY project).

Table 44: Classes of damage from thermal stress related to UTCI values, referring to the more vulnerable population groups (children under 15 years and elderly over 65 years) for the Naples climate zone. (Source: PLINIVS-LUPT, CLARITY project).

Damage class	Description	UTCI
D0	No Damage	26
D1	Level of caution (moderated heat stress)	32
D2	Level of caution (strong heat stress)	38
D3	Damage (very hard heat stress)	46
D4	Extreme damage (extreme heat stress)	> 46

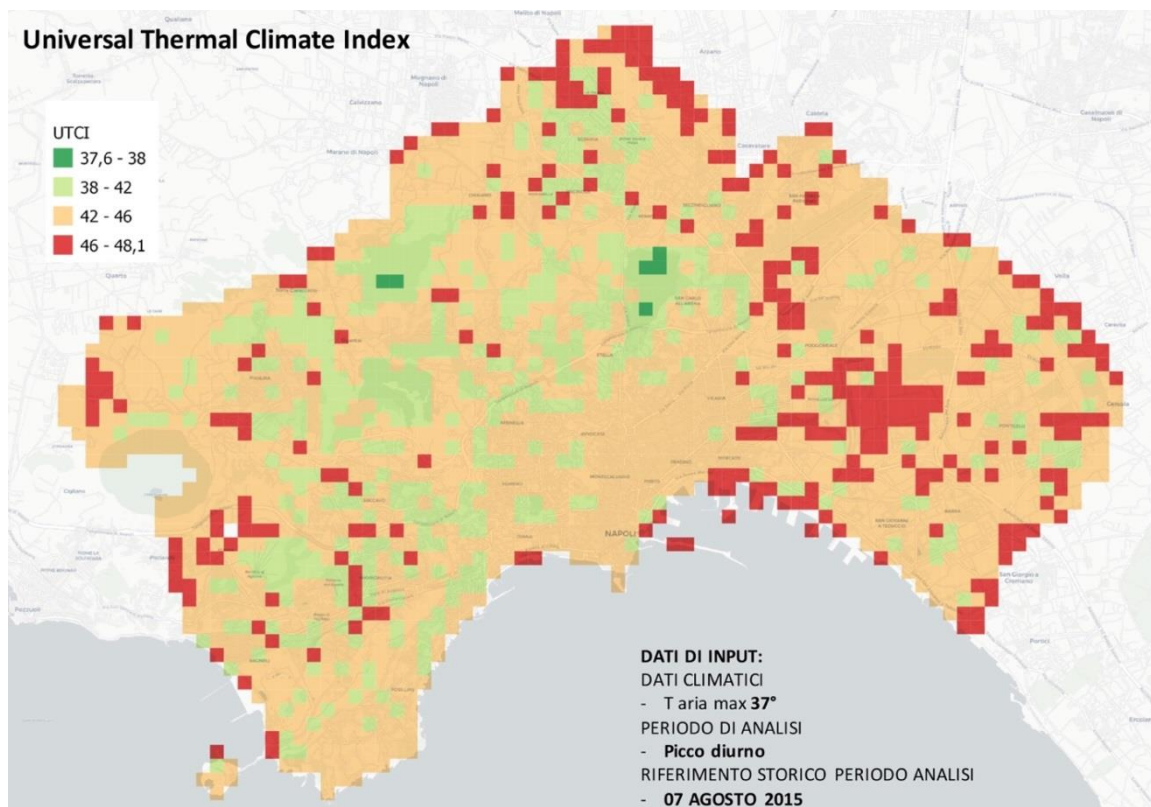
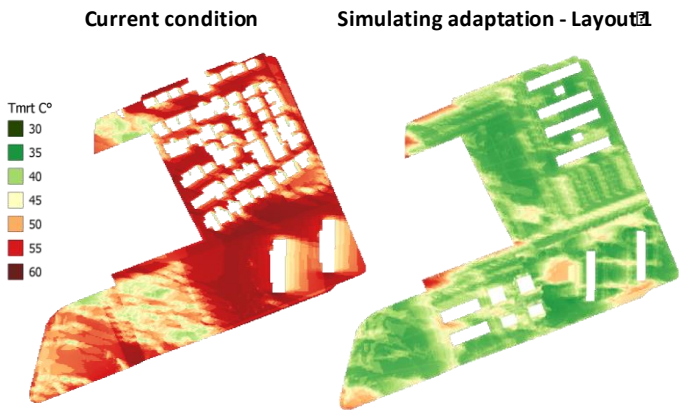


Figure 58: Universal Thermal Climate Index (UTCI) map for a typical day of heat wave with an air temperature of 36-37 ° C (on 250 m x 250 m grid). (Source: PLINIVS-LUPT, CLARITY project).

Following specific requests from the Municipality of Naples to provide support to the implementation of the Ponticelli Urban Regeneration plan, further expert analyses have been produced in this area of the city. These have assessed the effect of different configurations of building and open spaces, as well as of different surface covers, starting from the baseline projects developed by the Social Housing Department, in charge of implementing the plan.

The following figures show the first tests carried out using SOLWEIG in combination with an original parametric workflow developed in Grasshopper, based on the combination of available plug-ins such as Ladybug, Honeybee and ENVI-met.



INPUT:

CLIMATE DATA

- T_{air}max 37.40°
- T_{air}min 28.40°
- T_{ground} max 65.09
- T_{ground} min 28.40°
- K_{global} 14.323.7
- K_{in} 19.011.86
- K_d 12.299.99
- RH_{min} 33%
- RH_{max} 52%
- WIND speed 3.0 kst

HUMAN EXPOSURE PARAMETERS

- Absorption, shortwave radiation: 0.7
- Absorption, longwave radiation: 0.97

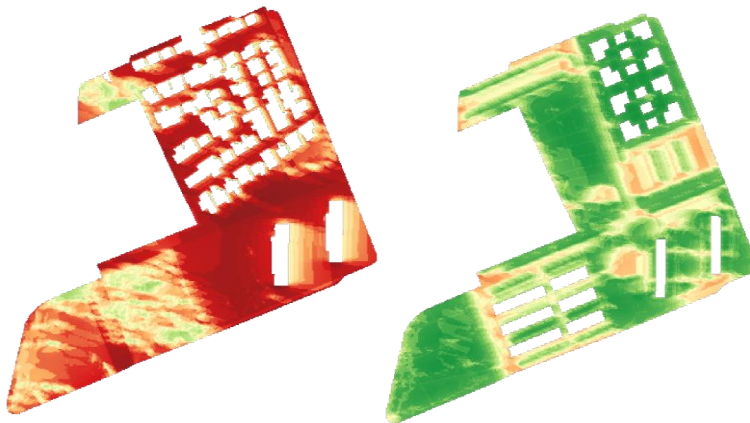
ANALYSIS PERIOD

- Mean h. 07:00-20:00

HISTORICAL REFERENCE ANALYSIS PERIOD

- 07 AUGUST 2015

Current condition Simulating adaptation – Layout 2



INPUT:

CLIMATE DATA

- T_{air}max 37.40°
- T_{air}min 28.40°
- T_{ground} max 65.09
- T_{ground} min 28.40°
- K_{global} 14.323.7
- K_{in} 19.011.86
- K_d 12.299.99
- RH_{min} 33%
- RH_{max} 52%
- WIND speed 3.0 kst

HUMAN EXPOSURE PARAMETERS

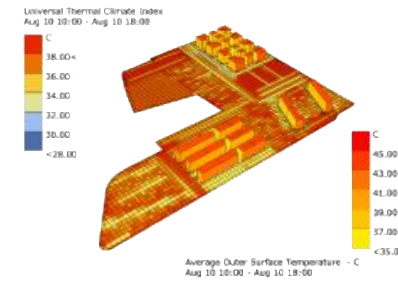
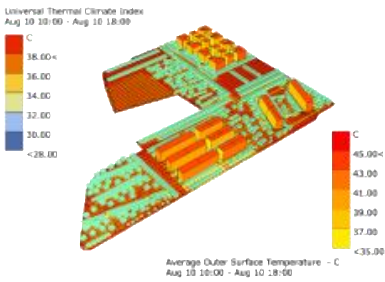
- Absorption, shortwave radiation: 0.7
- Absorption, longwave radiation: 0.97

ANALYSIS PERIOD

- Mean h. 07:00-20:00

HISTORICAL REFERENCE ANALYSIS PERIOD

- 07 AUGUST 2015



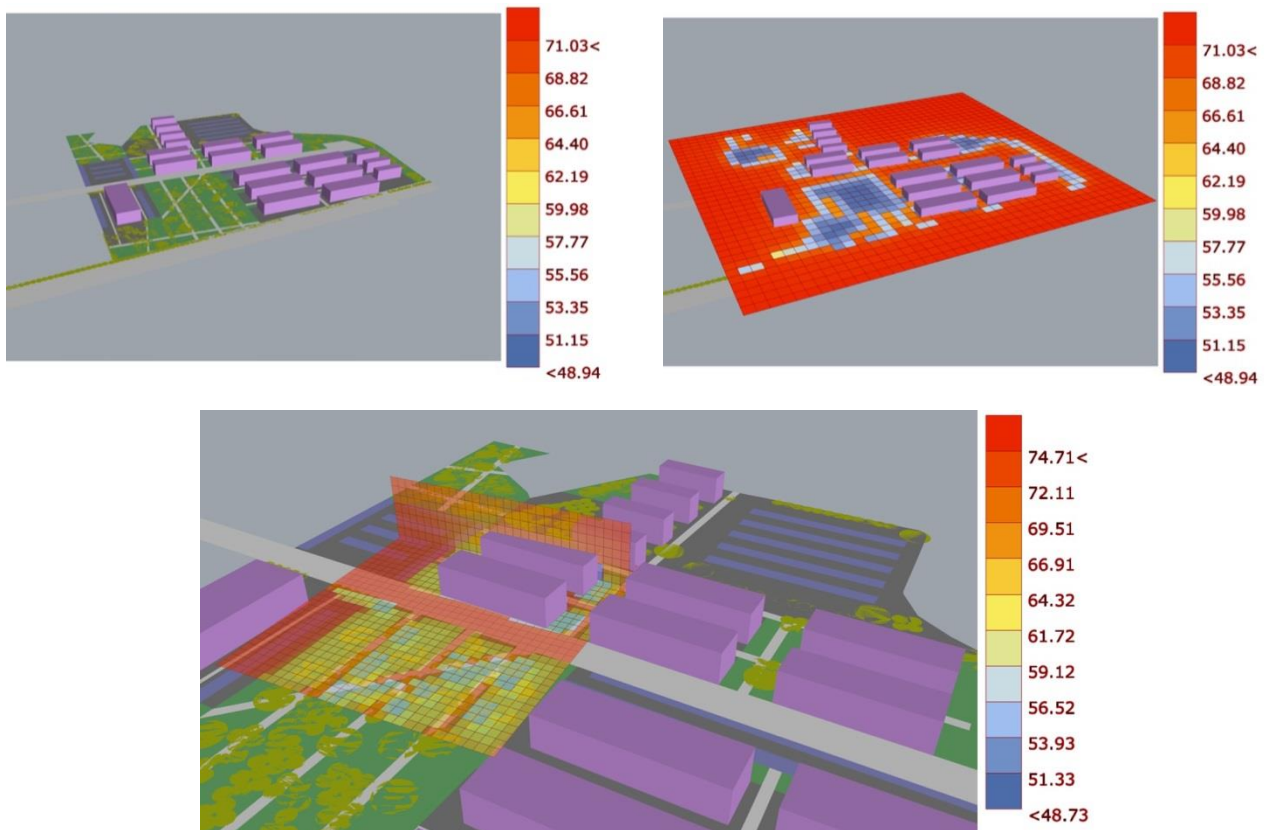


Figure 59: Detailed simulations in the Ponticelli area showing Tmrt which are used as input for the implementation of the Ponticelli Urban Regeneration project.

3.1.3 Flood – local effect

The hazard indicators for extreme rainfall used in the model are the water depth (units of mm) and flood velocity (units of m/s) of the rainwater not absorbed by sewage systems, which determine the occurrence of surface flooding.

The PLINIVS-LUPT simplified model, described in Section 2.1.2.3, has been used to identify urban areas that are more prone to pluvial flooding, considering the key factors that could aggravate the impact of extreme precipitation events. Meteorological datasets, layers related to geomorphology, buildings, open spaces and vegetation, as well as hydrological data sets have been used as input for this model. Most of these data have been extracted from the processing of Naples’ DSM and DTM provided by Municipality of Naples.

The model was preliminarily tested, as in the case of heat waves, on sample areas. The results will be subsequently extended to the entire Metropolitan area.

The implementation of the model involved several phases. First, through the interpolation of the original points with the Kriging estimator, the digital elevation model (DEM) data has been converted to GRID format, which is more suitable for the following processing steps because of its regular structure. Subsequently, in order to remove small imperfections in the data, the identification and the filling of the “pits” has been carried out. In the meantime, using the eight-flow direction (D8) model, the surface flow direction has been defined. In the last step, the flow accumulation dataset has been extracted and that output allows one to detect different micro-basins by applying various outlets. Once this preparatory step is completed, the PLINIVS-LUPT simplified model is finally computed (**Figure 60**).

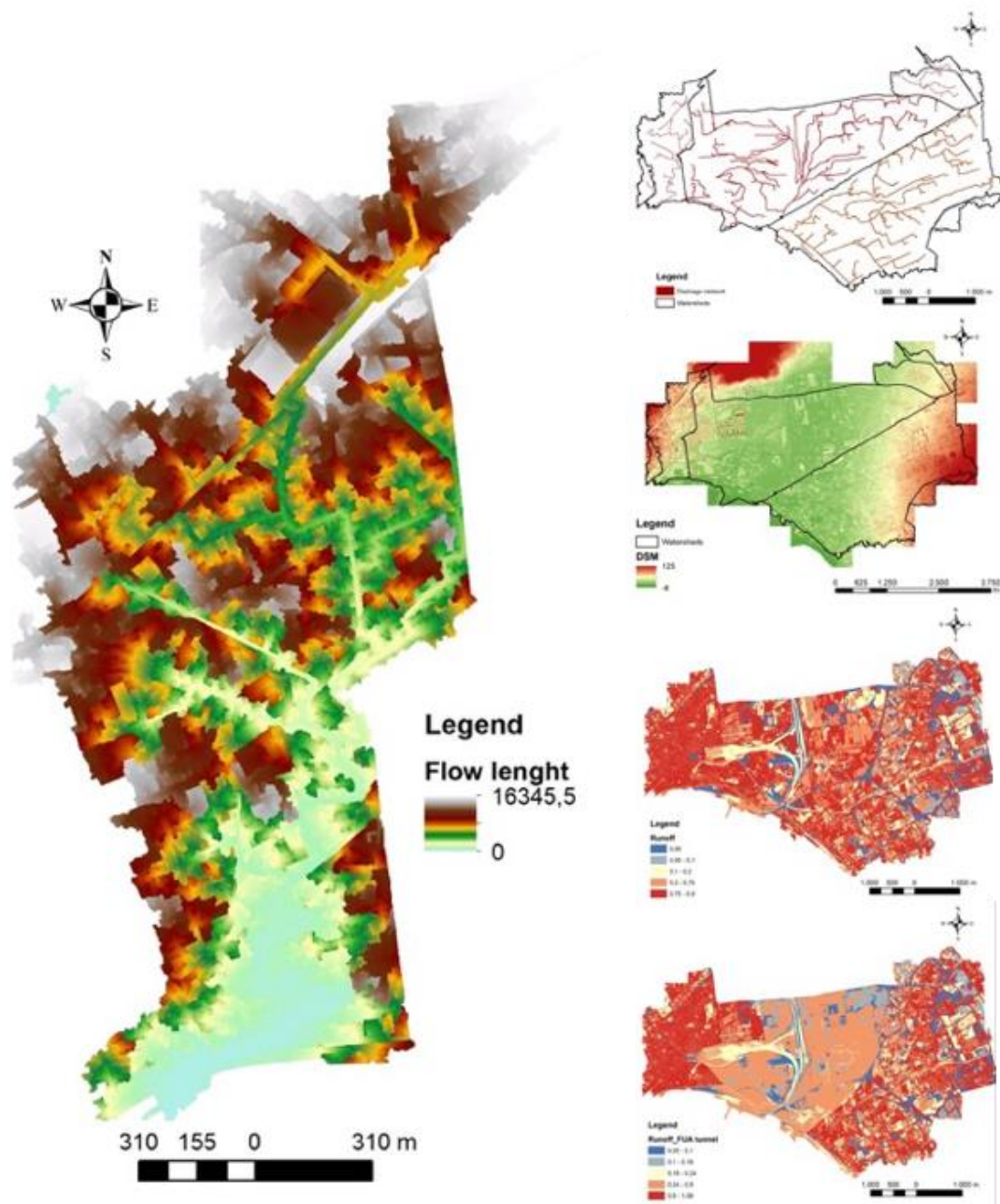


Figure 60: Examples of PLINIVS-LUPT simplified model output. The left panel is the far right segment of the four panels shown on the right side, and shows the flow length coloured.

Flooding simulations are extremely complex due to the amount of parameters involved. The level of detail needed to represent the dynamics of the phenomenon depends on the duration and intensity of the event. The simplified model developed within the CLARITY project does not currently evaluate the contribution of the disposal systems within the city. Typically for an extreme rain event in the city, the maximum capacity of the sewage network is reached within several minutes, and most of the rainwater will then flow along the surface, not being absorbed by drainage surfaces such as parks and green areas.

The main variables are linked to the absorption capacity of urban surfaces, calculated on the basis of the run-off index (**Figure 61**), as well as the morphology of the water catchment areas present in the municipal area (**Figure 62**) and therefore from the orographic characteristics, which determine the presence of

"channels" (streams) of water run-off. Most of the city's sewer system follows the natural orography, and almost all-natural streams are today converted in urban roads, in which most of the rainwater is channelled.

In relation to the urban planning objectives, together with the maintenance and adaptation of the sewage systems, the drainage capacity of urban surfaces is of particular importance, and must be balanced in relation to the specific characteristics of each river basin and other hydraulic characteristics (including the height of the groundwater which can be very near to the surface in some areas of the city).

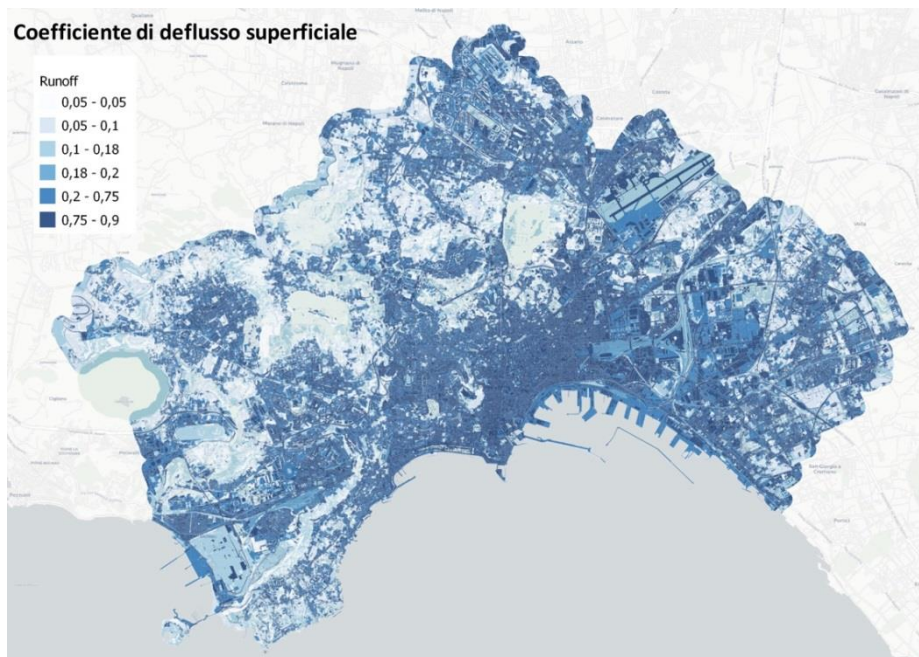


Figure 61: Run-off coefficient in relation to land use. (Source: PLINIVS-LUPT, CLARITY project).

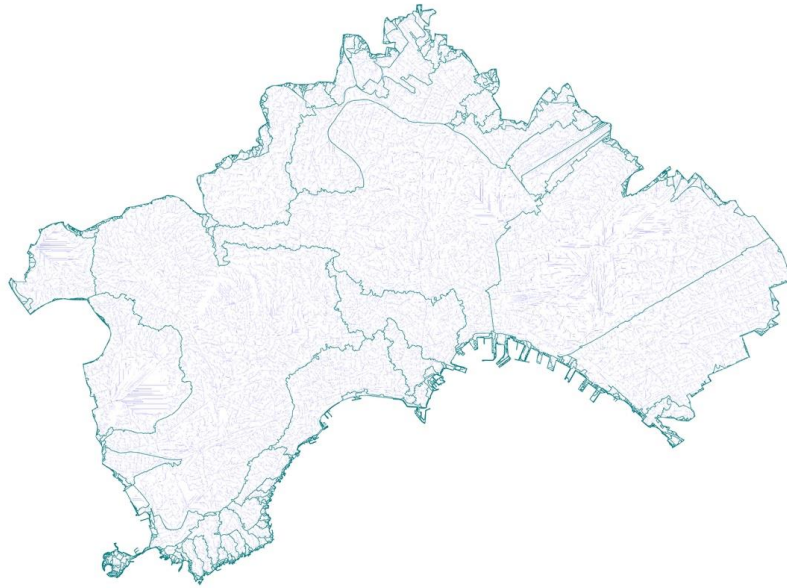


Figure 62: Drainage basins and run-off streams in the Municipality of Naples. (Source: PLINIVS-LUPT, CLARITY project).

An estimate of the water depth and velocity levels for each urban catchment has been produced (left panel of **Figure 63** shows a simulation test for the drainage basin of east Naples). During the calibration of the model, the results relating to these parameters were compared with the geo-localized data relating to emergency calls made by citizens for flooding cases (right panel of **Figure 63**). A majority of the calls are concentrated at the "minor" branches of the run-off channels, which often correspond to sewer branches with a lower flow rate.

A first assessment of the propensity of urban areas to flooding was made by integrating the above parameters (orography, drainage basins, surface run-off channels, run-off factor of the different uses of the soil, emergency calls related to flooding events), and assigning to each a "risk coefficient". This produces an overall picture at city level which highlights the areas with the greatest probability of flooding in case of extreme precipitation events (**Figure 64**).

Simulations related to the various drainage basins are currently being developed, which will be used for the assessment of the expected impacts in terms of interruption of road networks and economic damage to property or production activities.

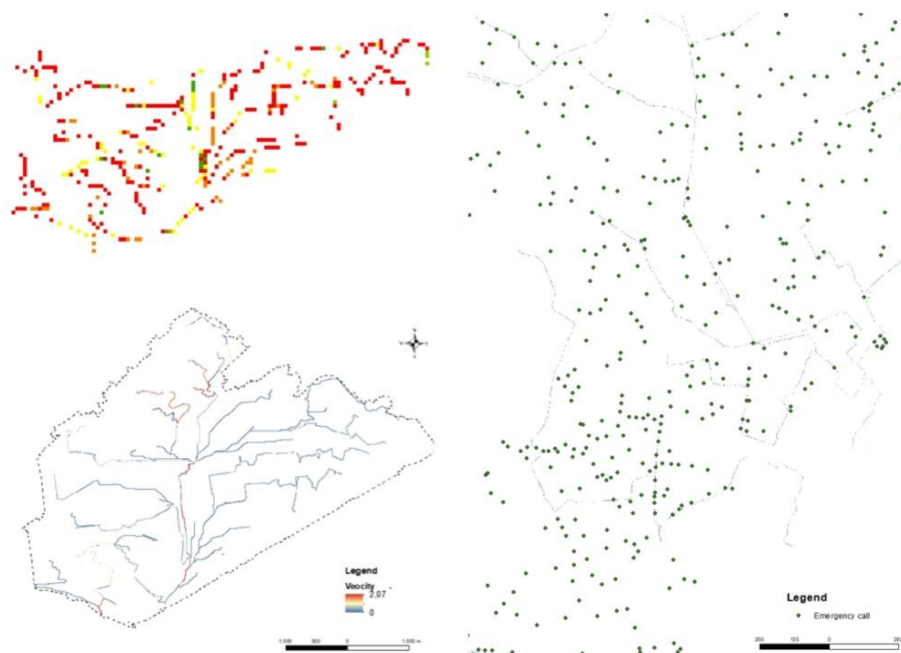


Figure 63: Simulations of the water depth and speed values in the catchment area of Naples east (on the left) and geolocation of emergency calls following extreme precipitation events (on the right). (Source: Civil Protection, PLINIVS-LUPT, CLARITY project).

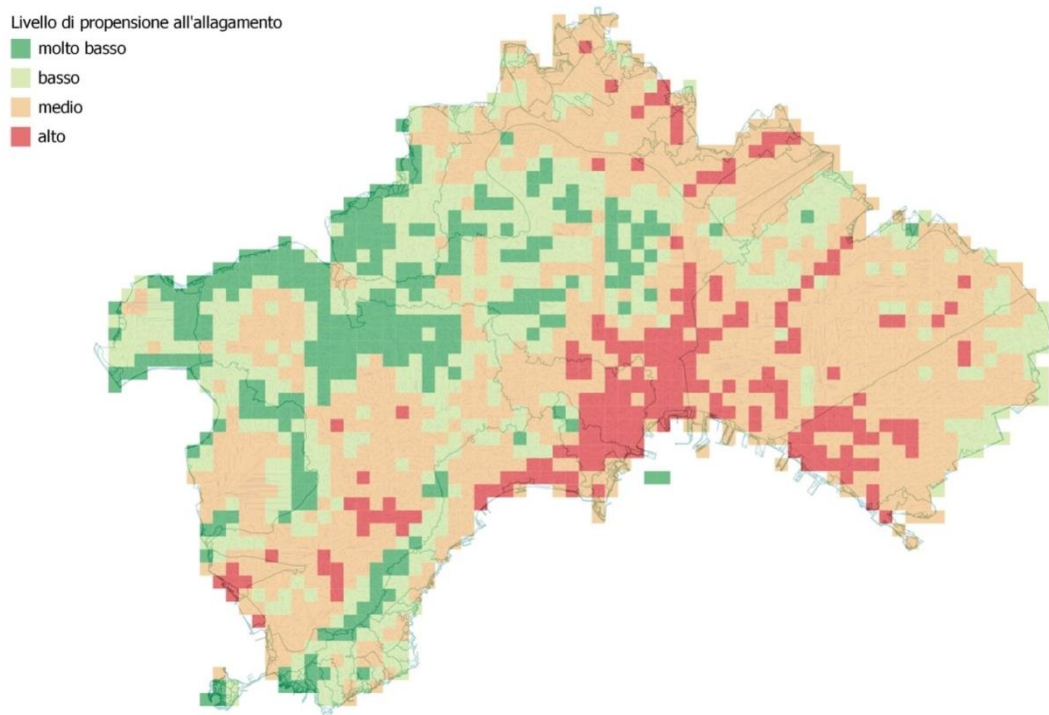


Figure 64: Risk propensity for flooding of urban spaces. Colour scale is: dark green = very low, light green = low, orange = medium, red = high. (Source: PLINIVS-LUPT, CLARITY project).

3.1.4 Climate adaptation strategies for the city of Naples

The goal of integrating climate adaptation measures into urban planning is a strategic priority at an international level. The available literature allows one to identify a series of adaptation measures in response to the impacts of extreme temperature and precipitation events that can be implemented at the local level based on an accurate analysis of the expected climate change scenarios. The assessment of the effectiveness of these measures can be linked to a series of indicators that define the contribution of each measure to the control of the urban microclimate.

Within CLARITY, a systematization of relevant literature resulted in the identification of a catalogue of most recurring adaptation measures (see Section 2.5), classified according to their ability to provide climate benefits in terms of:

- 1) reduction of impacts from heat waves, acting on the surface temperatures of buildings and open spaces and obtaining an improvement in the conditions of perceived thermal stress and the reduction of the Urban Heat Island (UHI);
- 2) reduction of the impacts of flood events, acting on the capacity of urban surfaces to guarantee adequate rainwater drainage and storage.

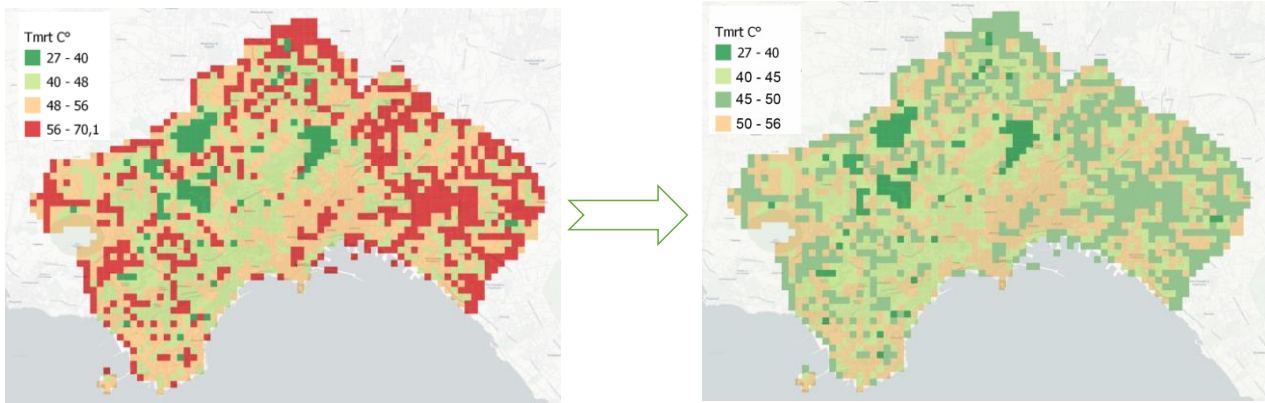
In relation to both categories of climate risk, however, it is worth highlighting the additional benefits associated with some types of adaptation measures, in particular green infrastructures such as green roofs, bioswales, trees or urban green areas, which contribute to carbon sequestration and climate mitigation (i.e. reducing CO₂ emissions), in terms of a local contribution to global warming [33].

The solutions "inspired and supported by nature" (NBS-Nature-Based Solutions) represent in this sense a priority in the international agendas on the issues of climate resilience and sustainable development, precisely for the ability to simultaneously provide environmental, social and economic benefits through systemic interventions adapted locally and resource efficient [34]. NBS provide additional benefits related to "ecosystem services" which can be defined as "the direct and indirect contributions of ecosystems to human well-being" [35]. In addition to climate adaptation and mitigation, ecosystem services convey additional environmental benefits for cities, such as reducing air pollution and increasing biodiversity, but also social benefits such as higher quality public spaces and fewer health impacts [36], [37].

A preliminary test has been carried out using the methodology outlined in Section 2.5, whereby adaptation measures are implemented within the cells showing a high value of the local effect hazard for heat waves and floods. **Figure 65** shows an example of these calculations.

The Adaptation Measures Technical Cards (see **Annex III: Adaptation Measures Technical Cards**) have been translated in Italian and will be used to support the co-design of adaptation strategies with local stakeholders in relation to the different planning levels identified.

During the DC1 Workshop in January 2020, the Technical Departments of the Municipality of Naples have identified the general framework that defines the potential contribution of CLARITY climate services in the context of a multi-scale integrated urban adaptation planning. **Figure 66** summarizes such framework, highlighting the need to use the same approach for technological support across the different planning phases/stages relevant in the context of the city of Naples, as to enhance the coherence of concepts, methods and assessments at the levels of Strategic Planning, City Planning and Urban Design.



Adaptation costs	€/m ²	€ totNapoli
Open spaces	€ 49,38	€ 2.153.138.128,29
Buildings	€ 216,26*	€ 13.514.906.677,95
Maintenance and enhancing of sewage systems	€ 35,00	€ 2.842.172.459,38

*per m² of surface cover

Figure 65: Example of the calculations of the impacts of adaptation measures in terms of cost.

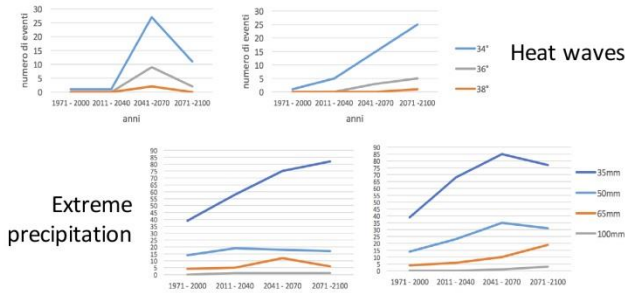
3.1.5 Summary

This demonstration case addressing issues for the Naples region has shown how the EU-GL methodology is applied to investigate the effect of climate change and what relevant adaptation measures can be taken. The focus is on the hazards of heat waves, floods, as well as landslides. A **hazard characterisation** of the heat wave and flooding hazards is performed in Section 3.1.1. Here it is illustrated that the duration and intensity of heat waves is projected to increase in the future. Similarly, heavy precipitation events are projected to increase in the future. Given this information, it is thus necessary to investigate what adaptation measures can be implemented in order to mitigate these damages.

The first step involves calculating the local effect on the urban scale of each hazard using available land use data sets. For heat waves (Section 3.1.2), indices of temperature and perceived comfort (e.g. Tmrt, UTCI) relevant for the **element of exposure**, population, are calculated for the baseline climate, with the focus on a proper calibration of the model. Once the model has been calibrated, it can then be used to calculate these parameters for the future climate of the RCP scenarios. Appropriate damage classes for the population were devised to consider the **vulnerability** aspect necessary for the calculation of the hazard impact. The calculation for the local effect of flooding (Section 3.1.3) uses a run-off index together with the orographic characteristics of Naples such as elevation, land use, and drainage basins and streams and to determine a risk coefficient. This coefficient gives a measure of the probability of flooding in an extreme precipitation event.

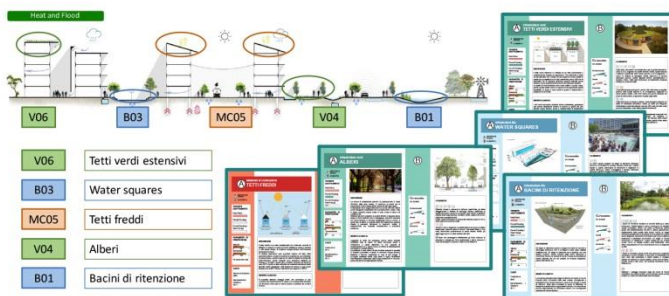
Adaptation measures relevant for Naples have been investigated (Section 3.1.4) with the aim of reducing the impacts of heat waves and floods. Preliminary tests of the proposed calculation methodology to **assess their benefits** have been conducted for various adaptation measures, and the results are currently being analysed.

CLIMATE PROJECTIONS



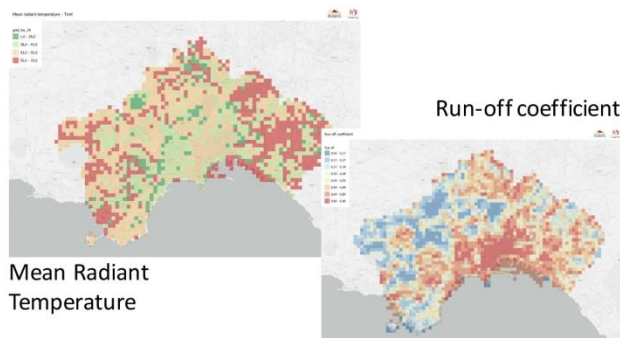
Climate change profile **Napoli 2020-2100**

STRATEGIC PLANNING



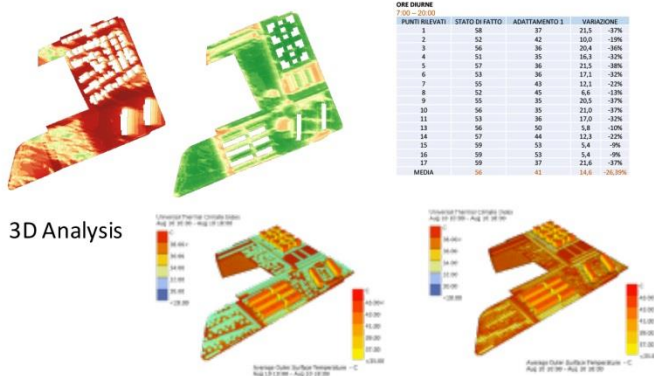
Support to the implementation of the **Sustainable Energy and Climate Action Plan for Napoli (SECAP)**

CITY PLANNING



Update of **Napoli City Plan (PUC)**

DISTRICT PLANNING



Ponticelli Urban Regeneration Plan (PRU)

Figure 66: General framework of CLARITY climate services support for the Municipality of Naples.

3.2 DC2

The DC2 user case focuses on expert services for Sweden. We are working with several sample expert services within two fields, water and health.

The workflow of DC2 according to the EU-GL methodology described in D3.1 is summarized in **Table 45**.

Table 45: Overview of the workflow of DC2 and its relation to the EU-GL methodology.

Hazard Characterisation	Element at risk	Vulnerability	Impact	Adaptation Options
Heat waves	People	High for very young/old age groups	Excess heat mortality Productivity loss	Investigate role of vegetation (location, type)
Pluvial Flooding	Buildings Infrastructure	High for objects in poor drainage areas and close to lakes	Damage Economic costs for repair / resource unavailability	Increased vegetation to control flow rates, infiltration
Air quality / Pollution	People	High for very young/old age groups	Reduced ventilation from vegetation results in locally high pollution concentrations	Investigate role of vegetation (location, type)

3.2.1 Water Hazards and Supply (US-DC2-100)

The user story US-DC2-100 is a parent story that summarizes common information needs for all water related user stories for Sweden in CLARITY. The goal is to provide input to city planners to both present city structure and when planning new buildings, infrastructure and other actions related to water supply, intense precipitation and expected changes in the future. For Sweden, several Swedish authorities produce open data that can be used as basis for expert studies. **Table 46** gives an overview of datasets used and exemplifies in which EU-GL step they are useful.

In our work we have identified that there is a lack of high resolution data for future hydrological studies in Sweden. So part of our work has been to build this national resource that will increase the possibility for hazard characterisation in Sweden. This work is further described in 3.2.1.1. Secondly, we have put an effort in reusing available resources from authorities and making use of input from already ongoing climate adaptation discussions and plans in Stockholm and Jönköping in the validation of adaptation plans from a climate effect perspective. This part of the work is further described in Section 3.2.1.2.

Table 46: Overview of available datasets used for this case study and for which EU-GL step they are mainly useful.

Authority, source	Example of datasets	EU-GL step
Swedish Authority for Land Survey (Lantmäteriet)	Land use, Elevation data, Orthophoto, Terrain maps, Topography Buildings	Hazard Characterisation Evaluation of Exposure
Geological Survey of Sweden (SGU)	Soil data	Hazard Characterisation
Jönköping Municipality	Overview map of plans, Mapping downpour, Water level,	Evaluation of exposure Hazard Characterisation
Jönköping County Board	Climate adaptation plans	Adaptation Options
Swedish meteorological and hydrological institute (SMHI)	Catchments in Sweden, Hydrological variables Climate projections	Hazard Characterisation
Swedish Civil Contingencies Agency (MSB)	Landslide flood	Hazard Characterisation
Statistics Sweden (SCB)	Critical services for the society such as schools, hospitals, population	Vulnerability Analysis
Swedish transport administration (Trafikverket)	Roads and railways	Evaluation of Exposure

3.2.1.1 Hazard Characterization – High resolution future hydrological data for Sweden using HYPE

Hydrological data in Sweden is made available by SMHI via the Vattenweb¹³ portal. In this portal, river flow modelled data using a process-based hydrological model HYPE is available across Sweden at a daily time resolution. HYPE is a continuous process-based hydrological model developed at SMHI, which simulates components of the catchment water cycle at a daily or hourly time step. The model is a semi-distributed conceptual model, in which a river basin may be subdivided into multiple sub-basins, which can further be subdivided into homogeneous hydrological response units (HRUs) based on combined soil type and land use classes. Normally, model outputs are generated at the sub-basin outlet. The model has conceptual routines for most of the major land surface and subsurface processes (e.g. including snow/ice accumulation and melting, evapotranspiration, surface and macro-pore flow, soil moisture, discharge generation, groundwater fluctuation, aquifer recharge/discharge, irrigation, abstractions and routing through rivers, lakes and reservoirs). The model requires input data that describe the land surface features of the catchment, such as topographic, soil and land use maps, as well as daily or hourly surface meteorological data (precipitation and temperature). Optional local information on irrigation and river/reservoir regulation may be used as well.

In CLARITY, the model has been employed in DC2 to provide information on the risk of riverine flooding in areas located along a small to meso-scale river basin. The results can, in particular, be used to assess the risk of flash flooding that can result from heavy precipitation of short duration. The model is setup to run at an hourly time step to enable simulation of discharge and runoff at a temporal resolution relevant for assessment of flooding due to intense precipitation events. The model is calibrated and validated for the southern part of Sweden using Radar based hourly precipitation [38] and hourly temperature from SMHI's reanalysis system MESAN [39].

Climate projections are performed using a subset of the EURO-CORDEX hourly data at 0.11° spatial resolution (see **Table 47**). The data received so far have emissions scenarios RCP4.5 and RCP8.5.

¹³ <http://vattenweb.smhi.se>

Table 47: List of hourly EURO-CORDEX configurations used for climate projections of flooding for DC2.

Name	RCM	GCM	Institute
RCA4-MPI-ESM-LR	RCA4	MPI-ESM-LR	SMHI
RCA4-IPSL-CM5A-MR	RCA4	IPSL-CM5A-MR	SMHI
RCA4-HadGEM2-ES	RCA4	HadGEM2-ES	SMHI
HIRHAM5-EC-Earthr03	HIRHAM5	EC-Earth	DMI

The hourly precipitation data from most of the climate models were found to underestimate the extremes [40]. Therefore, they were bias adjusted against gridded daily observed data covering Sweden. After bias correction, the extremes of the simulated hourly river flow for the reference period at all river gauging stations, where enough hourly data is available for computation of the extreme statistics, were found to be in good agreement with that of the observations for a comparable period (see **Figure 67**).

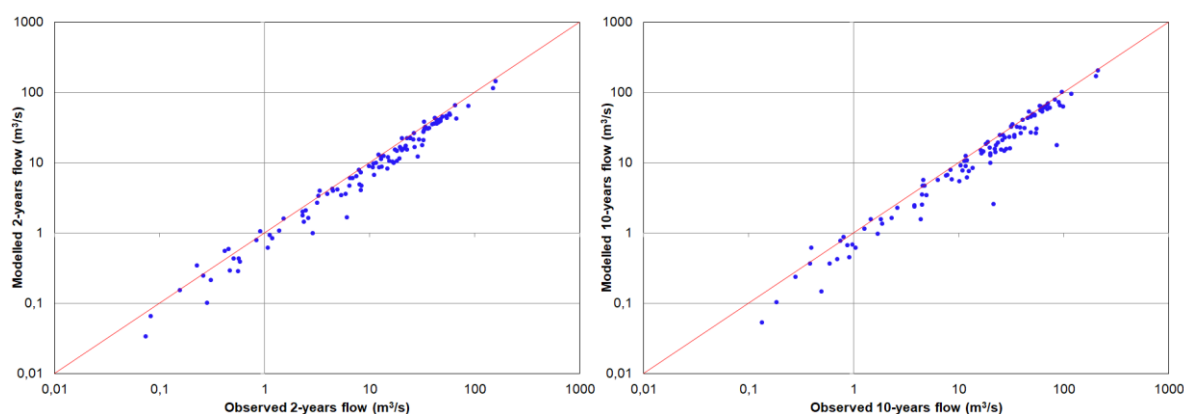


Figure 67: Comparison of extreme river flow simulated using bias-corrected hourly precipitation data and the corresponding observed extreme flows at river gauging stations across southern Sweden.

A set of hydrological indicators that are relevant for the assessment of flooding have been derived from model simulations corresponding both to the present climate and scenario periods. These include: river discharge, total runoff, and flood recurrence. **Figure 68** shows the projected percentage change in the 10 years hourly river flow across southern Sweden. The projection shows that a mild increase in the extreme river flow is expected for most part of southern Sweden with stronger increase in some regions with heavy settlement, such as Stockholm and Gothenburg.

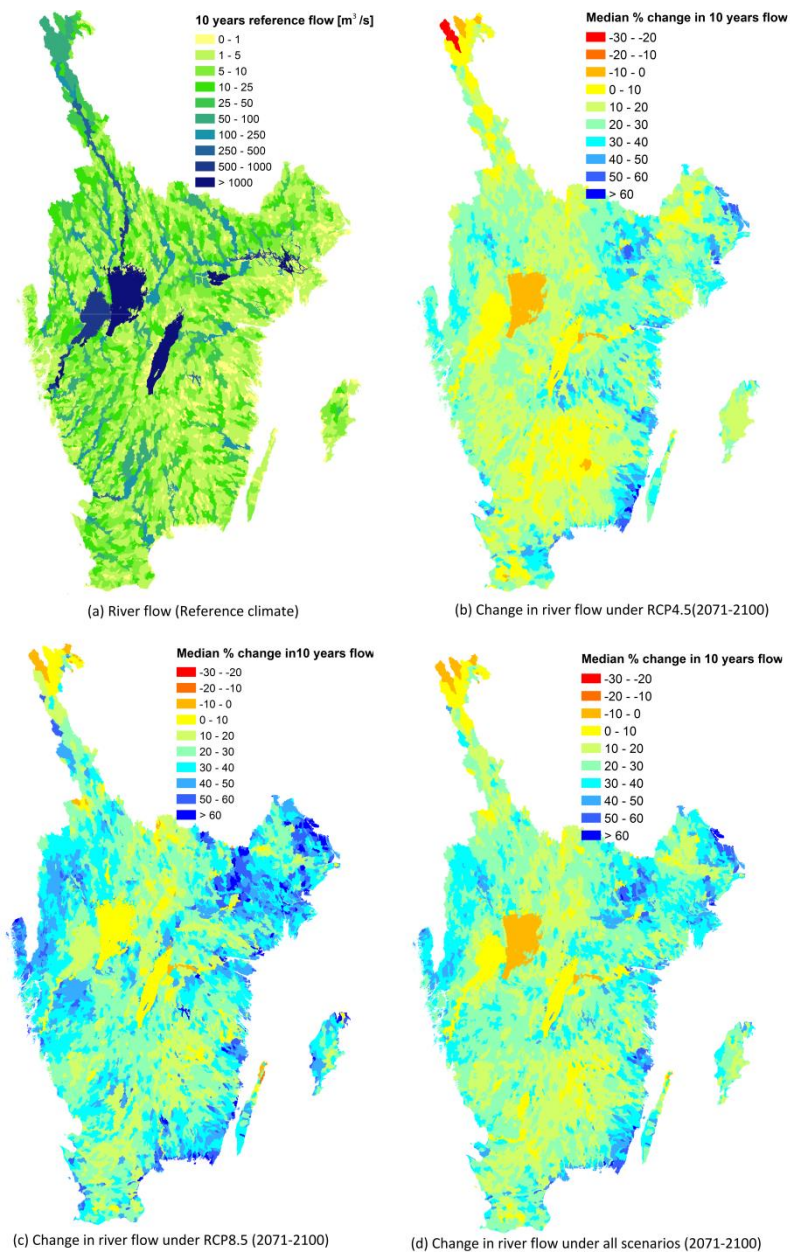


Figure 68: Projected percentage change in the 10-year extreme hourly river flow across southern Sweden.

3.2.1.2 Identifying Adaptation Options

3.2.1.2.1 Pluvial flooding mitigation study in Stockholm

In an early stage of CLARITY, a limited area in the city centre of Stockholm prone to pluvial flooding was identified. Thereafter a wide range of possible adaptation measures have been defined taking into account suggestions from a reference group containing representatives from different end-users. All suggested adaptation measures have then been selected for preliminary analysis in SCALGO (a less-time consuming methodology than doing a full, high-resolution hydrodynamic modelling in MIKE) to select the most efficient measures for incorporation in the MIKE model.

The MIKE products are developed by the Danish Hydraulic institute (DHI) for modelling water environments. Mike 21 is a fully dynamic, two-dimensional model that calculates water level and flow conditions. The model is commonly used for modelling the effect of extreme rainfall in urban areas. The

program requires high resolution topography data, land use, information about infiltration and rainfall data.

In the CLARITY project, the MIKE model is used in DC2 for Stockholm to simulate future scenarios of the effect of extreme rain on a high-resolution scale. The effect of vegetation on inundation depths and flow velocities is investigated by including potential green areas in the model. Based on the reference group and pre-study using SCALCO the most efficient measures have been selected for incorporation in the MIKE model that enables more detailed results. The results (expected early 2020) will be used to assess the risk of current and planned infrastructure and to evaluate the benefit of possible adaptation measures.

3.2.1.2.2 Analysing future flooding risk from combined events (case Jönköping)

A methodology for assessing and evaluating the effects and consequences of multiple future flood risks is performed in DC2 for Jönköping Sweden (CABJON). Available data sets and models with different scales is used to analyse joint probabilities and to conduct a multi-risk assessment for river floods, flooding from the lake and extreme rain. Focus is put on determining consequences for important societal functions (e.g. schools, infrastructure and hospitals). Within the DC2 case for Jönköping, a new cloudburst modelling scenario is performed taking future climate changes into account accounting for increasing rainfall volumes of up to 40%. The modelling (presently being made) will probably also be able to show the eventual success of the flood mitigation measures that have been performed during the last few years. The methodology is GIS-based and is supposed to help municipalities (and other end-users) to develop and prioritize adaptation measures to climate change and to serve as a basis for future infrastructure and urban planning.

3.2.1.2.3 Urban development in upstream areas and flood risk screening in downstream areas (Jönköping City)

There are plans to extend the amount of industrial areas in the southern (upstream) parts of the Tabergsån catchment, implying that paved areas will replace forest and farmland. The River Tabergsån eventually flows through the city centre of Jönköping and the case-study is performed to analyze the eventual consequences (increased flooding risk) downstream (in the city) of the upstream activities of increasing the amount of impervious area. By analysing the effect of the changed land use using the hydrologic model HYPE with simplified land use rearrangement within the model setup, no major difference can be seen when looking at major flood peaks (for example the flow peak in July 2004 having an expected return period of ~50 years). However, for average discharges, changes can be seen in terms of higher and “peakier” hydrographs after increased imperviousness. The conclusions are that this simplified analysis may be an indicator regarding the eventual need of making more detailed hydrologic/hydraulic modelling at an early landscape/city planning stage.

3.2.2 Health and Environment (US-DC2-200)

The city of Stockholm is facing a growing need of housing and roads, while the wellbeing and health of citizens needs to be safeguarded, today and in the future. To assess how the resilience of the city to climate-related hazards can be strengthened under intense on-going urban development is a priority. Measures combining grey, green and blue infrastructures have the potential to deliver robust and flexible solutions over long periods. In this context, SMHI is cooperating with Stockholm municipality, with the support of the Swedish Civil Contingency Agency, in the estimation of the effects of heat-waves in the wellbeing and health of city dwellers under current and future conditions.

In DC2 the urban climate of Stockholm is investigated, with a focus on the spatial variation of air temperature. High resolution climate simulations are carried out at $1 \times 1 \text{ km}^2$ grid spacing using a dynamical downscaling technique developed and validated over different European cities within the Copernicus Climate Change Service Urban SIS [41]. The work carried out in CLARITY within DC2's health and environment service was recently published in a Special Issue of the Urban Climate Journal [42].

3.2.2.1 Hazard Characterization – Baseline and future heat scenarios over Stockholm

Urban SIS was a proof-of-concept project within Copernicus Climate Change Service (C3S 441 Lot 3) providing city specific climate data and impact indicators to principally examine the infrastructure and health sectors acting in European cities. The demonstration of Urban SIS results is made for three $110 \times 100 \text{ km}^2$ areas centred over Stockholm, Bologna and Amsterdam/Rotterdam [41].

For the dynamical downscaling, the Numerical Weather Prediction system HARMONIE-AROME cycle 40h1.1 is used, with lateral boundary data provided by the UERRA-ALADIN reanalysis and surface observations retrieved from the ECMWF MARS archive. Surface/atmosphere interactions are computed by SURFEX (version 7.3). Depending on the type of surface, different modelling schemes are used in SURFEX, namely the Town Energy Balance (TEB) model over urban areas and the Interaction Soil-Biosphere-Atmosphere (ISBA) land surface model for soil and vegetation, while the fluxes over the urban vegetation are simulated by a simplified version of ISBA that enables the interaction with impervious surfaces. While the tiling of surfaces that underlies SURFEX offers the capability to account for sub-grid heterogeneity, on the other hand, it requires that detailed and accurate physiography information is provided. For this purpose we have compiled, processed and aggregated different open-access databases and products: the spatial coverage of land cover types from Urban Atlas 2012 (Copernicus Land Monitoring Services), building polygons from OpenStreetMap, building heights from Lidar measurements (available at the Swedish Forest Agency) and time series of leaf area index (LAI) from the Copernicus Global Land Service. The resulting grids, with a spatial resolution of approximately $300 \times 300 \text{ m}^2$, were then interpolated by SURFEX to the final model grid at $1 \times 1 \text{ km}^2$ and combined with the default European ecosystem classification and surface parameters dataset ECOCLIMAP-II. This methodology has shown to accurately capture the spatial variation of building density and vegetation fraction, as also the intricate interface land/water that characterises the landscape of this region. The Urban SIS information is based on climate re-analysis and climate scenario data, downscaled to be useful for individual cities. The Essential Climate Variables (ECVs) proposed for urban downscaling include hourly $\approx 1 \times 1 \text{ km}^2$ fields of several meteorological, air quality and hydrological variables. The ECVs are delivered for a historical 5-year period and for a climate scenario with two 5-year windows, one representing present and the other future conditions.

The ECVs can be accessed and downloaded as gridded time series or receptor point time series for use as input to further downscaling or impact modelling. Urban SIS also offers a series of statistical indicators for each ECV, e.g. daily/monthly/annual averages and extreme values. A full list of the available indicators from and how they were calculated can be found at <http://urbansis.climate.copernicus.eu/urban-sis-climate-indicators/> (in addition to [41]) and some examples are shown in **Figure 69** and **Figure 70**.

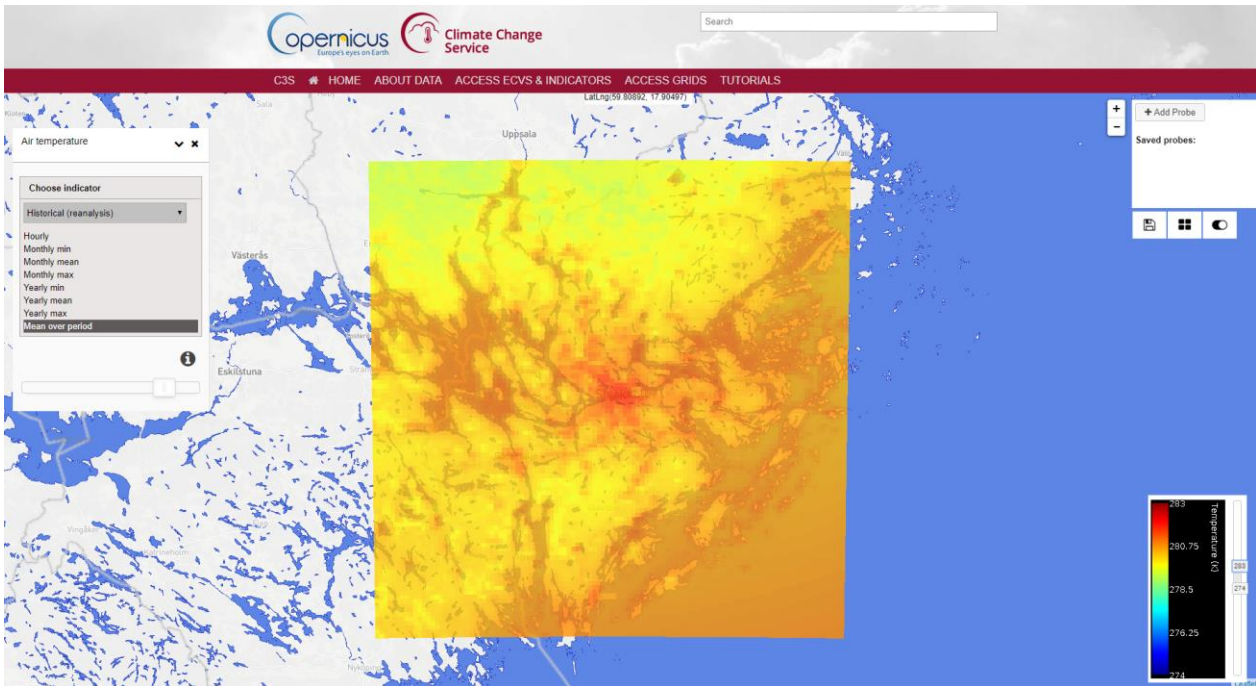


Figure 69: Example of the urban heat island over Stockholm visualized on the Urban SIS portal.

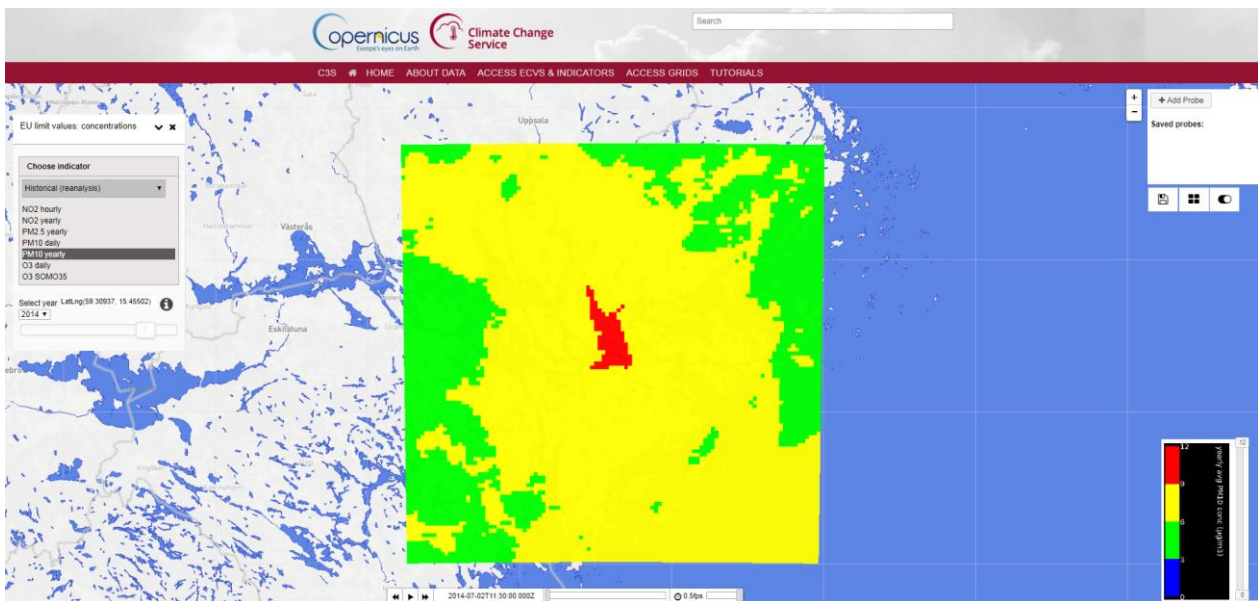


Figure 70: Example of PM10 concentrations over Stockholm from Urban SIS.

3.2.2.2 Vulnerability Analysis – Health indicators from Urban SIS

A number of the impact indicators available on the Urban SIS portal are related to the vulnerability of the population. One example is heat-induced mortality, defined as number of deaths associated with temperatures above the 75th percentile of daily mean temperature during summer months (Apr-Sep). Relative risks were extracted from a European multi-city study [43] and are used to describe the effect of high temperatures on mortality. A more extensive description of these calculations is given here: <http://urbansis.climate.copernicus.eu/annual-heat-related-deaths/> and an example is shown in **Figure 71**.

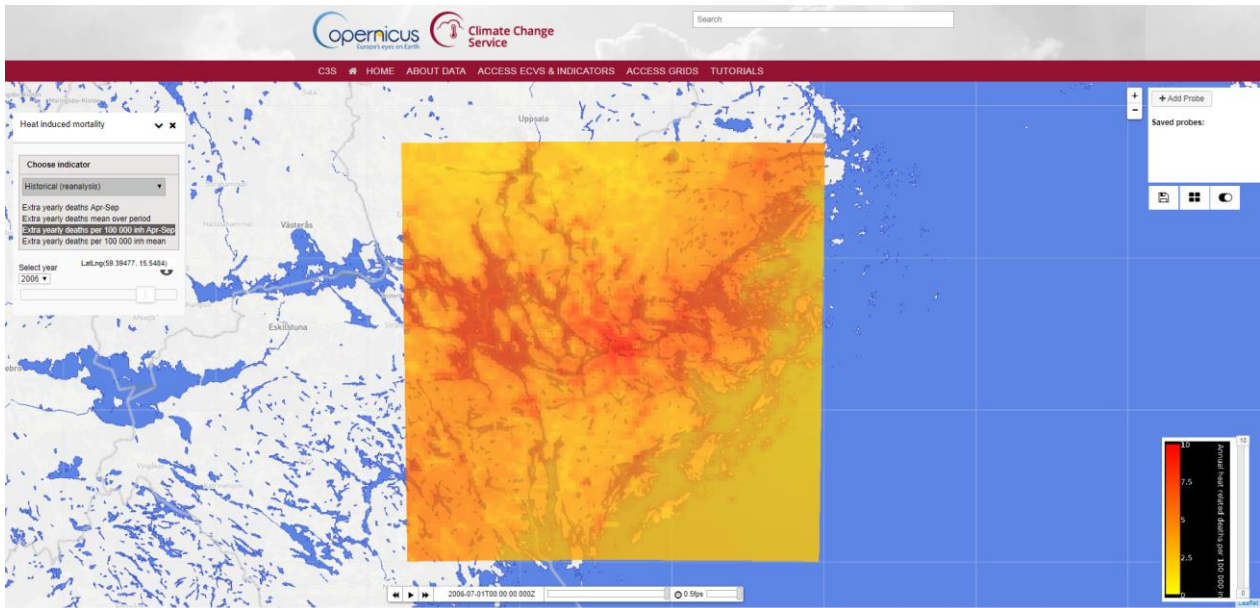


Figure 71: Example of heat induced mortality over Stockholm from the Urban SIS portal.

Other examples are given for air quality indicators where we have made estimations of mortality, as shown in **Figure 72**, with the estimated number of deaths in age group 30+ associated with long-term exposure to urban background levels of PM_{2.5} and NO₂. Relative risks are based on recommendations from WHO's HRAPIE Project [44] regarding PM_{2.5} and UK's [45] regarding NO₂. Estimates are presented both separately and combined for exposure to both pollutants. For details see <http://urbansis.climate.copernicus.eu/annual-deaths-due-to-no2-and-pm2-5-long-term-exposure/>. In addition we have estimated the number of preterm deaths due to ozone short-term exposure (for details visit: <http://urbansis.climate.copernicus.eu/annual-deaths-due-to-ozone-short-term-exposure/>).

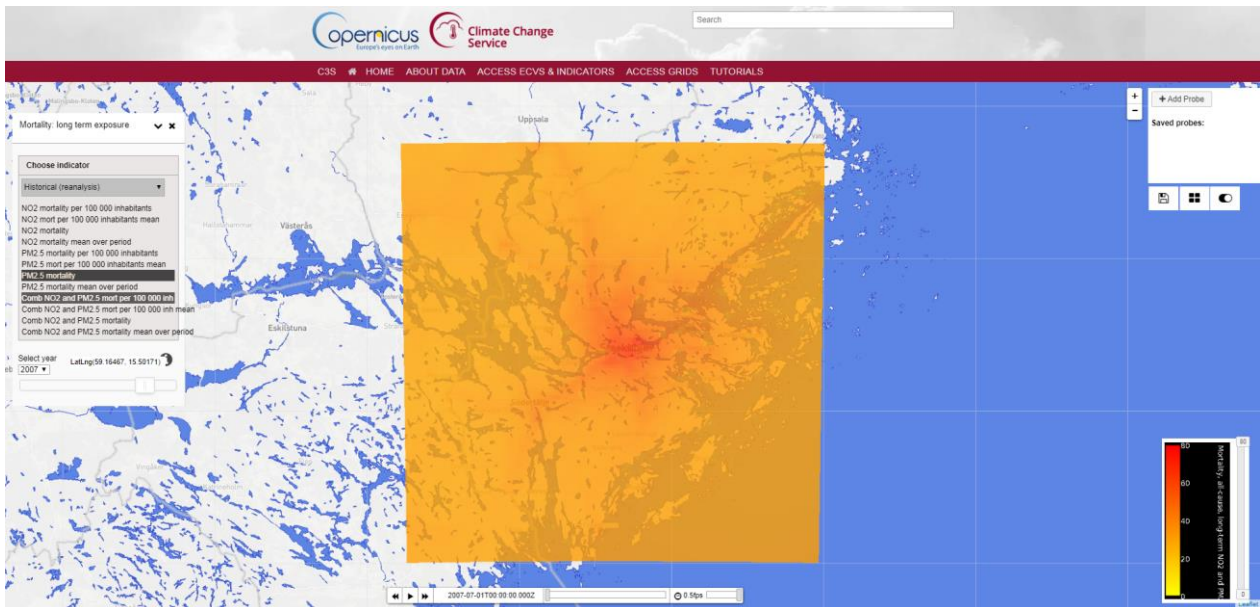


Figure 72: Example of combined NO₂ and PM_{2.5} mortality per 100 000 inhabitants over Stockholm.

3.2.2.3 Identifying Adaptation Options – Future development scenarios

In order to understand how the city's development might affect the future exposure to heat, four urban planning scenarios were defined for the city/region (see **Figure 73**) in cooperation with representatives from the municipality:

- the planned construction of 140 000 new homes by 2030, including one of Europe's largest urban development areas: the 'Stockholm Royal Seaport'. In this plan, the urban densification reduces the amount of vegetation in the intervened areas but the changes affect only the city;
- a "grey city" scenario that promotes the growth of the impervious surfaces in the region, mostly by increasing the density of buildings or constructing in areas that are currently occupied by forests. This scenario was calibrated against the regional development plan (RUF5 2050) and foresees a significant expansion and densification of the city,
- a "black city" scenario, with extreme densification and total absence of vegetation in the city. This is intended to quantify the current impact of vegetation over Stockholm's climate,
- a "green city" scenario, with a strong increase of green infrastructure, including street trees, parks and green roofs. The potential for the implementation of green roofs is maximized in public buildings.

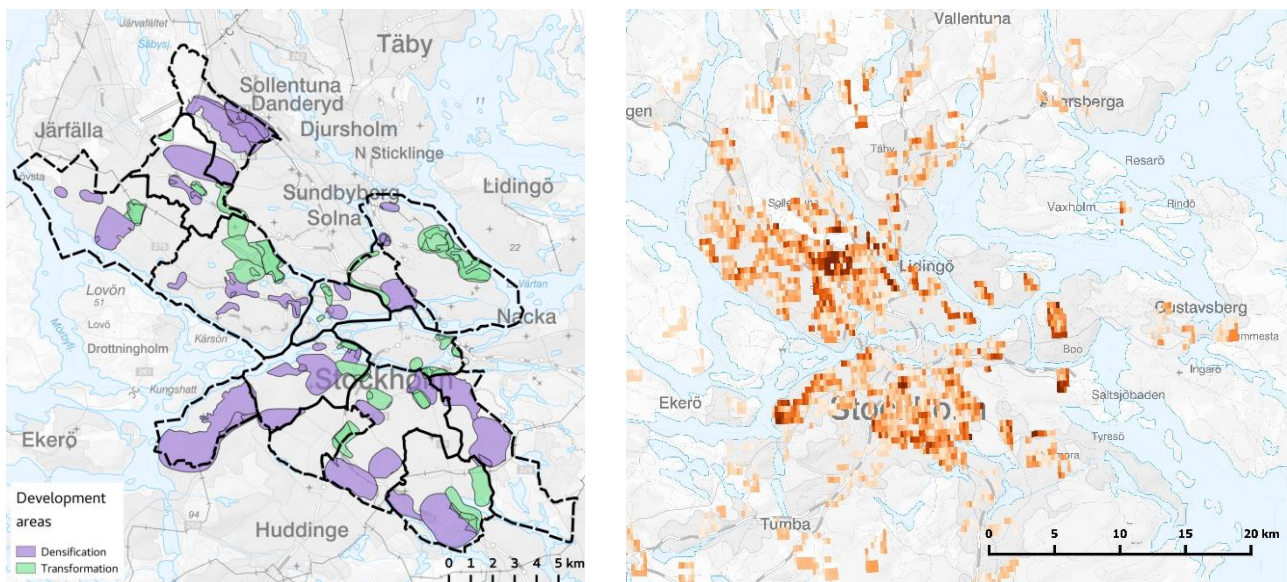


Figure 73: Planning scenarios developed for Stockholm. The construction of 140,000 new homes by 2030 (left) and the regional development plan for 2050 (right).

Baseline conditions for this comparative analysis were set for the summer of 2014, due to the hot weather conditions registered particularly during the last week of July. Meteorological boundary forcing was kept constant in all the experiments, and only physiography was changed according to the planning scenarios mentioned above.

The high-resolution urban climate data provided over Stockholm region reveals the full spatial coverage of the city's urban heat island (UHI), its intensity and temporal profile on a daily or seasonal basis. In addition to the urban-to-rural gradients, the dynamical downscaling applied in this work responds to the heterogeneity of the urban tissue, showing intense intra-city gradients that are intrinsically related, among other factors, with the interactions between impervious and vegetated surfaces. As an example, the local cooling induced by the 4 ha Observatorietlunden park was estimated as 1.82 °C in average during the summer, evidencing a strong diurnal cycle.

Results show that the 2014's summer temperature would increase by 0.29 °C in 2030, if the construction of 140 000 homes occurs as planned, with larger differences found over forest lands that will be urbanized (see **Figure 74**, left). The stronger densification and sprawling given by the 2050 regional development scenario induces an average warming of 0.46 °C, up to a local maximum of 1.35 °C (see **Figure 74**, centre). A preliminary analysis points out to an average cooling of 0.4 °C (monthly mean) as induced by Stockholm's existing vegetation, with heavily vegetated areas evidencing a local decrease in temperature of up to 1.0 °C (see **Figure 74**, right) [46].

This dataset is available in the CSIS as a demonstrator of an expert service focusing on heat in a Nordic city. Co-created climate services that include user-tailored downscaled urban climate data, in the example of Stockholm, provide new intelligence for urban planning that assimilates climate adaptation and fit-to-purpose Nature-based Solutions.

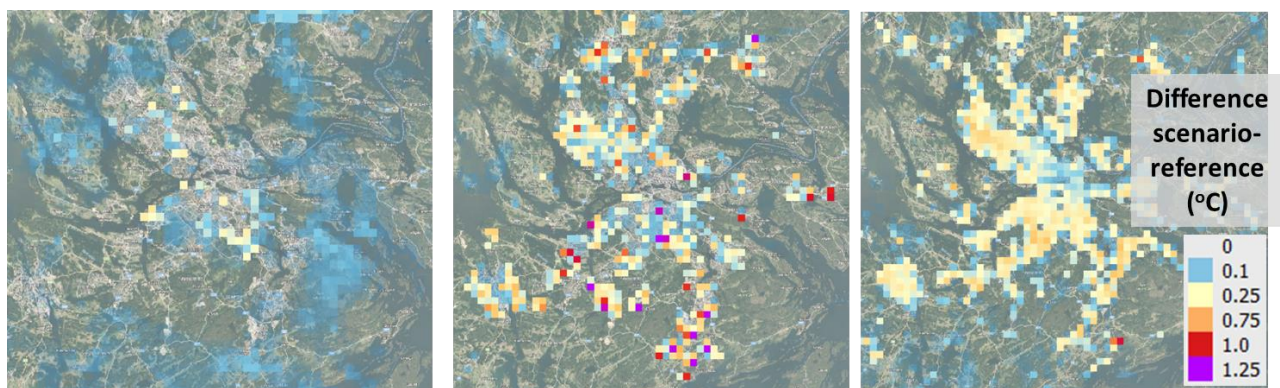


Figure 74: Monthly average temperature increase for future planning scenarios over Stockholm, 2030 with construction of 140 000 new homes (left), the 2050 regional development plan (middle), and a reference scenario where all urban vegetation is removed from today's city (right).

3.2.2.4 Appraise Adaptation Options – The Green Area Factor

The Green Area Factor (GAF), also known as Green Space Factor and Biotope Area Factor, is a planning tool that is used to create greener neighbourhoods in the city. This means that a certain portion of the plot of land must consist of vegetation and/or a water surface. The background is that greenery and water surfaces in the city environment contribute with many benefits: they provide an attractive appearance, they can be used for recreational activities and they contribute to increasing biodiversity, among other useful benefits. They also reduce the city's vulnerability to the adverse impacts of the climate change. More surfaces with vegetation can reduce vulnerability for flooding and lower the temperatures during heat waves and to some extent improve air quality.

The GAF is an urban site sustainability metric and a tool to enhance green infrastructure in the city. In Stockholm, the GAF is used early in the urban planning process in order to ensure that sustainability goals are achieved, and also to create greener outdoor environments that attract outdoor living, social meetings and improve people's quality of life. Many projects have high ambitions early in the process. The problems arise when it starts to cost money and one realizes that there are no short-term economic gains. With the green surface factor one cannot haggle away the green issues.

The GAF is equal to the ratio of the ecologically effective surface area to the total land area. Different target and minimum values are set to different land-use areas. The calculation requires knowing the areas covered with different green elements. This is a very flexible tool as it enables the target being met in several different ways through implementing different green elements.

Trees and other vegetation absorb and capture air pollutants, leading to the common perception that they, and trees in particular, can improve air quality in cities and provide an important ecosystem service for urban inhabitants. However, literature shows that different climate conditions, plant configurations, degree of urbanization and the scale of a study area yield variable potential of urban vegetation to reduce the levels of air pollutants. Air quality can be affected both positively (improved) and negatively by urban green infrastructure (UGI). The effect depends on many different factors like e.g. the pollutant being considered, type of vegetation and if the focus is on a local scale (street canyon) or urban scale. This complexity is the reason why air quality is not considered as a criterion in the GAF used in Stockholm.

In order to improve the knowledge and implement air quality in GAF, dispersion model simulations of a street in central Stockholm have been undertaken (**Figure 75**). Concentrations of particulate matter (PM10) were calculated for a situation with and without trees and all other factors being the same.

Figure 76 shows the effect of trees on the concentrations of PM10. Concentrations are higher with trees due to reduced ventilation (atmospheric dynamic effect). The deposition (filtering) of particles onto the leaves of the trees, even when assuming a very high deposition velocity, is far less important for the concentrations compared to the reduced dilution of the air. In conclusion, planting trees in street canyons may lead to higher air pollutant levels in the canyons. This result is consistent with other studies.

Lower vegetation, like hedges, would not have this negative effect on the ventilation. The uptake of different air pollutants on different types of vegetation depends on the leaf area, location of the vegetation in relation to the emissions of the pollutants and on the properties of the pollutants. This shows that the ecosystem services provided by the UGI depend on many synergetic but also counteracting factors. The suitability and effectiveness of a given vegetation species to ameliorate air quality, but also to regulate air temperature or to manage high precipitation can, therefore, be highly case-specific. Although in Nordic countries the UGI has been traditionally targeted at handling stormwater during cloudburst events, some relevant co-effects on air quality and heat are to be taken into consideration. In this scope, we will publish a systematic review of the scientific state of the art in the interactions of the UGI with urban climate and air quality, specifically in Nordic cities. This work characterizes the hazards represented by heat, flooding and air pollution in these regions; identifies green solutions in place; and analyses gaps in knowledge and in the communication to/with stakeholders.

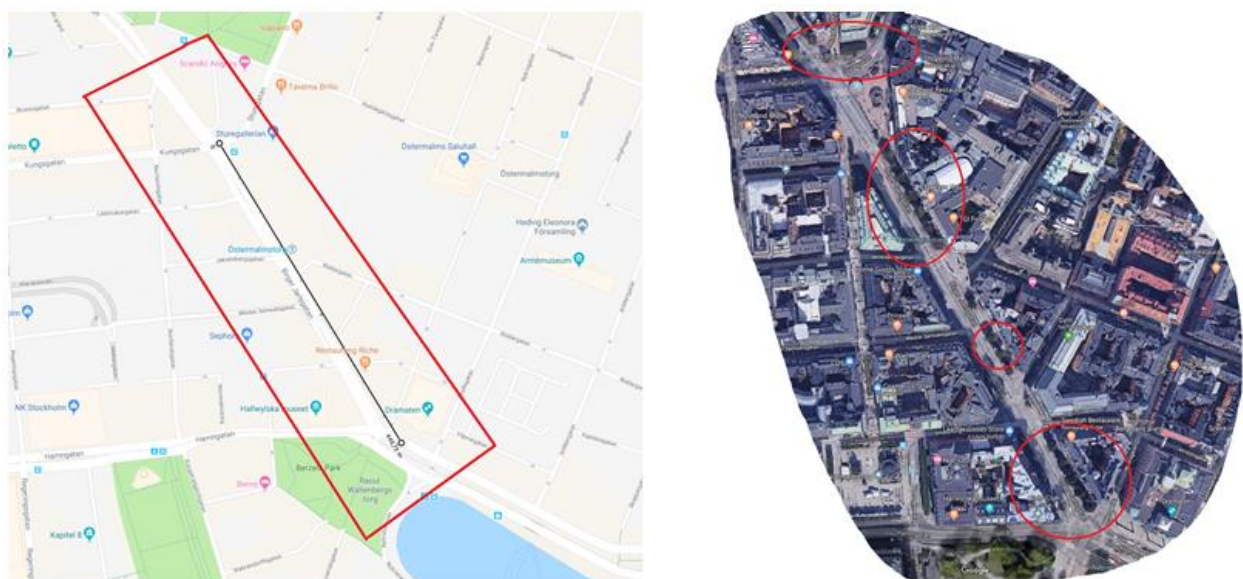


Figure 75: 3D modelling of a 450 m long street section in central Stockholm to see the effect of trees on air quality.

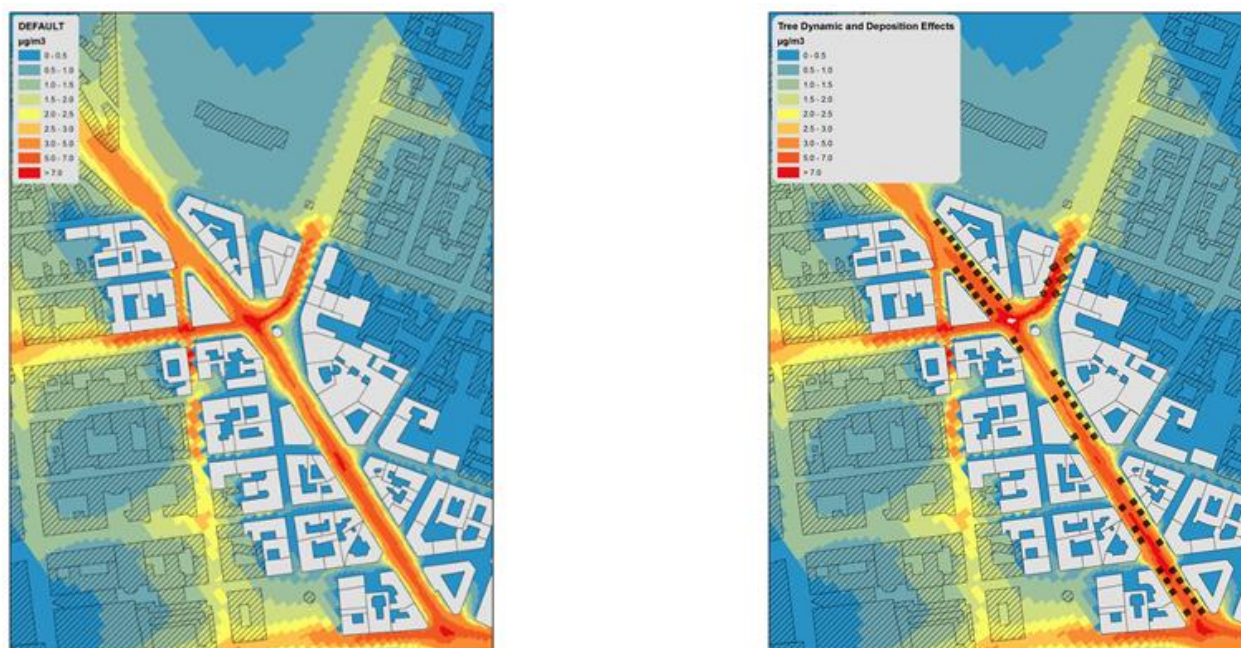


Figure 76: Effect of trees on street level annual PM10 concentrations along Birger Jarlsgatan in central Stockholm. Left: without trees, right: with trees (black dots). Colours indicate concentration in $\mu\text{g m}^{-3}$ (including only local traffic emissions).

3.2.3 Summary

This demonstration case addressing issues in Sweden has shown how the EU-GL methodology is applied to investigate how the effect of climate change can be mitigated.

The first user story concerns the hazard of pluvial flooding resulting from intense precipitation with the **elements of exposure** being buildings and infrastructure. This work has involved a consolidation of data as well as the development and implementation of a flow model in order to better **characterise the flooding hazard** for southern Sweden. As a second task, existing **adaptation measures were evaluated** in terms of their effect mitigating climate change for Jönköping, Sweden. This was performed through the use of two models (SCALGO for a preliminary analysis and MIKE), with the focus on determining consequences for important societal functions (e.g. schools, infrastructure, hospitals). Furthermore, the case of land use modification was addressed by investigating the change to the flooding hazard in Jönköping by the replacement of forest and farmland with increased paved areas upstream. A specific analysis of **vulnerability or the calculations of risk and impact** were not the focus for this study.

The second user story investigates the **hazard of heat waves** with the **element of exposure** being the urban population. The study made use of Urban SIS climate data and impact indicators as well as the SURFEX model to capture the small-scale elements of the urban environment (building density, vegetation fraction) at $1 \times 1 \text{ km}^2$ resolution. Impact indicators relating to the vulnerability of the population concerning heat (e.g. heat-induced mortality) and air quality were investigated. Relevant **adaptation options** of how the city develops in the future in terms of the amount of vegetation and density of buildings were **assessed** in terms of the changes in air temperature. Furthermore, it was shown that adaptation options involving increased vegetation need to be assessed in terms of their role in air pollution. Trees have the effect of reducing ventilation within the urban canyon and can thus lead to elevated levels of air pollution. As such, this shows that it is not always correct to assume that increasing vegetation to make the urban climate more liveable is an obvious solution, and shows the importance of conducting such **adaptation option assessments**.

3.3 DC3

The Linz Demonstration Case addresses heat hazards at the urban scale – including the urban heat island (UHI) effect – and aims to examine climate-change adaptation strategies to support climate-resilient urban planning and decision-making with respect to temperature increases.

The main objectives of DC3 are manifested through the parent user stories:

- US-DC3-100 Heat island adaptation measures-Linz-02
- US-DC3-200 Ventilation pattern adaptation measures-Linz-03

The workflow of DC3 according to the EU-GL methodology described in D3.1 is summarized in **Table 48**.

Table 48: Overview of the workflow of DC1 and its relation to the EU-GL methodology.

Hazard Characterisation	Element at risk	Vulnerability	Impact	Adaptation Options
Heat waves	People	High for very young/old age groups	Excess heat mortality Productivity loss	Green roofs, increased vegetation, albedo changes, reduction in soil-sealing

3.3.1 Regional and Urban Climate Modelling

As the majority of the work completed for this demonstration case concerning the climate modelling of the Linz, Austria, was already presented in D3.2, this section will concentrate on the results achieved since then with important points from D3.2 repeated here where relevant.

The Greater Linz area was first investigated at a spatial resolution of 1 km × 1 km with the COSMO-CLM. Here the Interest was on the heat wave hazard in terms of the temperature, and numbers of hot days and tropical nights and how these will look in the future. For the urban-scale climate modelling of Linz, MUKLIMO_3 was applied along with the cuboid method (dynamical statistical downscaling approach) to analyse the heat distribution over long-term climate periods. Both investigations showed an increase in the heat content over Linz in terms of the numbers of summer days and tropical nights.

With MUKLIMO_3, several adaptation measures such as through an increase in the albedo of roofs, roof greening, or unsealing of surfaces could be modelled and their effects assessed. Each adaptation measure showed a decrease in the number of summer days in the future compared with the 1971-2000 baseline climate of varying amounts.

3.3.2 Microclimate Modelling

Microclimate modelling of the Linz Demonstration case is primarily concerned with the **Identification and Appraisal of Adaptation Options** steps of the EU-GL methodology. Specifically, the work presented here addresses the following:

1. Adaptation options simulations for selected sample sites in the City of Linz
2. Validation of microclimate simulation results

3.3.2.1 Modelling of Adaptation Options within the City of Linz

Microclimate simulations were conducted to demonstrate the possible impact of hypothetical adaptation measures at selected sample sites (Linz city centre, Tabakfabrik Linz, Green Center, inner city street block). These results were presented and discussed in a stakeholder workshop in Linz and published at a press conference with following interviews for TV, radio and newspapers. The case of introducing increased greening within the city centre of Linz is shown in **Figure 77**. The location of the two areas of increased greening are above and to the left of centre, and above and to the right of centre in **Figure 77b**.

The effect of this adaptation option is presented in **Figure 78**, where the mean radiant temperature averaged over 24 hours is presented for both the current layout (panel a), and for the case of the increased greening (panel b). It is clear to see that where the greening has increased, the mean radiant temperature is reduced by about 10-12°C

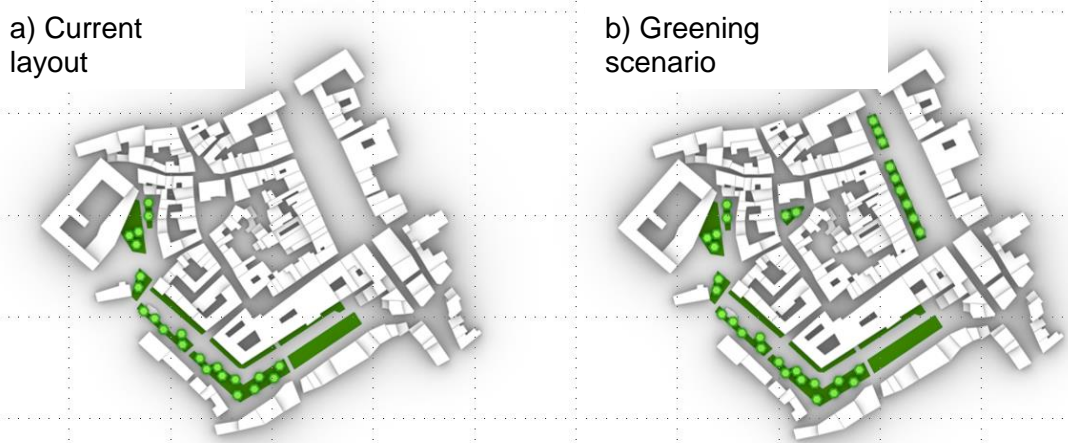


Figure 77: Hypothetical adaptation measure: a) current layout, b) proposed greening of the main square in the city centre.

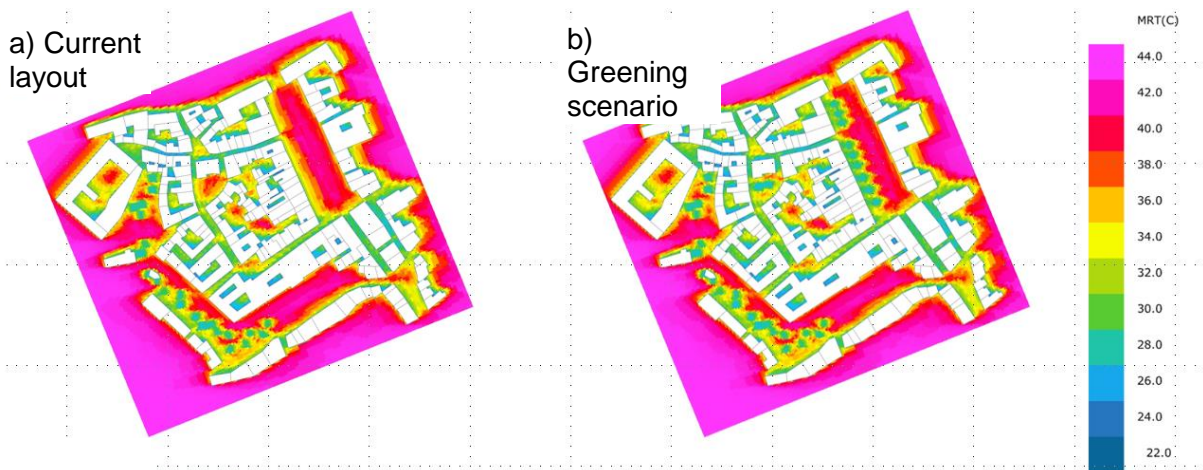


Figure 78: Simulations of the mean radiant temperature (MRT) averaged over 24 hours, a) with the current layer and b) with the increased greening.

3.3.2.2 Validation of the Micro-Climature Model Output

The results from the Micro-Climature Model were validated, which involved model tests, model extensions, and setting up test sites and applications to simulate the adaptation effects. The validation has been undertaken in two methods.

The first method utilizes infrared camera measurements of surfaces with different properties (asphalt, grass, facades – both sunny and shaded) using the AIT campus as a test site, which were compared to ENVI-MET and Rhino/Grasshopper simulations of surface temperature. **Figure 79** shows the locations of the infrared cameras used at the AIT campus. **Figure 80** shows the surface temperatures for two locations, one characterised by “asphalt, sun” and the other by “asphalt, shadow”. The measurements were made from just after 3pm to 9pm on one day and from about 7am to 5pm on the following day. The dark blue line shows this measurement of surface temperature, while the other coloured lines show mean radiant temperature and the UTCI calculated from ENVIMET and Rhino/Grasshopper (GH).

1 Asphalt sun	Parkinglot 65
2 Asphalt shadow	Parkinglot 62
3 Gravel (sun)	
4 Grass sun	near gravel
5 Grass under tree	
6 Window and Facade East	GG4
7 Window and Facade North	GG5
8 Window and Facade West	GG6
9 Window and Facade South	GG7
10 Asphalt South	Parkinglot 16
11 S/W Glass Facade	GG4
12 Tree (202)	behind GG6
13 Grass under tree (202)	behind GG6
14 Tree crown (202)	behind GG6
15 Tree asphalt (sun and shade)	
16 Facade	GG6
17 Energy Base	GG6
18 Terrace concrete	GG6
19 Terrace wood	GG6
20 Terrace greening	GG6
21 Terrace greening	GG6

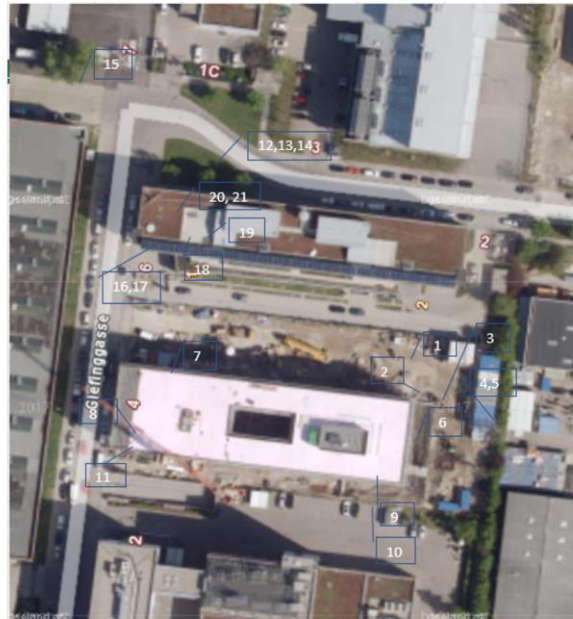


Figure 79: Locations of infrared camera measurements at AIT campus. The numbers in the leftmost column correspond to the numbers on the image at right.



Figure 80: Comparison of measured and simulated values for the locations a) “asphalt sun” and b) “asphalt shadow”. The dark blue line represents the measured surface temperature, while the other lines represent values calculated either from ENVI-MET or Rhino/Grasshopper (GH).

The second method of validation involved a three month monitoring campaign from August to October 2019, making use of two weather stations with several sensors (temperature, humidity, radiation) located at the Tabakfabrik Linz site in a fully shaded area below a tree and a fully sunny “grass island”. **Table 49** shows values of global radiation and temperature measured at several different locations at different times of the day. The different locations exhibit very similar temperatures but large deviations in global radiation, which suggests that the mean radiant temperature, which takes into account radiation, may be a better indicator for thermal comfort than temperature alone.

Table 49: Comparison between measurements of global radiation and temperature at different locations.

	Global Radiation (W/m ²)	Anzengruberstrasse	Tabakfabrik	Tabakfabrik Shadow
night 0:15-5:00		0,0	0,0	0,0
early morning 5:15-9:00		28,9	41,6	8,7
late morning 9:15-11:30		341,1	362,9	24,2
noon 11:45-14:30		497,7	432,3	24,4
early afternoon 14:45-16:30		352,6	369,6	21,4
late afternoon/evening 16:45-20:00		44,2	49,6	7,3
night 20:15-24:00		0,0	0,0	0,0
	Temperature (°C)	Anzengruberstrasse	Tabakfabrik	Tabakfabrik Shadow
night 0:15-5:00		14,1	13,7	13,9
early morning 5:15-9:00		13,1	13,0	13,1
late morning 9:15-11:30		16,5	16,4	16,0
noon 11:45-14:30		19,9	19,5	19,1
early afternoon 14:45-16:30		20,9	20,9	20,4
late afternoon/evening 16:45-20:00		19,4	19,3	19,4
night 20:15-24:00		16,5	16,1	16,3

The measurement results were compared to Rhino/Grasshopper simulations with the following conclusions made:

- ENVI-MET night-time results appear to be less plausible; Rhino3D-Grasshopper extensions (Ladybug, Honeybee and Dragonfly) produce more plausible results but also here the daytime results show higher validity as the night time results where the back-radiation of ground and building surfaces, heated up during the daytime hours, is not fully reflected by the simulations.
- AIT further started plausibility checking by screening (heat) downscaling indices and mortality impact index in Linz and other areas (e.g. Vienna, Naples, Salzburg, Innsbruck...)

3.3.3 Summary

This Demonstration Case for Linz has shown how the EU-GL methodology is applied to investigate how the effect of climate change can be mitigated. For this study it was previously determined through the **hazard characterisation** that heat was a relevant hazard to investigate. This was subsequently performed at three different spatial scales through climate modelling typical of an expert study (regional and urban scale in 3.3.1 and sections 3.3.1 and 3.3.2 of D3.2 and suburb scale in Section 3.3.2). Several heat indices calculated from several climate models for the baseline (historical) period and future periods allowed an assessment of the change for the **element of exposure** being the population of Linz. An analysis of the **vulnerability** and subsequent calculations of **risk and impact** were not necessary for this study. Instead, of interest was an **assessment** of possible Adaptation Options in mitigating the heat hazard. This analysis was performed on both the urban scale (changes to roof albedo, roof greening, reduction of soil sealing) affecting the entire urban area, and at the city-block/suburb scale (increased greening) affecting only certain streets, and showed how such changes can lead to a reduction in the heat load in the affected areas.

3.4 DC4

The partners of DC4 have worked on the preparation of a software tool to ease the implementation of the methodology adopted for the screening of CC risk in a road project. Such a tool is being designed to incorporate the EU-GL steps of Evaluation of Exposure, Vulnerability Analysis, and Risk and Impact Assessment. The tool is coherent with the schematization of the CLARITY modelling workflow that is implemented for urban areas, although adjusted to the specific assessment needs of road infrastructure managers.

The workflow of DC4 according to the EU-GL methodology described in D3.1 is summarized in **Table 50**.

Table 50: Overview of the workflow of DC4 and its relation to the EU-GL methodology.

Hazard Characterisation	Element at risk	Vulnerability	Impact	Adaptation Options
Heat waves	Road infrastructure	High for extreme temperatures and extended durations	Surface deformities, rutting, damage	Changes in road orientation / shadowing
Cold waves	Road infrastructure, People	High during winter	Snow and ice buildup on elevated road surfaces	Changes in routes to lower elevations
Floods	Road infrastructure, People		Insufficient drainage	Increases in drainage sizes / channels

The purpose of this demo case is to document the results of the climate change risk assessment of the "Autovía A-2", section Guadalajara - Alcolea del Pinar. This risk assessment has been carried out applying the recommendations contained in the "Climate Change Vulnerability and Risk Assessment Methodology for Road Projects", elaborated for its application in the Demonstration Case 4 of the Clarity Project.

The Project includes the section of the A-2 dual carriageway which is the object of the "Autovía de First Generation, N-II, from P.K. 62+000 to the limit of the province of Soria/Guadalajara, P.K. 139+500. Construction and Operation". This is a section of the State Highway Network located entirely within the province of Guadalajara with two lanes for each direction of circulation. From its link with the R-2 motorway in the municipality of Guadalajara crosses the municipalities of Torija, Trijueque, Muduex, Gajanejos, Ledanca, Almadrones, Mandayona, Mirabueno, Algora, Torremocha del Campo, Saúca and Alcolea del Pinar. The section, which is currently in operation, is concessioned by a 19-year period by shadow toll until 2026 to *ACCIONA Construction*.

As details about this DC have already been provided in Section 3.4 of D3.2, these will be left out here and only referred to where relevant.

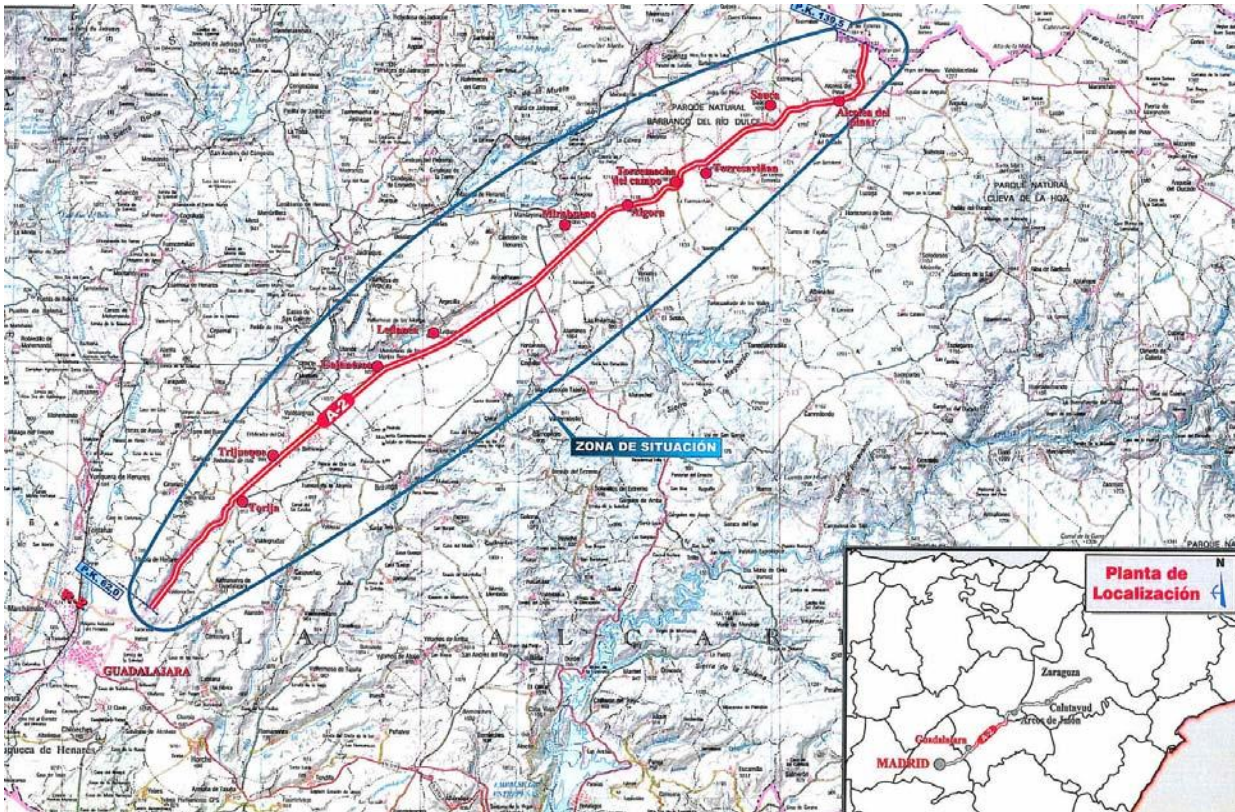


Figure 81: Map showing the region of interest.

The concession contract with *ACCIONA Construction* comprises three areas of activity:

- Adaptation, reform and modernisation works carried out at the start of the concession period, from 2007 to 2013, to adapt the infrastructure to the technical and functional characteristics required for the correct provision of the service. This entailed substantial modifications in terms of layout, construction and arrangement of links, etc. Also, it was necessary to carry out the rehabilitation works and replacement of existing infrastructure so that they were renovated and improved the initial conditions of the track. The works carried out include, in particular:
 - Route variants.
 - Population variants.
 - Improvement of curves with route variation.
 - Variations in the ground level that involve demolition and reconstruction of the road surface.
 - Construction or extension of service roads.
 - Construction or enlargement of collector roads.
 - Construction of links.
- Replacement, repair or rehabilitation work to be carried out during the life of the concession on those elements of the infrastructure whose estimated useful life is less than the term of the concession contract.
- Operation and maintenance work on the road from the entry into the contract and for the entire duration of the concession. It includes the ordinary conservation and the maintenance of the road, including during the execution of the works of adequacy and reform.

3.4.1 Adaptation elements and its economical appraisal

The selection of adaptation strategies opens a wide window of possibilities. A thorough assessment on adaptation strategies has been done in the framework of the *ROADADAPT project* [24], where a 10 step approach that can be applied to different climate hazards is proposed. The elements assessed are mainly: erosion of road embankments and foundations, landslides, loss of road structure integrity, loss of pavement integrity, and loss of driving ability (traffic conditions). This can be taken as a reference for the DC4.

The next step would be to perform the economic appraisal of the adaptation options. This issue has also been thoroughly studied within the *ROADADAPT*. From the analysis of the reports produced within the project one can see that it has a certain complexity. For each threat, different adaptation options can be proposed. The objective of these measures are to either eliminate the threat (so the risk disappears) or reduce the impact of the threat. The cost of the implementation of the adaptation measure can be compared with the cost of the impact. This cost benefit assessment (CBA) will be taken into consideration by the road authorities in the process of decision making.









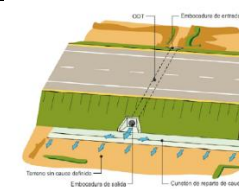
So in the first place, an economic analysis of the adaptation measures has to be done. The overall workflow of the process is shown in **Table 51**.






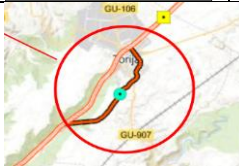
Table 51: Overall workflow including the cost parameters for the adaptation measure

Hazards	Elements	Damage Typologies	Vulnerability Assessment	Risk Assessment
<input type="checkbox"/> ok Extreme Precipitation Events	Paviment	Sliding of slopes	<input type="checkbox"/> ok Probability of Hazards	<input type="checkbox"/> ok Risk Level
Heat Waves	Transverse drainage	Structural movements		
Cold Waves	Road section	<input type="checkbox"/> ok Insufficient capacity to water evacuate	<input type="checkbox"/> ok Severity	<input type="checkbox"/> ok Cost parameters
Windstorms	<input type="checkbox"/> ok Traffic conditions	Snowdrifts		
Forest Fires		Affectation to the circulation by fires		

Table 52 shows in detail adaptation measures along with their economic cost, addressing each hazard and element at risk identified in DC4 (for more information, see D3.2). An implementation cost scale was defined to quantify adaptation investment, from 1 (cheap) to 3 (expensive). An expected efficiency scale based on expert criteria, was defined from A (good) to C (weak) to quantify the expected efficiency. Further information can be found in Annex II: Adaptation options.

Table 52: DC4 Adaptation measures for each element and risk with cost scale and expected efficiency.

Main potential hazards and impacts	Element at risk	Adaptation measures	Average Cost	Cost Scale	Expected Efficiency	
Falling materials and erosion as a consequence of intense rainfall	Traffic conditions	Afforestation of slopes with drought-resistant species		8,6 €/m ²	1	A-B
		Implementation of erosion control blankets or other type of protection (drains, berms, anchors, gunite or others)		11,5€/m ²	2	A-B
		Reduce the slope of the cut Soft soils: 6€/m ³ Rock soils 20€/m ³		13€/m ³ (average)	3	A-B
		Improvement of road maintenance resources		24.000€/k m	3	B
Structural movements in pontoon (pk 63+775) due to the presence of water	Pontoon (pk 63+775)	Reinforcement of of the pontoon		105€/m	3	A
		Improve drainage		65€/m ²	2	B
Structural movements in pontoon (pk 63+775) due to the presence of water	Traffic conditions	Signalisation (reduce speed)		300 €/unit	1	C
Insufficient drainage capacity of the road surface during episodes of very heavy rainfall	Traffic conditions (left lane of the section from PK 112+000 to 113+000)	Alternative mixtures for bituminous pavements and surface courses (porous asphalt)		+4€/ton	2	A
		Improve drainage within the section (transversal and longitudinal)		Project design	3	A

		Inspection and clean culverts regularly		1000 €/km	1	B
		Lane closure (personal, patrol, fuel, signalling)		660€/day	1	C
Snowfall and snowdrifts	Traffic conditions (from PK 92+700 to 93+300 and from PK 120+400 to 123+300; left side of the dual carriageway)	Increase surveillance of the section in case of unfavourable weather conditions		150€/km	1	B-C
		De-icing agents that cause the least possible damage to pavements and the environment.		500 €/km	2	A-B
		Improving the asphalt specification to increase its failure strain		+4€/ton	2	A
		Allow alternative routes in case of road closure		Project desing	1	B

The cost of the reparation can be estimated from the average costs of maintenance activities (ordinary and extraordinary maintenance activities). The cost of the impact on traffic conditions can be assessed from different points of view. For the *ROADAPT project* it was considered that the travel time was the main key indicator for impact assessment.

The cost benefit assessment has been done for the traffic conditions at **pk 72+900 to pk 73+150** because of its high risk, due to intense rainfalls that might cause rocks to fall on the carriage way:

“The level of risk in the three cuttings considered to be at risk is not expected to vary over the time horizon covered by the assessment (80 years). The slope with the highest risk level is the one from PK 72+900 to PK 73+150, with medium risk to the integrity of the element and high risk to the conditions of circulation. “

EVALUACIÓN DEL RIESGO DEL PROYECTO 'Autovía A-2 Tramo Guadalajara - Alcolea del Pinar'								
Deslizamiento de laderas y caída de materiales y erosión de taludes en desmonte			Integridad del elemento			Condiciones de circulación		
			2018	2048	2098	2018	2048	2098
Talud-1	A-2 PK 64+500 Calz. Decr.	Severidad afectación	4	4	4	3	3	3
		Probabilidad afectación	3	3	3	3	3	3
		Nivel del riesgo	Riesgo bajo	Riesgo bajo	Riesgo bajo	Riesgo bajo	Riesgo bajo	Riesgo bajo
Talud-2	A-2 PK 72+900 a 73+150 Calz. Decr.	Severidad afectación	4	4	4	4	4	4
		Probabilidad afectación	4	4	4	4	4	4
		Nivel del riesgo	Riesgo medio	Riesgo medio	Riesgo medio	Riesgo alto	Riesgo alto	Riesgo alto
Talud-3	A-2 PK 129+300 a 129+400	Severidad afectación	2	2	2	2	2	2
		Probabilidad afectación	3	3	3	2	2	2
		Nivel del riesgo	Riesgo despreciable	Riesgo despreciable	Riesgo despreciable	Riesgo despreciable	Riesgo despreciable	Riesgo despreciable



Figure 82: Side view of slope at pk 72+900 to pk 73+150

Cost of reparation:

In the event of slope collapse due to any of the analysed risks (falling materials and erosion as a consequence of intense rainfall) an average slope surface has been calculated according to the following estimation:

- slope length of 150 m and average slope high of 5 m
- overall surface of 750 m².

The cost of reparation was calculated in two different phases:

- Restoration of collapsed slope by refining, prefilling and disposal of remaining soil terrain at an average slope depth of 2 meters with an overall of 750 m²x2m =1,500 m³, with an average cost of 8,3 €/m³. Total restoration cost: 12,450 €
- Slope stabilization with erosion control blankets, at an average cost of 15 €/m² with a total stabilization cost of 11,250 €

The estimated total cost in the case of slope collapse and later stabilization and mitigation will be 23,700 €



Figure 83: Aerial view of the slope at pk 72+900 to pk 73+150 and surface estimation.

Cost of the affection to traffic conditions:

In the scenario analysed the right lane of the road has to be closed for a week. This means delays of up to 1 hour every day (because of traffic jams at peak hours and speed reductions). A simple calculation has been done in order to calculate the cost of time that is lost due to this event.

The average daily traffic (ADT) values are:

ADT (light vehicles): 21,905 vehicles

ADT (heavy vehicles): 7,403 vehicles

It is assumed that, for the distribution of the traffic flow within a day for an interurban road (see **Figure 84**), the delays will only take in place during peak hours; this is expected to happen during approximately 4 hours a day. The intensity at peak hours can be estimated as 7% of ADT (light vehicles). Therefore, it is going to be considered that only 28% of the ADT suffers this 1 hour delay. In the case of heavy vehicles, the intensity at peak hour can be estimated at 5% of the ADT (heavy vehicles), so only 20% of the trucks might be affected by delays.

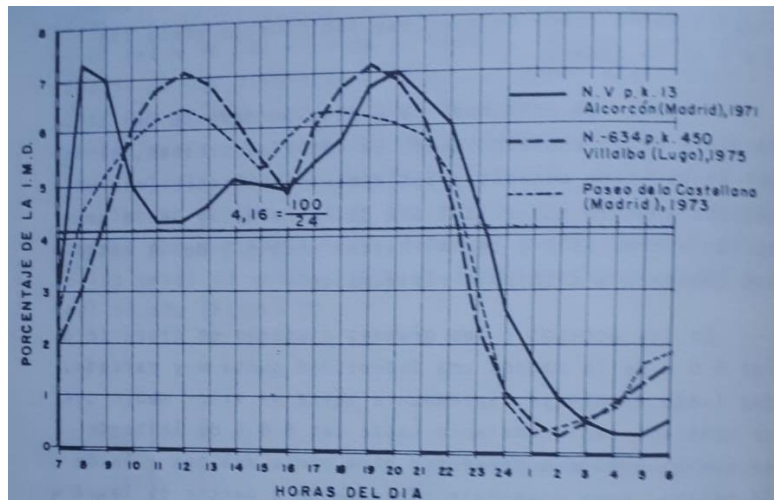


Figure 84: Average daily traffic distribution per hour.

The value of time has been considered 25.95€/h for light vehicles and 34.53 €/h for heavy vehicles¹⁴.

Table 53: Estimation of costs related to closure of lane between PK 72+900 to PK 73+150,

	Value for LV	Value for HV	Total (LV+HV)
Duration of incident (days)	7		
Number of vehicles per day	21.905	7.403	29.308
Percentage of vehicles affected	0,28	0,2	
Individual time loss (h)	1	1	
Value of time (€/h)	25,95	34,53	
Total loss time €	1.114.132,11	357.875,83	1.472.007,94

¹⁴ Source: https://www.mitma.gob.es/recursos_mfom/ns_32014.pdf

In the case that the whole road section had to be closed, the socioeconomic impact would be bigger because the traffic has to be deviated. Therefore, costs associated to vehicle operation have to be added. In the case of the section between PK 72+900 to PK 73+150 the alternative route would not suppose a big increase in distance but it is a difference in the road section capacity. In other sections of the pilot, the increase in distance would be severe as it can be seen in the map below.

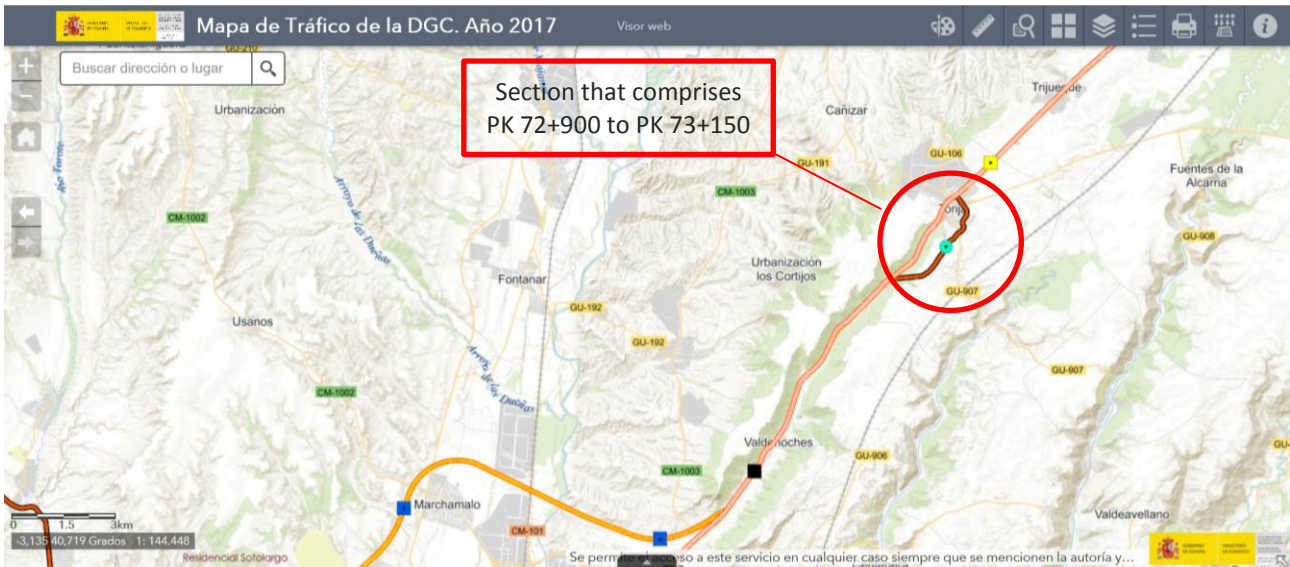


Figure 85: Traffic map (source: <https://mapas.fomento.gob.es/mapatrafico/2017/>)

3.4.2 Summary

This Demonstration Case for Spain has shown how the EU-GL methodology is applied to investigate how the effect of climate change can be mitigated, with the focus over the last year being on assessing adaptation options. The relevant **hazards** for this study include heat and cold waves, and floods, with the **element of exposure** being road infrastructure, and indirectly people which are dependent on such transport routes and the maintenance thereof. An analysis of the **vulnerability** showed that the road infrastructure was at most risk to damage during extended periods of extreme heat or cold. The **impacts** on the road included surface damage and deformities during extreme heat, and the build-up of snow and ice on elevated and exposed road sections during extreme cold. A number of **adaptation options** were proposed with **economic appraisals** made, with the case presented of what costs would be incurred for failing to implement adaptation options for a section of motorway with a slope. Erosion and subsequent slope collapse leading to debris on the road would provide significant costs in terms of restoration and delays in the traffic.

4 Conclusions

The main objective of this deliverable is to give a report on the work performed in WP3 since the last deliverable D3.2 and thus conclude the Scientific Support part of CLARITY.

The **EU-GL methodology** employed within CLARITY is the basis for the **Basic Screening Level, Advanced Screening Level and Expert Level** of service provided through CSIS. The backbone of the basic screening level has been the development of the pan-European climate indices as well as the integration of various datasets from portals such as Urban Atlas encompassing land usage, vegetation, orography, population, etc. The calculations of the climate indices necessary for the **hazard characterisation** step of the EU-GL has involved the initial bias-correction of the EURO-CORDEX climate model data. Of relevance were climate indices related to heat waves and floods, and to a lesser extent on wind storms, droughts, and landslides. Further flooding indicators were obtained from SWICCA. Much of this data has been imported into the CSIS in the form of data packages and is available for users of the CSIS.

As the resolution of the pan-European datasets is too coarse to be directly applied to urban settings, methods for calculating the local effect based on physical principles and the pan-European datasets has been developed and refined in the case of the heat waves, through calibration and validation (ongoing) on the Naples area and smaller areas within. This forms the foundation of the advanced screening level. The method of calculating the local effect for flooding has been developed and implemented for sub-areas within Naples and calibration and validation is still ongoing. Both methods consider not only the hazard, but also the **elements** which are **exposed** to the hazard (people for heat, and buildings and infrastructure for floods), and also assesses their **vulnerability**.

The calculations of the **hazard impact** can be made with estimates of mortality, in the case of heat waves, provided as a function of heat wave duration and intensity. This is currently available within the CSIS but is still in a testing and calibration phase. Methods have been presented to evaluate the **impact economically** for both heat waves and floods by focussing on both the direct and indirect costs which affect people (heat waves) and buildings and infrastructure (floods). An extension of these methods is made to encompass the role of **adaptation measures** in order to **evaluate** their costs and benefits. This is vital aspect in deciding which measures should be implemented.

The four demonstration cases examine different steps of the EU-GL at various levels of complexity according to the requirements of the users involved.

DC1 concerns **Naples, Italy** and examines the hazards of heat waves, floods, and to a lesser extent, landslides, the **hazard characterisation** step showed that the duration and intensity of heat waves is projected to increase in the future. Similarly, heavy precipitation events are projected to increase in the future, which will also affect landslides. Measures were examined to assess the impact on the **elements of exposure**, such as indices of temperature and perceived comfort relevant for humans in the case of heat waves, and runoff and flooding probability relevant for buildings and infrastructure in the case of floods. Both were calculated using local effect models operating at 250×250m² developed by PLINIVS. In the case of heat waves, appropriate damage classes for the population were devised to consider the **vulnerability** aspect necessary for the calculation of the hazard impact. Relevant **adaptation measures** have been investigated with the aim of reducing the impacts of heat waves and floods. Preliminary tests of the proposed calculation methodology to **assess their benefits** have been conducted for various adaptation measures, and the results are still under analysis.

DC2 investigates several cities/towns in **Sweden** and examines the hazards of pluvial flooding from intense precipitation, and heat waves. In the case of flooding, the **elements of exposure** are buildings and infrastructure, with the **hazard characterisation** occurring on the basis of a consolidation of climate index data as well as the development and implementation of a flow model for southern Sweden. Existing **adaptation measures were evaluated** in terms of their effect mitigating climate change for Jönköping, Sweden performed through the use of two models (SCALGO for a preliminary analysis and MIKE), with the

focus on societal functions (e.g. schools, infrastructure, hospitals). Furthermore, the case of land use modification was addressed by investigating the change to the flooding hazard in Jönköping by the replacement of forest and farmland with increased paved areas upstream. In the case of heat waves with the **element of exposure** being the urban population, Urban SIS climate data and impact indicators as well as the SURFEX model were employed to capture the small-scale elements of the urban environment (building density, vegetation fraction) at 1×1 km² resolution. Impact indicators relating to the **vulnerability** of the population concerning heat (e.g. heat-induced mortality) and air quality were investigated. Relevant **adaptation options** of how the city develops in the future in terms of the amount of vegetation and density of buildings were **assessed** in terms of the changes in air temperature and pollution.

DC3 concerns **Linz, Austria** and the **hazard characterisation** step (along with communication with the users) showed that heat was the relevant hazard to investigate. This investigation occurred at three different spatial scales through climate modelling typical of an expert level study. Several heat indices calculated from several climate models for the baseline (historical) period and future periods allowed an assessment of the change for the **element of exposure**, that being the population of Linz. An analysis of the **vulnerability** and subsequent calculations of **risk and impact** were not necessary for this study. Instead, of interest was an **assessment** of possible **adaptation options** in mitigating the heat hazard. This analysis was performed on both the urban scale (changes to roof albedo, roof greening, reduction of soil sealing) affecting the entire urban area, and at the city-block/suburb scale (increased greening) affecting only certain streets, and showed how such changes can lead to a reduction in the heat load in the affected areas.

DC4 concerns **Spain**, where the relevant **hazards** for this study include heat and cold waves, and floods, with the **element of exposure** being road infrastructure, and indirectly people which are dependent on such transport routes and the maintenance thereof. An analysis of the **vulnerability** showed that the road infrastructure was at most risk to damage during extended periods of extreme heat or cold. The **impacts** on the road included surface damage and deformities during extreme heat, and the build-up of snow and ice on elevated and exposed road sections during extreme cold. A number of **adaptation options** were proposed, including changes in road orientation or shadowing to minimise solar radiation in the case of heat, or changes to routes to lower elevations in the case of cold. For the flooding hazard caused by heavy precipitation in short periods of time, a necessary adaptation measure would be to increase the size of drainage channels to accommodate the water. An **economic appraisal** of failing to implement adaptation options showed the costs that would be incurred for the example of a section of motorway with a slope. Erosion and subsequent slope collapse leading to debris on the road would provide significant costs in terms of restoration and delays in the traffic.

5 Acknowledgement

According to Article 38.1.2 of the model grant agreement, all the documents related to CLARITY (deliverables, presentations, papers, newsletters, leaflets etc.) shall contain the following statement: ***“This project has received funding from the European Union’s Horizon 2020 research and innovation programme under grant agreement No 730355.”***

6 References

- [1] Directorate-General Climate Action, "Non-paper Guidelines for Project Managers: Making vulnerable investments climate resilient," European Commission, 2011. [Online]. Available: <http://climate-adapt.eea.europa.eu/metadata/guidances/non-paper-guidelines-for-project-managers-making-vulnerable-investments-climate-resilient/guidelines-for-project-managers.pdf>. [Accessed November 21 2017].
- [2] Taylor, K. E., Stouffer, R. J., Meehl, G. A., "An overview of CMIP5 and the experiment design," *Bulletin of the American Meteorological Society*, no. April, pp. 485-498, 2012.
- [3] IPCC, "Climate Change 2014: Synthesis Report," Contribution of Working Groups I, II and III to the Fifth Assessment Report of the Intergovernmental Panel on Climate Change [Core Writing Team, R.K. Pachauri and L.A. Meyer (eds.)], IPCC, Geneva, Switzerland, 2014.
- [4] P. J. Robinson, "On the definition of a heat wave," *Journal of Applied Meteorology*, vol. 40, pp. 762-775, 2001.
- [5] S. E. Perkins, "A review on the scientific understanding of heatwaves - Their measurement, driving mechanisms, and changes at the global scale," *Atmospheric Research*, no. 164-165, pp. 242-267, 2015.
- [6] Perkins, S. E., Alexander, L. V., "On the measurement of heat waves," *Journal of Climate*, no. 26, pp. 4500-4517, 2013.
- [7] D'Ippoliti, D., Michelozzi, P., Marino, C., de'Donato, F., Menne, B., Katsouyanni, K., Kirchmayer, U., Analitis, A., Medina-Ramon, M., Paldy, A., Atkinson, R., Kovats, S., Bisanti, L., Schneider, A., Lefranc, A., Iniguez, C., Perucci, C. A., "The impact of heat waves on mortality in 9 European cities: Results from the EuroHEAT project," no. 9, pp. 1-9, 2010.
- [8] Lindberg, F., Grimmond, C. S. B., "SOLWEIG_v2018a," Department of Earth Sciences, University of Gothenburg, Sweden, University of Reading, UK, 2019.
- [9] Defra, "Surface Water Management Plan Technical Guidance," Department for Environment, Food and Rural Affairs, London, UK, 2010.
- [10] Parker, D. J., Priest, S. J., McCarthy, S. S., "Surface water flood warnings requirements and potential in England and Wales," *Applied Geography*, vol. 31, no. 3, pp. 891-900, 2011.
- [11] European Environmental Agency, "Climate Change, impacts and vulnerability in Europe 2016," Publications Office of the European Union, Luxembourg, 2017.
- [12] Smith, L. S., Liang, Q., Quinn, P. F., "A flexible hydrodynamic modelling framework for GPUs and CPUs: Application to the Carlisle 2005 floods," in *International Conference on Flood Resilience: Experiences in Asia and Europe*, Newcastle University, 2013.
- [13] Pitt, M., "The Pitt Review: Learning lessons from the 2007 floods, London, UK," Cabinet Office, London, UK, 2008.
- [14] Dhakal, N., Fang, X., Cleveland, T. G., Thompson, D. B., Asquith, W. H., Marzen, L. J., "Estimation of volumetric runoff coefficients for Texas watersheds using land-use and rainfall-runoff data," *Journal of Irrigation and Drainage Engineering*, vol. 138, 2011.
- [15] Viessman, W. L. G., Introduction to Hydrology, Upper Saddle River, New Jersey: 5th ed. Prentice Hall, 2003.
- [16] de Almeida, I. K., Almeida, A. K., Anache, J. A. A., Steffen, J. L., Sobrinho, T. A., "Estimation on time of concentration of overland flow in watersheds: a review," *Geociências*, vol. 33, no. 4, pp. 661-671, 2014.
- [17] N. i. England, "Sito ufficiale del Sistema Sanitario del Regno Unito," [Online]. Available: <http://www.nhs.uk/Conditions/Heat-exhaustion-and-heatstroke/Pages/Diagnosis.aspx>. [Accessed 31 January 2020].

- [18] Merrill, C. T., Miller, M., Steiner, C., "Hospital Stays Resulting from Excessive Heat and Cold Exposure Due to Weather Conditions in U.S. Community Hospitals," HEALTHCARE COST AND UTILIZATION PROJECT, Agency for Healthcare Research and Quality, 2005.
- [19] Liss, A., Wu, R., Chui, K. K. H, Naumova, E. N., "Heat-Related Hospitalizations in Older Adults: An Amplified Effect of the First Seasonal Heatwave," *Scientific Reports*, vol. 7, 2017.
- [20] Huizinga, J., Moel, H. de, Szewczyk, W., "Global flood depth-damage functions. Methodology and the database with guidelines," JRC Technical Reports, EC, 2017.
- [21] H. J. Huizinga, "Flood damage functions for EU member states," HKV Consultants, Implemented in the framework of the contract, 2007.
- [22] Bosch Slabbers, "Climate Adaptation App," Landscape + Urban Design, Deltares, Sweco, KNMI, Witteveen+Bos, [Online]. Available: <http://www.climateapp.nl>. [Accessed 2019].
- [23] ATELIER GROENBLAUW, "Urban green-blue grids for sustainable resilient cities," 2016. [Online]. Available: <https://www.urbangreenbluegrids.com>.
- [24] ROADAPT, "Roads for today, adapted for tomorrow. Guideline part E: Selection of adaptation measures and strategies for mitigation.," 2015.
- [25] Zygowicz, W. M., "Developing Key Performance Indicators to Improve Patient Care and Outcome at Littleton Fire Rescue," [Online]. Available: <https://www.hsdl.org/?view&did=692160>. [Accessed 31 January 2019].
- [26] Yager, R. R., "On ordered weighted averaging aggregation operators in multi-criteria decision," *IEEE Transactions on Systems, Man and Cybernetics*, vol. 18, no. 1, pp. 183-190, 1988.
- [27] D'Ambrosio, V., Leone, M. F. (Eds.), "Progettazione ambientale per l'adattamento al Climate Change. Modelli innovativi per la produzione di conoscenza.," CLEAN, Napoli, 2018.
- [28] Kantor, N., Unger, J., "The most problematic variable in the course of human-biometeorological comfort assessment – the mean radiant temperature," *Central European Journal of Geosciences*, vol. 3, pp. 90-100, 2011.
- [29] Thorsson, S., Rocklöv, J., Rayner, D., Konarska, J., Lindberg, F., Holmer, B., "Mean radiant temperature—a measure for evaluating the impact of climate(change) on health.," in *The 8th International Conference on Urban Climate*, Dublin, Ireland, 2012.
- [30] Ng, E., Ren, C. (Eds.), *The urban climatic map: A methodology for sustainable urban planning.*, Routledge, 2015.
- [31] Oke, T. R., Mills, G., Christen, A., Voogt, J. A., *Urban climates*, New York/London: Cambridge University Press, 2017.
- [32] Błażejczyk, K., Jendritzky, G., Bröde, P., Fiala, D., Havenith, G., Epstein, Y., Psikuta, A., Kampmann, B., "An introduction to the universal thermal climate index (UTCI)," *Geographia Polonica*, vol. 86, pp. 5-10, 2013.
- [33] Strohbach, M. W., Arnold, E., Haase, D., "The carbon footprint of urban green space: A lift cycle approach," *Landscape and Urban Planning*, vol. 104, no. 2, pp. 220-229, 2012.
- [34] EC, "Policy Topics: Nature-Based Solutions," 2019. [Online]. Available: <https://ec.europa.eu/research/environment/index.cfm?pg=nbs>.
- [35] TEEB, "The Economics of Ecosystems and Biodiversity: Ecological and Economic Foundation.," Routledge, 2010.
- [36] Kabisch, N., Korn, J., Stadler, J., Bonn, A., *Nature-Based Solutions to Climate Change Adaptation in Urban Areas: Linkages Between Science, Policy and Practice*, 1st ed., Springer Verlag, 2017.
- [37] Rosenzweig, C., Solecki, W., Romero-Lankao, P., Mehrotra, S., Dhakal, S., Ibrahim, S. A., "ARC3.2: Climate Change and Cities: Second Assessment Report of the Urban Climate Research Network.," Columbia University, New York, 2018.
- [38] Berg, P., Noring, L., and Olsson, J., "Creation of a high resolution precipitation data set by merging

- gridded gauge data and radar observations for Sweden.," *Journal of Hydrology*, vol. 541(A), pp. 6-13, 2016.
- [39] Häggmark, L., Ivarsson, K.-I., Gollvik, S. and Olofsson, P.-O., "Mesan, an operational mesoscale analysis system.," *Tellus*, vol. 52A, pp. 2-20, 2000.
- [40] Berg, P., Christensen, O.B., Klehmet, K., Lenderink, G., Olsson, J., Teichmann, C., and Yang, W., "Summertime precipitation extremes in a EURO-CORDEX 0.11 ensemble at an hourly resolution.," *Nat. Hazards Earth Syst. Sci.*, vol. 19, pp. 957-971, 2019.
- [41] Gidhagen L., Olsson J., Amorim J.H., Asker C., Belusic D., Carvalho A.C., Engardt M., Hundecha Y., Körnich H., Lind P., Lindstedt D., Olsson E., Rosberg J., Segersson D., Strömbäck L., "Towards climate services for European cities: Lessons learnt from the Copernicus project Urban SIS," *Urban Climate*, vol. 31, 2020.
- [42] Amorim J.H., Segersson D., Körnich H., Asker C., Olsson E., Gidhagen L., "High resolution simulation of Stockholm's air temperature and its interactions with urban development.," *Urban Climate*, vol. 32, 2020.
- [43] de Donato, F.K., Leone, M., Scortichini, M., De Sario, M., Katsouyanni, K., Lanki, T., Basagana, X., Ballester, F., Astrom, C., Paldy, A., Pascal, M., Gasparri, A., Menne, B., Michelozzi, P., "Changes in the effect of heat on mortality in the last 20 years in nine European cities. Results from the PHASE Project.," *Int. J. Environ. Res. Public Health*, vol. 12, pp. 15567-15583, 2015.
- [44] WHO, "Health risks of air pollution in Europe – HRAPIE," in *Recommendations for Concentration-response Functions for Cost-benefit Analysis of Particulate Matter, Ozone and Nitrogen Dioxide*, Copenhagen, http://www.euro.who.int/__data/assets/pdf_file/0006/238956/Health_risks_air_pollution_HRAPIE_project.pdf?ua=1, 2013.
- [45] COMEAP, "Interim statement on quantifying the association of long-term average concentrations of nitrogen dioxide and mortality.," in *Public Health England*, UK, https://assets.publishing.service.gov.uk/government/uploads/system/uploads/attachment_data/file/485373/COMEAP_NO2_Mortality_Interim_Statement.pdf, 2015.
- [46] Amorim J.H., Segersson D., Körnich H., Asker C., Olsson E., Gidhagen L., "High resolution simulation of Stockholm's air temperature and its interactions with urban development," *Urban Climate*, under revision.
- [47] Alfieri, L., Burek, P., Feyen, L. and Forzieri, G., "Global warming increases the frequency of river floods in Europe," *Hydrology and Earth System Sciences*, vol. 19, no. 5, pp. 2247-2260, 2015.
- [48] Themeßl, M., Gobiet, A., Leuprecht, A., "Empirical-statistical downscaling and error correction of daily precipitation from regional climate models," *Int. J. Climatol.*, pp. 1530-1544, 2011.
- [49] Feigenwinter, I., Kotlarski, S., Casanueva, A., Fischer, A.M., Schwierz, C., Liniger, M. A., "Exploring quantile mapping as a tool to produce user-tailored climate scenarios for Switzerland," Technical Report MeteoSwiss No. 270, Zürich, 2018.
- [50] Donat, M. G., Leckebusch, G. C., Wild, S., Ulbrich, U., "Future changes in European winter storm losses and extreme wind speeds inferred from GCM and RCM multi-model simulations," *Nat. Hazards Earth Syst. Sci.*, vol. 11, pp. 1351-1370, 2011.
- [51] Van Wagner, C. E., "Development and structure of the Canadian Forest Fire Weather Index System," Canadian Forestry Service, Headquarters, Ottawa, 1987.
- [52] Floater, G. Heckt, C. Ulterino, M. Mackie, L. Rode, P. Bhardwaj, A. Carvahlo, M. Gill, D. Bailey, T. and Huxley. R. , "Taxonomy of architecture and infrastructure indicators: Adaptation measures and corresponding indicators for resilient architecture and infrastructure," 2015.
- [53] Floater, G. Heckt, C. Ulterino, M. Mackie, L. Rode, P. Bhardwaj, A. Carvahlo, M. Gill, D. Bailey, T. and Huxley. R., "Co-benefits of urban climate action: A framework for cities.," <http://eprints.lse.ac.uk/id/eprint/68876>, 2016.

- [54] A. Eggert, "Building Urban Resilience by Integrating Co-Benefits of Climate Adaptation into Urban Planning Processes.," Masters Degree Thesis, https://projekter.aau.dk/projekter/files/335107665/Masters_Thesis_EGGERT.pdf, 2020.
- [55] JASPERS, "JASPERS Guidance Note. The Basics of Climate Change Adaptation Vulnerability and Risk Assessment," Joint Assistance in Supporting Projects in European Regions, 2017.
- [56] Mahgoub, Mohamed H., Neveen Hamza, Steven Dudek, "Urban morphology impact on microclimate of the Fatimid city, Cairo, Egypt," in *International Conference on "Changing Cities": Spatial, morphological, formal & socio-economic dimensions*, Skiathos island, Greece, 2013.
- [57] Thorsson, Sofia, D. Rayner, F. Lindberg, A. Monteiro, L. Katzschner, K. Lau, S. Campe, A. Katzschner, J. Konarska, S. Onomura, S. Velho, B. Holmer, "Present and projected future mean radiant temperature for three European cities," *Int. J. Biometeorol.*, vol. 61, pp. 1531-1543, 2017.
- [58] Rakha, Tarek, P. Zhand, C. Reinhart, "A Framework for Outdoor Mean Radiant Temperature Simulation: Towards Spatially Resolved Thermal Comfort Mapping in Urban Spaces," in *Proceedings of the 15th IBPSA Conference*, San Francisco, CA, USA, 2017.

7 Annex I: Climate Indices

A summary of the indices available is shown in **Table 54**.

Table 54: Summary of the climate indices used for hazard characterisation.

Hazard	Index
HEAT: Heat waves	Consecutive summer days
	Consecutive hot days $\geq 75^{\text{th}}$ percentile
HEAT: Extreme heat	Hot days
	Summer days
	Tropical nights
	Maximum temperature $\geq 75^{\text{th}}$ percentile
COLD: Cold waves	Consecutive frost days
COLD: Extreme cold	Frost days
	Ice days
	Minimum temperature $\leq 10^{\text{th}}$ percentile
Thermal stress	Extreme temperature range
FLOODS: Extreme precipitation	Maximum 1-day precipitation
	Maximum 5-day precipitation
	Snow days
FLOODS: Wet periods	Consecutive wet days
	Wet days
	Heavy precipitation days
	Days where daily precipitation $\geq 90^{\text{th}}$ percentile
FLOODS: River flooding	Flood recurrence
	River flow
FLOODS: Pluvial flood	Water runoff
STORMS: Extreme wind speed	Wind speed $\geq 98^{\text{th}}$ percentile
	Maximum wind speed
	Damaging wind speed Torro
DROUGHTS	Consecutive dry days

In addition to the indices listed above, efforts were made to include flood hazard data provided by the Joint Research Centre (JRC), online and from the PESETA IV project. We have downloaded flood hazard maps (<https://data.jrc.ec.europa.eu/collection/id-0054>), and were in contact with JRC regarding the data from the PESETA IV project and processed the provided data to investigate how it can be best integrated.

The difference in baseline-time period definition between this data and that used already in CLARITY, along with the time constraints at the end of the project meant that it was not possible to include the data in a meaningful way. That is, it was not possible to make the data coherent with the current CSIS setup and with what is already published (e.g. [47]) and useful for the user. However, this could potentially be done in a follow up project.

For now, we have included links in the respective EU-GL steps in CSIS to the flood hazard maps and the corresponding papers (under the steps: hazard characterization and risk and impact assessment) and to the PESETA website (Adaptation Options step), where adaptation options for river floods were assessed: <https://ec.europa.eu/jrc/en/peseta-iv/river-floods>.

7.1 Data used for the calculation of the indices

The daily E-OBS dataset at 0.22° spatial resolution is a gridded observational dataset based on daily ECA&D station data for precipitation, minimum, mean and maximum temperature and sea level pressure in Europe. E-OBS version 17.0 forms the basis for the current climate of several climate indices and is used for bias correction of temperature and precipitation data of the climate model data provided by the EURO-CORDEX initiative. From the many bias correction methods listed in D3.1 (section 3.2.5) we have chosen to apply the quantile mapping method [48] for bias correction of the EURO-CORDEX data. Pros and cons of bias correction were already discussed in D3.1.

The daily EURO-CORDEX climate model data at 0.11° spatial resolution forms the basis for the future climate projections of most of the climate indices. The climate model configurations that are available are shown in **Table 55**. All configurations have data on the greenhouse gas emissions scenarios (Representative Concentration Pathways) RCP4.5 (effective measures) and RCP8.5 (business as usual / worst case) and only a subset have the lower emission scenario RCP2.6 (early response) [3]. **Figure 86** shows the evolution of the forcing due to the greenhouse gases used in the climate models.

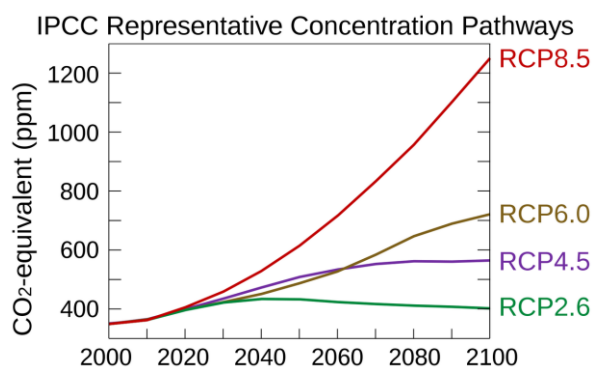


Figure 86: Evolution of the forcing agents' atmospheric CO₂-equivalent concentrations (in parts-per-million-by-volume (ppmv)) of the four RCPs used by the fifth IPCC Assessment Report to make predictions. (Source: https://en.wikipedia.org/wiki/Representative_Concentration_Pathway)

It was planned to calculate the indices using all of the climate model configurations shown in **Table 55** to establish an ensemble of members, so that a mean and a spread can be calculated with the latter giving an indication as to the reliability of the former quantity. However, our analysis of the EURO-CORDEX errata¹⁵ showed that not all model combinations could be considered due to problems discovered during independent external studies. Examples include, the GCM “IPSL-INNERIS” with RCM “WRF331F” where spurious precipitation patterns north of the Alps and over Greece were discovered, or that for GCM “CNRM-ALADIN53” and RCM “CNRM-CM5” that SSTs were wrongly remapped from the driving GCM

15 <https://www.hzg.de/ms/euro-cordex/078730/index.php.en>

leading to uncertainty in the land surface temperatures for coastal zones. The GCM “MPI-ESM” was also affected by interpolation problems when mapping the EUR11 (European) grid, and so these models were also left out. In the end, the models that remained for the study are those highlighted in **Table 55** in green. It should be pointed out, that although the models with RCM “SMHI-RCA4” also exhibited a patchy pattern in summer/winter rainfall, it was felt that excluding these models would result in too few models for an adequate analysis of the uncertainty of the climate result. From the selected models the ensemble mean and ensemble standard deviation was calculated for each index.

The relevant climate index is calculated from the daily EURO-CORDEX data and is averaged over one of the 30-year periods being investigated (1971-2000, 2011-2040, 2041-2070, 2071-2100). The use of the 1971-2000 period from the model acts as a baseline in which to compare the results of the future periods indicating the *change* of climate indices under different RCP scenarios until the end of the 21st century.

The decision to select the GCM/RCM combinations shown in **Table 55** was based on similar climate analysis studies such as in the BRIGAD Project (BRIGAD D5.1 TIF¹⁶) and the Pan-European Urban Climate Services (PUCS; D5.2 Urban Climate Data for Demonstration Cases¹⁷) and what climate model data was already available at the host institutions.

For the flood hazard, CLARITY will provide precipitation indices calculated as described above as well as flood indices, which are available from SWICCA (<https://swicca.eu/>).

Table 55: List of EURO-CORDEX climate model configurations showing the institute, driving global model (GCM) and regional climate model (RCM). The last three columns show the availability of the emissions scenarios RCP2.6 (early response), RCP4.5 (effective measures), and RCP8.5 (business as usual / worst case). The rows highlighted in green show the model combinations ultimately used after taking into account the EURO-CORDEX errata.

Institute	Driving GCM	RCM	RCP2.6	RCP4.5	RCP8.5
CLMcom	CNRM-CERFACS-CNRM-CM5	CCLM4-8-17	no	yes	yes
	ICHEC-EC-EARTH	CCLM4-8-17	yes	yes	yes
	MOHC-HadGEM2-ES	CCLM4-8-17	no	yes	yes
	MPI-M-MPI-ESM-LR	CCLM4-8-17	no	yes	yes
CNRM	CNRM-CERFACS-CNRM-CM5	ALADIN53	no	yes	yes
DMI	ICHEC-EC-EARTH	HIRHAM5	yes	yes	yes
	NCC-NorESM1-M	HIRHAM5	no	yes	yes
IPSL-IPSL-IPSL-CM5A-MR	IPSL-IPSL-CM5A-MR	WRF331F	no	yes	yes
KNMI	ICHEC-EC-EARTH	RACMO22E	yes	yes	yes
	MOHC-HadGEM2-ES	RACMO22E	yes	yes	yes

16 https://brigaid.eu/wp-content/uploads/2016/10/BRIGAD_D5.1_TIF.pdf

17 <https://climate-fit.city/wp-content/uploads/2018/11/D5.2-Urban-Climate-Data-For-Demonstration-Cases.pdf>

MPI-CSC	MPI-M-MPI-ESM-LR	REMO2009	yes	yes	yes
SMHI	CNRM-CERFACS-CNRM-CM5	RCA4	no	yes	yes
	ICHEC-EC-EARTH	RCA4	yes	yes	yes
	IPSL-IPSL-CM5A-MR	RCA4	no	yes	yes
	MOHC-HadGEM2-ES	RCA4	yes	yes	yes
	MPI-M-MPI-ESM-LR	RCA4	yes	yes	yes

The following sections show the results of the various climate indices available in the CSIS. A definition of the index is shown together with a basic description as to where the index may be useful for the user. It is organized such that for each index plot for the baseline period 1971-2000 is shown followed by the three emissions scenarios (RCP2.6, RCP4.5, RCP8.5) for each of the two future time periods¹⁸ (2041-2070, 2071-2100). In each of the plots, the left panels show the ensemble mean and the right panels show the ensemble standard deviation. The ensemble consists of the seven GCM/RCM model combinations highlighted in **Table 55**.

7.1.1 Ensemble standard deviation

The ensemble standard deviation represents a measure of the spread of the model results, with large values indicating uncertainty in the results. This has been scaled from black (low uncertainty) to white (high uncertainty) according to the units of the index. These plots should be used in conjunction to the ensemble mean plots in order to establish how confident one should be in interpreting the results. One point to note about the ensemble standard deviation is the following. For some historical period, some indices involving temperature, such as hot days, summer days, tropical nights, frost days, and ice days exhibit very low values of about 0.5-0.75 days (i.e. less than 1 day) over the European landmass. In contrast, when one examines the standard deviation over the water (not shown due to masking) or coastal regions (e.g. the islands of Greece), the standard deviations have "normal" values in the range 10-40 days depending on the index.

This effect is due to the quantile mapping technique employed in the bias-correction of the climate model data which has been performed using the E-OBS dataset¹⁹ over land. This has the effect of adjusting all of the model datasets to the temperature distribution curve (specifically the cumulative distribution function) of the (E-OBS) observations [48] [49], as illustrated in **Figure 87**.

There do exist a couple of temperature index types which display a more typical distribution of standard deviation across Europe (i.e. not everywhere black), namely the indices involving "consecutive" time periods (e.g. consecutive summer or frost days), or those involving extreme percentiles (e.g. 10th percentile of T_n or 90th percentile of T_x). For the first case of consecutive days, the quantile mapping does not change the timing when a (e.g.) summer day is. That is, the days when summer days occur is still a characteristic of a particular model. The second case of the extreme percentiles considers values at the extreme ends of the cumulative distribution function of temperature. The ends of the distribution (upper or lower 10 percent) cover a greater temperature range than when one considers temperatures at the, say, 60th percentile which may correspond to the 25°C temperature threshold for summer days (**Figure 87**). As the quantile mapping method adjusts only the mean temperature of each percentile/quantile rather than its temperature spread, this latter aspect still remains a characteristic of the climate model, and it is this difference which appears in the standard deviation map.

¹⁸ The time period 2011-2040 is omitted to save space.

¹⁹ https://surfobs.climate.copernicus.eu/dataaccess/access_eobs.php

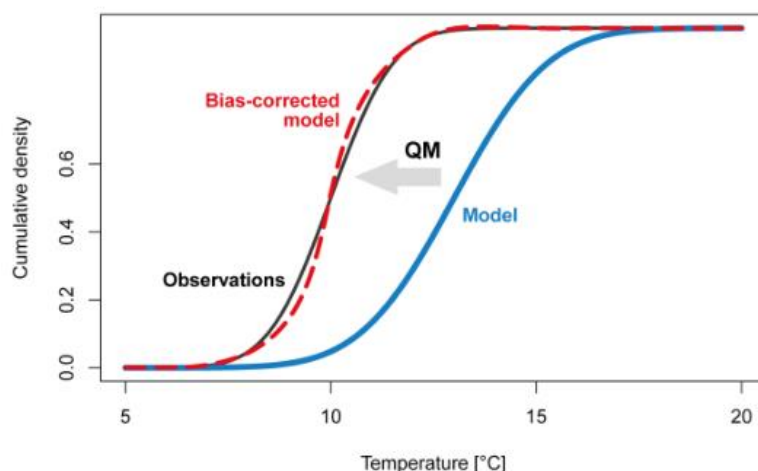


Figure 87: The effect of quantile mapping s to correct the temperature distribution of the model (blue curve) to that of the observations. (Source: [49]).

7.1.2 Generalized discussion of results

In discussing the results of each index, several generalisations about the trends can be made which apply to multiple heat indices. These are addressed here in order to avoid repetition. Exceptions to these generalizations are indicated under the relevant index.

Heat indices (CSU, Tx75p HD, SD, TN, Tx90p), RCP2.6: An increase from the baseline period (1971-2000) to the 2041-2070 period followed by a slight decrease from the 2041-2070 to 2071-2100 period across Europe (e.g. Consecutive Summer Days, **Figure 89a** and **Figure 90a**, France²⁰). This is in accordance with the decrease in the forcing from greenhouse gas emissions associated with the scenario (**Figure 86**).

Heat indices (CSU, Tx75p HD, SD, TN, Tx90p), RCP4.5 / RCP8.5: An increase from the baseline period (1971-2000) to the 2041-2070 period followed by a continued / large increase to the 2071-2100 period across Europe (e.g. Consecutive Summer Days, **Figure 89c** and **Figure 90c**, France) . This is in accordance with the slight / large increase in the forcing from greenhouse gas emissions associated with the scenario between these two periods (**Figure 86**).

Cold indices (CFD, FD, ID), RCP2.6: A decrease from the baseline period (1971-2000) to the 2041-2070 period followed by a further decrease, i.e. continued warming in Southern Europe from 2041-2070 to 2071-2100 (e.g. Frost Days, **Figure 110a** and **Figure 111a**, Turkey), but an increase, i.e. cooling in Northern Europe (e.g. Frost Days, **Figure 110a** and **Figure 111a**, Germany).

Cold indices (CFD, FD, ID), RCP4.5 / RCP8.5: A decrease from the baseline period (1971-2000) to the 2041-2070 period followed by a further /large decrease, i.e. continued / large warming to the 2071-2100 period across Europe (e.g. Frost Days, **Figure 110a** and **Figure 111a**, Germany).

²⁰ Owing to the colour scheme the change is often best seen over France.

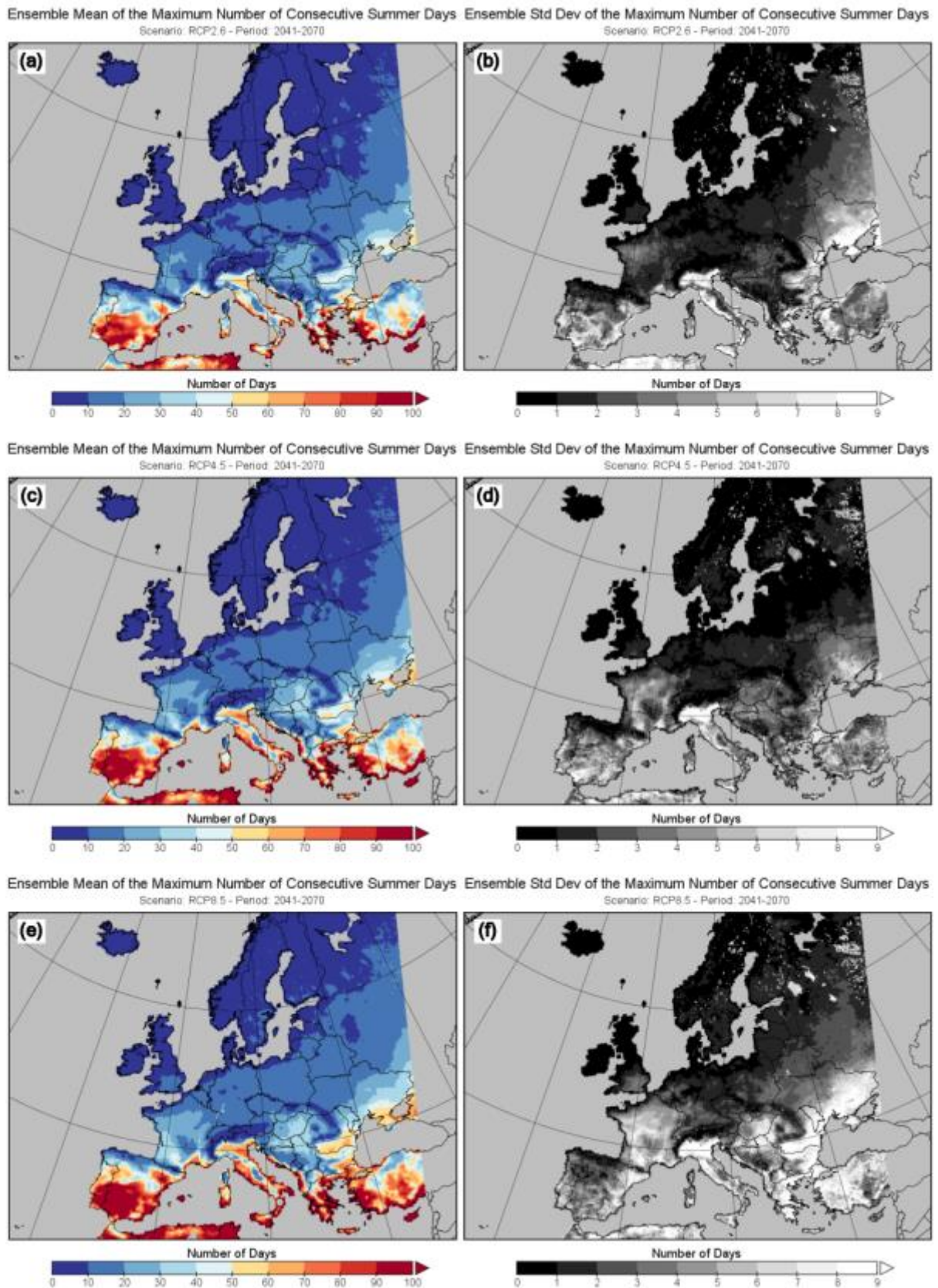


Figure 89: Maximum number of consecutive summer days for 2041-2070. (left panels) Ensemble mean and (right panels) ensemble standard deviation. (a, b) RCP2.6, (c, d) RCP4.5, (e, f) RCP8.5.

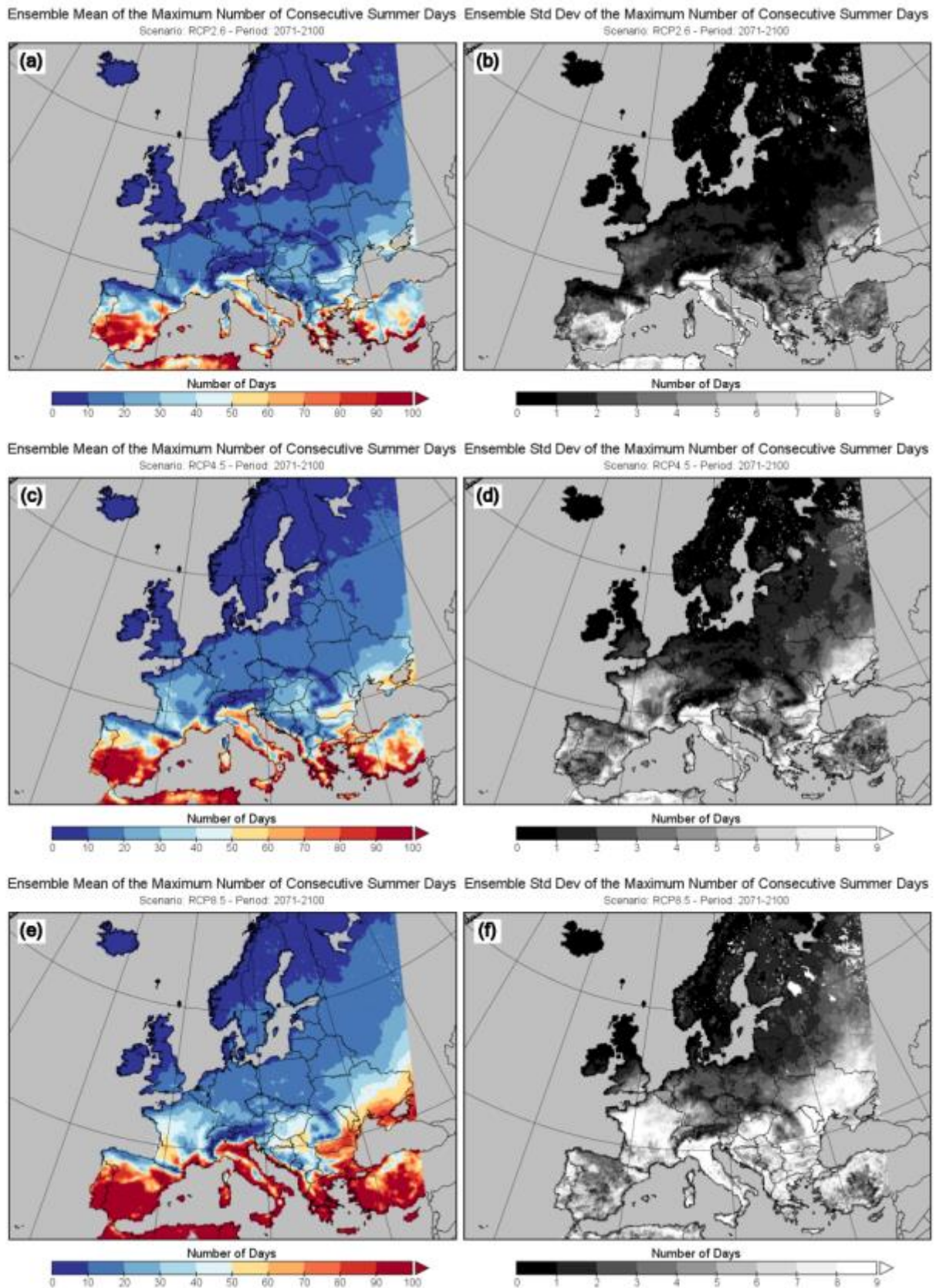


Figure 90: Maximum number of consecutive summer days for 2071-2100. (left panels) Ensemble mean and (right panels) ensemble standard deviation. (a, b) RCP2.6, (c, d) RCP4.5, (e, f) RCP8.5.

7.3 Heat wave days exceeding 75th percentile of consecutive daily maximum temperature

Definition: Maximum number of consecutive days where the daily maximum temperature exceeds the 75th percentile of maximum temperature during the baseline period 1971-2000 for the warm months April-September. This is averaged for each year in the 30-year period.

Units: Days

Background: This climate index is a measure of daytime heat, with high values corresponding to warm conditions. An increase of this index with time means that the chance of warmer conditions will increase.

Results: See description regarding the heat indices in Section 7.1.2.

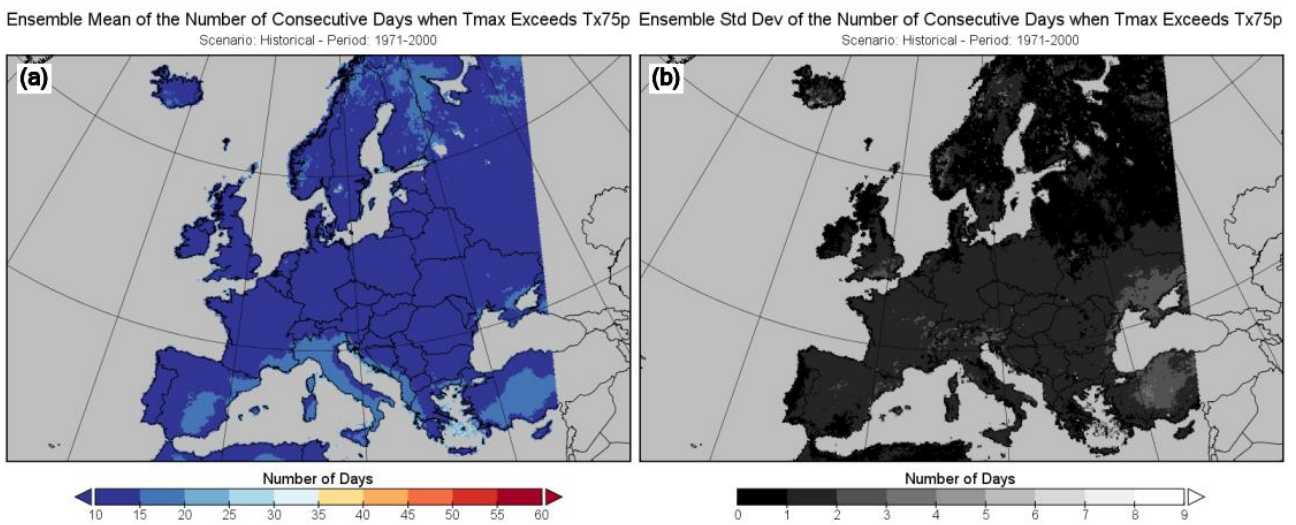
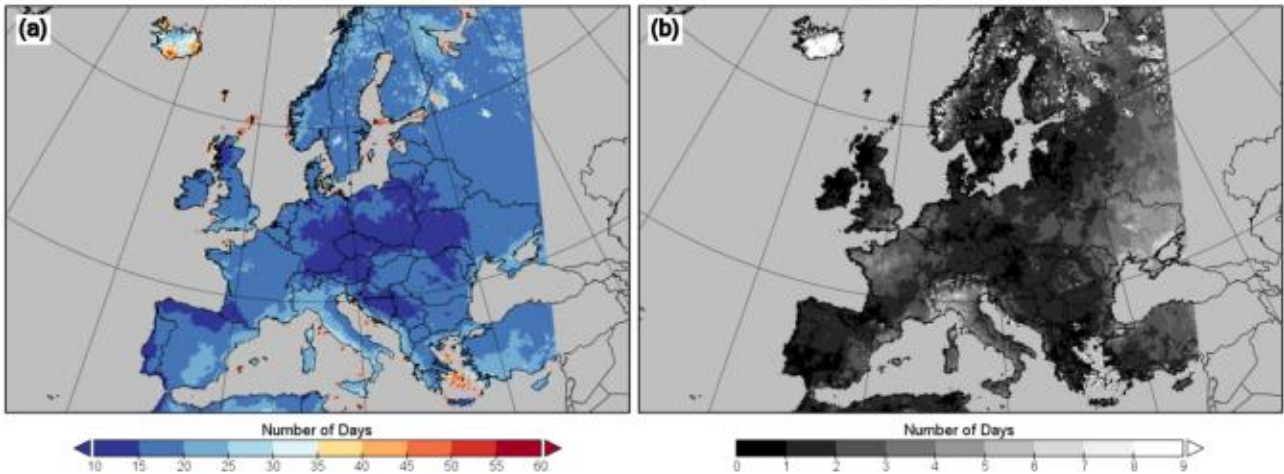
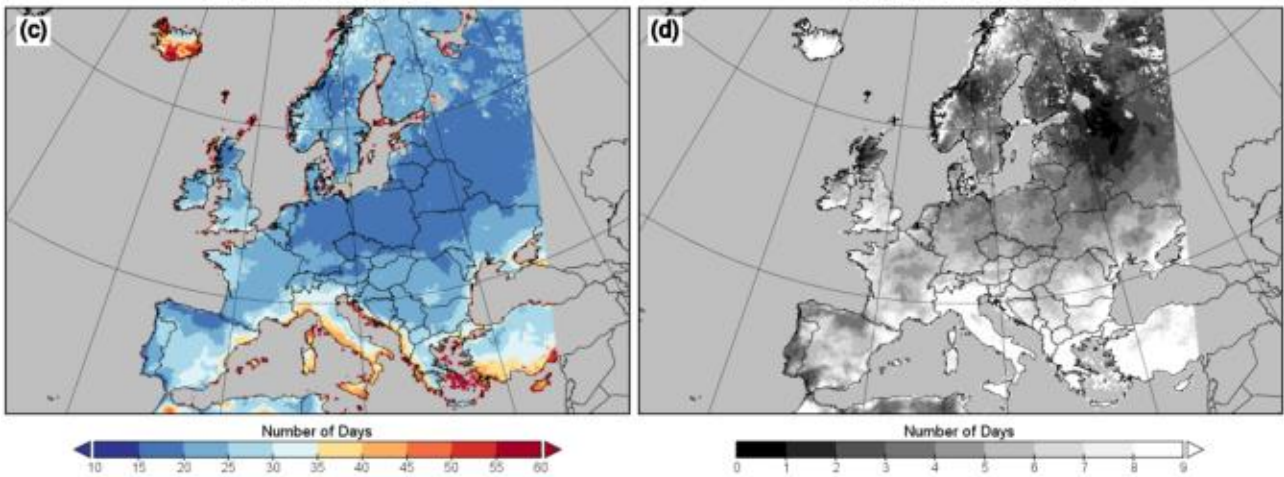


Figure 91: Tx75p maximum consecutive for the baseline period 1971-2000. (a) Ensemble mean and (b) ensemble standard deviation.

Ensemble Mean of the Number of Consecutive Days when Tmax Exceeds Tx75p Scenario: RCP2.6 - Period: 2041-2070 Ensemble Std Dev of the Number of Consecutive Days when Tmax Exceeds Tx75p Scenario: RCP2.6 - Period: 2041-2070



Ensemble Mean of the Number of Consecutive Days when Tmax Exceeds Tx75p Scenario: RCP4.5 - Period: 2041-2070 Ensemble Std Dev of the Number of Consecutive Days when Tmax Exceeds Tx75p Scenario: RCP4.5 - Period: 2041-2070



Ensemble Mean of the Number of Consecutive Days when Tmax Exceeds Tx75p Scenario: RCP8.5 - Period: 2041-2070 Ensemble Std Dev of the Number of Consecutive Days when Tmax Exceeds Tx75p Scenario: RCP8.5 - Period: 2041-2070

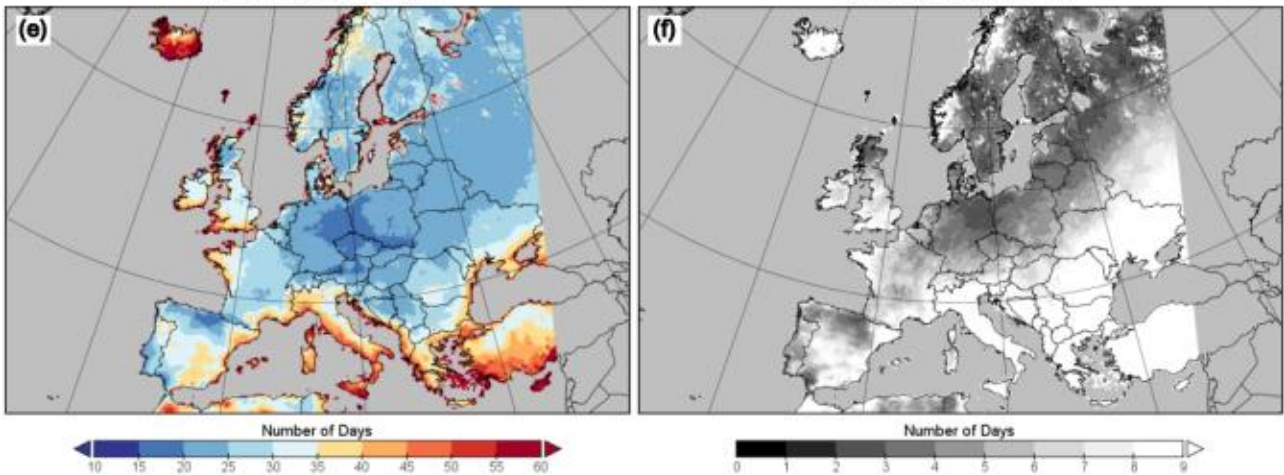
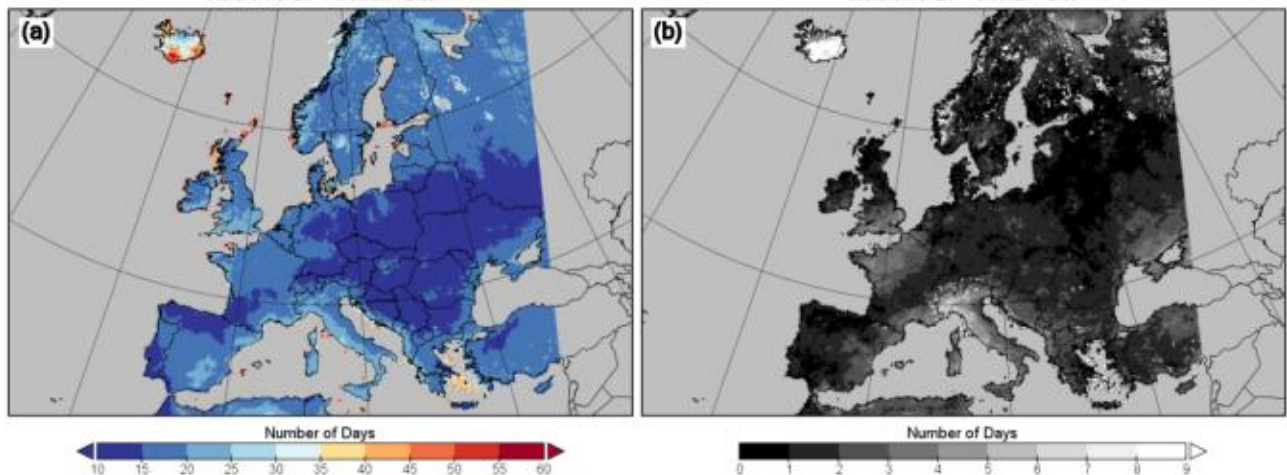
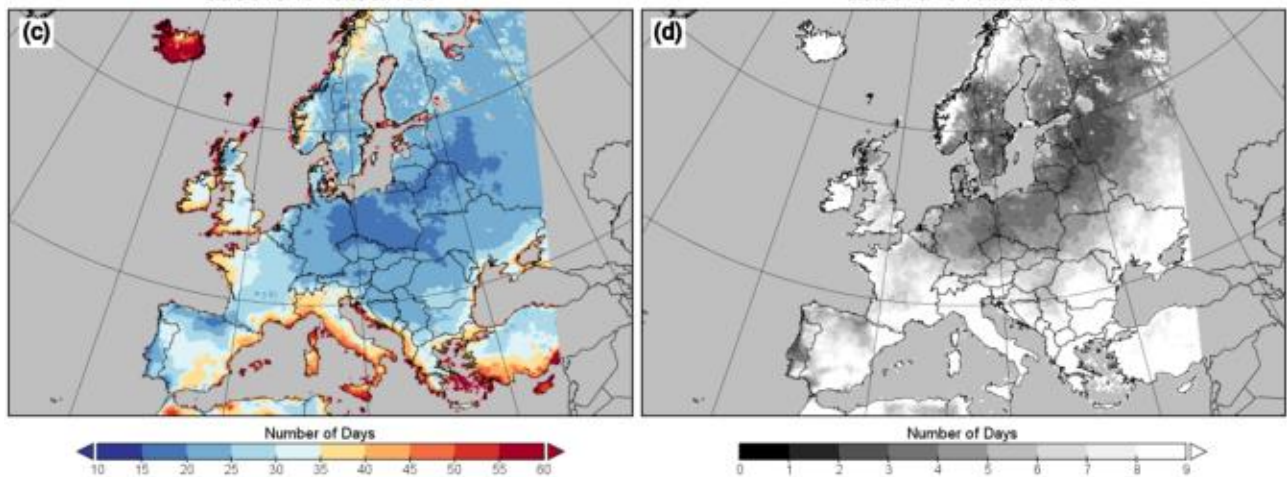


Figure 92: Tx75p maximum consecutive for the period 2041-2070. (left panels) Ensemble mean and (right panels) ensemble standard deviation. (a, b) RCP2.6, (c, d) RCP4.5, (e, f) RCP8.5.

Ensemble Mean of the Number of Consecutive Days when Tmax Exceeds Tx75p Scenario: RCP2.6 - Period: 2071-2100 Ensemble Std Dev of the Number of Consecutive Days when Tmax Exceeds Tx75p Scenario: RCP2.6 - Period: 2071-2100



Ensemble Mean of the Number of Consecutive Days when Tmax Exceeds Tx75p Scenario: RCP4.5 - Period: 2071-2100 Ensemble Std Dev of the Number of Consecutive Days when Tmax Exceeds Tx75p Scenario: RCP4.5 - Period: 2071-2100



Ensemble Mean of the Number of Consecutive Days when Tmax Exceeds Tx75p Scenario: RCP8.5 - Period: 2071-2100 Ensemble Std Dev of the Number of Consecutive Days when Tmax Exceeds Tx75p Scenario: RCP8.5 - Period: 2071-2100

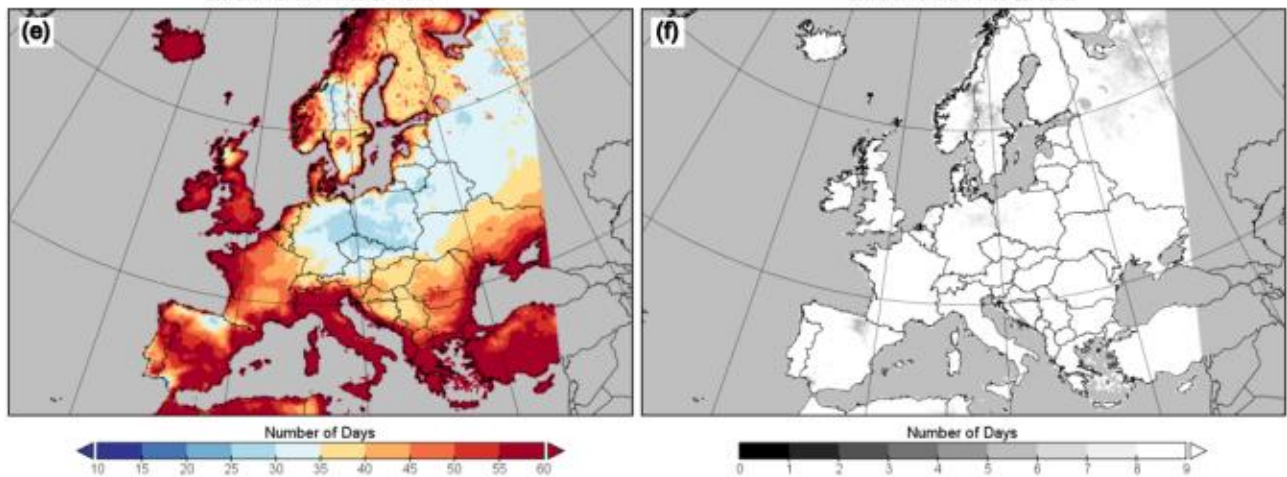


Figure 93: Tx75p maximum consecutive for the period 2071-2100. (left panels) Ensemble mean and (right panels) ensemble standard deviation. (a, b) RCP2.6, (c, d) RCP4.5, (e, f) RCP8.5.

7.4 Hot days (HD)

Definition: The average yearly number of hot days in Europe, averaged over a 30-year period.. A hot day is a day where the daily maximum temperature exceeds 30.0 °C.

Units: Days

Background: This climate index is a measure of daytime heat, with high values corresponding to warm conditions. An increase of this index with time means that the chance of warmer conditions will increase.

Results: See description regarding the heat indices in Section 7.1.2.

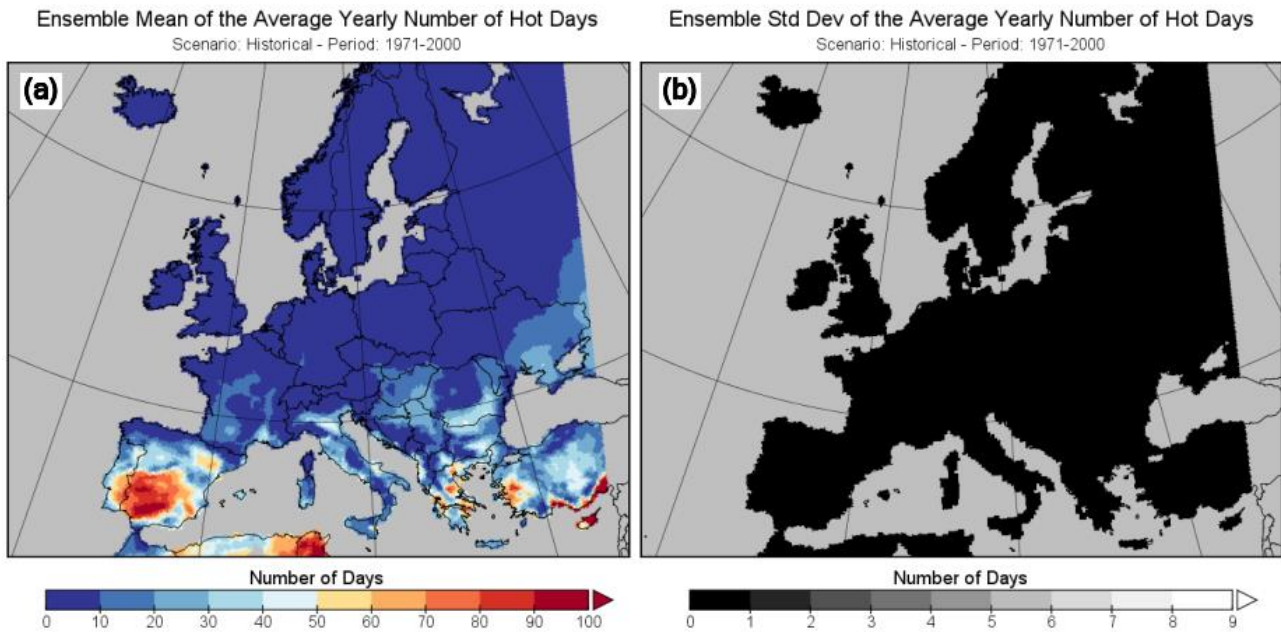


Figure 94: Hot days for the baseline period 1971-2000. (a) Ensemble mean and (b) ensemble standard deviation.

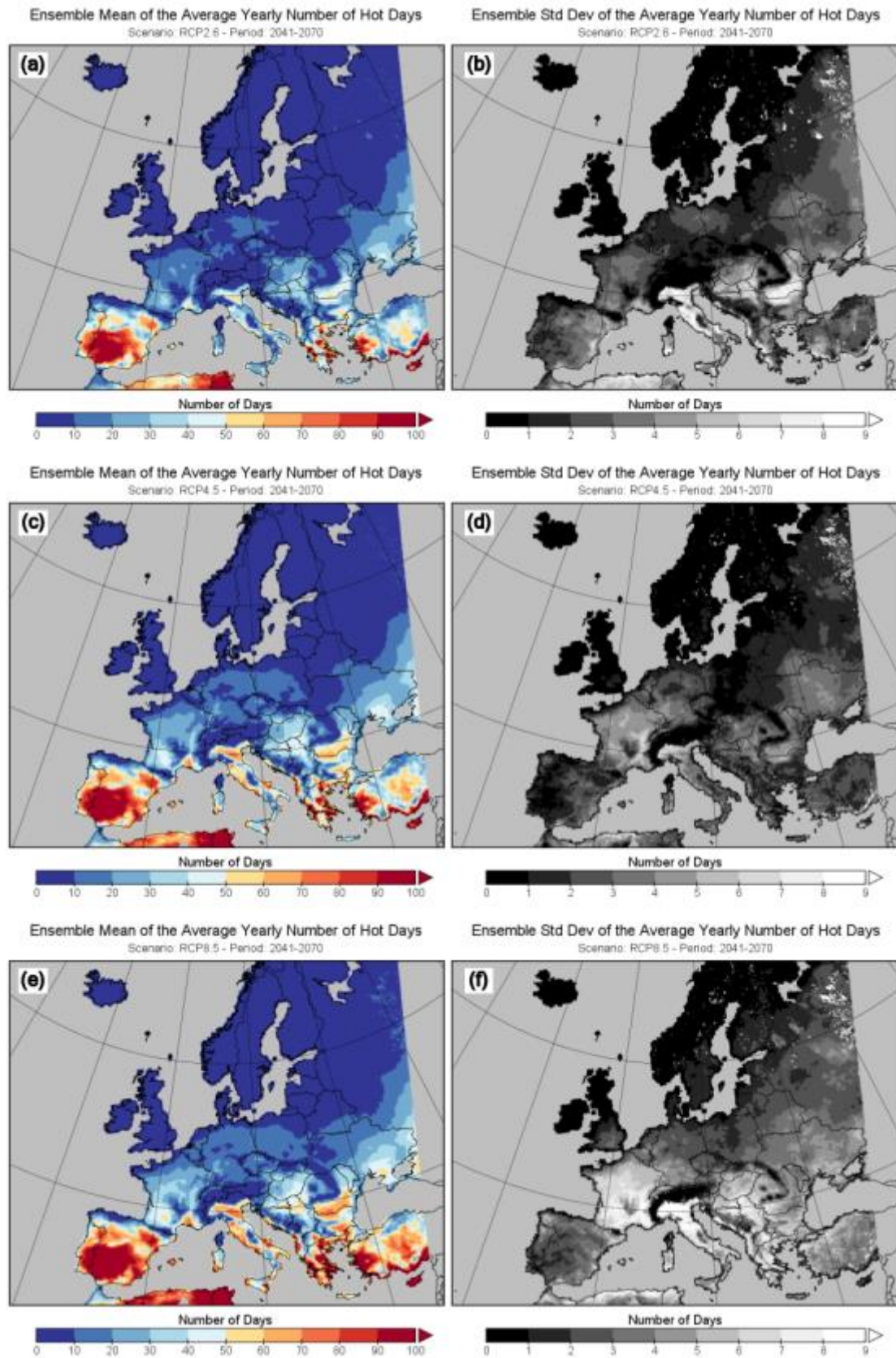


Figure 95: Hot days for the period 2041-2070. (left panels) Ensemble mean and (right panels) ensemble standard deviation. (a, b) RCP2.6, (c, d) RCP4.5, (e, f) RCP8.5.

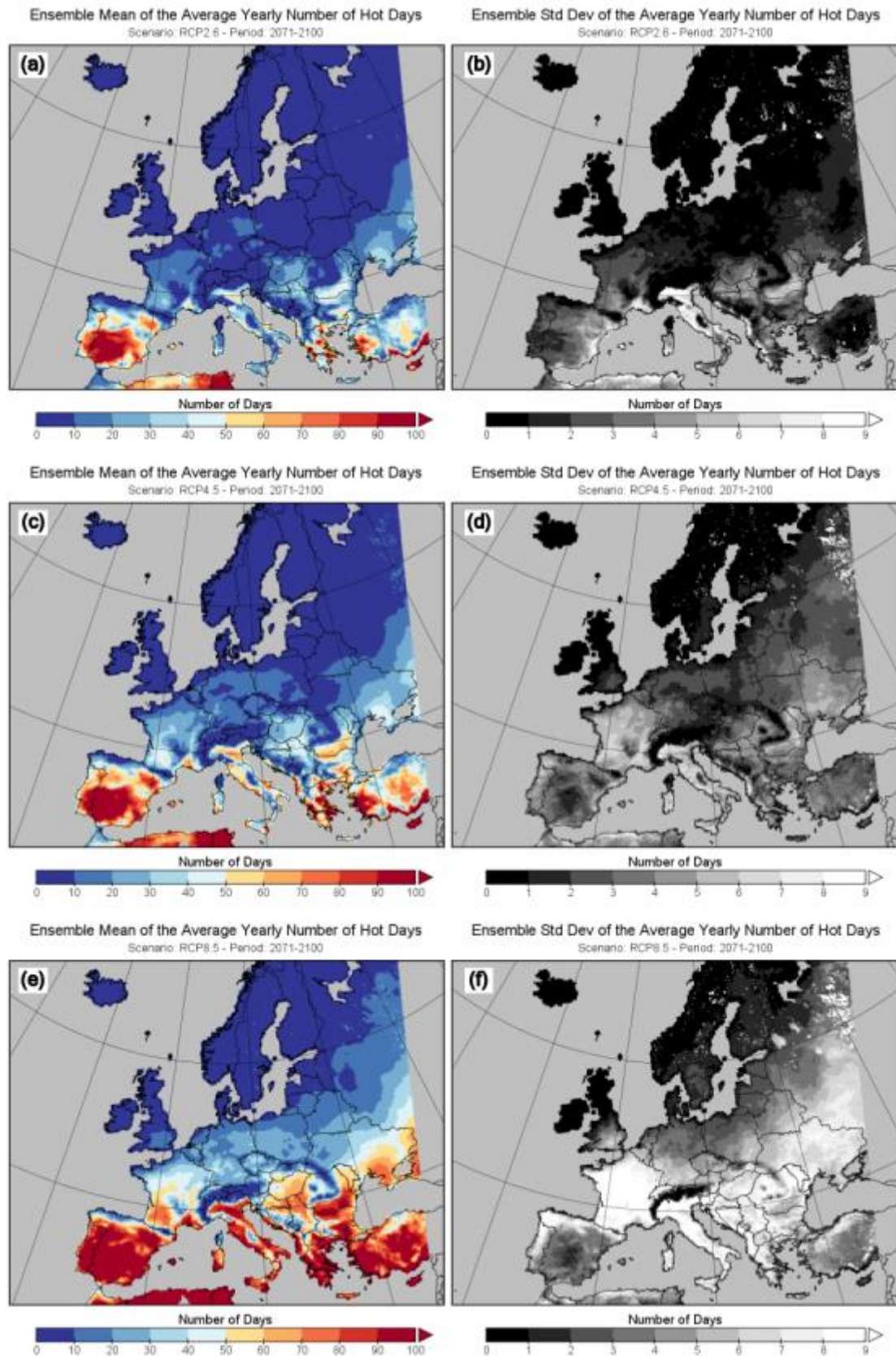


Figure 96: Hot days for the period 2071-2100. (left panels) Ensemble mean and (right panels) ensemble standard deviation. (a, b) RCP2.6, (c, d) RCP4.5, (e, f) RCP8.5.

7.5 Summer days (SD)

Definition: The average yearly number of summer days in Europe averaged over a 30-year period. A summer day is a day where the daily maximum temperature exceeds 25.0 °C.

Units: Days

Background: This climate index is a measure of daytime heat, with high values corresponding to warm conditions. An increase of this index with time means that the chance of warmer conditions will increase.

Results: See description regarding the heat indices in Section 7.1.2. The RCP4.5 scenario shows a slight increase in the number of summer days for most of Europe. However, Central and Eastern Europe show a slight decrease in the number of summer days from 2041-2070 to 2071-2100 (**Figure 98c**, **Figure 99c**, e.g. Germany, Poland, Ukraine, Belarus).

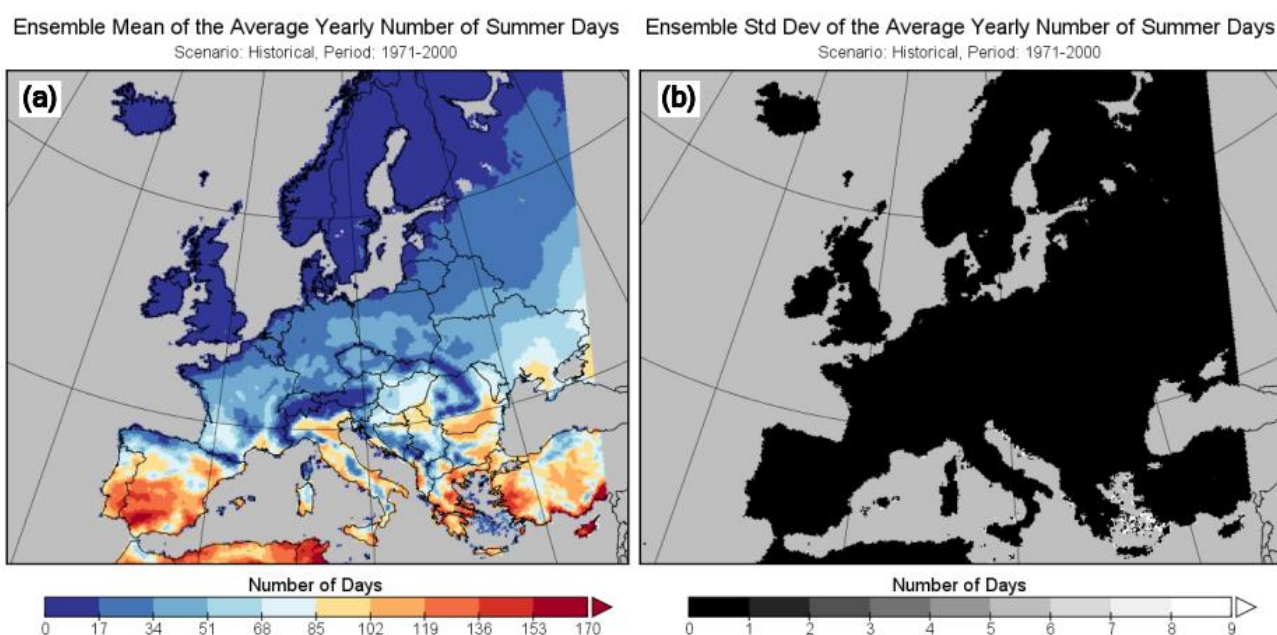


Figure 97: Summer days for the baseline period 1971-2000. (a) Ensemble mean and (b) ensemble standard deviation.

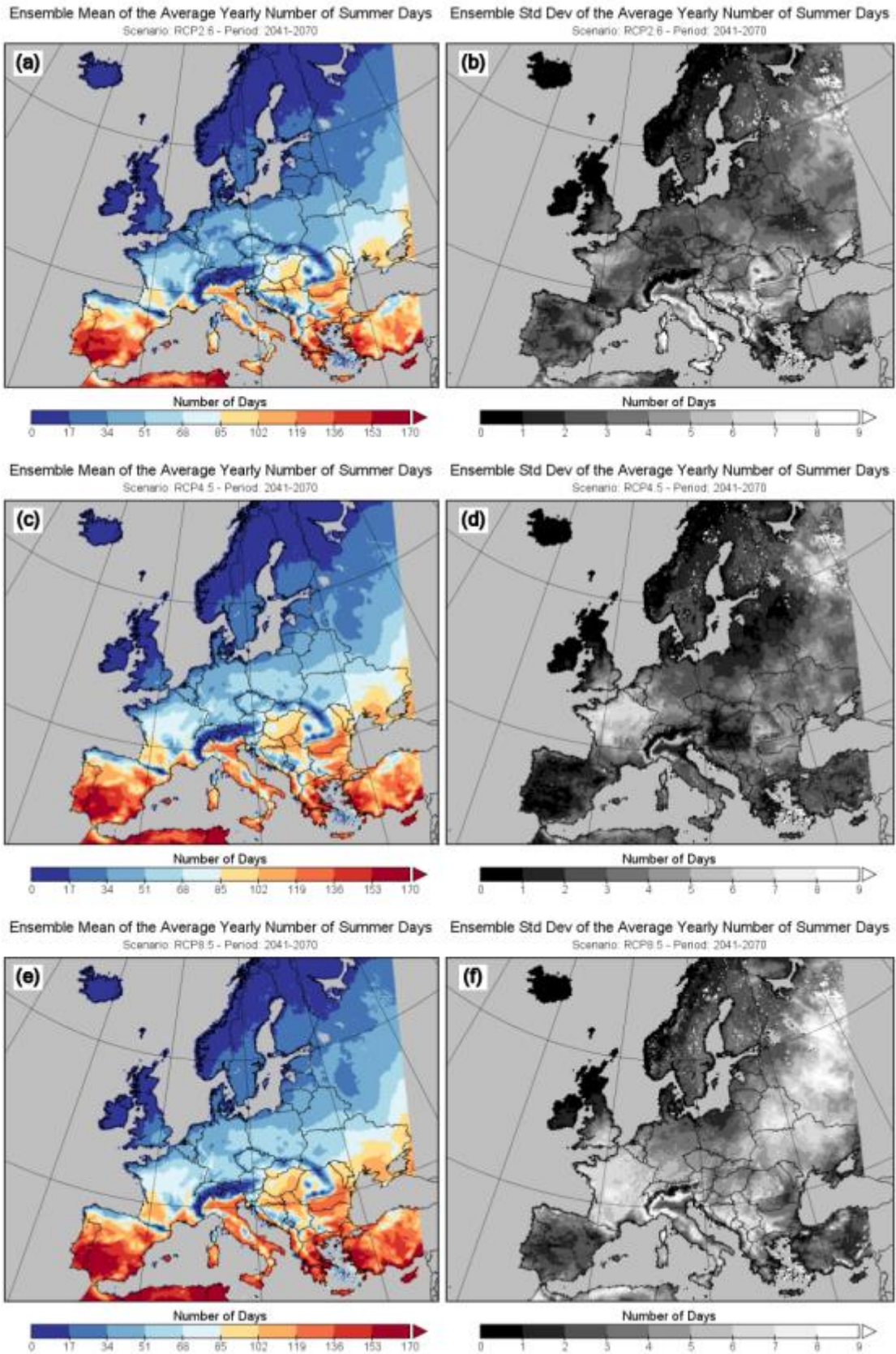


Figure 98: Summer days for the period 2041-2070. (left panels) Ensemble mean and (right panels) ensemble standard deviation. (a, b) RCP2.6, (c, d) RCP4.5, (e, f) RCP8.5.

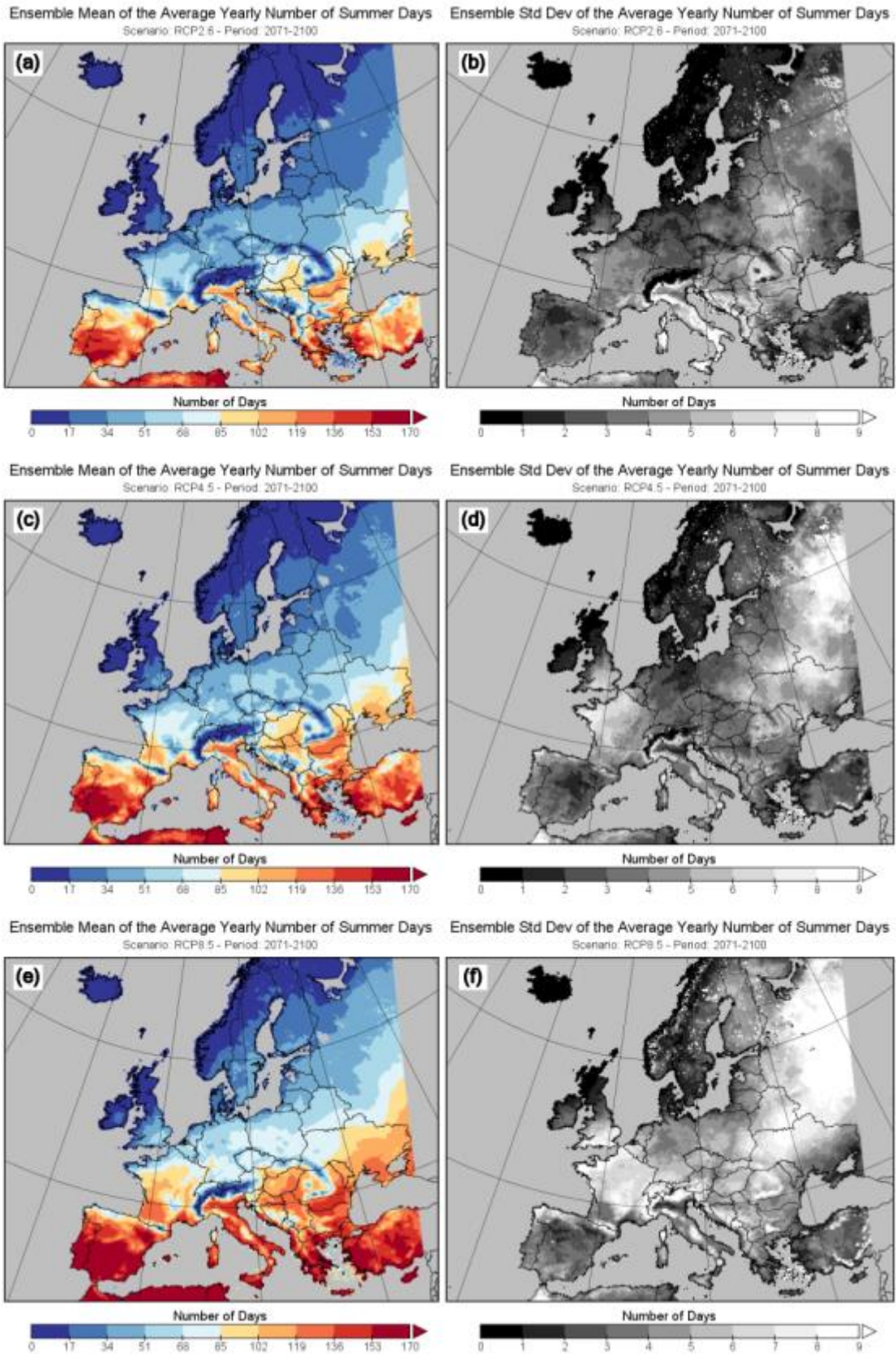


Figure 99: Summer days for the period 2071-2100. (left panels) Ensemble mean and (right panels) ensemble standard deviation. (a, b) RCP2.6, (c, d) RCP4.5, (e, f) RCP8.5.

7.6 Tropical nights (TN)

Definition: The average yearly number of tropical nights in Europe averaged over a 30-year period. A tropical night is where the daily minimum temperature exceeds 20.0 °C.

Units: Nights

Background: This climate index is a measure of nighttime heat, with high values corresponding to warm conditions. An increase of this index with time means that the chance of warmer conditions will increase.

Results: See description regarding the heat indices in Section 7.1.2.

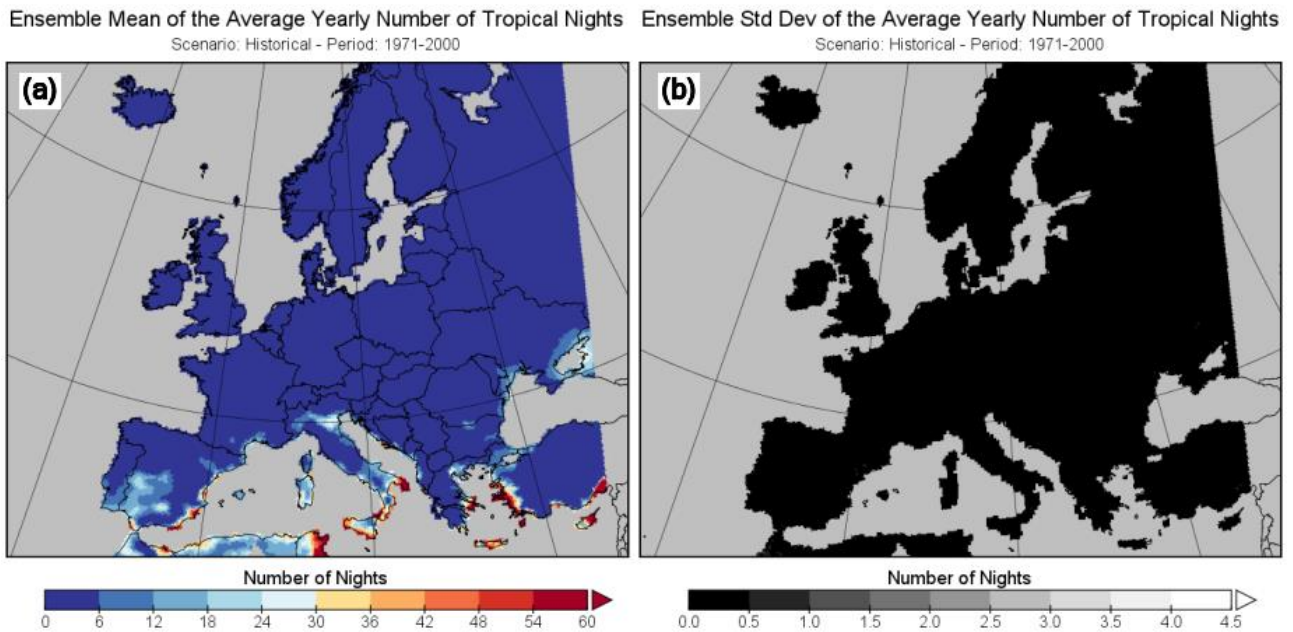


Figure 100: Tropical nights for the baseline period 1971-2000. (a) Ensemble mean and (b) ensemble standard deviation.

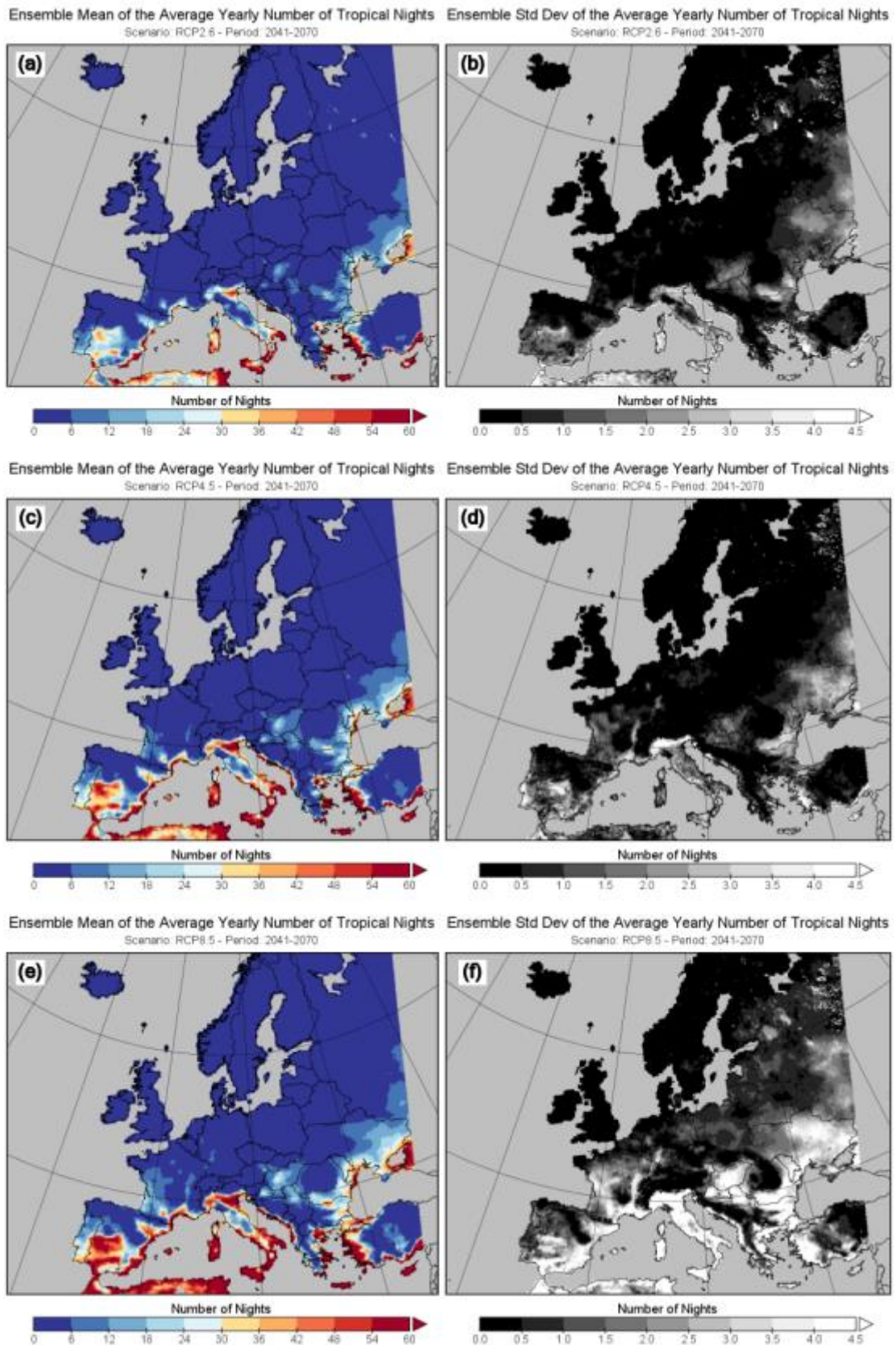


Figure 101: Tropical nights for the period 2041-2070. (left panels) Ensemble mean and (right panels) ensemble standard deviation. (a, b) RCP2.6, (c, d) RCP4.5, (e, f) RCP8.5.

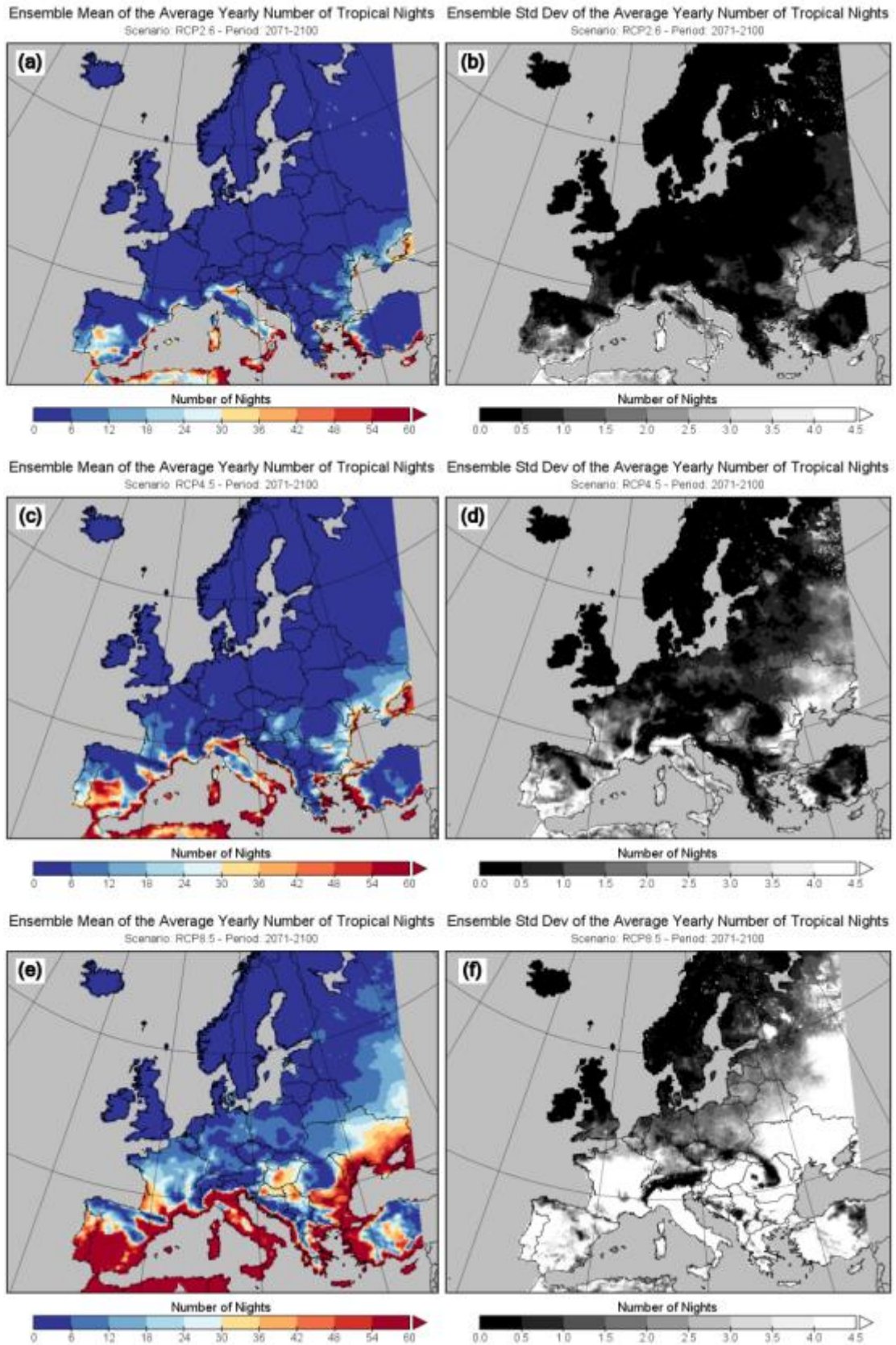


Figure 102: Tropical nights for the period 2071-2100. (left panels) Ensemble mean and (right panels) ensemble standard deviation. (a, b) RCP2.6, (c, d) RCP4.5, (e, f) RCP8.5.

7.7 Hot days with respect to the 90th percentile of daily maximum temperature (Tx90p)

Definition: The number of days where the daily maximum temperature exceeds the 90th percentile of maximum temperature during a five day window centred on each calendar day of the baseline period 1971-2000. The value for each year is averaged over a 30-year period.

Units: Days

Background: This climate index is a measure of daytime heat, with high values corresponding to warm conditions. An increase of this index with time means that the chance of warmer conditions will increase.

Results: See description regarding the heat indices in Section 7.1.2.

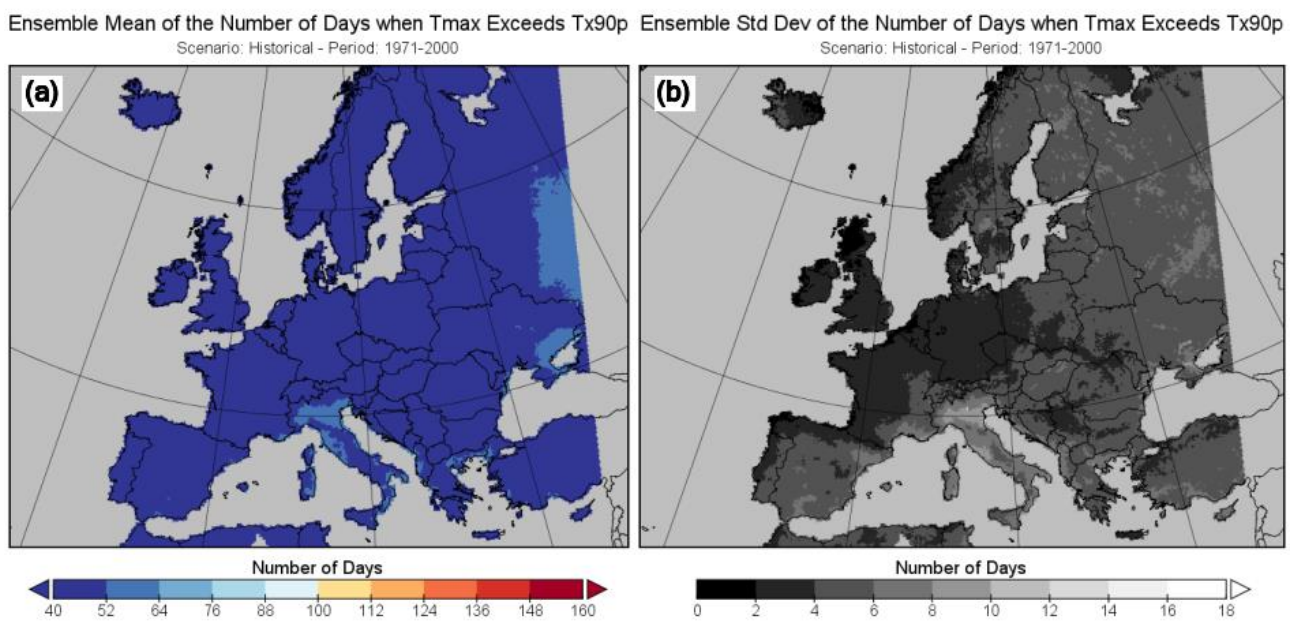


Figure 103: Tx90p for the baseline period 1971-2000. (a) Ensemble mean and (b) ensemble standard deviation.

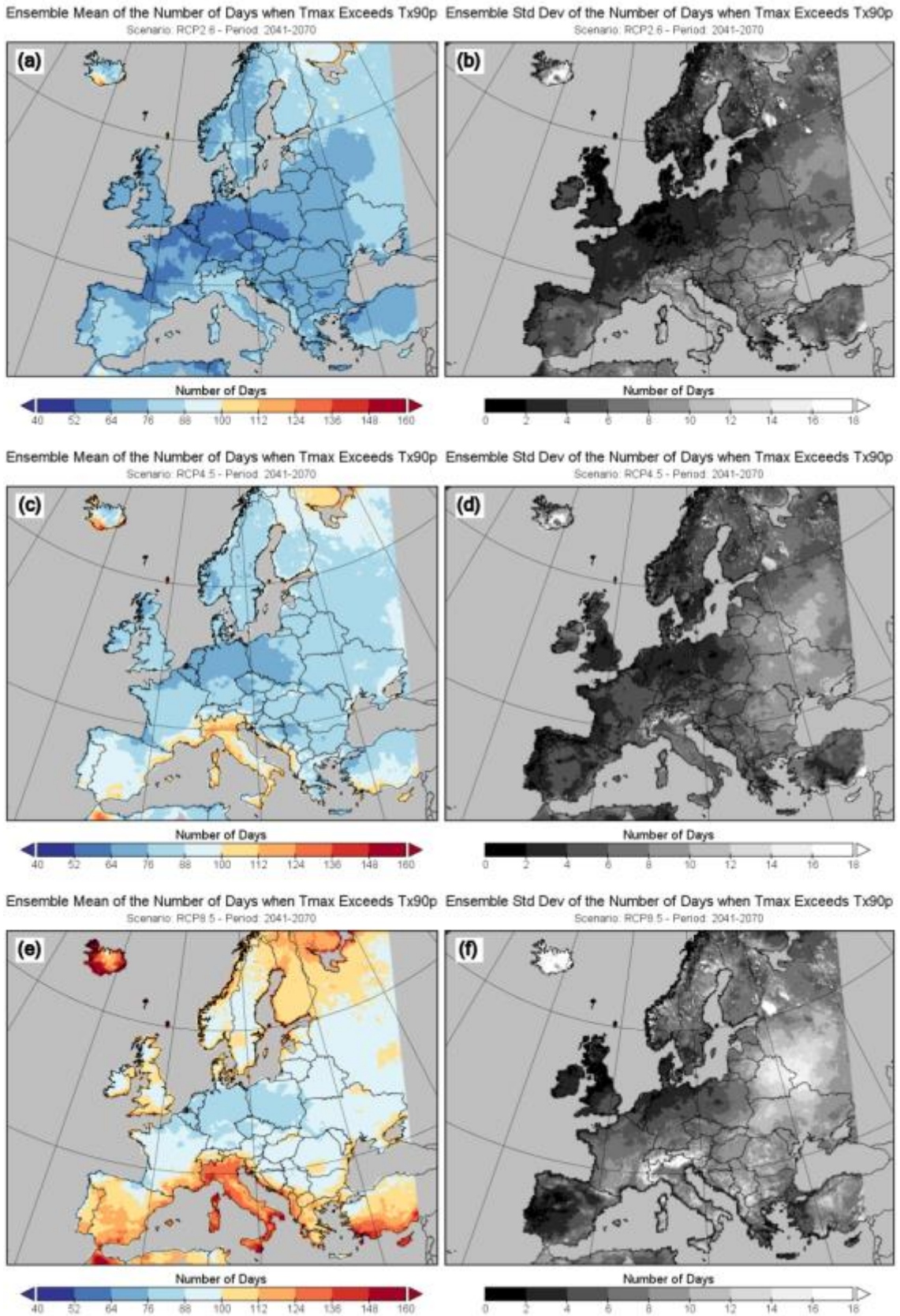


Figure 104: Tx90p for the period 2041-2070. (left panels) Ensemble mean and (right panels) ensemble standard deviation. (a, b) RCP2.6, (c, d) RCP4.5, (e, f) RCP8.5.

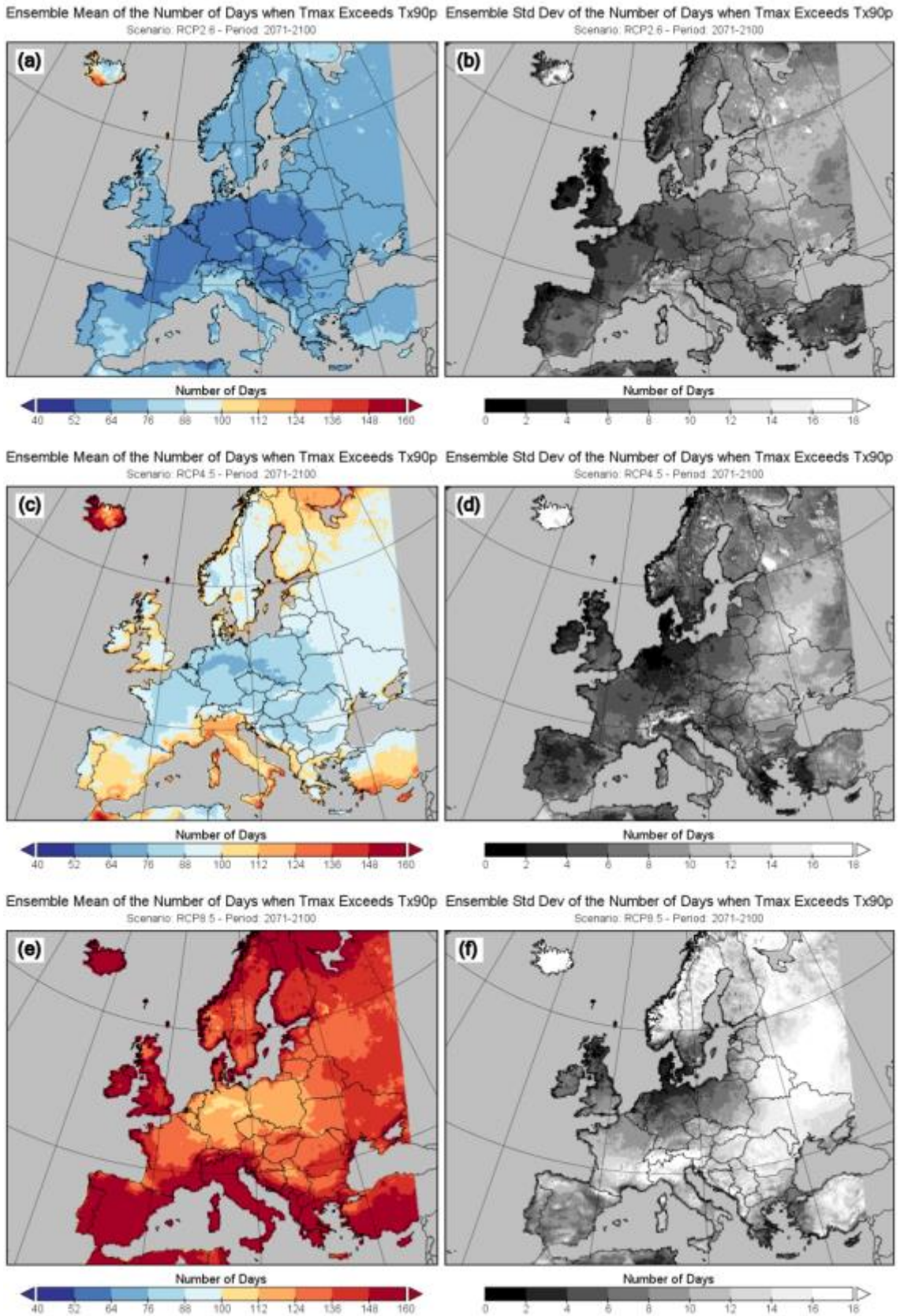


Figure 105: Tx90p for the period 2071-2100. (left panels) Ensemble mean and (right panels) ensemble standard deviation. (a, b) RCP2.6, (c, d) RCP4.5, (e, f) RCP8.5.

7.8 Consecutive frost days (CFD)

Definition: The maximum number of consecutive frost days in Europe for each year averaged over a 30-year period. A frost day is a day where the daily minimum temperature is less than 0.0 °C.

Units: Days

Background: This climate index is a measure of daytime cold, with high values corresponding to cold conditions. An increase of this index with time means that the chance of colder conditions will increase.

Results: See description regarding the cold indices in Section 7.1.2.

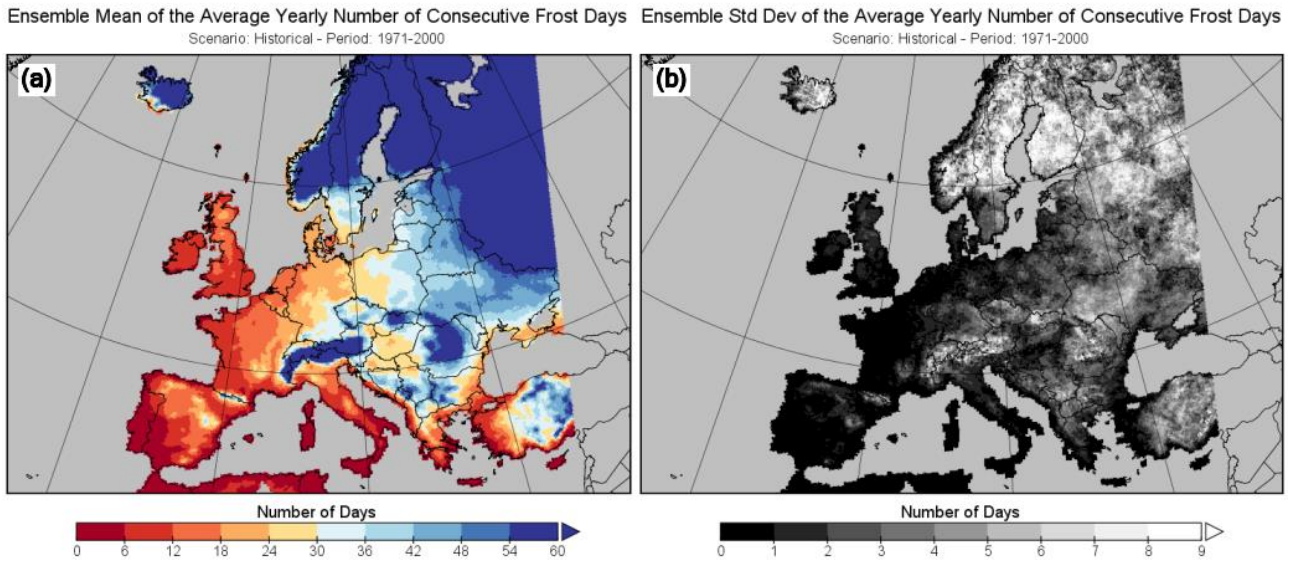


Figure 106: Consecutive frost days for the baseline period 1971-2000. (a) Ensemble mean and (b) ensemble standard deviation.

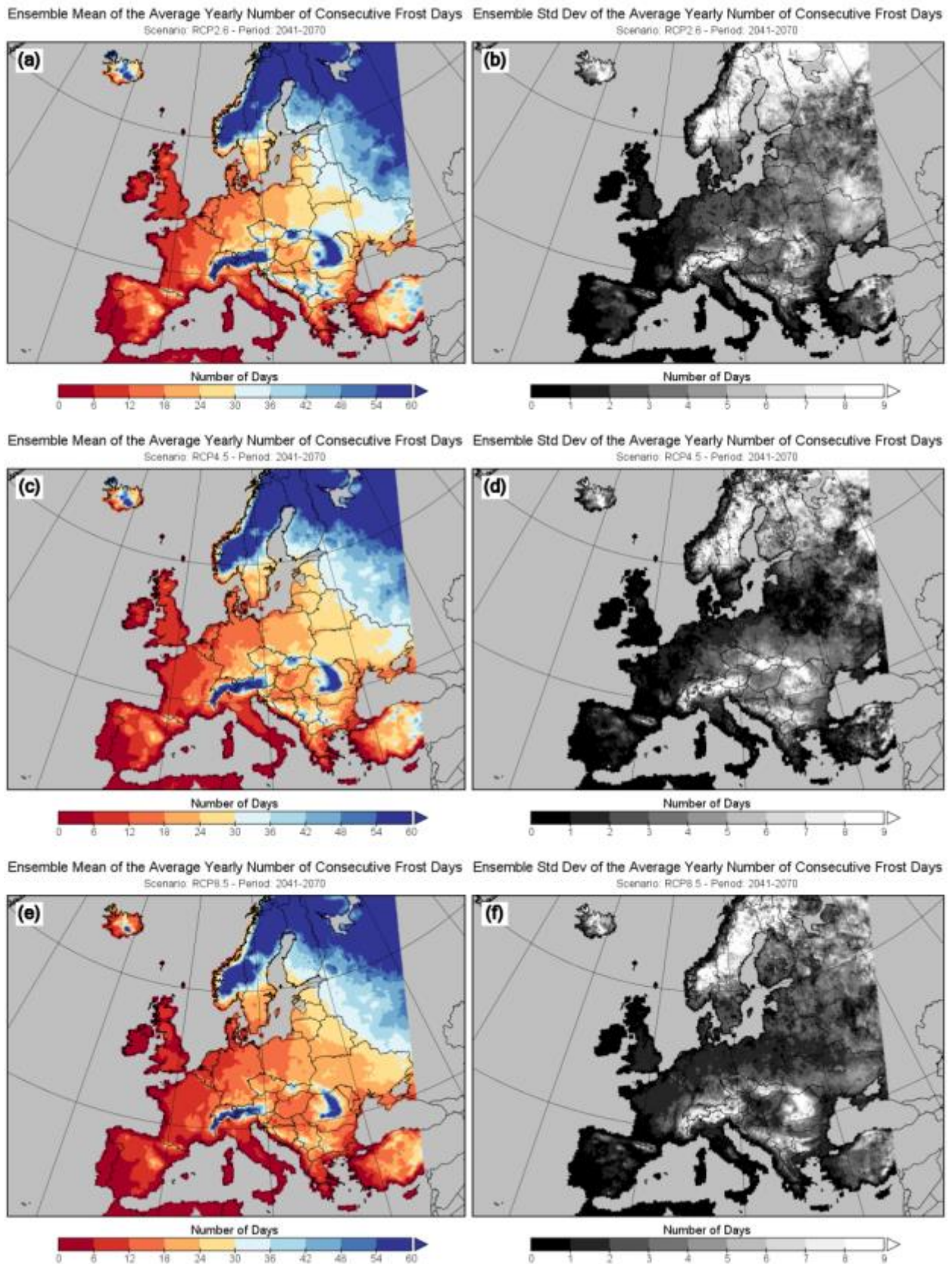
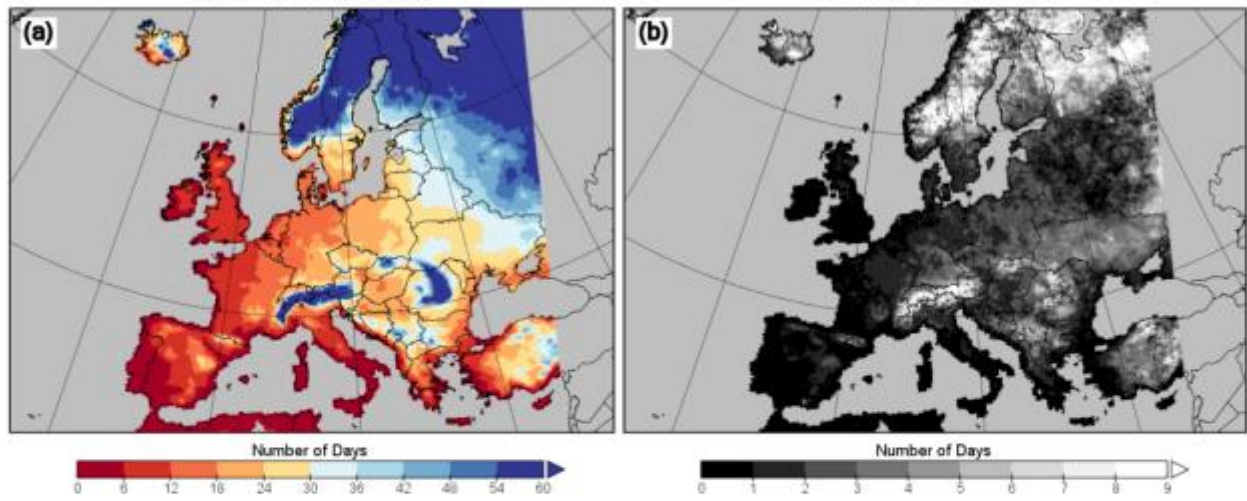
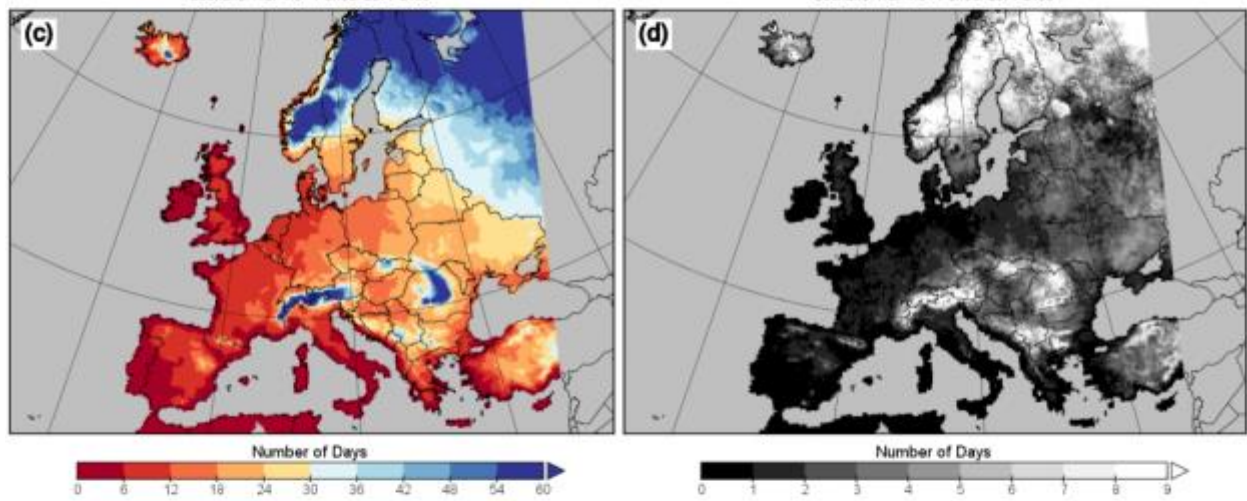


Figure 107: Consecutive frost days for the period 2041-2070. (left panels) Ensemble mean and (right panels) ensemble standard deviation. (a, b) RCP2.6, (c, d) RCP4.5, (e, f) RCP8.5.

Ensemble Mean of the Average Yearly Number of Consecutive Frost Days Scenario: RCP2.6 - Period: 2071-2100 Ensemble Std Dev of the Average Yearly Number of Consecutive Frost Days Scenario: RCP2.6 - Period: 2071-2100



Ensemble Mean of the Average Yearly Number of Consecutive Frost Days Scenario: RCP4.5 - Period: 2071-2100 Ensemble Std Dev of the Average Yearly Number of Consecutive Frost Days Scenario: RCP4.5 - Period: 2071-2100



Ensemble Mean of the Average Yearly Number of Consecutive Frost Days Scenario: RCP8.5 - Period: 2071-2100 Ensemble Std Dev of the Average Yearly Number of Consecutive Frost Days Scenario: RCP8.5 - Period: 2071-2100

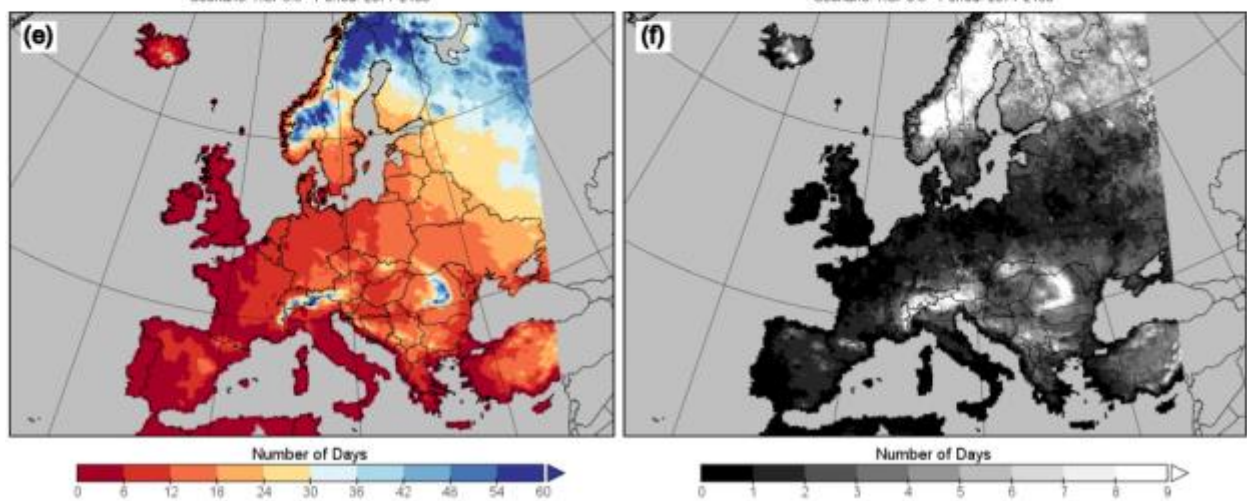


Figure 108: Consecutive frost days for the period 2071-2100. (left panels) Ensemble mean and (right panels) ensemble standard deviation. (a, b) RCP2.6, (c, d) RCP4.5, (e, f) RCP8.5.

7.9 Frost days (FD)

Definition: The average yearly number of frost days in Europe averaged over a 30-year period. A frost day is a day where the daily minimum temperature is less than 0.0 °C.

Units: Days

Background: This climate index is a measure of daytime cold, with high values corresponding to cold conditions. An increase of this index with time means that the chance of colder conditions will increase.

Results: See description regarding the cold indices in Section 7.1.2.

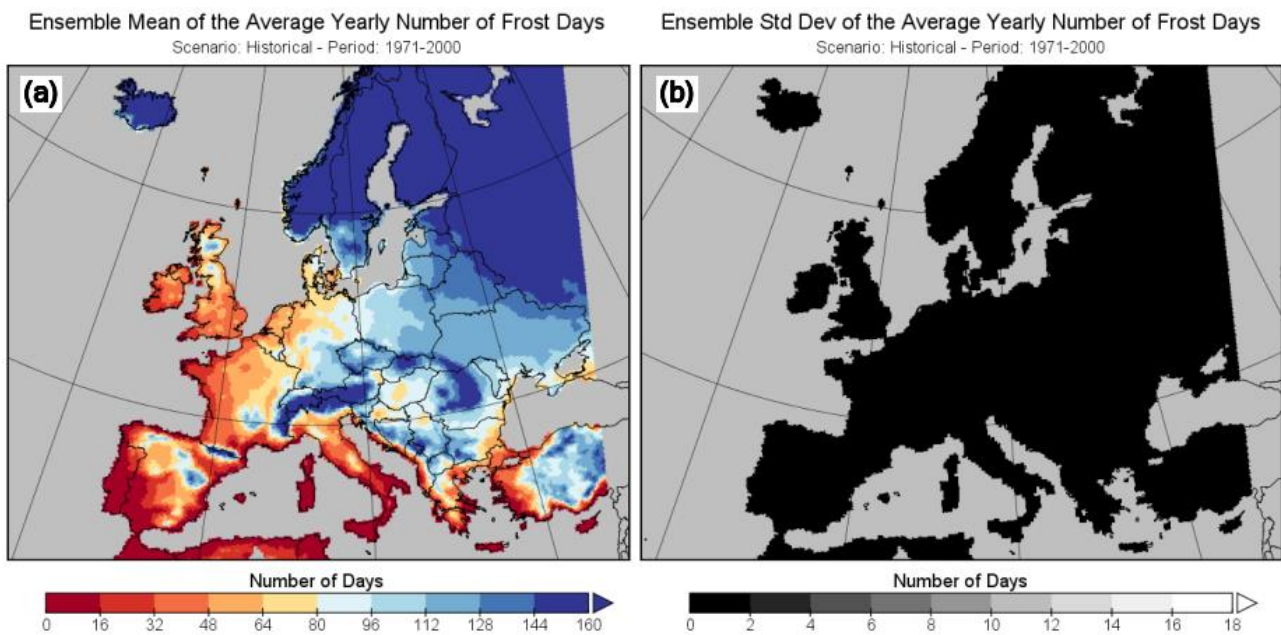


Figure 109: Frost days for the baseline period 1971-2000. (a) Ensemble mean and (b) ensemble standard deviation.

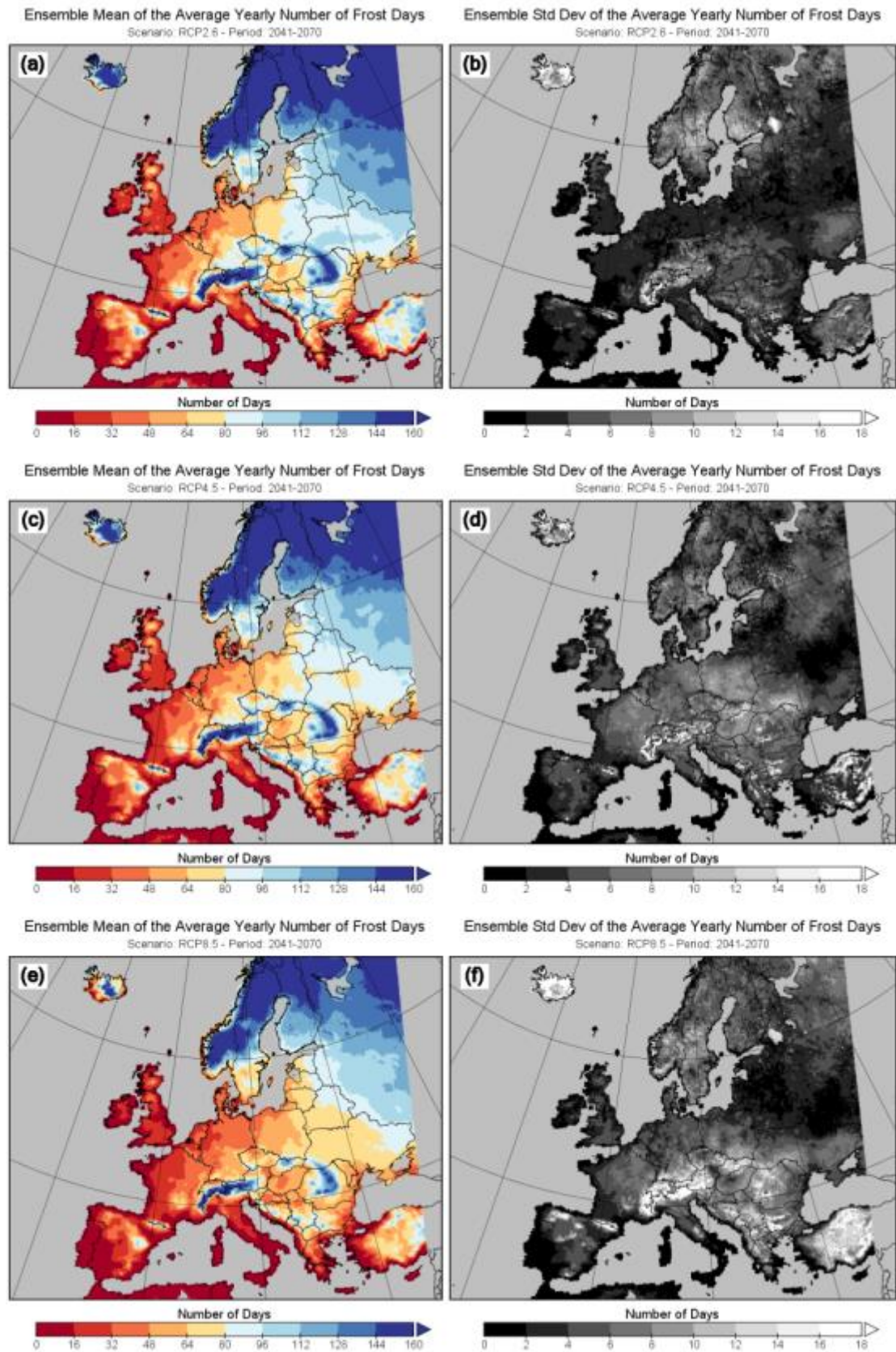


Figure 110: Frost days for the period 2041-2070. (left panels) Ensemble mean and (right panels) ensemble standard deviation. (a, b) RCP2.6, (c, d) RCP4.5, (e, f) RCP8.5.

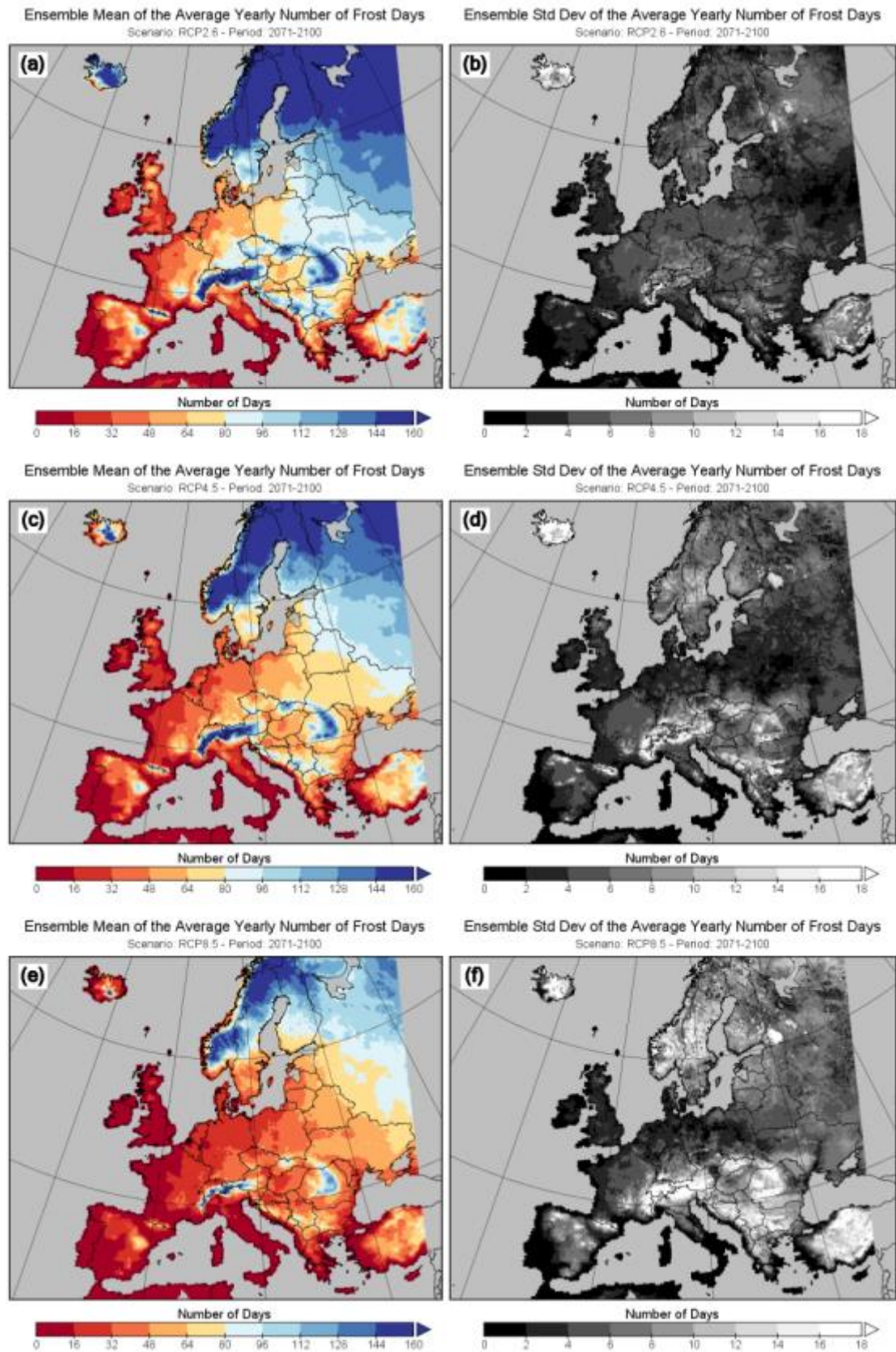


Figure 111: Frost days for the period 2071-2100. (left panels) Ensemble mean and (right panels) ensemble standard deviation. (a, b) RCP2.6, (c, d) RCP4.5, (e, f) RCP8.5.

7.10 Ice days (ID)

Definition: The average yearly number of ice days in Europe averaged over a 30-year period. An ice day is a day where the maximum temperature is less than 0.0 °C.

Units: Days

Background: This climate index is a measure of daytime cold, with high values corresponding to cold conditions. An increase of this index with time means that the chance of colder conditions will increase.

Results: See description regarding the cold indices in Section 7.1.2.

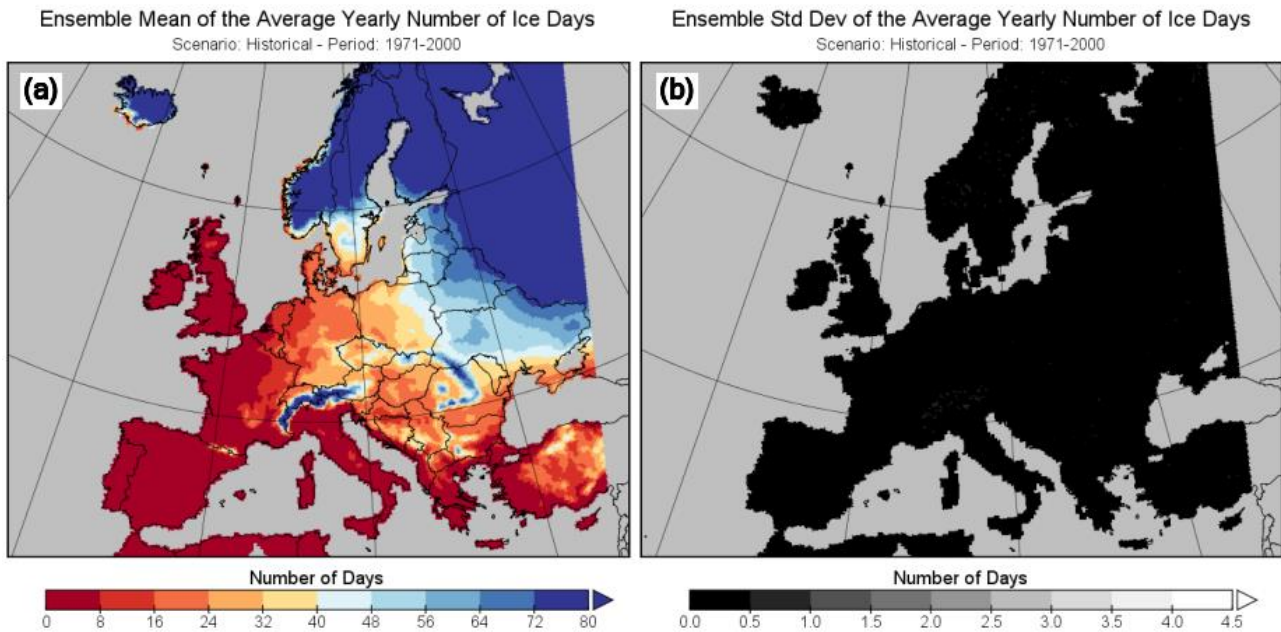


Figure 112: Ice days for the baseline period 1971-2000. (a) Ensemble mean and (b) ensemble standard deviation.

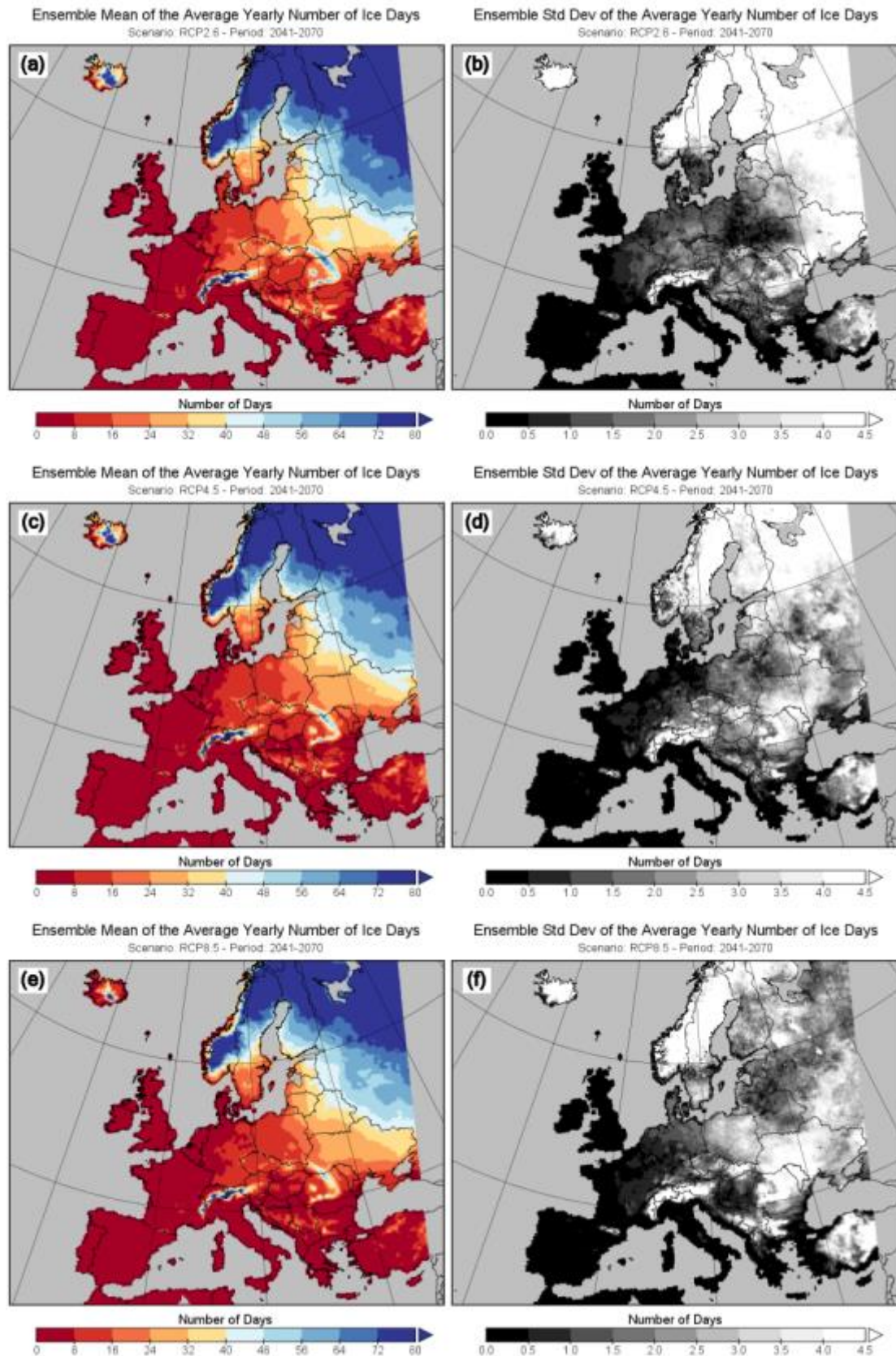


Figure 113: Ice days for the period 2041-2070. (left panels) Ensemble mean and (right panels) ensemble standard deviation. (a, b) RCP2.6, (c, d) RCP4.5, (e, f) RCP8.5.

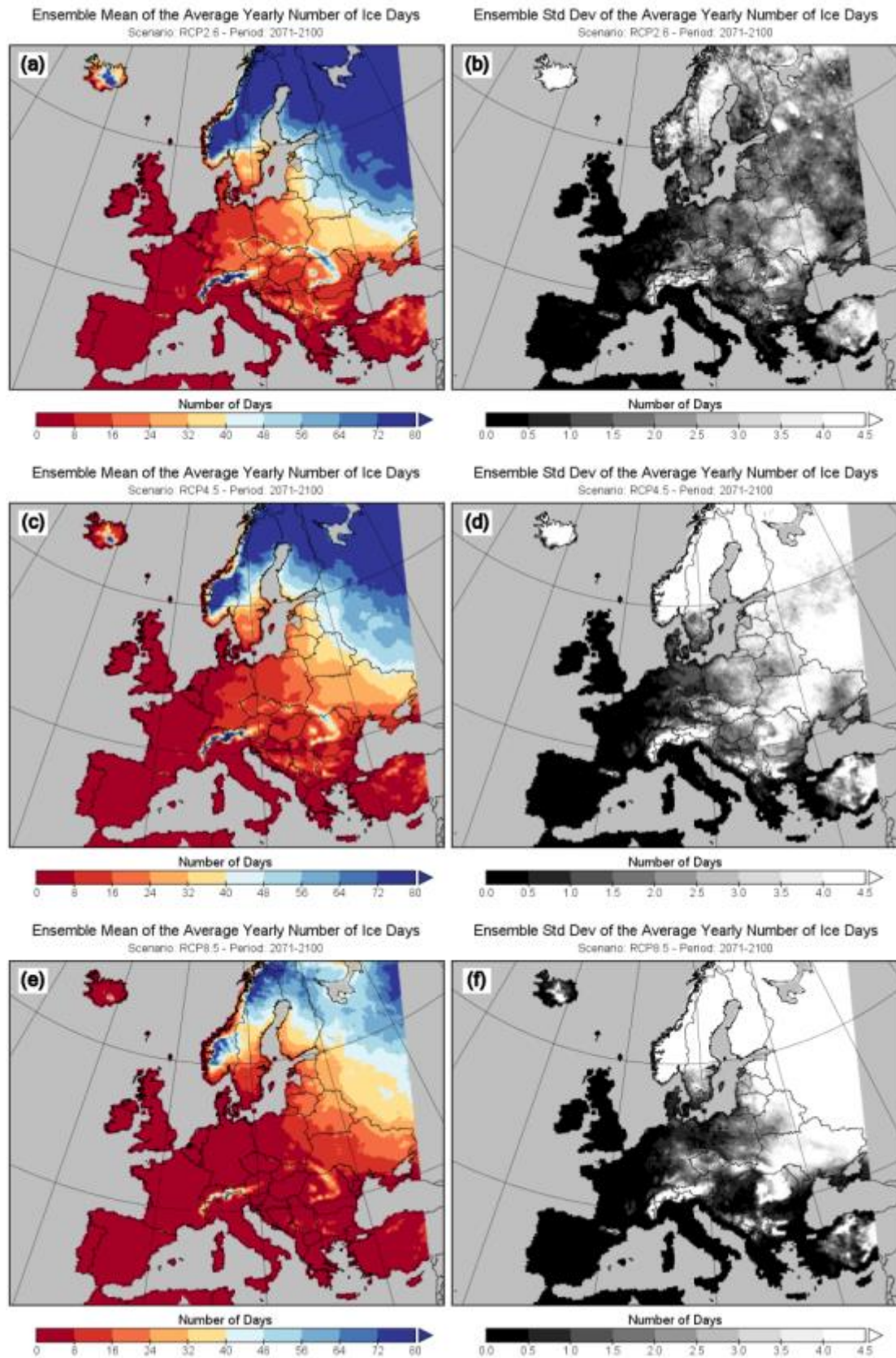


Figure 114: Ice days for the period 2071-2100. (left panels) Ensemble mean and (right panels) ensemble standard deviation. (a, b) RCP2.6, (c, d) RCP4.5, (e, f) RCP8.5.

7.11 Cold days with respect to the 10th percentile of daily minimum temperature (Tn10p)

Definition: Maximum number of days where the daily minimum temperature is below the 10th percentile of minimum temperature during the baseline period 1971-2000. The value for each year is averaged over a 30-year period.

Units: Days

Background: This climate index is a measure of daytime cold, with high values corresponding to cold conditions. An increase of this index with time means that the chance of colder conditions will increase.

Results: There is a decrease in Tn10p over Europe for all RCP scenarios from the baseline period (1971-2000, **Figure 115**) to the 2041-2070 period (**Figure 116**) with the biggest change occurring over Northern Europe. The trend from the 2041-2070 to 2071-2100 period (**Figure 117**) for RCP2.6 shows an increase in Tn10p over Eastern Europe and a decrease over Western Europe. For RCP4.5 and RCP8.5 however, a decrease occurs throughout Europe with the biggest change occurring for the RCP8.5 scenario

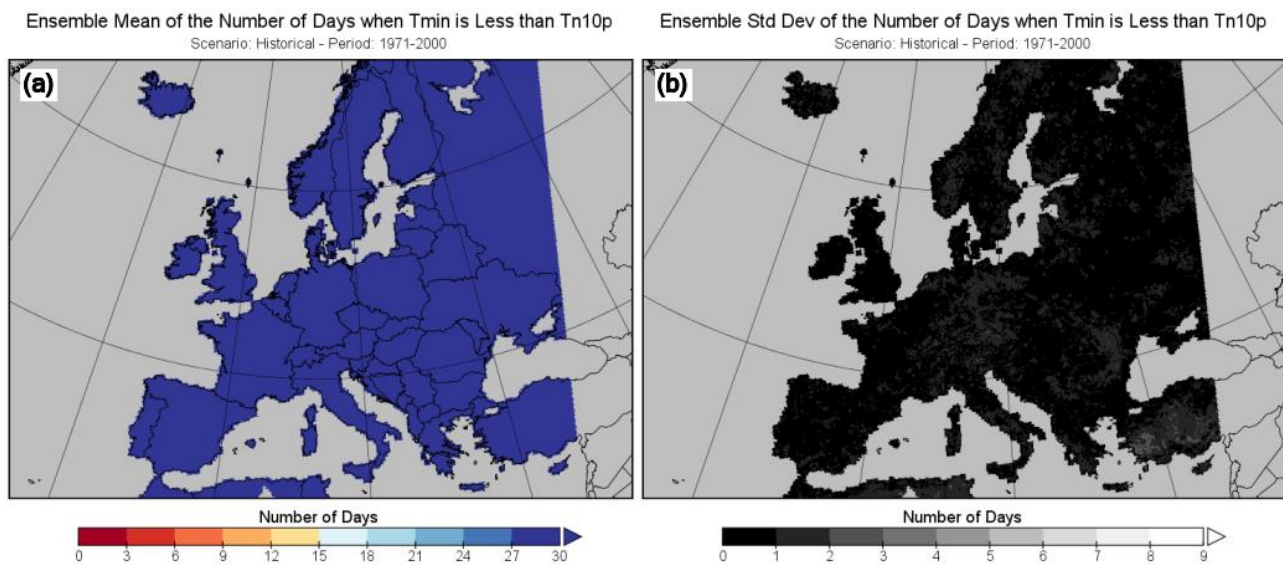


Figure 115: Tn10p for the baseline period 1971-2000. (a) Ensemble mean and (b) ensemble standard deviation.

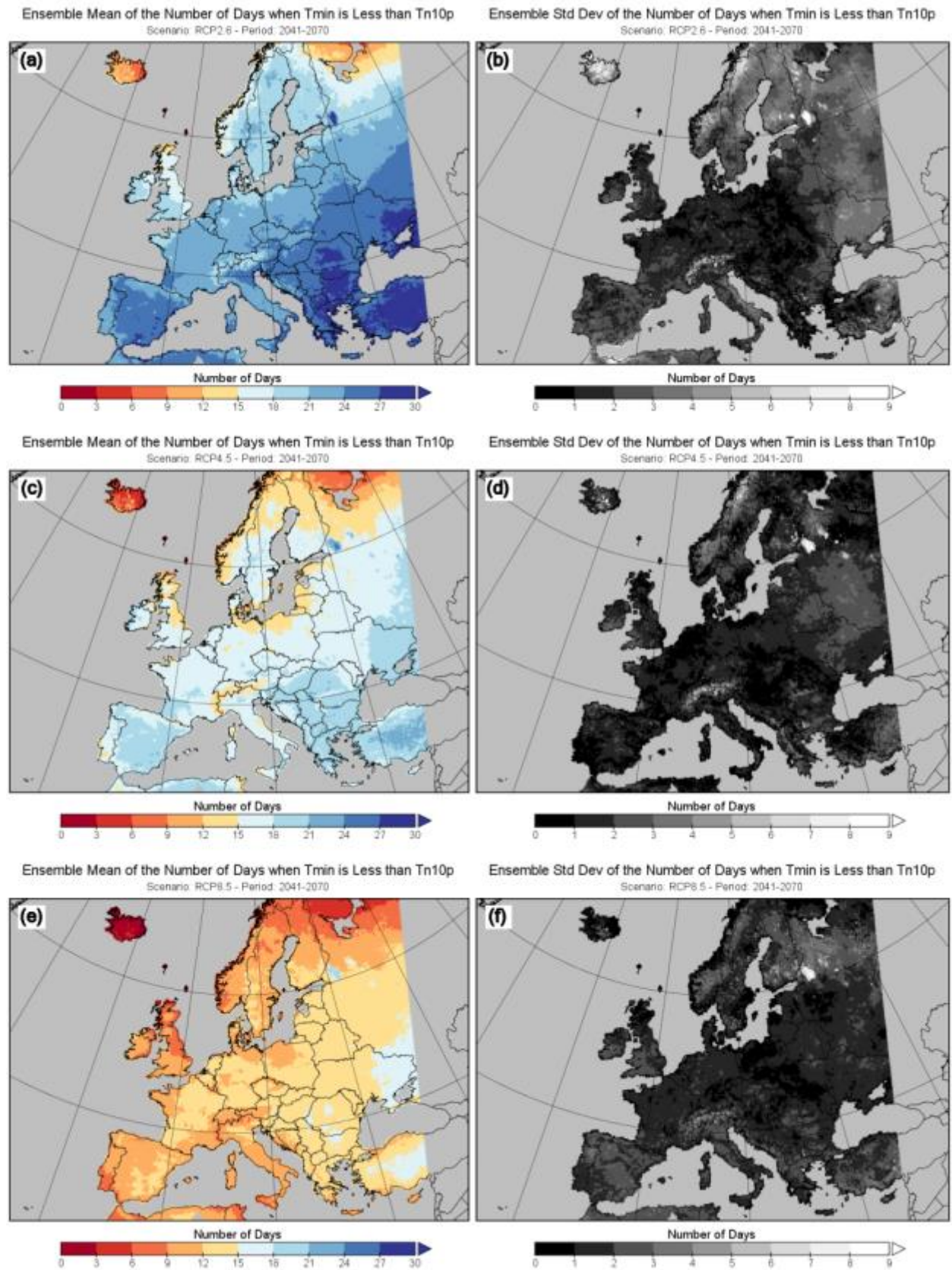


Figure 116: T_{n10p} for the period 2041-2070. (left panels) Ensemble mean and (right panels) ensemble standard deviation. (a, b) RCP2.6, (c, d) RCP4.5, (e, f) RCP8.5.

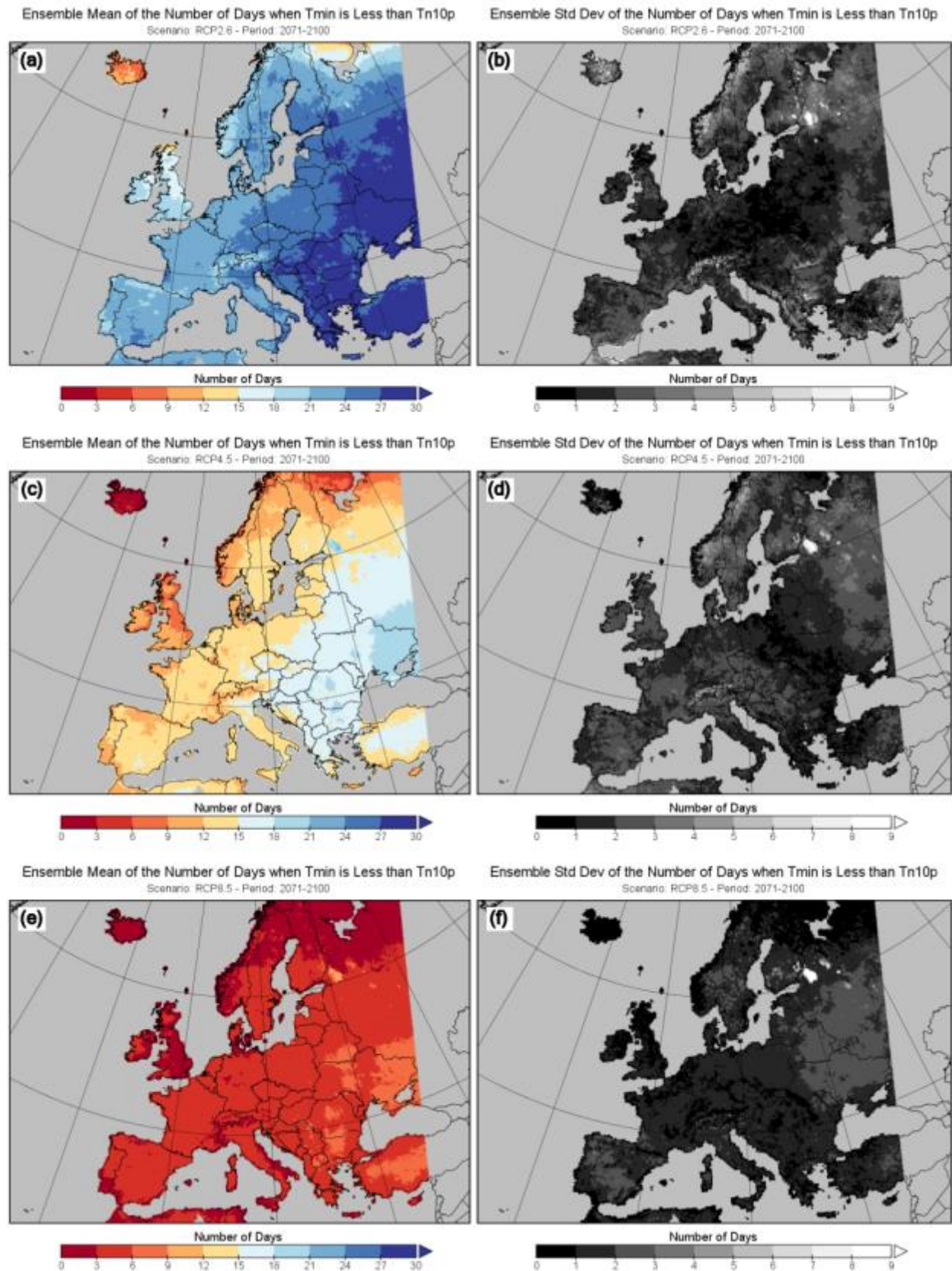


Figure 117: T_{n10p} for the period 2071-2100. (left panels) Ensemble mean and (right panels) ensemble standard deviation. (a, b) RCP2.6, (c, d) RCP4.5, (e, f) RCP8.5.

7.12 Extreme temperature range (ETR)

Definition: The Extreme Temperature Range is a measure of thermal stress and is the greatest difference between the daily maximum and minimum temperatures for a year, averaged over a 30-year period.

Units: Degrees Celsius (°C)

Background: This climate index is a measure of the day-night temperature difference, with small values suggesting reduced cooling during the night if the daytime temperature was high.

Results: There is a general decrease in ETR from the baseline period (1971-2000, **Figure 118**) to the 2041-2070 period (**Figure 119**) over Northeastern Europe and an increase over Western Europe for all RCP scenarios. For the RCP2.6 scenario from 2041-2070 to the period 2071-2100 (**Figure 120**), there is an increase in ETR over Northeastern Europe. For RCP4.5 and RCP8.5 (**Figure 120**) there is a decrease over Northern Europe, but an overall increase over the rest of Europe with the changes greatest for RCP8.5.

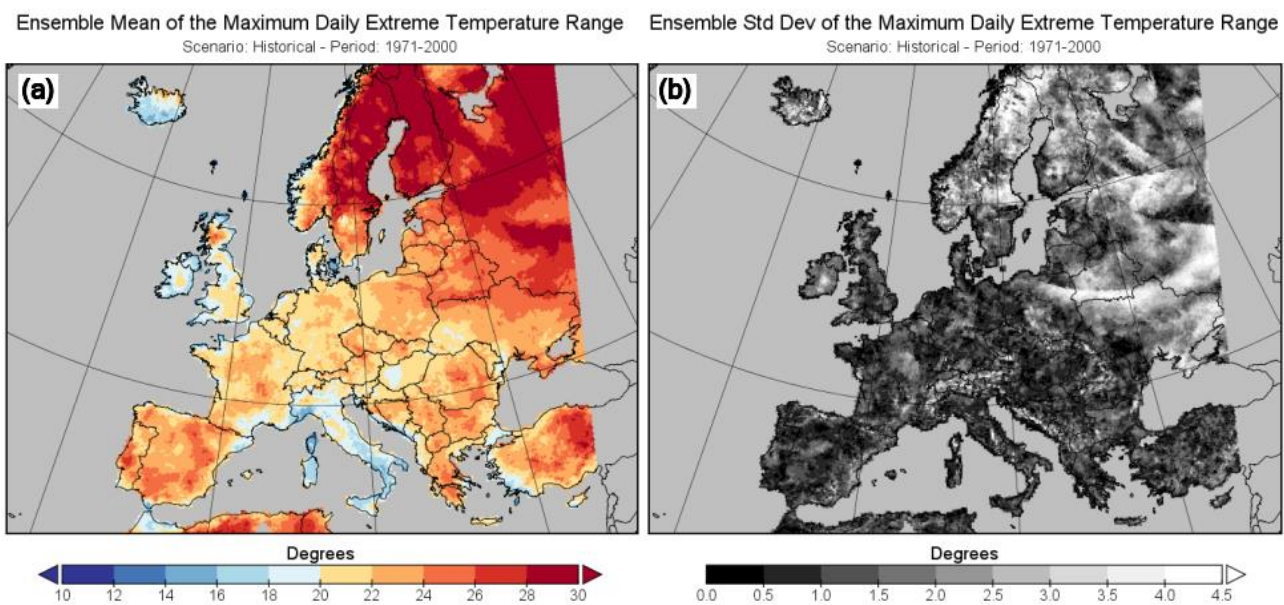


Figure 118: Extreme temperature range for the baseline period 1971-2000. (a) Ensemble mean and (b) ensemble standard deviation.

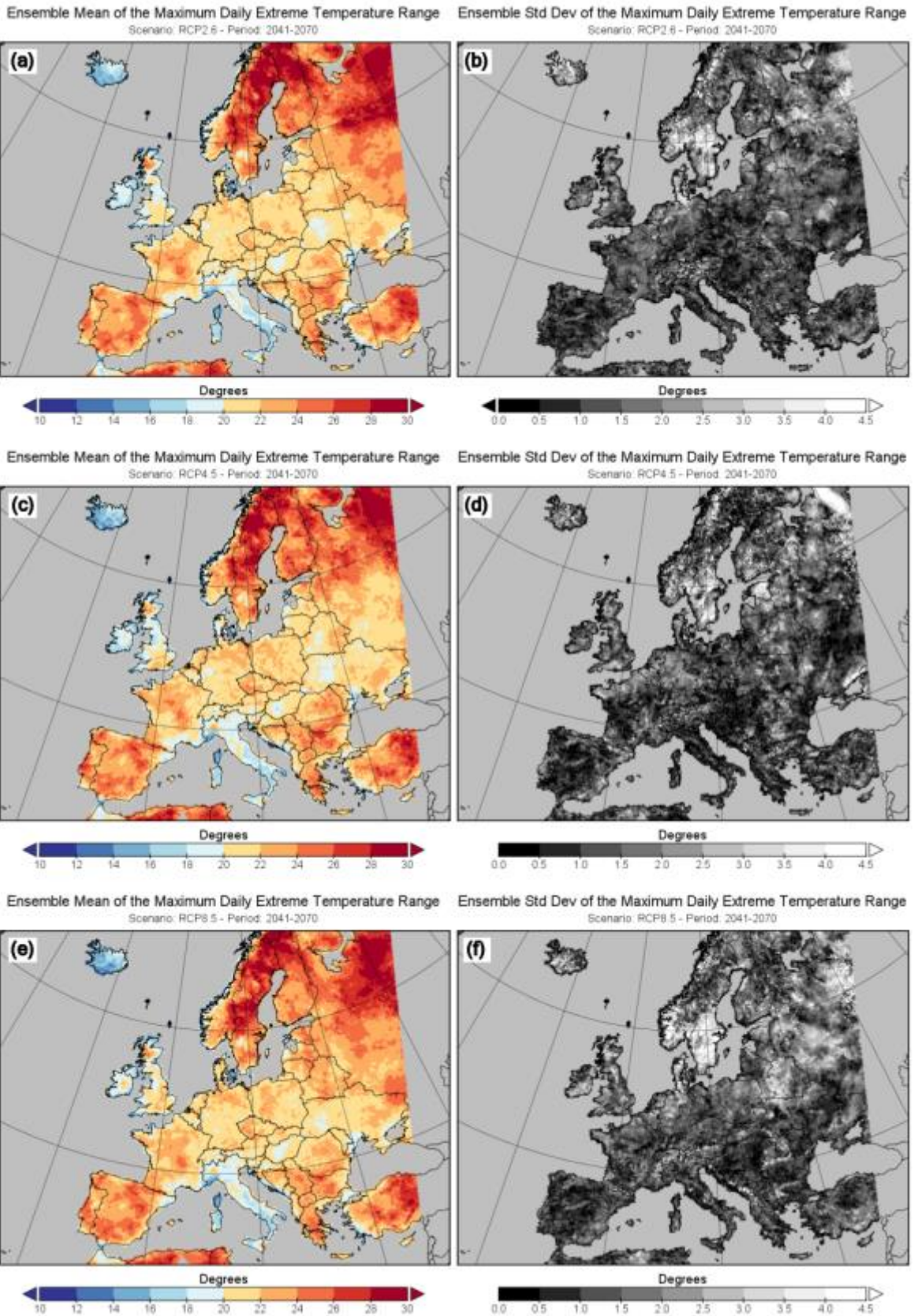
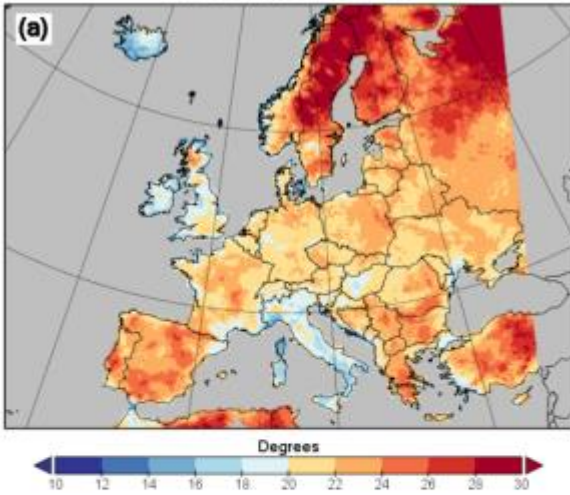
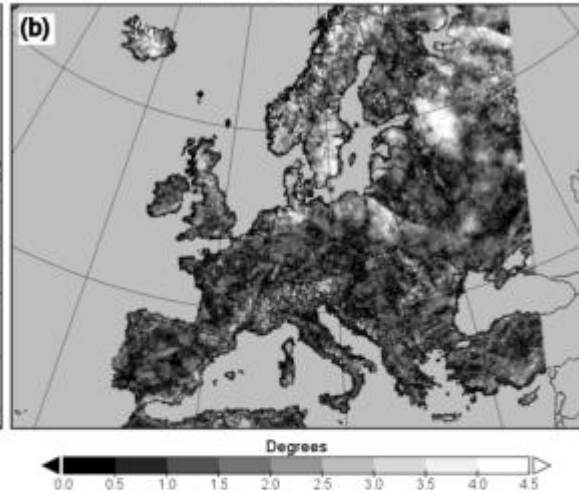


Figure 119: Extreme temperature range for the period 2041-2070. (left panels) Ensemble mean and (right panels) ensemble standard deviation. (a, b) RCP2.6, (c, d) RCP4.5, (e, f) RCP8.5.

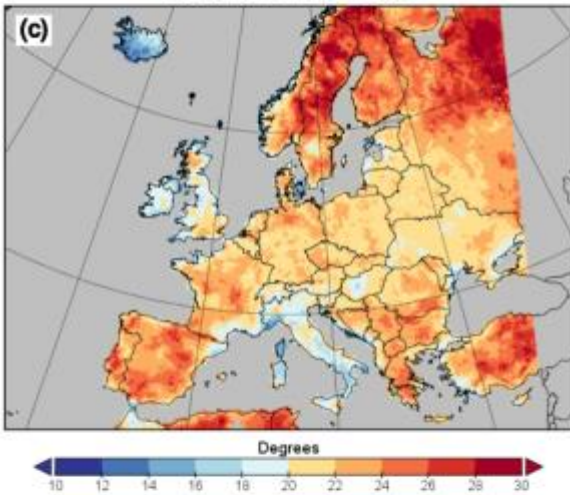
Ensemble Mean of the Maximum Daily Extreme Temperature Range
Scenario: RCP2.6 - Period: 2071-2100



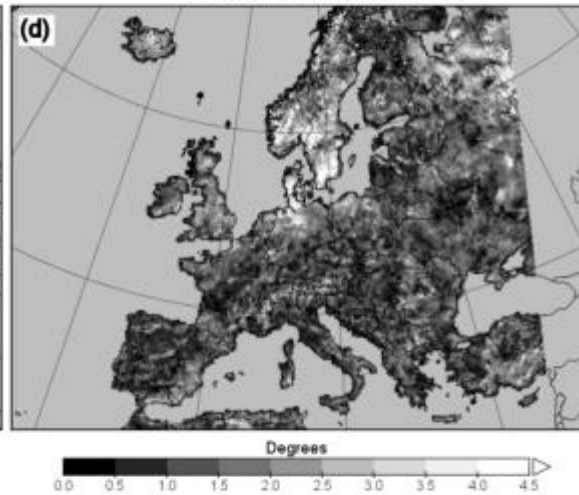
Ensemble Std Dev of the Maximum Daily Extreme Temperature Range
Scenario: RCP2.6 - Period: 2071-2100



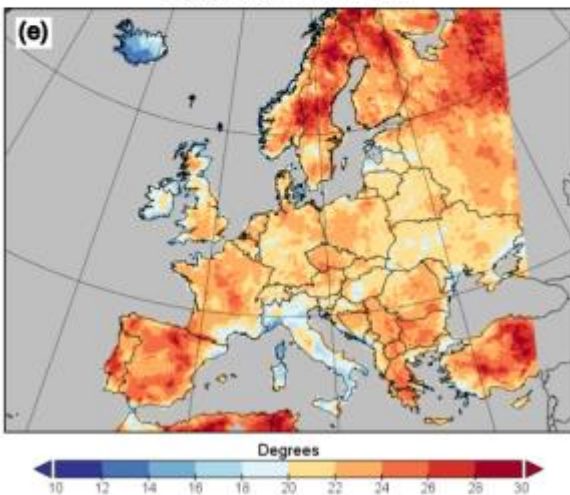
Ensemble Mean of the Maximum Daily Extreme Temperature Range
Scenario: RCP4.5 - Period: 2071-2100



Ensemble Std Dev of the Maximum Daily Extreme Temperature Range
Scenario: RCP4.5 - Period: 2071-2100



Ensemble Mean of the Maximum Daily Extreme Temperature Range
Scenario: RCP8.5 - Period: 2071-2100



Ensemble Std Dev of the Maximum Daily Extreme Temperature Range
Scenario: RCP8.5 - Period: 2071-2100

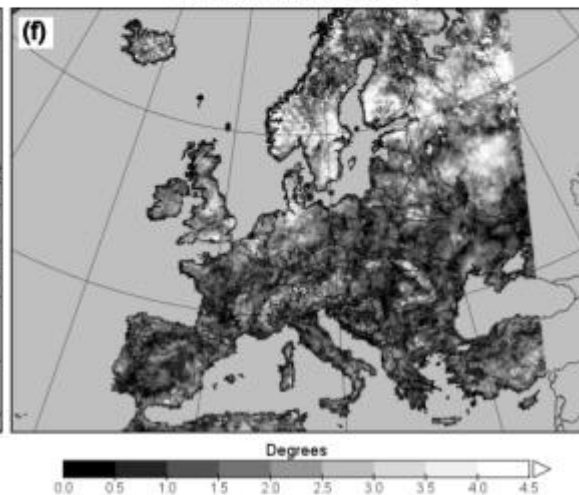


Figure 120: Extreme temperature range for the period 2071-2100. (left panels) Ensemble mean and (right panels) ensemble standard deviation. (a, b) RCP2.6, (c, d) RCP4.5, (e, f) RCP8.5.

7.13 Highest 1-day precipitation amount (RX1day)

Definition: Maximum of one day precipitation amount for each year, averaged over a 30-year period.

Units: Millimetre (mm)

Background: This climate index is a measure of heavy precipitation, with high values corresponding to a high chance of flooding. An increase of this index with time means that the chance of flood conditions will increase.

Results: There is a general increase from the baseline period (1971-2000, **Figure 121**) to the 2041-2070 period (**Figure 122**, e.g. northern Italy) for all RCP scenarios. From 2041-2070 to the period 2071-2100 (**Figure 123**) there appears to be only small changes for the RCP2.6 scenario, whereas the RCP4.5 and RCP8.5 scenarios exhibit a general increase over Europe, with RCP8.5 showing the greatest change.

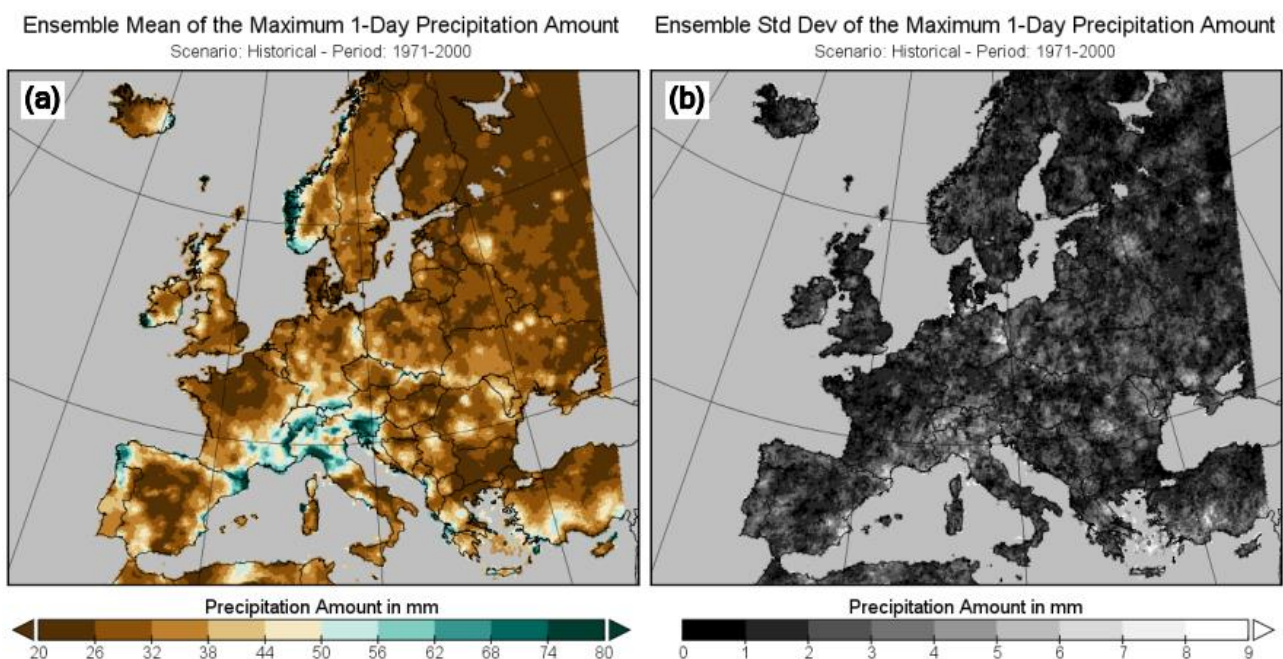


Figure 121: RX1day for the baseline period 1971-2000. (a) Ensemble mean and (b) ensemble standard deviation.

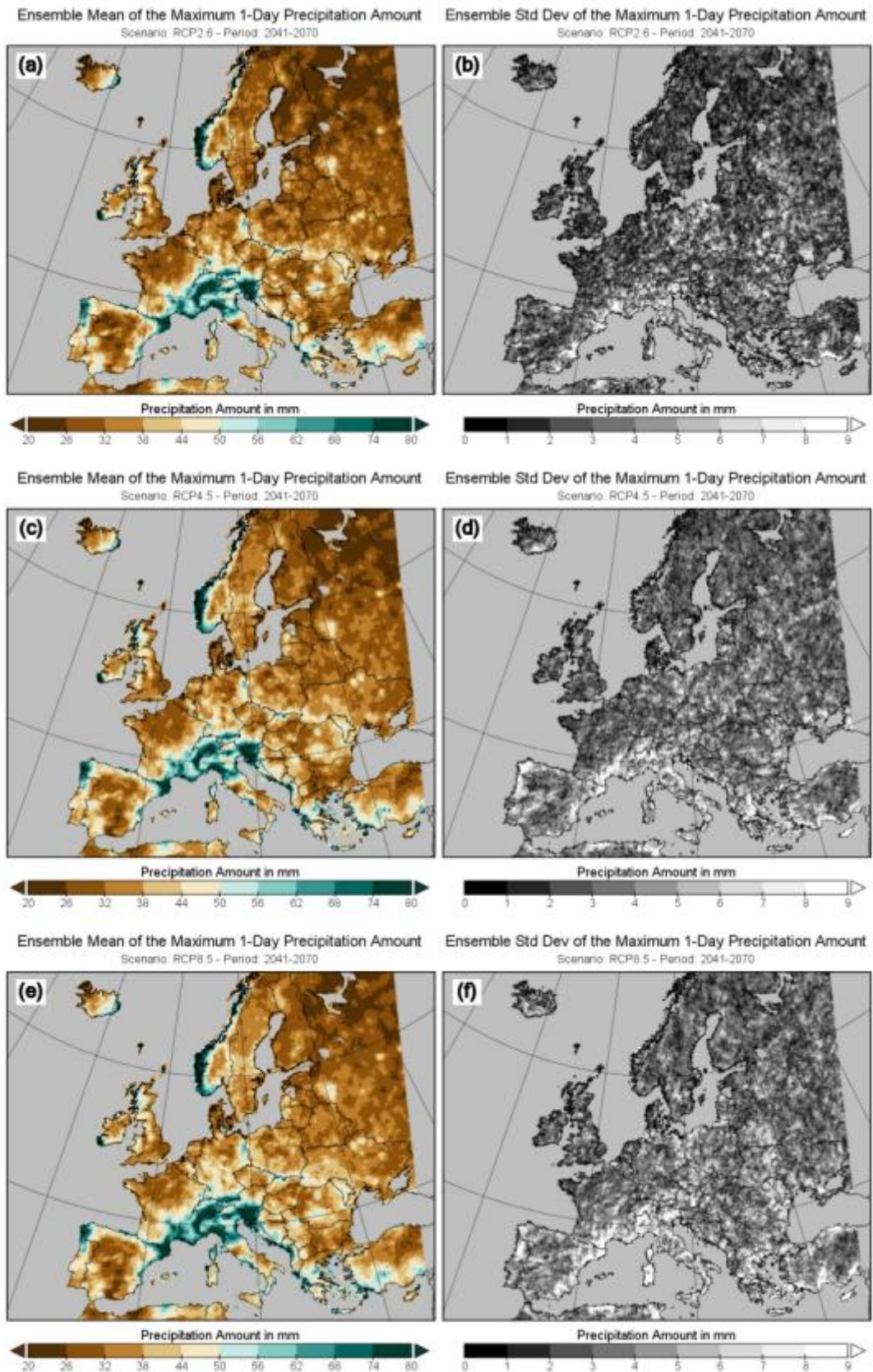


Figure 122: RX1day for the period 2041-2070. (left panels) Ensemble mean and (right panels) ensemble standard deviation. (a, b) RCP2.6, (c, d) RCP4.5, (e, f) RCP8.5.

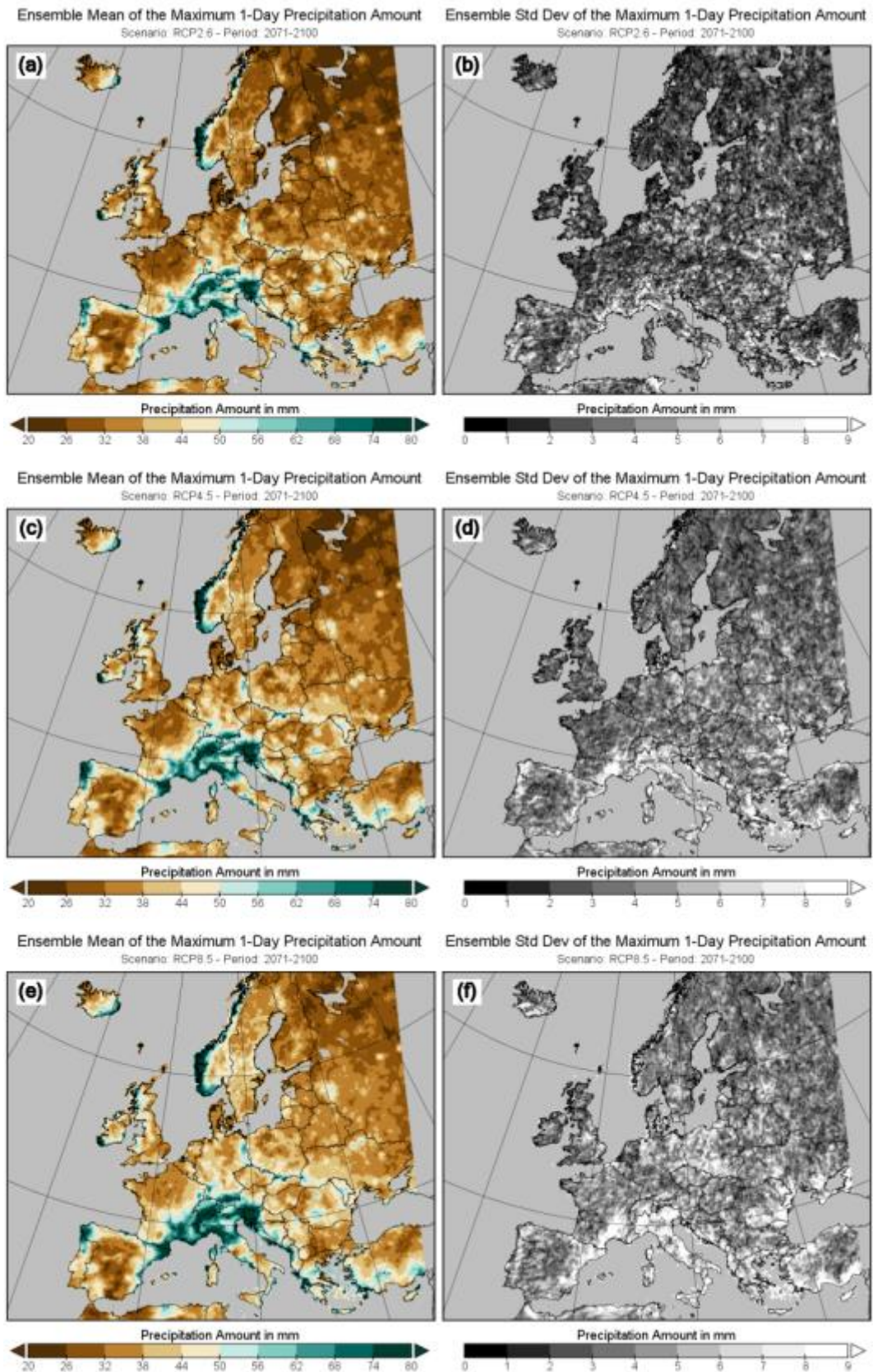


Figure 123: RX1day for the period 2071-2100. (left panels) Ensemble mean and (right panels) ensemble standard deviation. (a, b) RCP2.6, (c, d) RCP4.5, (e, f) RCP8.5.

7.14 Highest 5-day precipitation amount (RX1day)

Definition: Maximum of the daily precipitation amount summed over five days for each year, averaged over a 30-year period..

Units: Millimetre (mm)

Background: This climate index is a measure of heavy precipitation, with high values corresponding to a high chance of flooding. An increase of this index with time means that the chance of flood conditions will increase.

Results: As for RX1day, there is an increase from the baseline period (1971-2000, **Figure 124**) to the 2041-2070 period (**Figure 125**, e.g. northern Italy) for all RCP scenarios. From 2041-2070 to the period 2071-2100 (**Figure 126**), the changes appear locally confined and less coherent over larger regions (e.g. increase over Northwestern Spain, decrease over eastern Germany). However, as for RX1day, the RCP4.5 and RCP8.5 scenarios exhibit a general increase over Europe, with RCP8.5 showing the greatest change

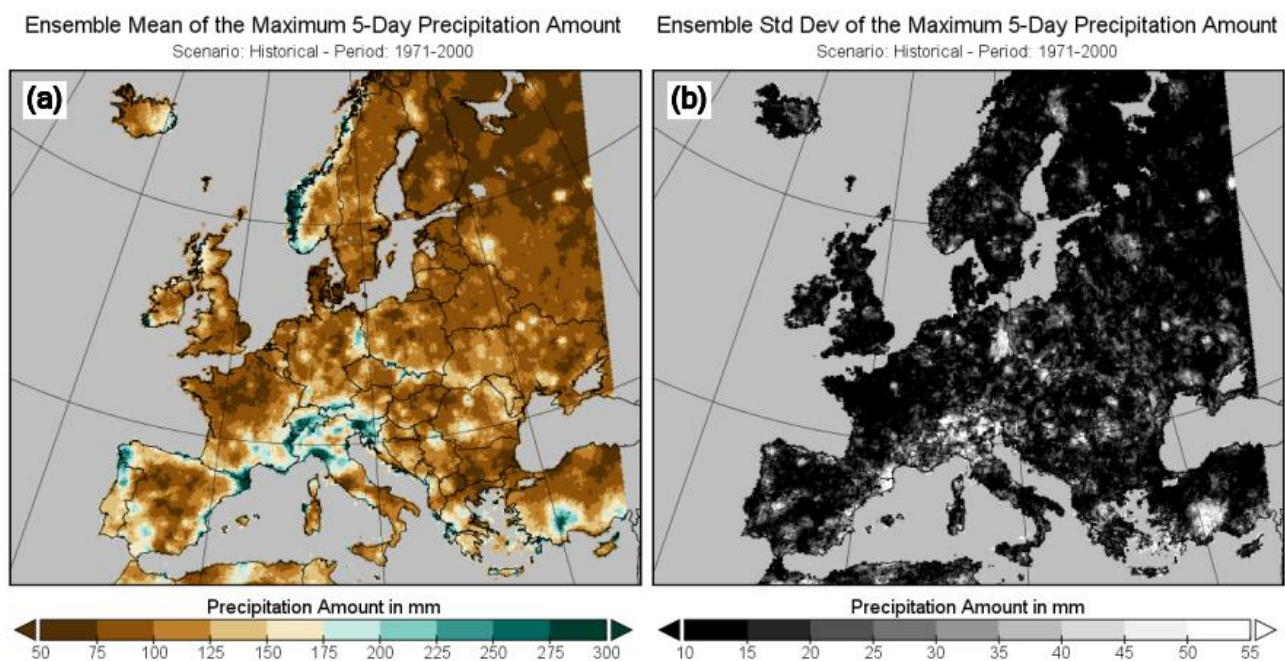


Figure 124: RX5day for the baseline period 1971-2000. (a) Ensemble mean and (b) ensemble standard deviation.

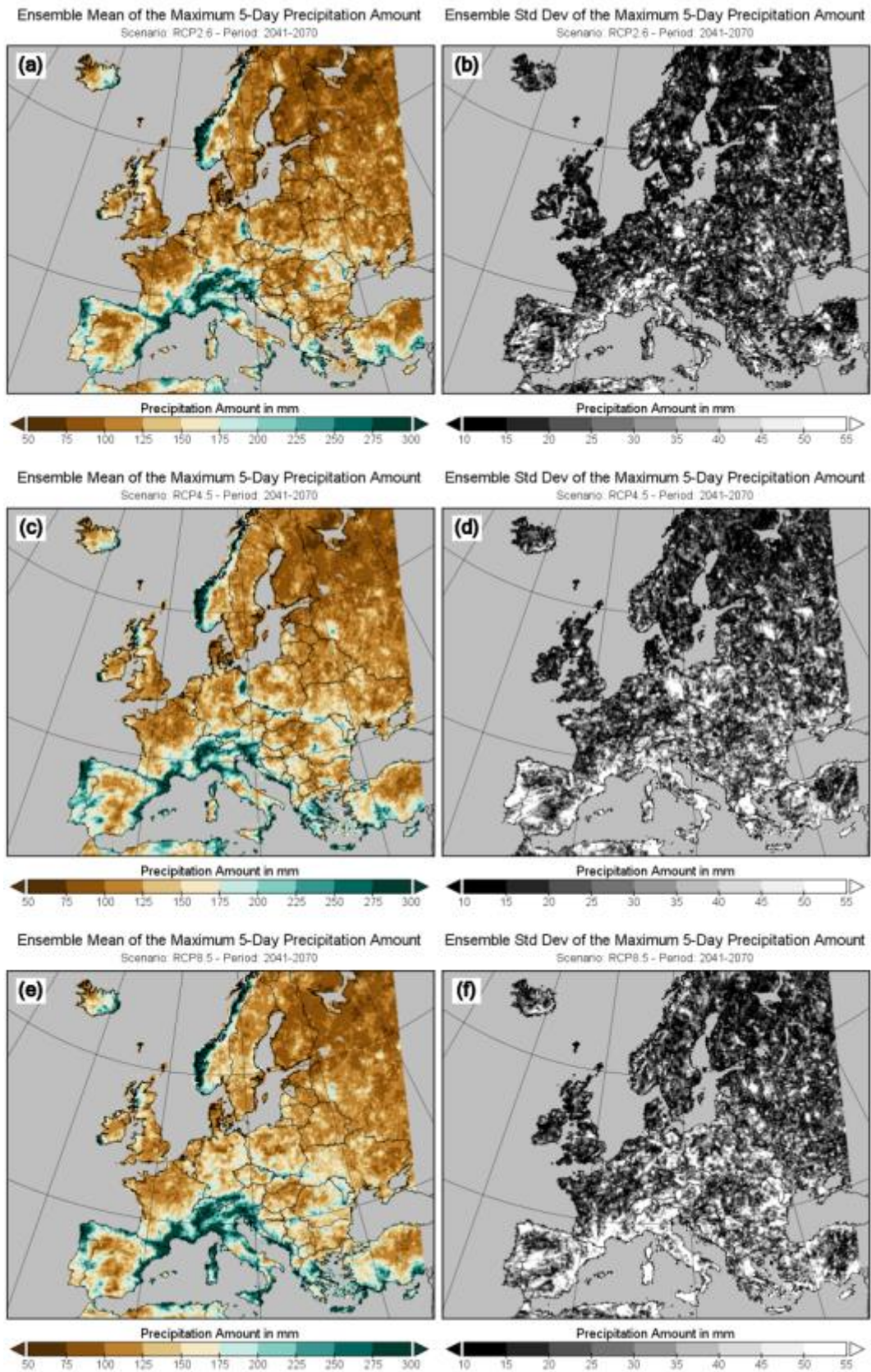


Figure 125: RX5day for the period 2041-2070. (left panels) Ensemble mean and (right panels) ensemble standard deviation. (a, b) RCP2.6, (c, d) RCP4.5, (e, f) RCP8.5.

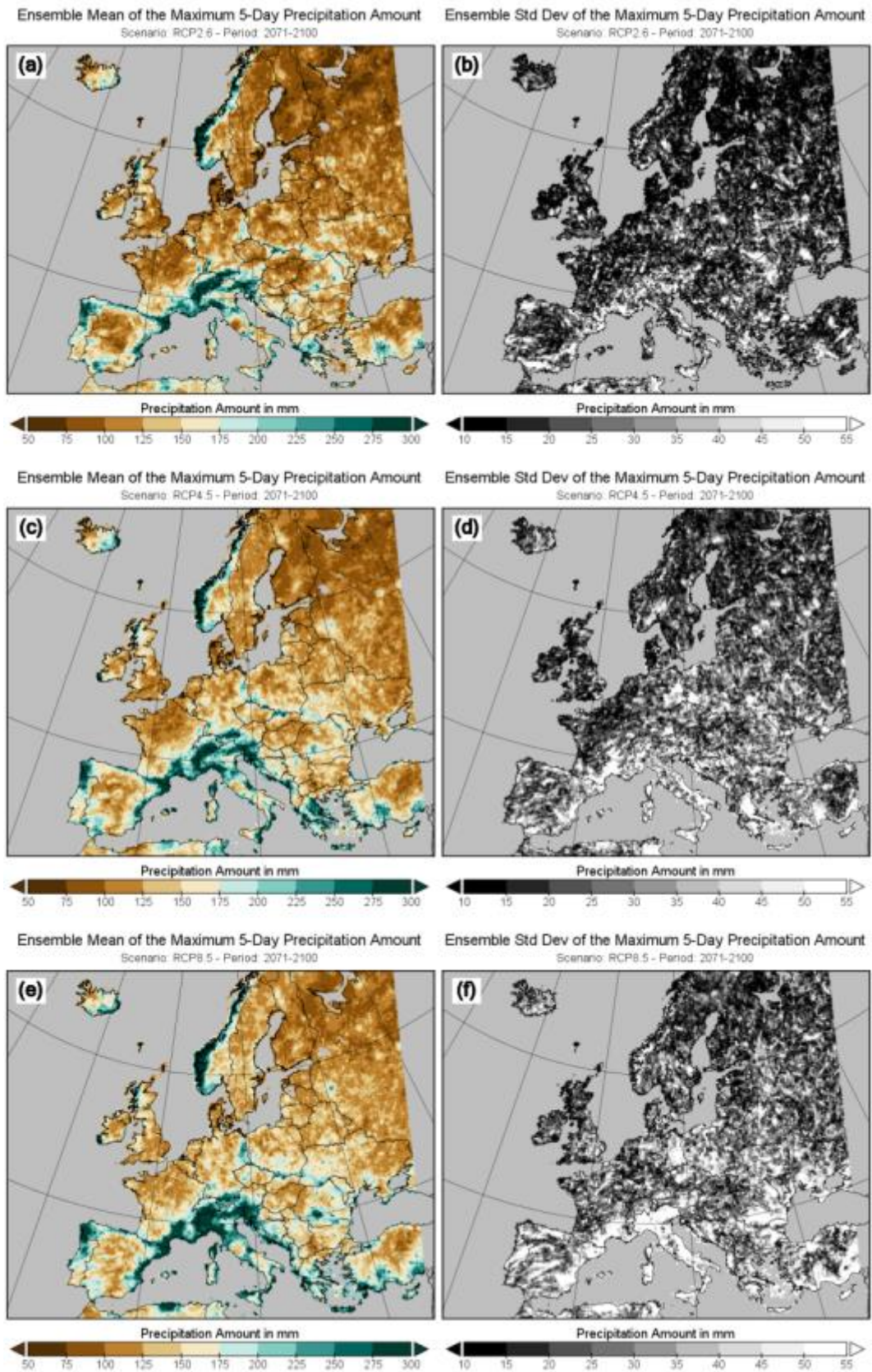


Figure 126: RX5day for the period 2071-2100. (left panels) Ensemble mean and (right panels) ensemble standard deviation. (a, b) RCP2.6, (c, d) RCP4.5, (e, f) RCP8.5.

7.15 Snow days

Definition: Number of days with daily precipitation of at least 1mm and a daily maximum temperature below 4 °C for each year, averaged over a 30-year period

Units: Days

Background: This climate index is a measure of the potential of snow, with high values corresponding to long periods of days of snow. An increase of this index with time means that the chance of snow conditions will increase.

Results: There is a decrease in the number of snow days over Southern Europe and an increase over Northern Europe from the baseline period (1971-2000, **Figure 127**) to the 2041-2070 period (**Figure 128**) with the change increasing for increasing RCP scenario. The trend from the 2041-2070 to 2071-2100 period (**Figure 129**) for RCP2.6 shows an increase overall except for far Northern Europe, while for RCP4.5 and RCP8.5 there is an increase over much of Europe except over Southern Europe., with the latter scenario showing greater changes.

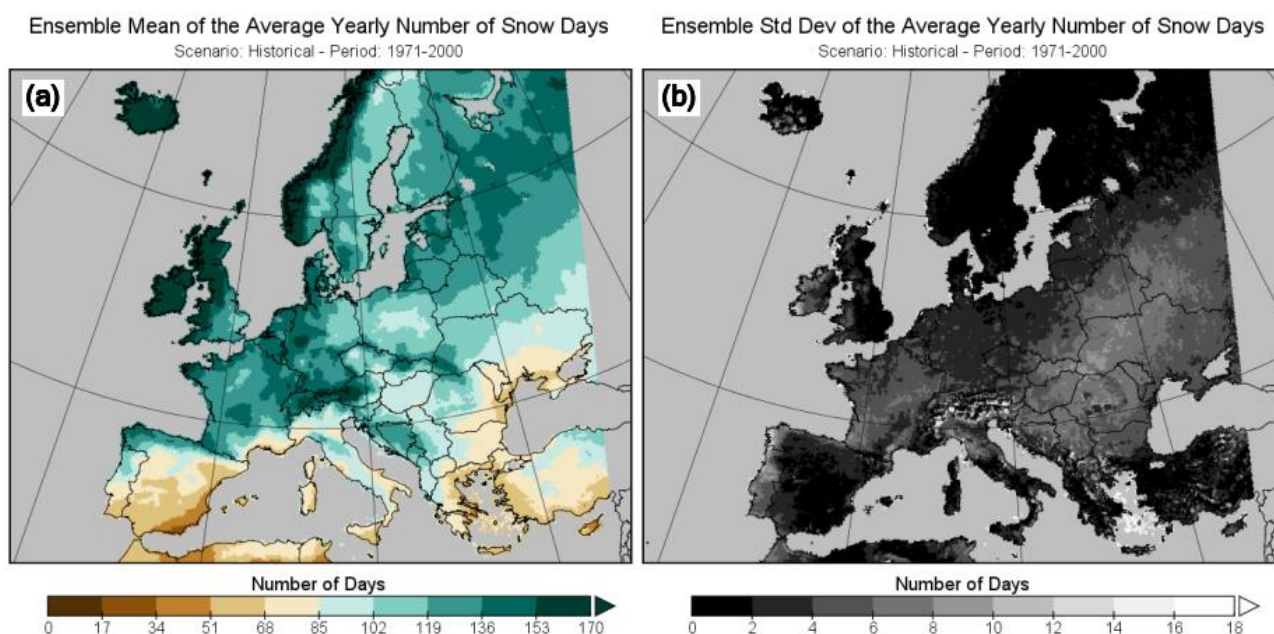


Figure 127: Snow days for the baseline period 1971-2000. (a) Ensemble mean and (b) ensemble standard deviation.

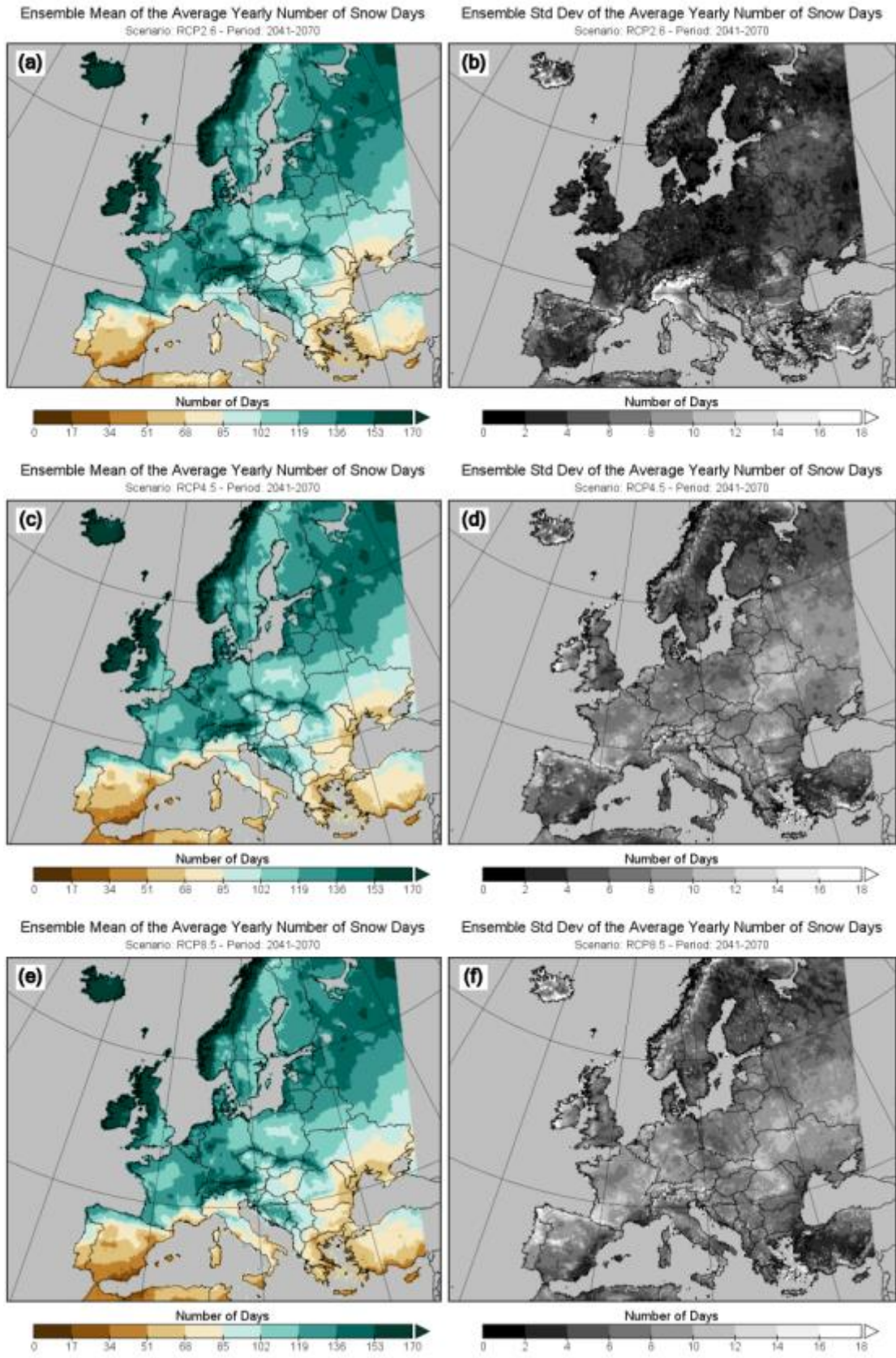


Figure 128: Snow days for the period 2041-2070. (left panels) Ensemble mean and (right panels) ensemble standard deviation. (a, b) RCP2.6, (c, d) RCP4.5, (e, f) RCP8.5.

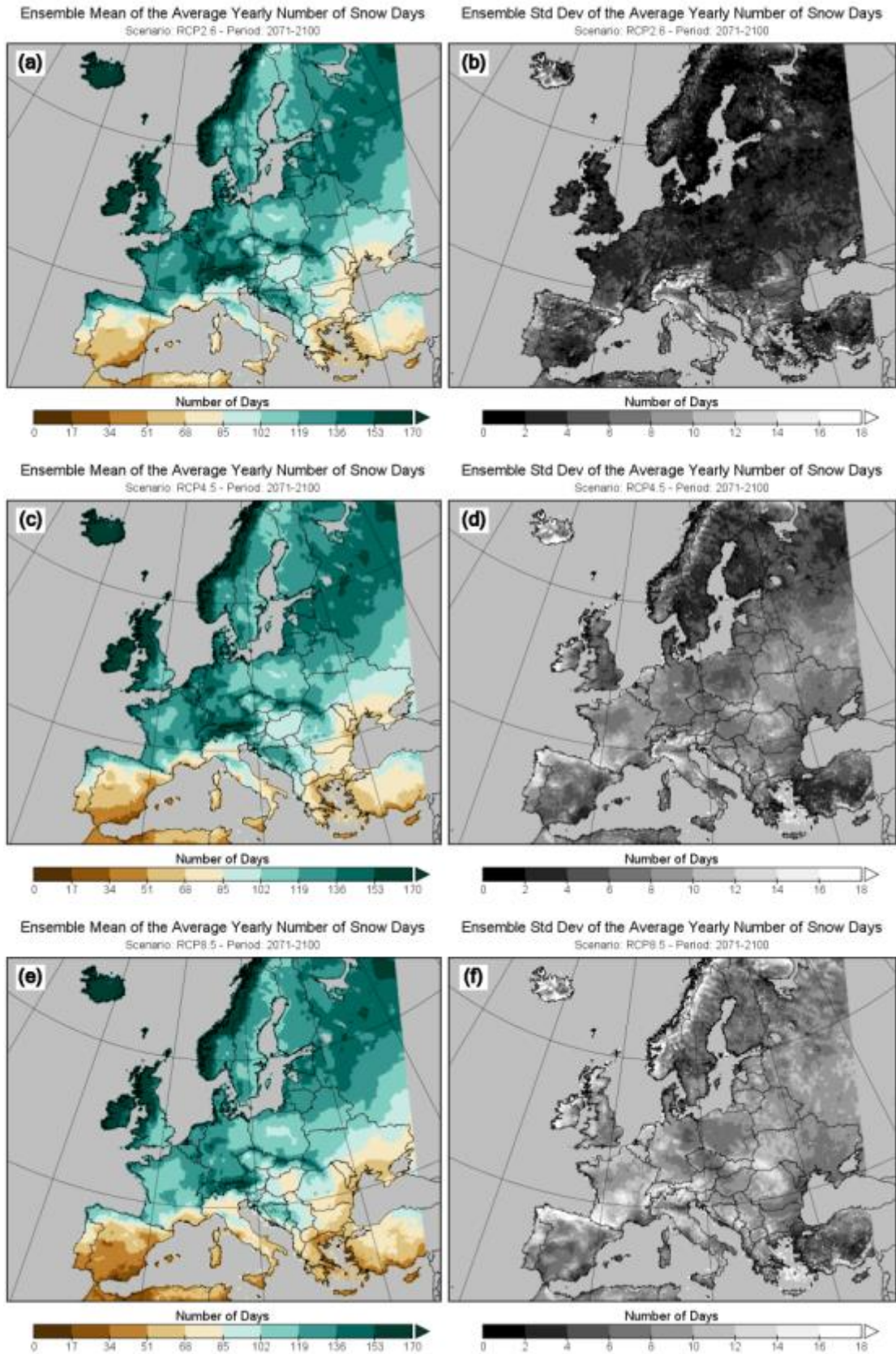


Figure 129: Snow days for the period 2071-2100. (left panels) Ensemble mean and (right panels) ensemble standard deviation. (a, b) RCP2.6, (c, d) RCP4.5, (e, f) RCP8.5.

7.16 Consecutive wet days (CWD)

Definition: Maximum number of consecutive days per time period with daily precipitation amount at least 1 mm for each year, averaged over a 30-year period.

Units: Days

Background: This climate index is a measure of precipitation, with high values corresponding to a high chance of flooding. An increase of this index with time means that the chance of flood conditions will increase.

Results: There is no obvious consistent change from the baseline period (1971-2000, **Figure 130**) to the 2041-2070 (**Figure 131**) for either RCP scenario (e.g. Spain exhibits a slight decrease, France a slight increase). The trend to the 2071-2100 period (**Figure 132**) shows a slight increase for RCP2.6 over central and Northern Europe. The trend for RCP4.5 shows also an increase over much of Europe (e.g. Iberian Peninsula), while for RCP8.5, the trend in Southern Europe is a decrease with an increase in Northern Europe.

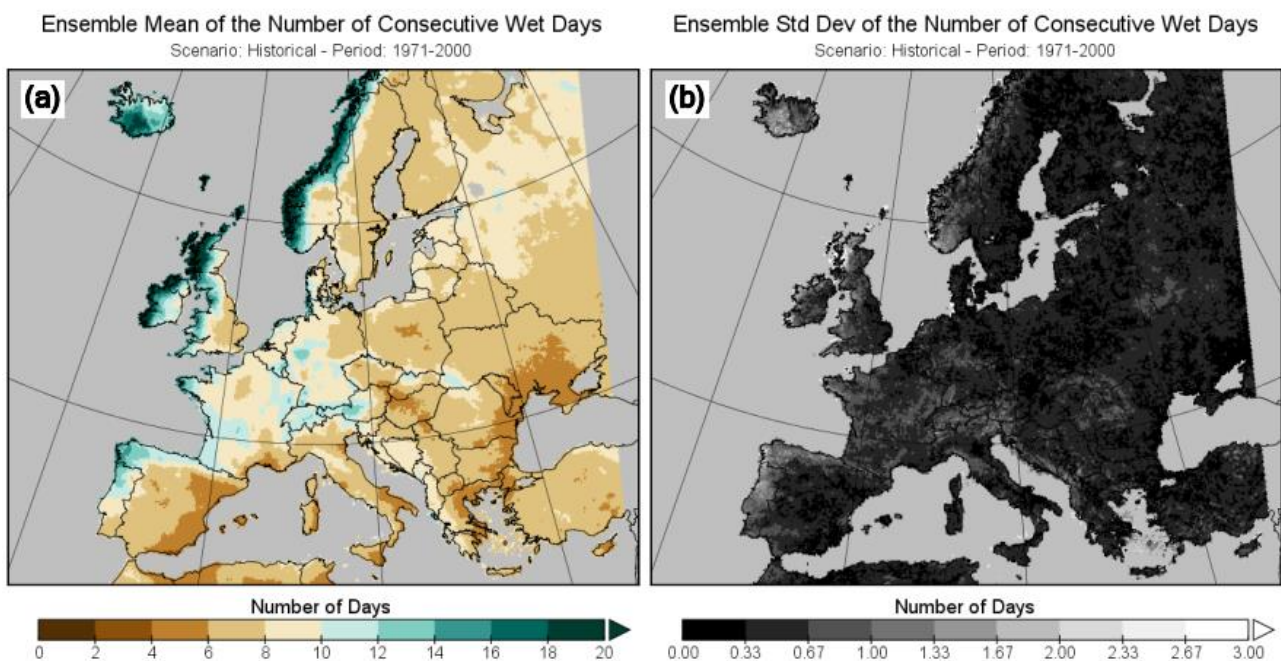


Figure 130: Consecutive wet days for the baseline period 1971-2000. (a) Ensemble mean and (b) ensemble standard deviation.

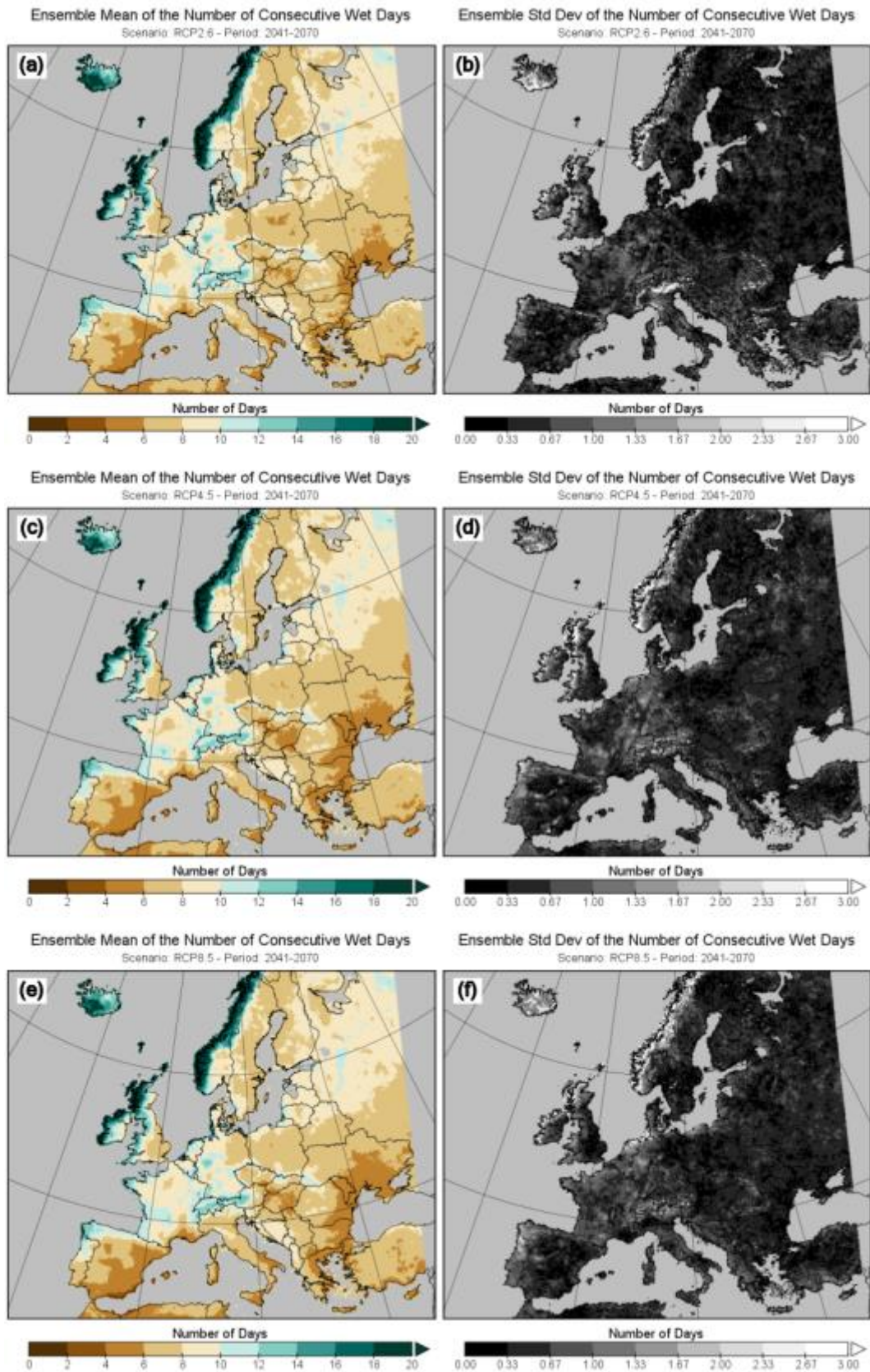


Figure 131: Consecutive wet days for the period 2041-2070. (left panels) Ensemble mean and (right panels) ensemble standard deviation. (a, b) RCP2.6, (c, d) RCP4.5, (e, f) RCP8.5.

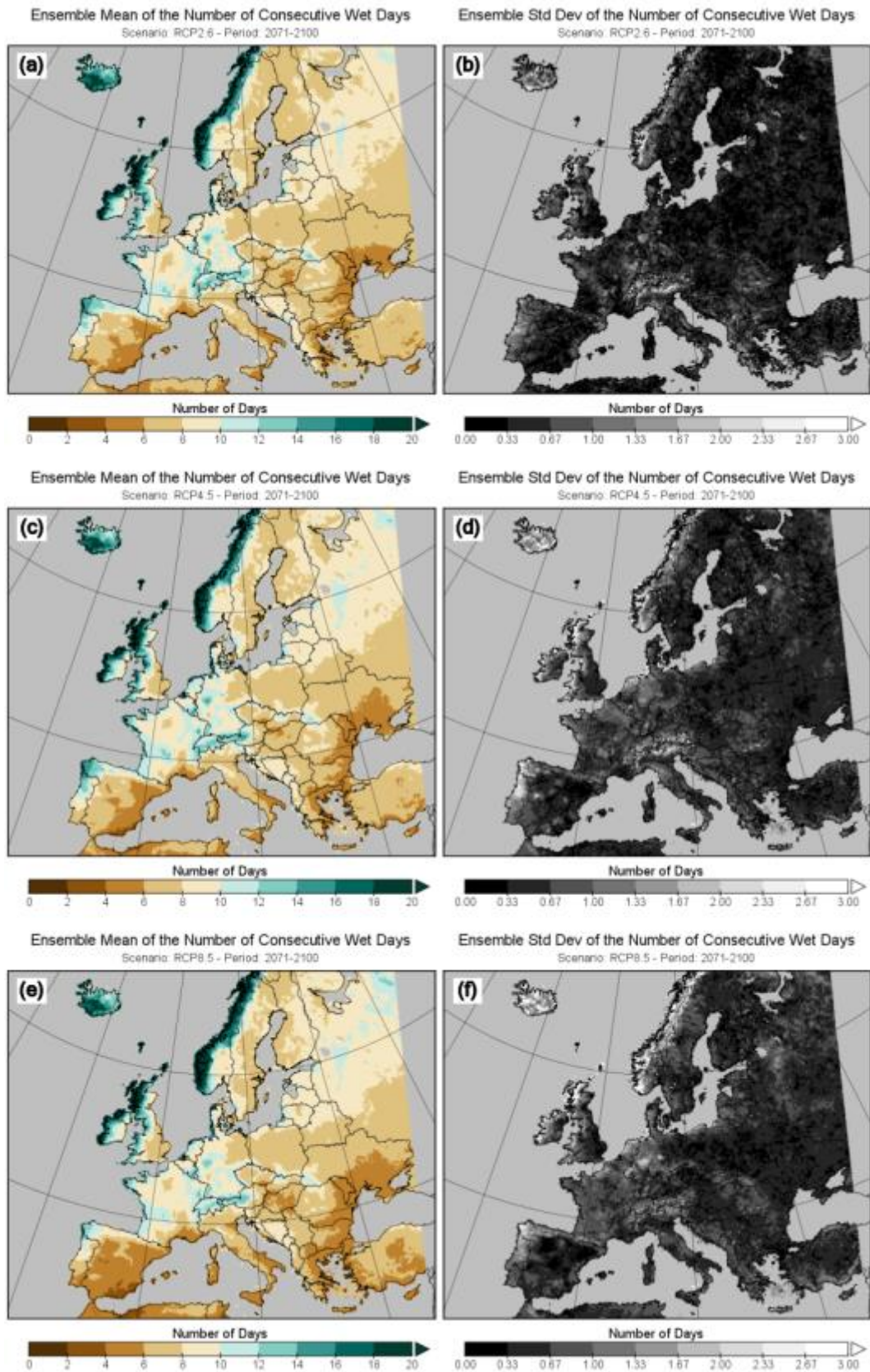


Figure 132: Consecutive wet days for the period 2071-2100. (left panels) Ensemble mean and (right panels) ensemble standard deviation. (a, b) RCP2.6, (c, d) RCP4.5, (e, f) RCP8.5.

7.17 Wet days (RR1mm)

Definition: Number of days per year with daily a precipitation amount of at least 1 mm for each year, averaged over a 30-year period

Units: Days

Background: This climate index is a measure of precipitation, with high values corresponding to a high chance of flooding. An increase of this index with time means that the chance of flood conditions will increase.

Results: There is a decrease in the number of wet days over Western and Southern Europe from the baseline period (1971-2000, **Figure 133**) to the 2041-2070 period (**Figure 134**) with the change increasing for increasing RCP scenario. The trend from the 2041-2070 to 2071-2100 period (**Figure 135**) for RCP2.6 and RCP4.5 show an increase to some degree Europewide with a decrease for southern, Mediterranean countries. For RCP8.5 the increase is confined to Northern Europe with a decrease occurring for the rest of Europe with the biggest change occurring in Southern European countries.

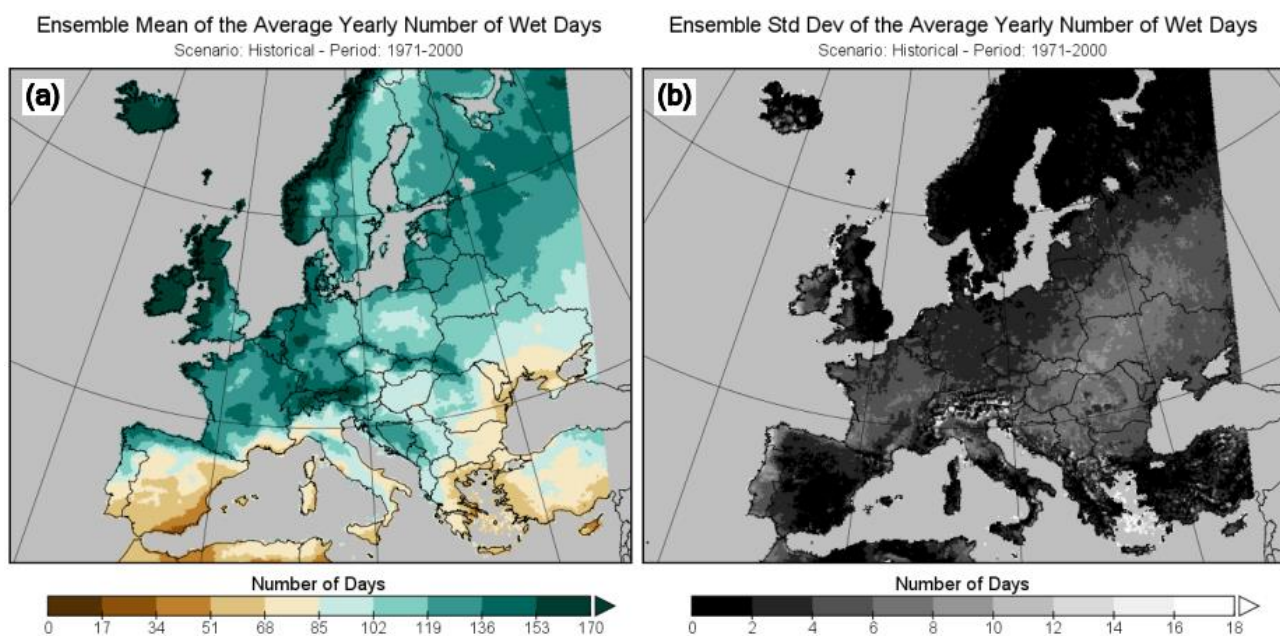


Figure 133: RR1mm for the baseline period 1971-2000. (a) Ensemble mean and (b) ensemble standard deviation.

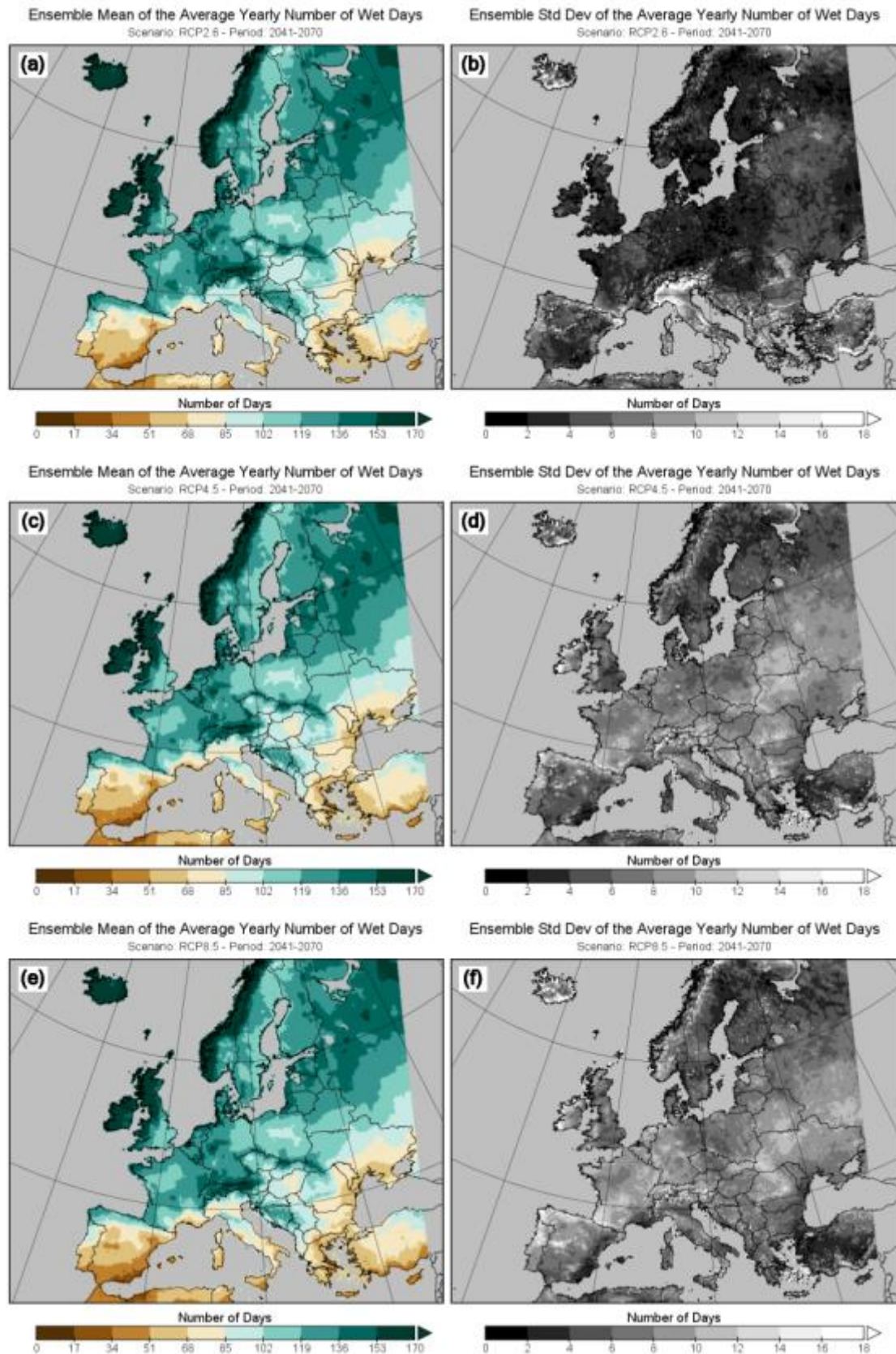


Figure 134: Wet days for the period 2041-2070. (left panels) Ensemble mean and (right panels) ensemble standard deviation. (a, b) RCP2.6, (c, d) RCP4.5, (e, f) RCP8.5.

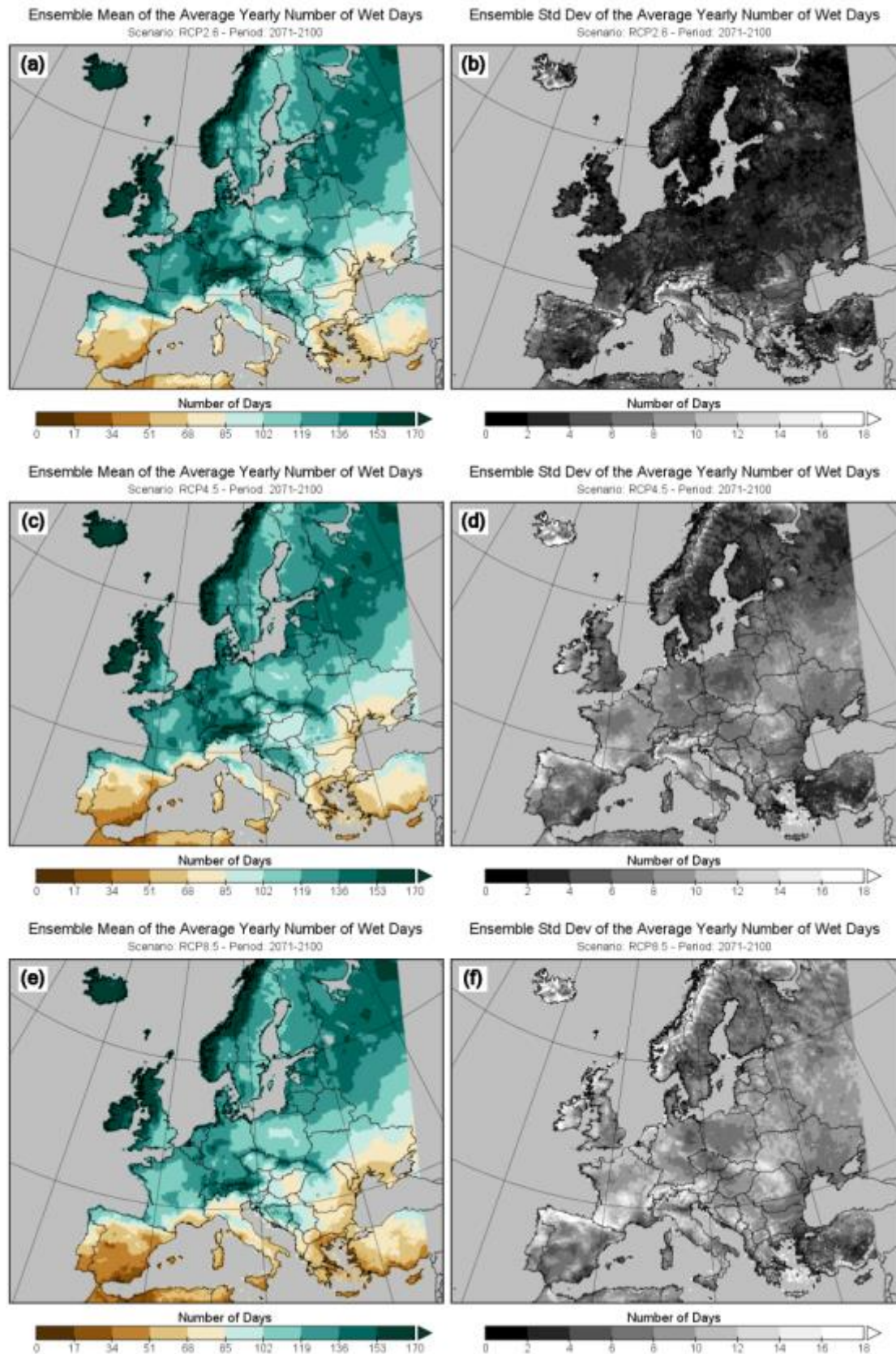


Figure 135: Wet days for the period 2071-2100. (left panels) Ensemble mean and (right panels) ensemble standard deviation. (a, b) RCP2.6, (c, d) RCP4.5, (e, f) RCP8.5.

7.18 Heavy precipitation days (RR20mm)

Definition: Number of days per year with a daily precipitation amount of at least 20 mm for each year, averaged over a 30-year period.

Units: Days

Background: This climate index is a measure of heavy precipitation, with high values corresponding to a high chance of flooding. An increase of this index with time means that the chance of flood conditions will increase.

Results: There is little change in the number of heavy precipitation days from the baseline period (1971-2000, **Figure 136**) to the 2041-2070 period (**Figure 137**) for all RCP scenarios. The trend from the 2041-2070 to 2071-2100 period (**Figure 138**) for RCP2.6 is not clear, while for RCP4.5 and RCP8.5 there is a general decrease across most of Europe, while the Alpine area, the northern half of Italy, and Northwestern Spain and Portugal exhibit an increase in the number of wet days.

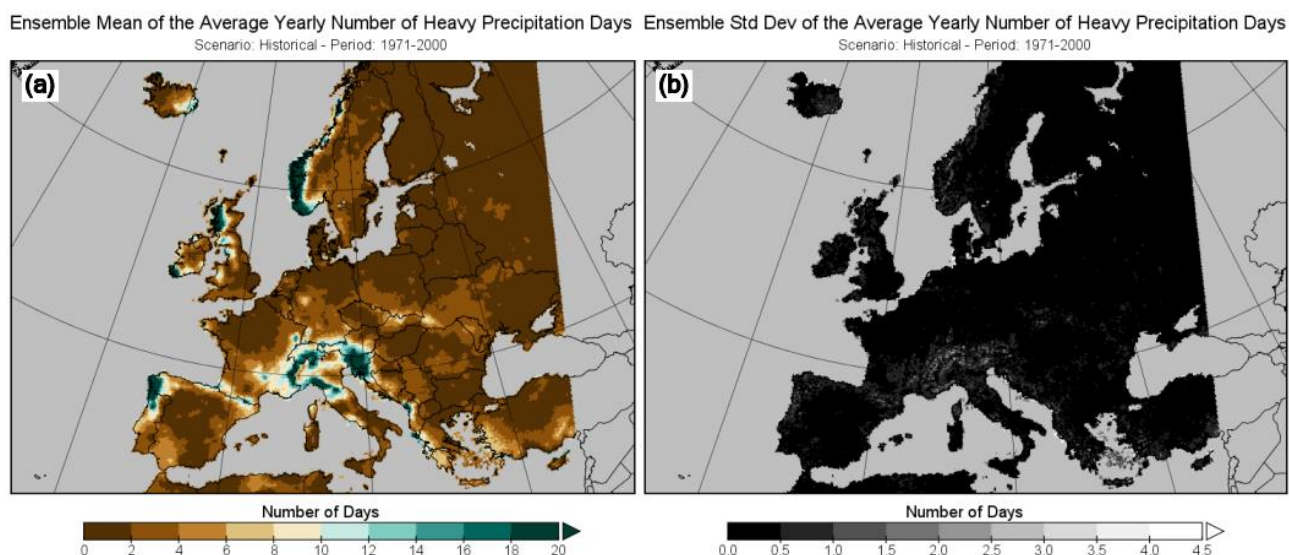
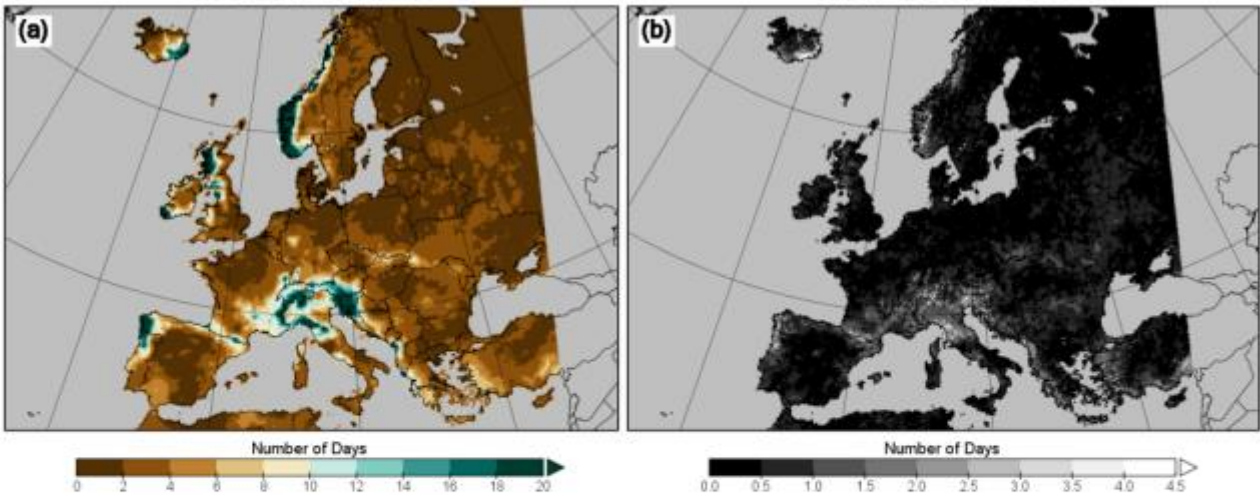
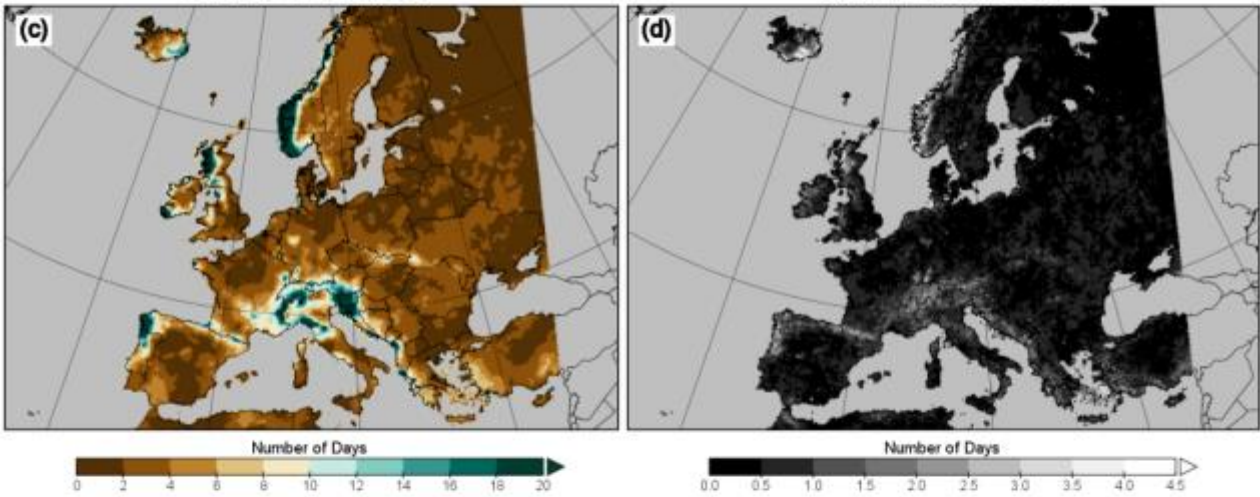


Figure 136: RR20mm for the baseline period 1971-2000. (a) Ensemble mean and (b) ensemble standard deviation.

Ensemble Mean of the Average Yearly Number of Heavy Precipitation Days Scenario: RCP2.6 - Period: 2041-2070
 Ensemble Std Dev of the Average Yearly Number of Heavy Precipitation Days Scenario: RCP2.6 - Period: 2041-2070



Ensemble Mean of the Average Yearly Number of Heavy Precipitation Days Scenario: RCP4.5 - Period: 2041-2070
 Ensemble Std Dev of the Average Yearly Number of Heavy Precipitation Days Scenario: RCP4.5 - Period: 2041-2070



Ensemble Mean of the Average Yearly Number of Heavy Precipitation Days Scenario: RCP8.5 - Period: 2041-2070
 Ensemble Std Dev of the Average Yearly Number of Heavy Precipitation Days Scenario: RCP8.5 - Period: 2041-2070

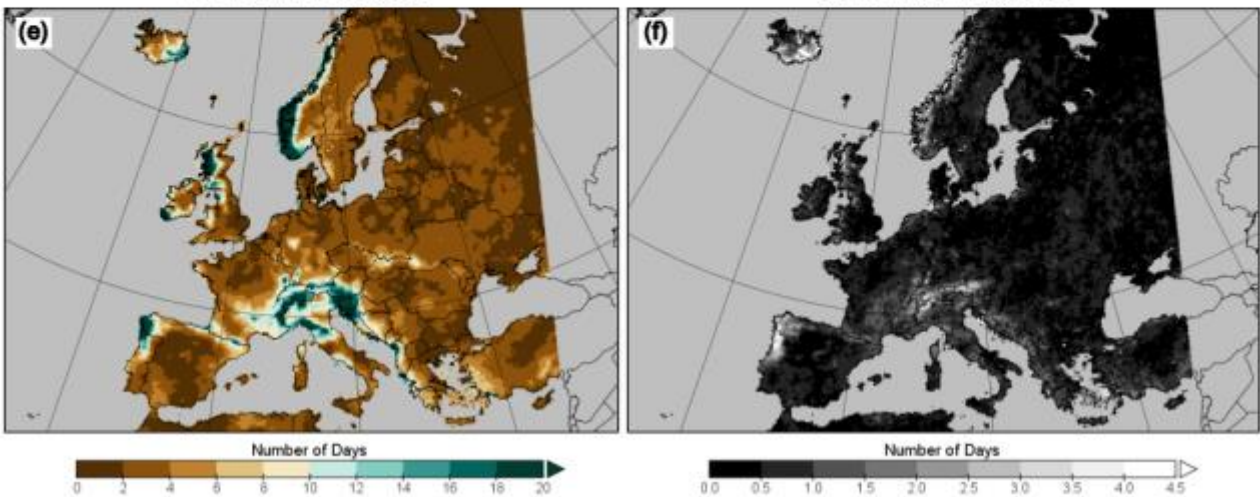
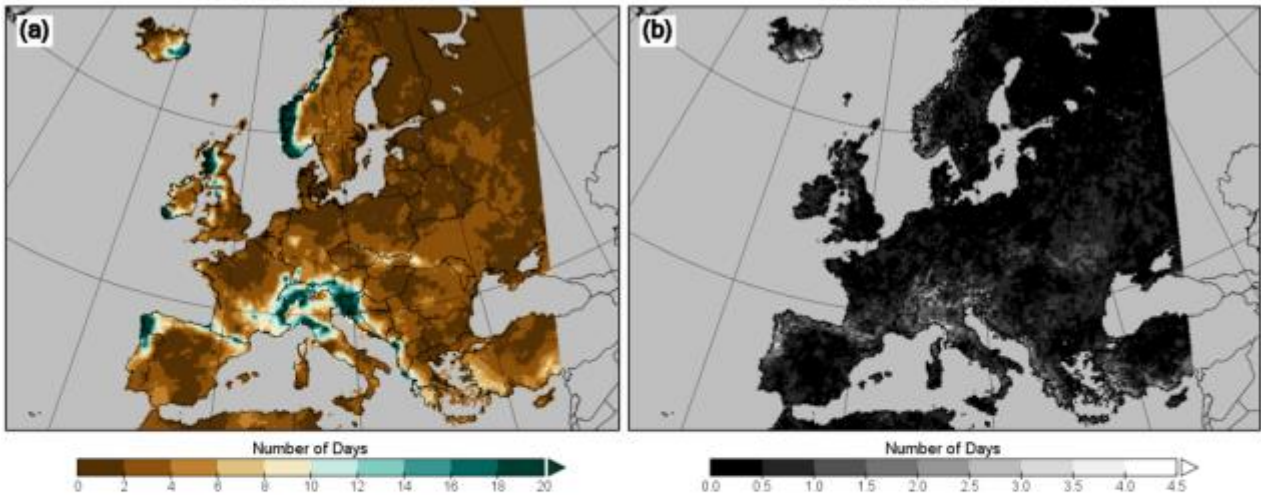
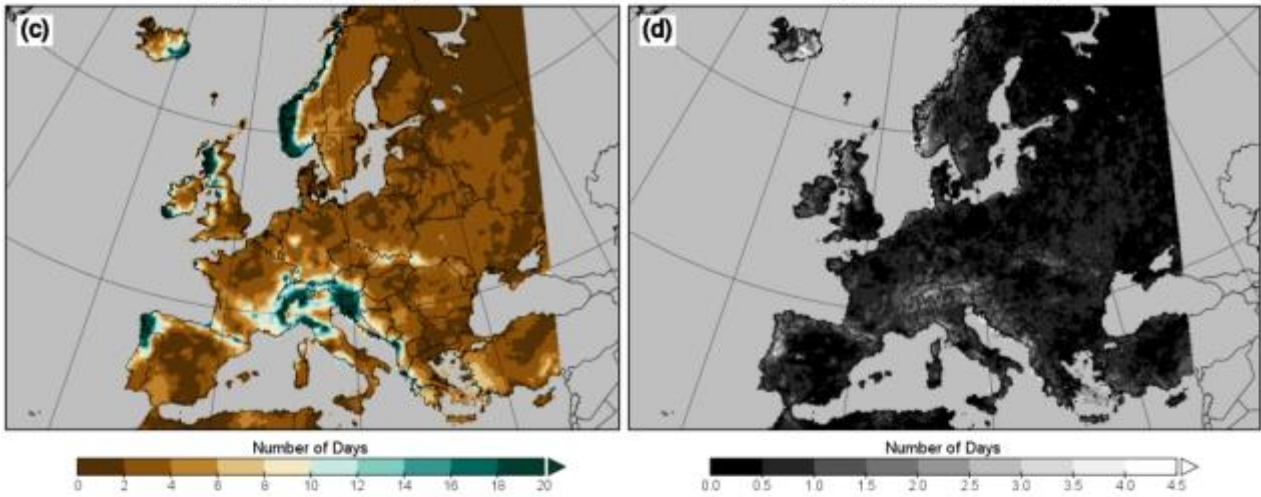


Figure 137: Very heavy precipitation days for the period 2041-2070. (left panels) Ensemble mean and (right panels) ensemble standard deviation. (a, b) RCP2.6, (c, d) RCP4.5, (e, f) RCP8.5.

Ensemble Mean of the Average Yearly Number of Heavy Precipitation Days Scenario: RCP2.6 - Period: 2071-2100 Ensemble Std Dev of the Average Yearly Number of Heavy Precipitation Days Scenario: RCP2.6 - Period: 2071-2100



Ensemble Mean of the Average Yearly Number of Heavy Precipitation Days Scenario: RCP4.5 - Period: 2071-2100 Ensemble Std Dev of the Average Yearly Number of Heavy Precipitation Days Scenario: RCP4.5 - Period: 2071-2100



Ensemble Mean of the Average Yearly Number of Heavy Precipitation Days Scenario: RCP8.5 - Period: 2071-2100 Ensemble Std Dev of the Average Yearly Number of Heavy Precipitation Days Scenario: RCP8.5 - Period: 2071-2100

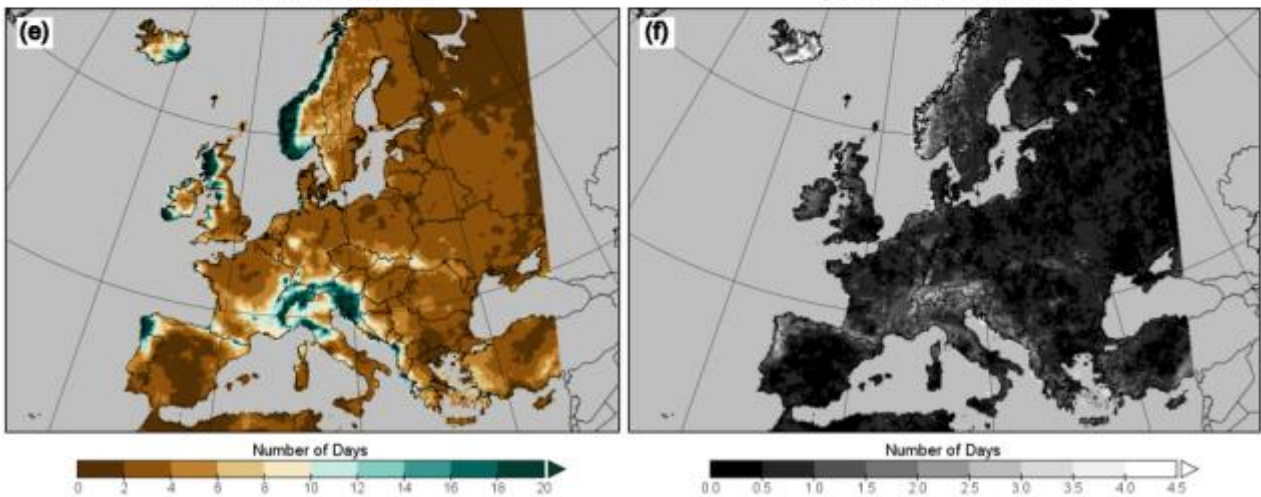


Figure 138: Very heavy precipitation days for the period 2071-2100. (left panels) Ensemble mean and (right panels) ensemble standard deviation. (a, b) RCP2.6, (c, d) RCP4.5, (e, f) RCP8.5.

7.19 Wet days with respect to the 90th percentile of daily precipitation (RR90p)

Definition: The number of days where the daily precipitation is higher than the calendar 90th percentile (centred on a 5-day window) of the baseline period 1971-2000. The values for each year are averaged over a 30-year period.

Units: Days

Background: This climate index is a measure of heavy precipitation, with high values corresponding to a high chance of flooding. An increase of this index with time means that the chance of flood conditions will increase.

Results: There is a general increase in RR90p from the baseline period (1971-2000, **Figure 139**) to the 2041-2070 period (**Figure 140**), each RCP over most of Europe, with the exception being nearly all southern, Mediterranean countries where a decrease occurs. The changes are progressively larger with increasing RCP scenario. The trend from the 2041-2070 to 2071-2100 period (**Figure 141**) differs according to the RCP, with RCP2.6 showing an increase to some degree Europe-wide, while RCP4.5 and RCP8.5 continue the trend from the earlier period, showing an increase over most of Europe and a decrease for southern, Mediterranean countries.

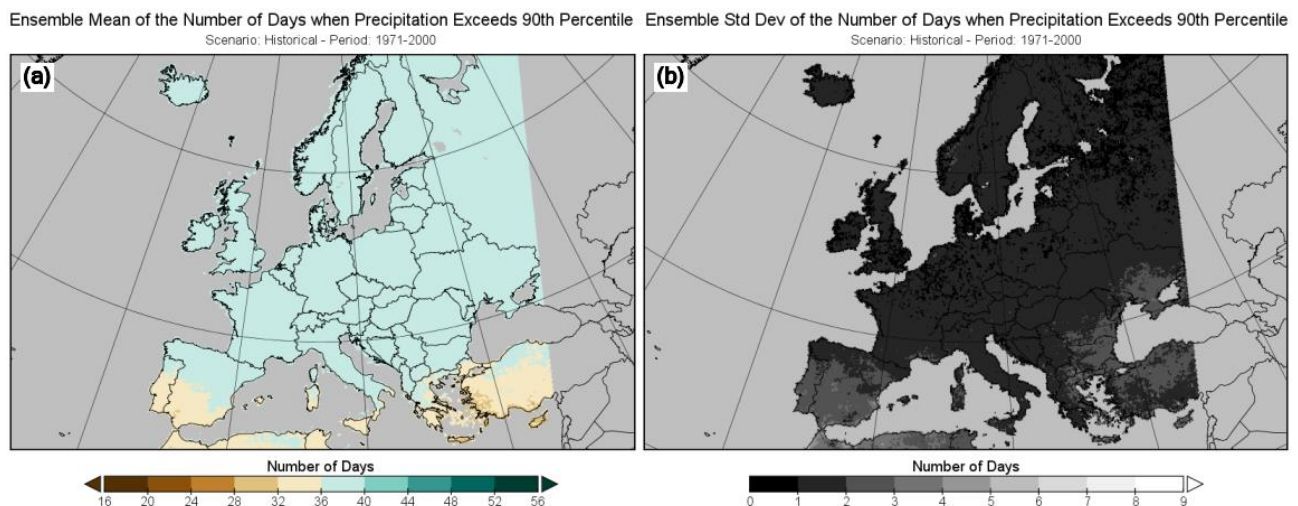


Figure 139: RR90p for the baseline period 1971-2000. (a) Ensemble mean and (b) ensemble standard deviation.

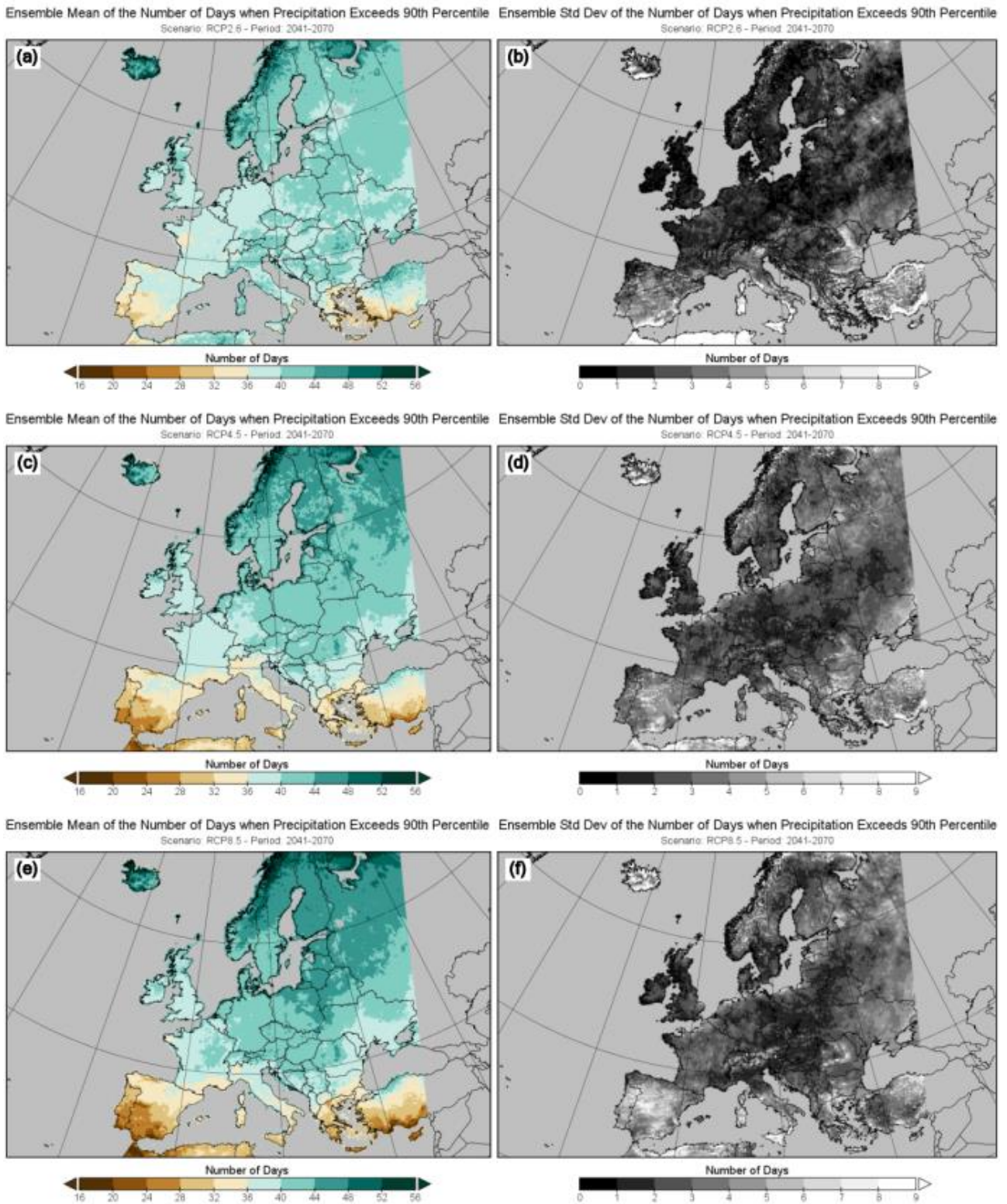


Figure 140: RR90p for the period 2041-2070. (left panels) Ensemble mean and (right panels) ensemble standard deviation. (a, b) RCP2.6, (c, d) RCP4.5, (e, f) RCP8.5.

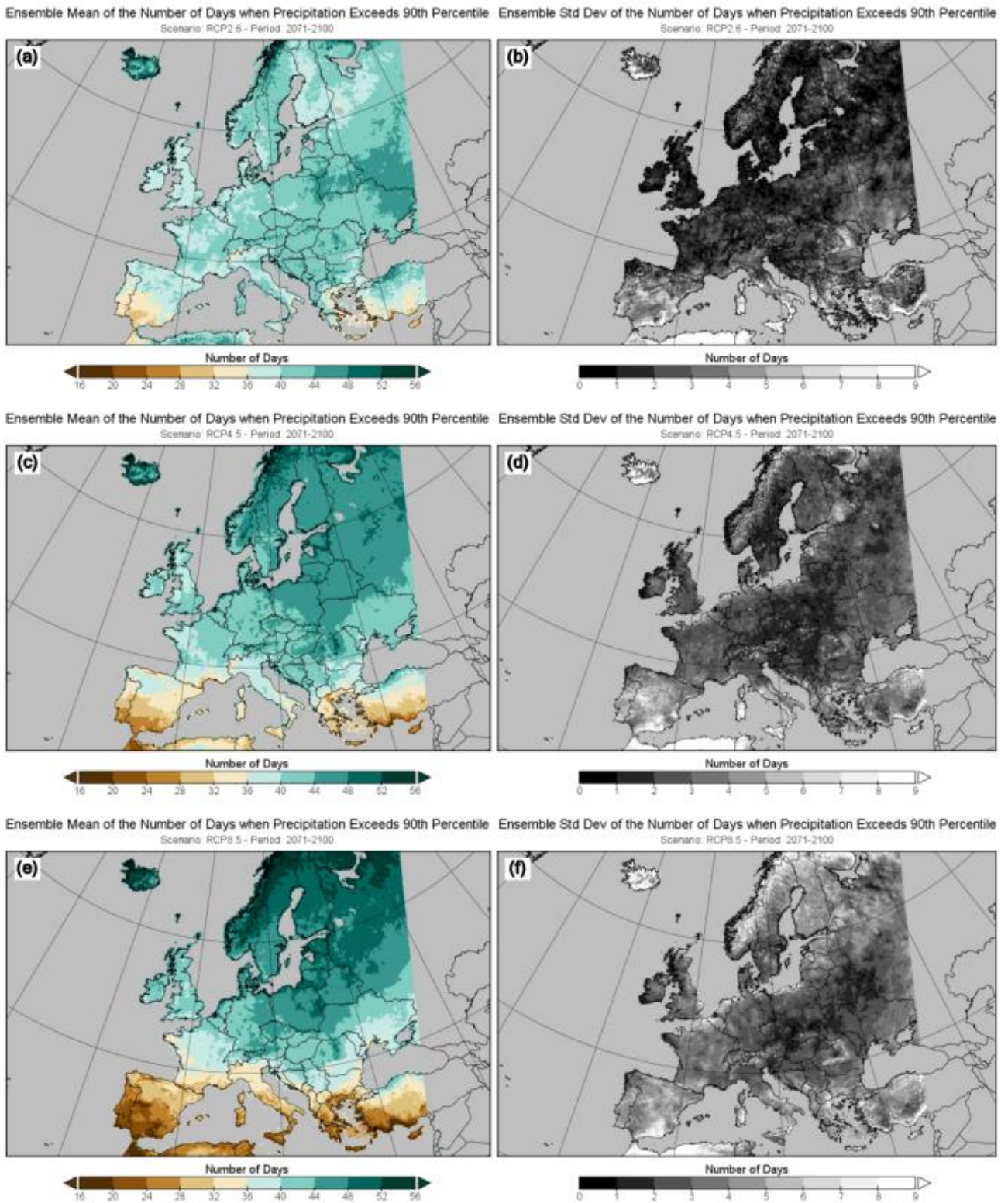


Figure 141: RR90p for the period 2071-2100. (left panels) Ensemble mean and (right panels) ensemble standard deviation. (a, b) RCP2.6, (c, d) RCP4.5, (e, f) RCP8.5.

7.20 Maximum wind speed

Definition: The annual maximum of daily maximum wind speed, averaged over a 30-year period.

Units: Metres per second (m/s)

Background: This climate index is a measure of wind, with high values corresponding to windy and potentially damaging conditions. An increase of this index with time means that the chance of windier conditions will increase.

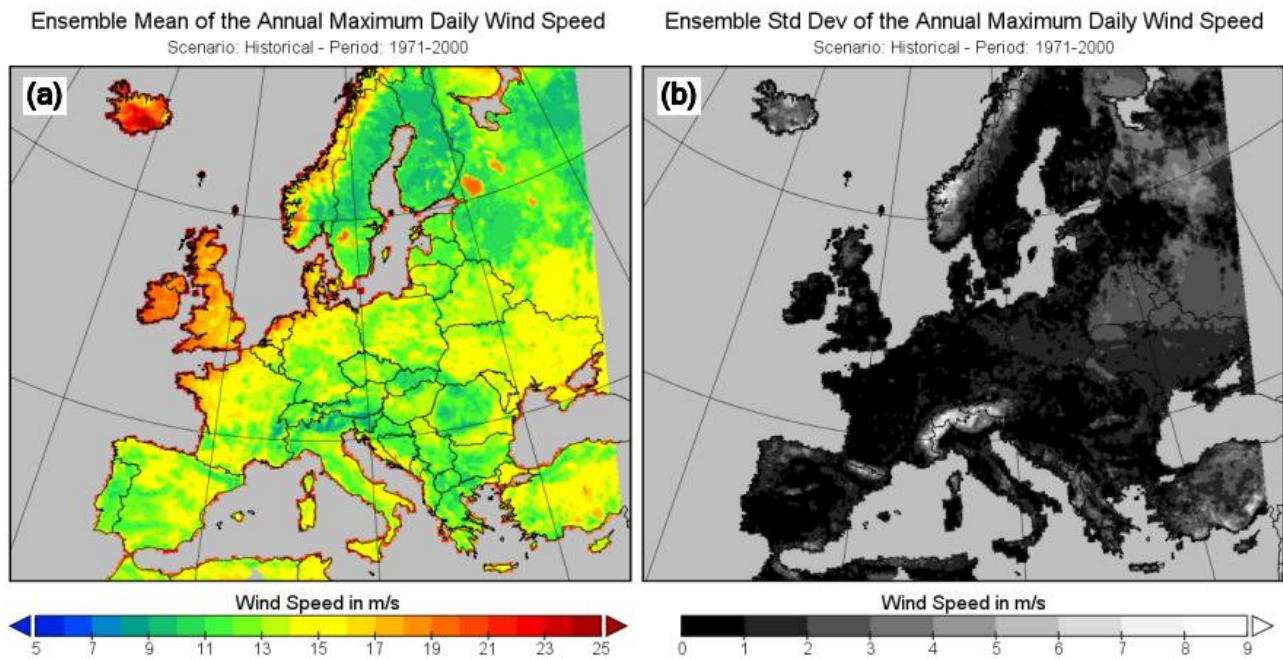


Figure 142: Maximum wind speed for the baseline period 1971-2000. (a) Ensemble mean and (b) ensemble standard deviation.

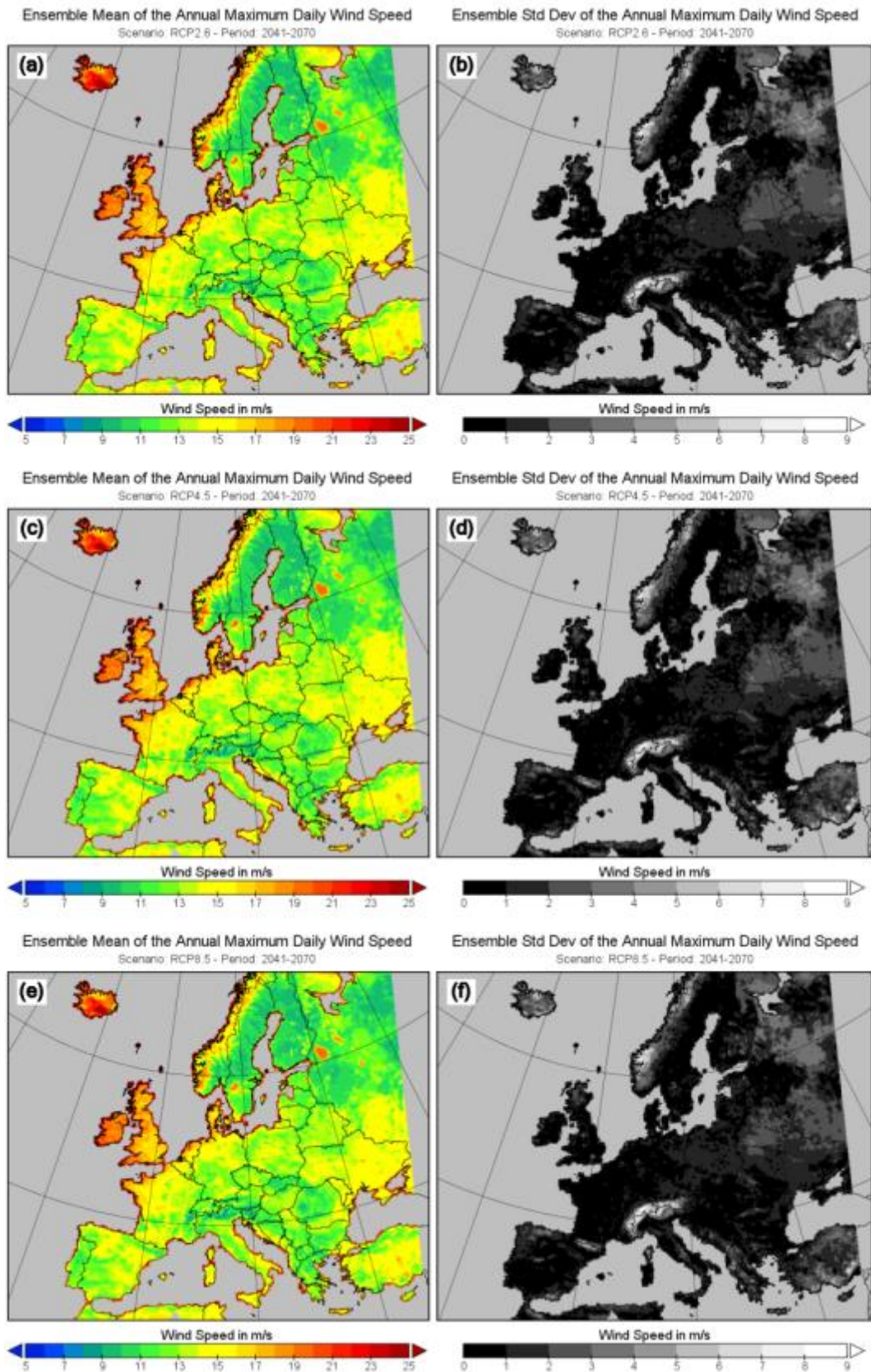


Figure 143: Maximum wind speed for the period 2041-2070. (left panels) Ensemble mean and (right panels) ensemble standard deviation. (a, b) RCP2.6, (c, d) RCP4.5, (e, f) RCP8.5.

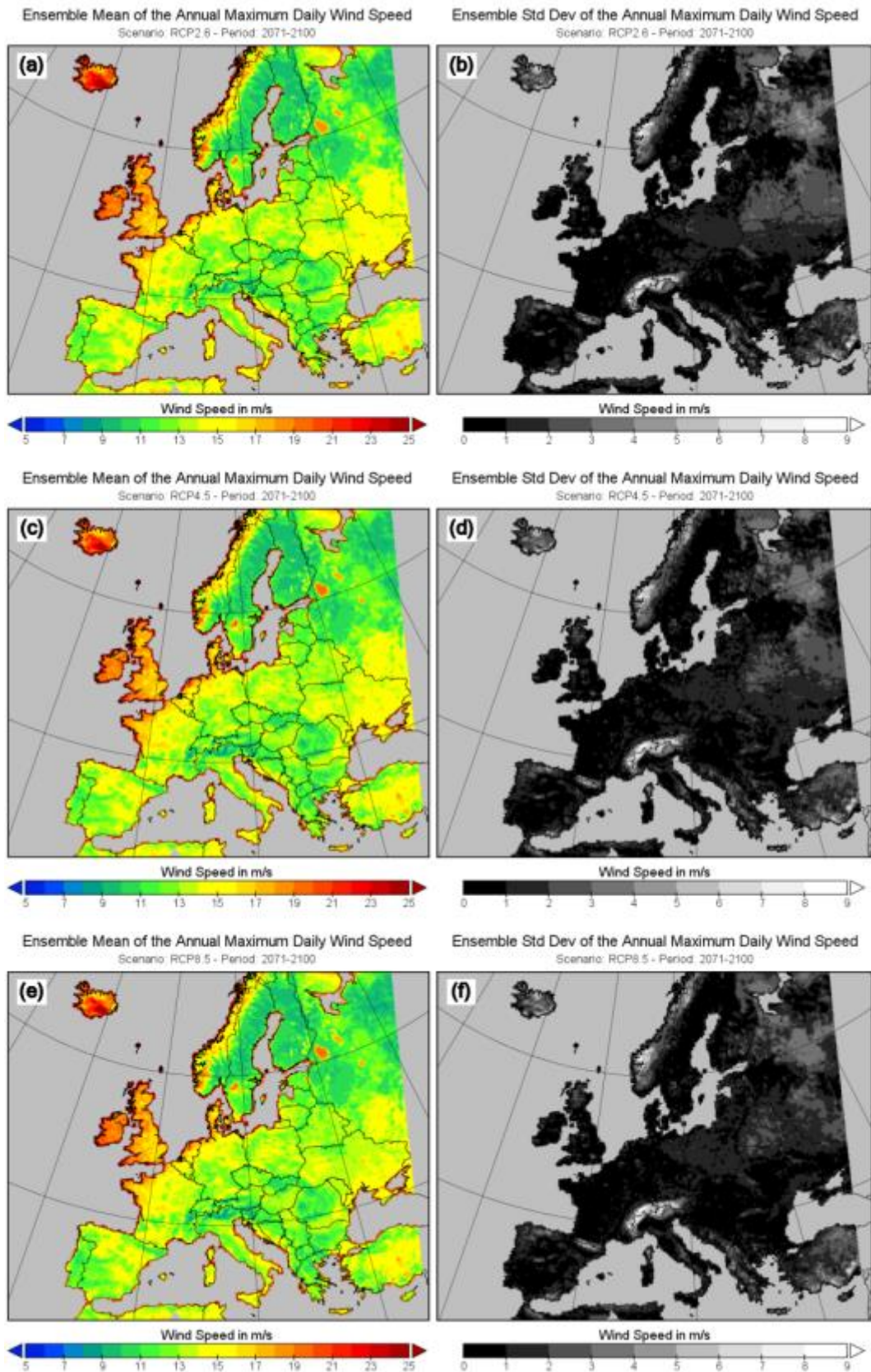


Figure 144: Maximum wind speed for the period 2071-2100. (left panels) Ensemble mean and (right panels) ensemble standard deviation. (a, b) RCP2.6, (c, d) RCP4.5, (e, f) RCP8.5.

7.21 Wind speed with respect to the 98th percentile of daily wind (Wind98p)

Definition: The 98th percentile of the daily maximum wind speed (calculated for each year, averaged over a 30- year period)

Units: Metres per second (m/s)

Background: This climate index is a measure of wind, with high values corresponding to windy and potentially damaging conditions. An increase of this index with time means that the chance of windier conditions will increase.

Results: This index has been used by [50] to estimate European winter storm losses. The most prominent features are the high wind speeds on the west-coasts of Norway, Great Britain, Iceland, Denmark Benelux and the northern parts of France and Germany. Highest variations in wind speed between models occur along the west coast of Norway as well as over the Alps and the Pyrenees. Changes in Wind98p for the different emissions scenarios are difficult to ascertain based on these plots alone. Climate signal maps indicate only slight changes of Wind98p over the continent when looking at the end of the century. While in large parts of Europe the different RCP scenarios predict contrasting changes, all RCP scenarios indicate a slight increase in Wind98p in the western part of the Balkan Peninsula and a reduction of Wind98p in Iceland, Denmark, along the west coast of Norway, east of Poland and north-east of Romania.

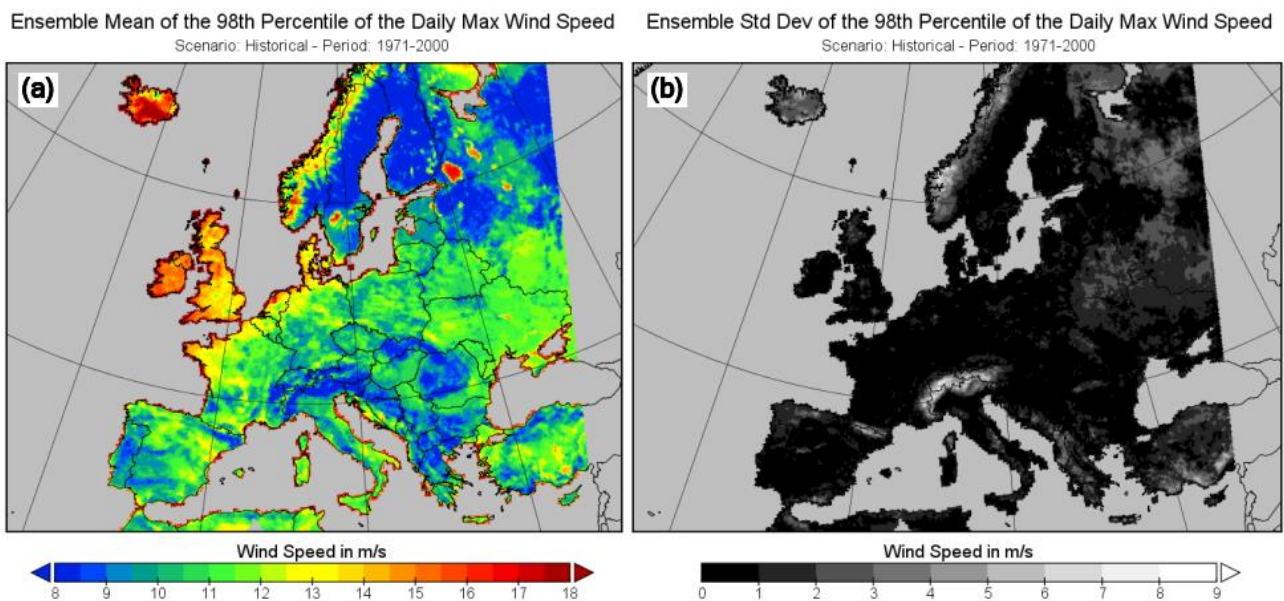


Figure 145: Wind98p for the baseline period 1971-2000. (a) Ensemble mean and (b) ensemble standard deviation.

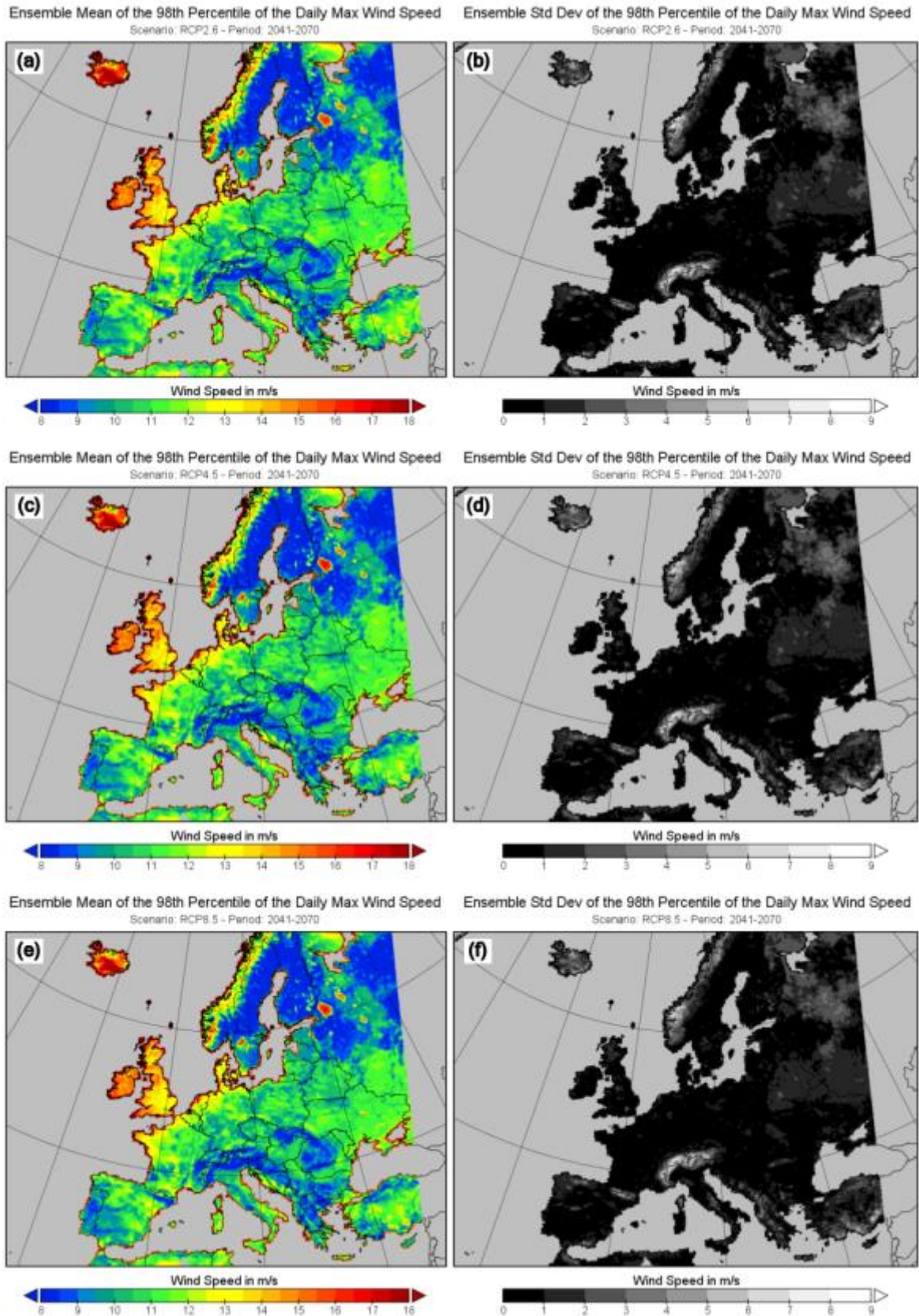


Figure 146: Wind98p for the period 2041-2070. (left panels) Ensemble mean and (right panels) ensemble standard deviation. (a, b) RCP2.6, (c, d) RCP4.5, (e, f) RCP8.5.

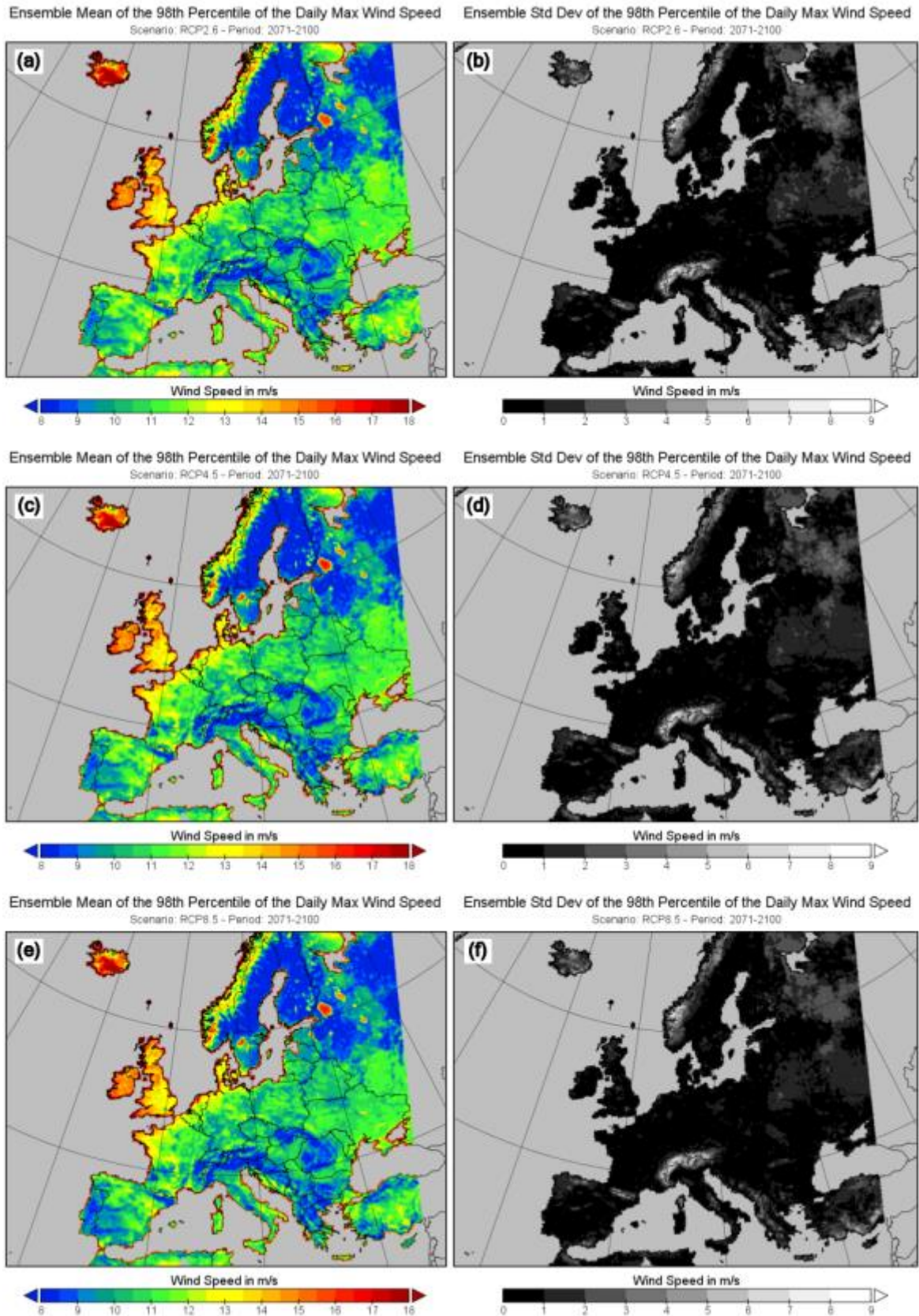


Figure 147: Wind98p for the period 2071-2100. (left panels) Ensemble mean and (right panels) ensemble standard deviation. (a, b) RCP2.6, (c, d) RCP4.5, (e, f) RCP8.5.

7.22 Torro17

Definition: Number of days per year with the daily maximum wind speed equal to or greater than 17 m/s, (average over 30 year period). Wind speeds at or above this value are classified as damaging winds according to the Torro wind damage scale²¹.

Units: Days

Background: This climate index is a measure of wind, with high values corresponding to windy and potentially damaging conditions. An increase of this index with time means that the chance of windier conditions will increase.

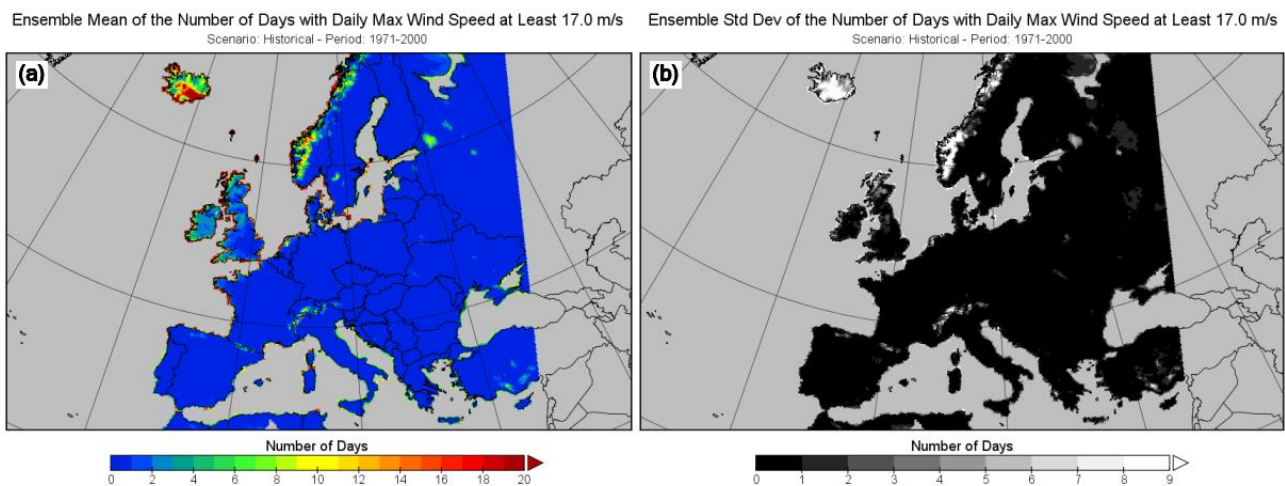
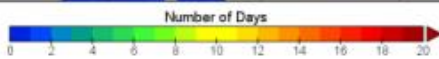


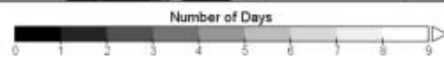
Figure 148: Torro17 for the baseline period 1971-2000. (a) Ensemble mean and (b) ensemble standard deviation.

21 <http://www.torro.org.uk/tscale.php>

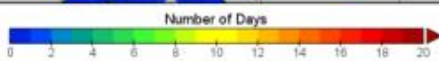
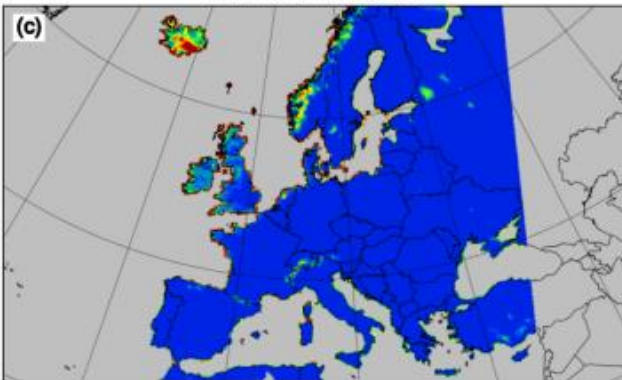
Ensemble Mean of the Number of Days with Daily Max Wind Speed at Least 17.0 m/s
Scenario: RCP2.6 - Period: 2041-2070



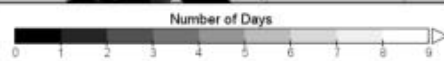
Ensemble Std Dev of the Number of Days with Daily Max Wind Speed at Least 17.0 m/s
Scenario: RCP2.6 - Period: 2041-2070



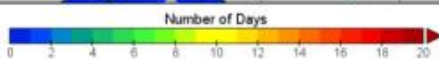
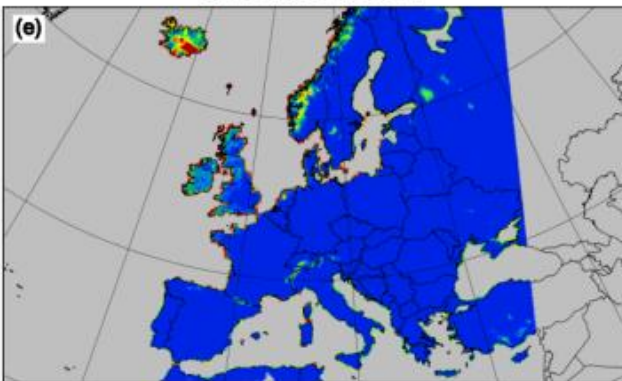
Ensemble Mean of the Number of Days with Daily Max Wind Speed at Least 17.0 m/s
Scenario: RCP4.5 - Period: 2041-2070



Ensemble Std Dev of the Number of Days with Daily Max Wind Speed at Least 17.0 m/s
Scenario: RCP4.5 - Period: 2041-2070



Ensemble Mean of the Number of Days with Daily Max Wind Speed at Least 17.0 m/s
Scenario: RCP8.5 - Period: 2041-2070



Ensemble Std Dev of the Number of Days with Daily Max Wind Speed at Least 17.0 m/s
Scenario: RCP8.5 - Period: 2041-2070

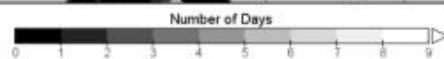
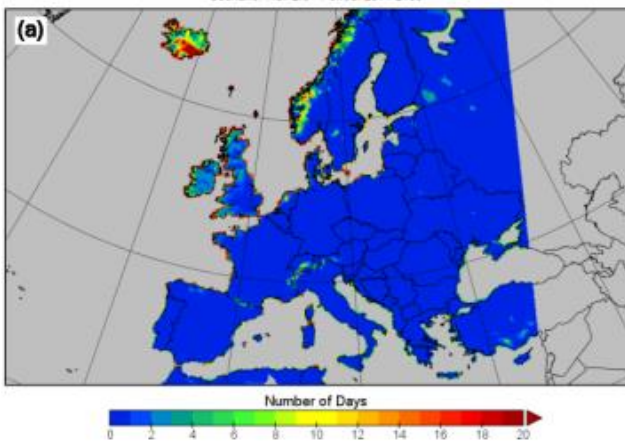
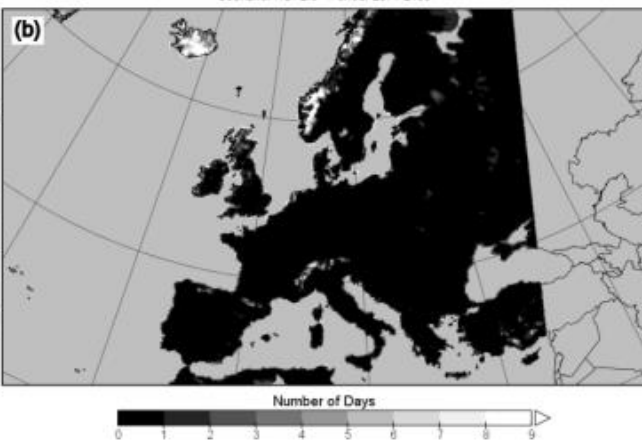


Figure 149: Torro17 for the period 2041-2070. (left panels) Ensemble mean and (right panels) ensemble standard deviation. (a, b) RCP2.6, (c, d) RCP4.5, (e, f) RCP8.5.

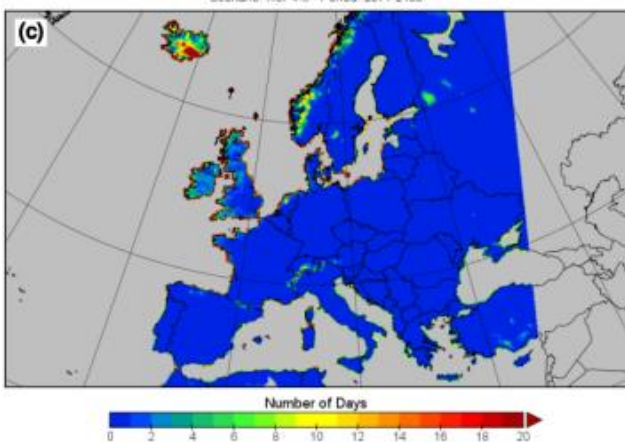
Ensemble Mean of the Number of Days with Daily Max Wind Speed at Least 17.0 m/s
Scenario: RCP2.6 - Period: 2071-2100



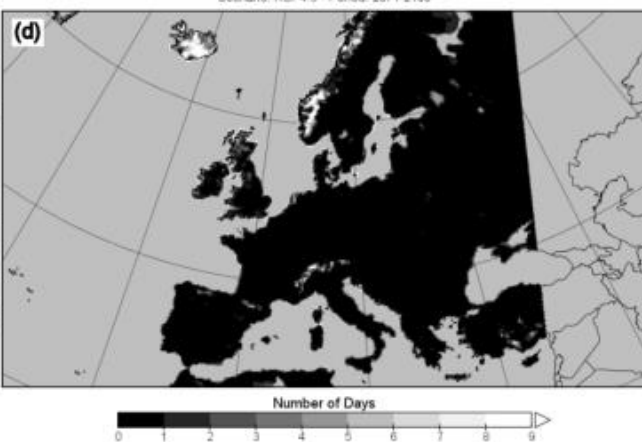
Ensemble Std Dev of the Number of Days with Daily Max Wind Speed at Least 17.0 m/s
Scenario: RCP2.6 - Period: 2071-2100



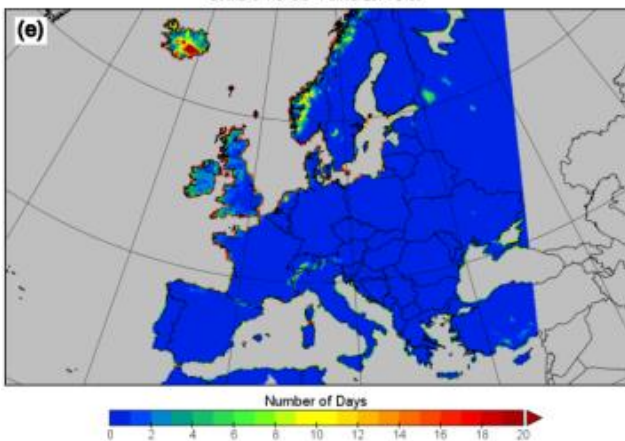
Ensemble Mean of the Number of Days with Daily Max Wind Speed at Least 17.0 m/s
Scenario: RCP4.5 - Period: 2071-2100



Ensemble Std Dev of the Number of Days with Daily Max Wind Speed at Least 17.0 m/s
Scenario: RCP4.5 - Period: 2071-2100



Ensemble Mean of the Number of Days with Daily Max Wind Speed at Least 17.0 m/s
Scenario: RCP8.5 - Period: 2071-2100



Ensemble Std Dev of the Number of Days with Daily Max Wind Speed at Least 17.0 m/s
Scenario: RCP8.5 - Period: 2071-2100

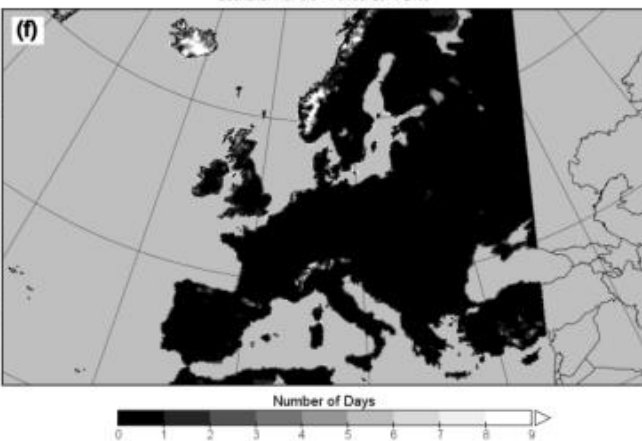


Figure 150: Torro17 for the period 2071-2100. (left panels) Ensemble mean and (right panels) ensemble standard deviation. (a, b) RCP2.6, (c, d) RCP4.5, (e, f) RCP8.5.

7.23 Consecutive dry days (CDD)

Definition: Maximum number of consecutive dry days per year for each year, averaged over a 30-year period. A dry day is a day with the daily precipitation amount less than 1 mm.

Units: Days

Background: This climate index is a measure of low precipitation, with high values corresponding to long periods of low precipitation and potentially drought-favouring conditions. An increase of this index with time means that the chance of drought conditions will increase.

Results: There is a general decrease in consecutive dry days from the baseline period (1971-2000, **Figure 151**) to the 2041-2070 (**Figure 152**) for all RCP scenarios with the change more apparent with increase RCP scenario. (e.g.. France). The trend to the 2071-2100 period (**Figure 153**) shows a decrease for RCP2.6 over much of Europe. The trend for RCP4.5 shows also a reduction over much of Europe (e.g. Eastern Europe), while for RCP8.5, the trend in Southern Europe is an increase with a decrease in Northern Europe.

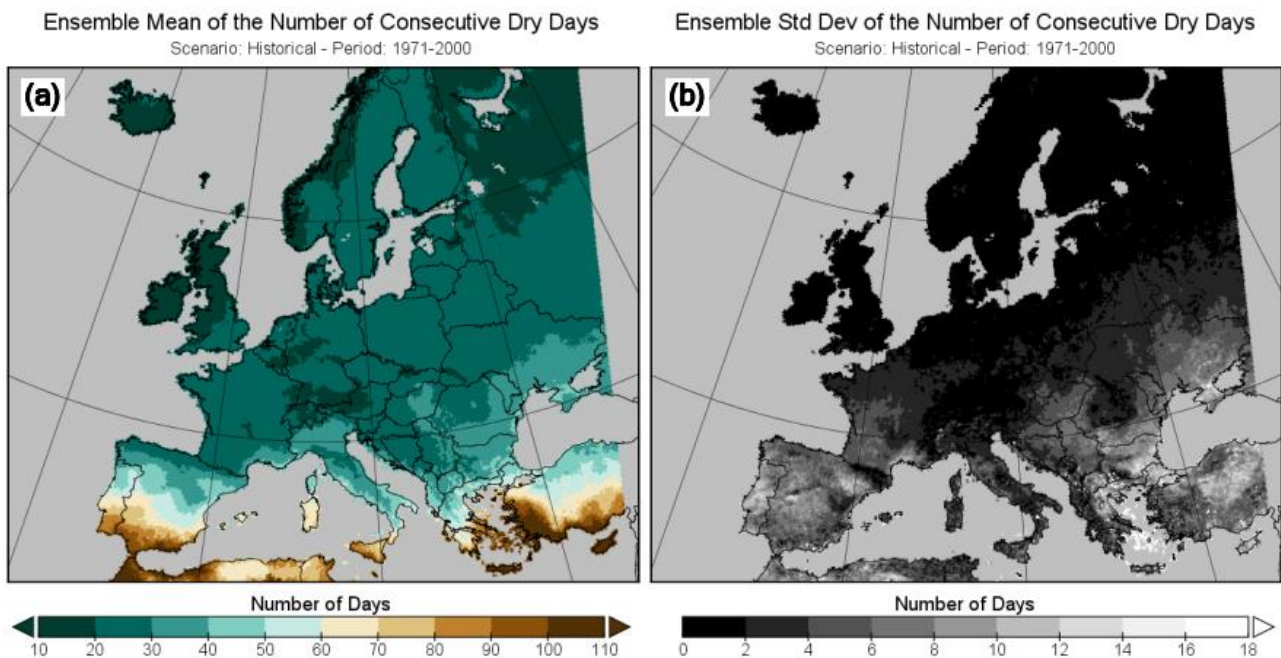


Figure 151: Consecutive dry days for the baseline period 1971-2000. (a) Ensemble mean and (b) ensemble standard deviation.

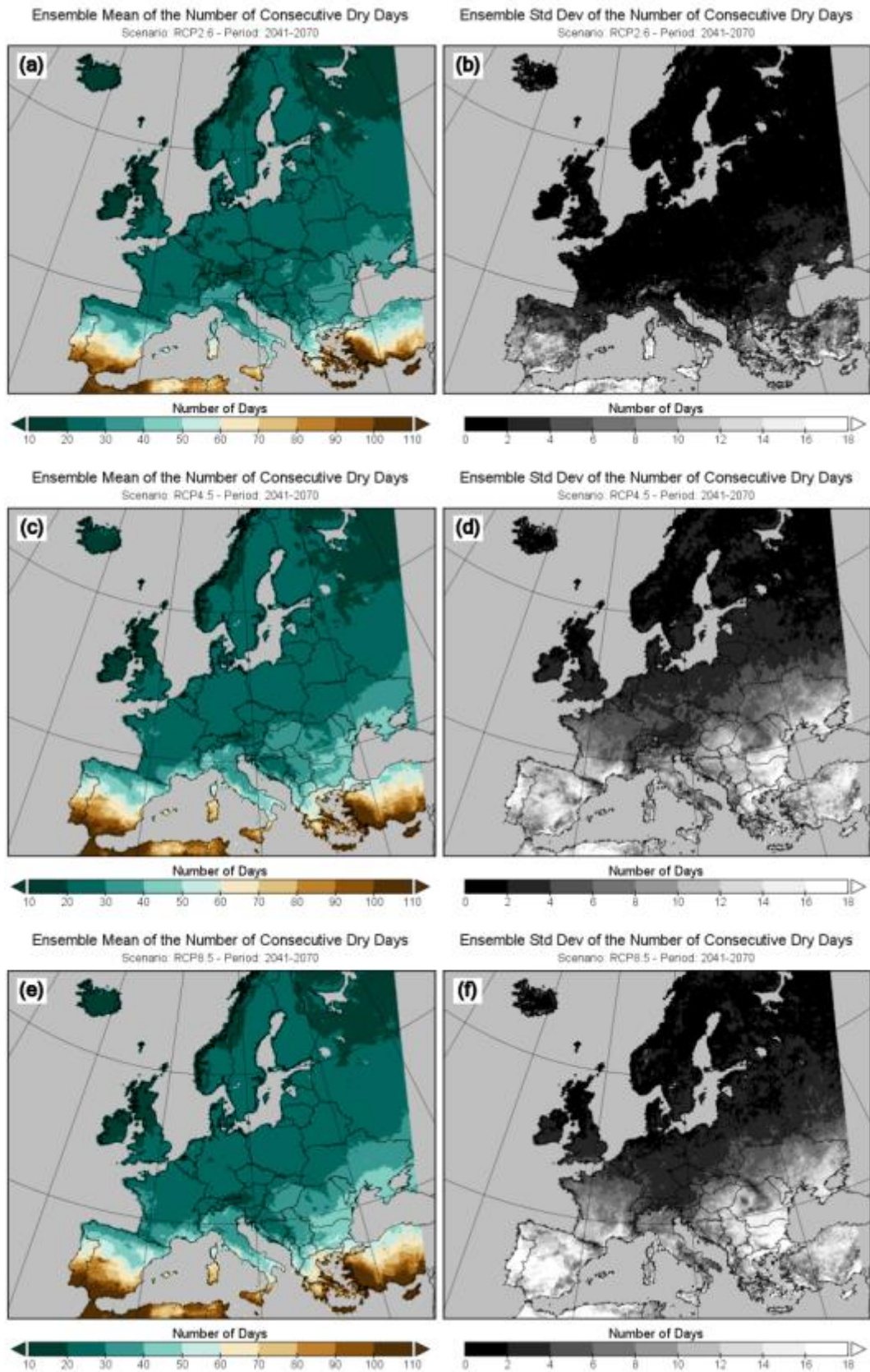


Figure 152: Consecutive dry days for the period 2041-2070. (left panels) Ensemble mean and (right panels) ensemble standard deviation. (a, b) RCP2.6, (c, d) RCP4.5, (e, f) RCP8.5.

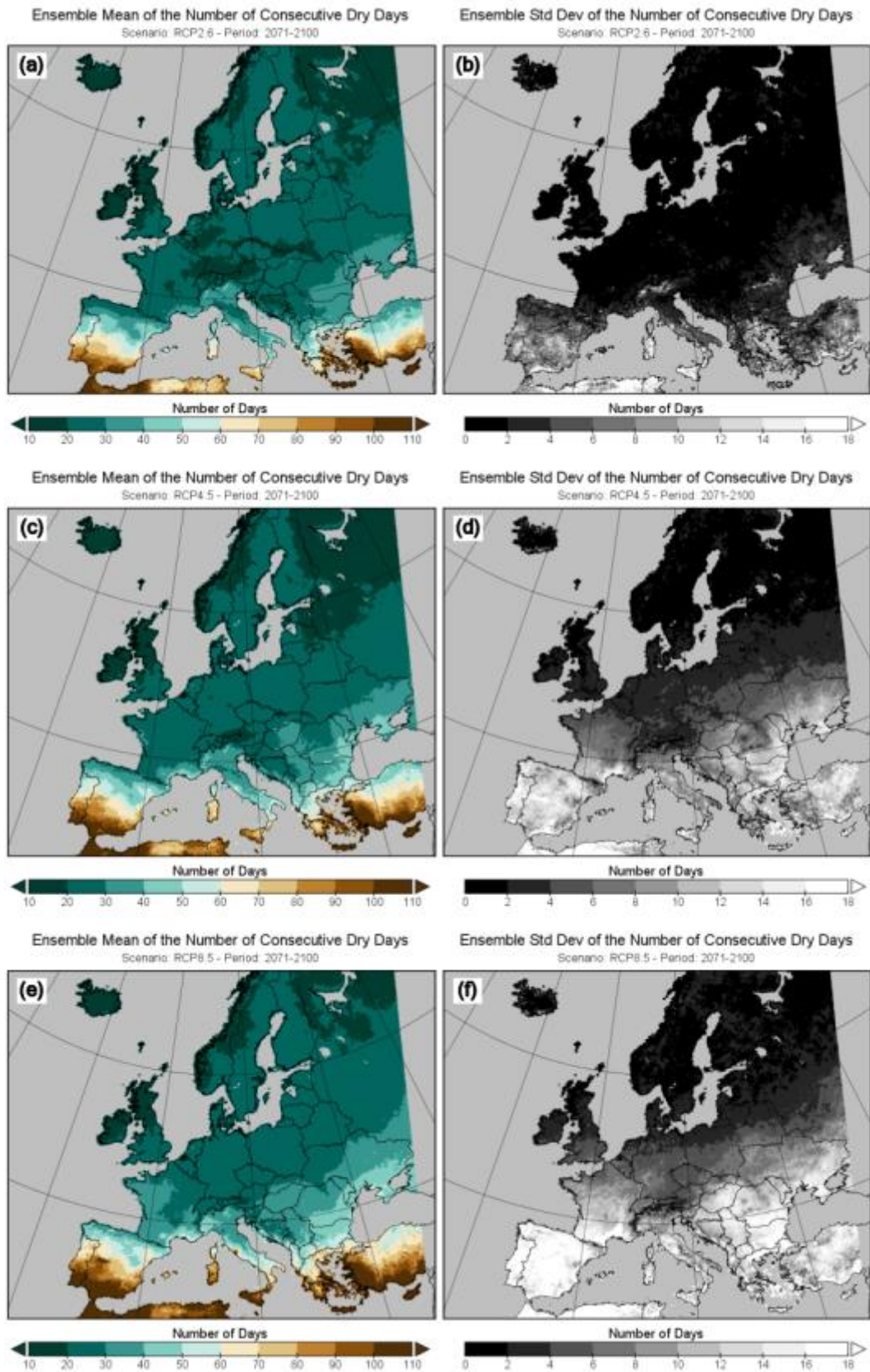


Figure 153: Consecutive dry days for the period 2071-2100. (left panels) Ensemble mean and (right panels) ensemble standard deviation. (a, b) RCP2.6, (c, d) RCP4.5, (e, f) RCP8.5.

7.24 River flooding

River flooding is described using daily river flows corresponding to different return periods. The river flows are estimated through simulation by employing hydrological models. Three different models of varying spatial resolution are used to enable ensemble simulation of river flows: VIC, Lisflood, and E-HYPE. The first two are grid based models with resolutions of 0.5 degree and 5 km, respectively. The third one is a sub-catchment based model with an average catchment size of 215 km². River discharge values are provided on a common 0.5 degree grid, which is the native grid of VIC. Lisflood and E-HYPE results are up-scaled to this resolution. Daily precipitation and temperature from the climate models shown in **Table 56** are used to force the hydrological models. The return period values are calculated using a Gumbel distribution fitted to the simulated yearly maximum daily river flows for each of the 30-year periods. Return periods of 2, 5, 10, 50, and 100 years are considered. The analysis is performed within the EU FP7 project IMPACT2C (grant agreement 282746) and more information on the analysis can be found at: http://impact2c.hzg.de/imperia/md/content/csc/projekte/impact2c_d5.1_fin.pdf.

Table 56: EURO-CORDEX climate model configurations used for climate impact analysis of river flooding.

Institute	Driving GCM	RCM	RCP2.6	RCP4.5	RCP8.5
IPSL-INERIS	IPSL-IPSL-CM5A-MR	WRF331F	no	yes	no
KNMI	ICHEC-EC-EARTH	RACMO22E	yes	yes	yes
MPI-CSC	MPI-M-MPI-ESM-LR	REMO2009	yes	yes	yes
SMHI	ICHEC-EC-EARTH	RCA4	yes	yes	yes
	MOHC-HadGEM2-ES	RCA4	yes	yes	yes

Figure 154 shows the projected ensemble mean changes in the 10-years river flow over the three future time periods in relation to the reference period. The ensemble consists of all combinations of hydrological models and climate models used for the analysis under all three RCPs. The projections show a coherent spatial pattern of changes in the extreme river flow. Extreme flows are projected to decrease in the northern and eastern parts of Europe and increase in the central, western, and Southern Europe, as well as southern parts of Scandinavia for the all three time horizons.

In addition, the full period mean of river flow and of water runoff (surface and subsurface runoff) is available from SWICCA (<http://swicca.eu/>) and might be integrated into the CLARITY Climate Services Information System (CSIS) as well.

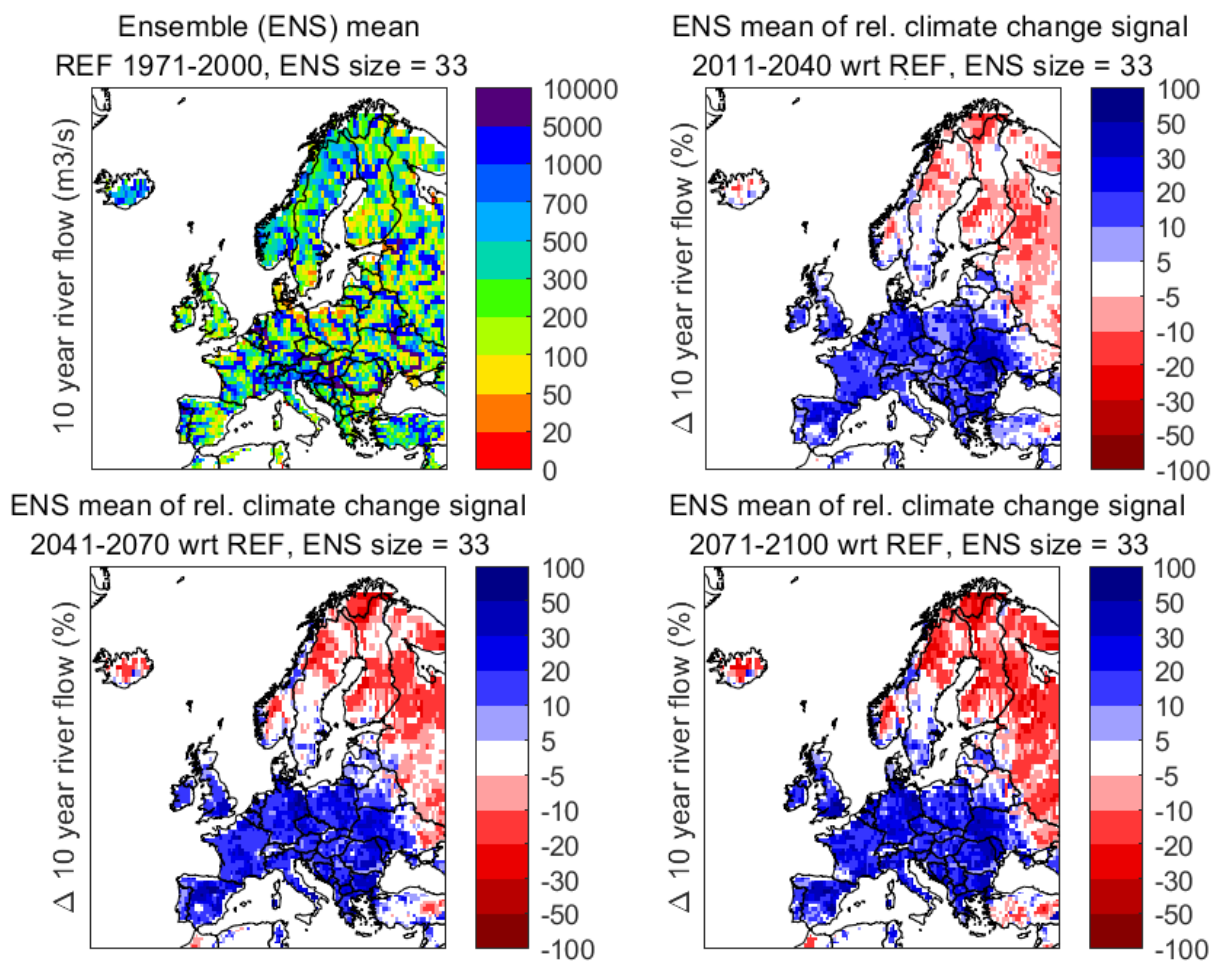


Figure 154: Projected changes in the 10-year river flow relative to the reference period for three future time periods across Europe.

7.25 Forest fires

Forest fires are represented by the index FWI. The six components of the FWI (see) System for the effects of meteorological conditions and fuel moisture on fire behaviour [51] have been computed:

- 1) Fine Fuel Moisture Code (FFMC) – temperature, relative humidity, wind and rain.
- 2) Duff Moisture Code (DMC) – temperature, relative humidity and rain.
- 3) Drought Code (DC) – temperature and rain.
- 4) Initial Spread Index (ISI) – FFMC and wind
- 5) Buildup Index (BUI) – DMC and DC
- 6) Fire Weather Index (FWI) – ISI and BUI

The first three components are numeric ratings of the average moisture content of the 1) litter and other fine fuels, 2) loosely compacted organic layers of moderate depth, and 3) deep, compact organic layers. High values indicate dry fuels. Only the DC is capable of carrying over fall moisture conditions into the spring.

The last three components represent, 4) the rate of fire spread, 5) the fuel available for combustion, and 6) the frontal fire intensity. The values of these components rise as the fire danger increases.

The Daily Severity Rating (DSR) and its time-averaged value, the Seasonal Severity Rating (SSR), are extensions of the FWI System. The DSR is a transformation of the daily FWI value, calculated as follows:

$$DSR = 0.0272 (FWI)^{1.77}$$

The DSR can be accumulated over time as the cumulative DSR, or it may be averaged over time as the SSR:

$$SSR = \sum_{i=1}^n \frac{DSR_i}{n}$$

where n is the total number of days, and DSR_i is the DSR value for day i.

For this study, fire weather severity was evaluated by comparing the projected monthly SSR over the 21st century against the hindcast SSR obtained with the corresponding model historical run. Currently, there is an ongoing process to calculate FWI due to some issues with the data available at EURO-CORDEX. The climatic data needed for these indices' calculation are temperature, relative humidity, and wind at noon. Additionally, daily accumulated precipitation will also be needed. Not all the models listed before were used for the calculations due to the fact that the relative humidity and wind were only available for the models shown in **Table 57**.

Table 57: EURO-CORDEX climate model configurations considered in the calculation of the FWI.

Institute	Driving GCM	RCM	RCP2.6	RCP4.5	RCP8.5
KNMI	ICHEC-EC-EARTH	RACMO22E	no	yes	Yes
	MOHC-HadGEM2-ES	RACMO22E	no	yes	yes
SMHI	CNRM-CERFACS-CNRM-CM5	RCA4	no	yes	yes
	IPSL-IPSL-CM5A-MR	RCA4	no	yes	yes
	MPI-M-MPI-ESM-LR	RCA4	no	yes	yes
	MOHC-HadGEM2-ES	RCA4	no	yes	yes

A detailed analysis of the data showed that relative humidity offered by EURO-CORDEX is a mean relative humidity instead of instant relative humidity at noon. This led to the decision of discarding these indices in favour of new ones determined using ESM outputs, even if their spatial resolution is coarse. The models used along with the workflow for the calculation are shown in the **Figure 155**.

The resulting indices are expected to be available by the end of March 2020. Once this process is completed, statistics will be obtained for the following:

- 90th percentile of the FWI for periods of 20 years centred on the years of the different RCPs for each season,
- 90th percentile of the seasonal SSR for periods of 20 years centred on the years of the different RCPs.

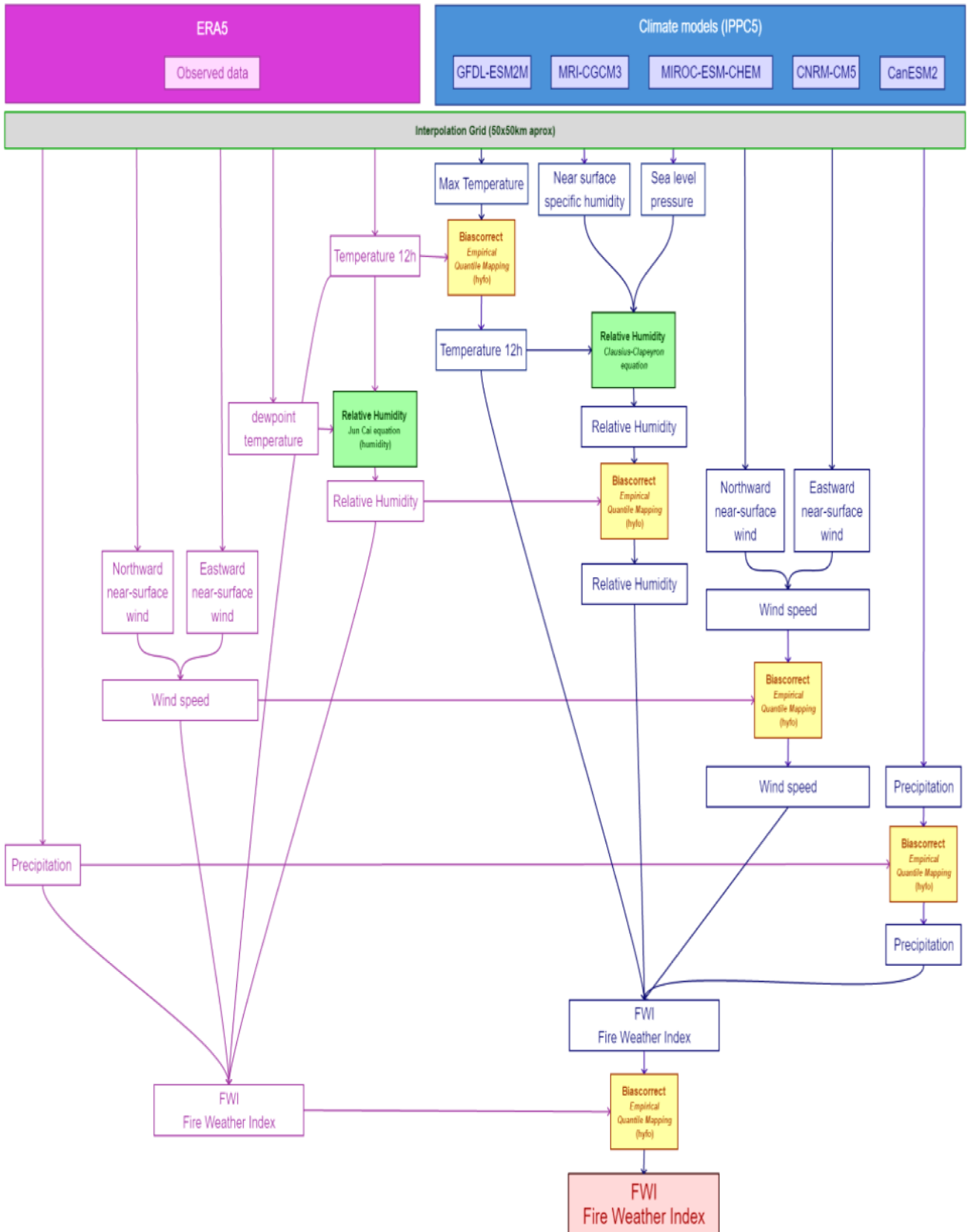


Figure 155: Models and workflow used for FWI calculations.

7.26 Landslides

Landslides are represented by the Landslide Susceptibility index. This data has been downloaded from the European Soil Data Center (ESDAC²²). This data accounts for actual landslide susceptibility but does not contain information about future trends.

In order to estimate the impact of climate change on this hazard, it is necessary to combine the exposure obtained from the aforementioned map with indicators of possible triggering effects such as maximum rainfall intensities in 1 or 5 days, already obtained as indexes associated with floods.

There are no further calculations planned due to the complexity of determining the way in which precipitation can affect the stability of the slopes depending on the existing types of soil.

7.27 Hazard scale maps


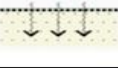
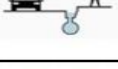



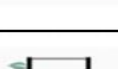









An idea at the beginning of the project was to represent each hazard in terms of a hazard scale in order to classify the magnitude of the hazard for the time period in question. A basic three level hazard scale (1=low, 2=medium, 3=high) was chosen. The hazard scale for the baseline period (1971-2000) is defined by grouping the values of a particular climate index *over space* into three terciles with the lower (upper) tercile corresponding to a low (high) hazard level. The hazard scale for the three future periods is similarly defined *over space*, but instead of using the absolute values of the climate index, the difference from the baseline period is used. That is, for the future periods, the hazard level refers to the *change* in the index between the baseline and future scenario. This definition of hazard level is similar to that used in the BRIGAD project (BRIGAD D5.1 TIF; quintiles are used instead of the terciles here). Section 2.1 of Deliverable 3.2 shows an example of this hazard scale map.





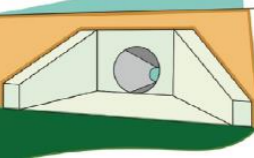




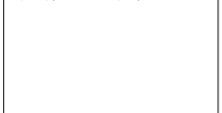
Alternative definitions for the hazard scale were examined. For example, for the future scenarios, the hazard scale was defined in terms of the amount of change from the baseline climate. For example one could define the tercile levels for the low, medium, and high hazard levels in terms of relative changes (50% and 100% increase, respectively) or absolute changes (increases of 20 and 40 days, respectively). One disadvantage of this method is that these thresholds are dependent on the climate index being considered and need to be carefully chosen to yield meaningful²³ results each time. For this reason, defining the hazard level in terms of spatial terciles presented first will be preferred here.

22 <https://esdac.jrc.ec.europa>

23 Meaningful, in this case, means maps which are not everywhere classified as being of low or high hazard level for all time periods.

8 Annex II: Adaptation options

ADAPTATION	TOWARDS WHICH HAZARD	VARIATION ON HAZARD'S LOCAL EFFECT	VARIATION ON VULNERABILITY OF ELEMENTS AT RISK	COST		CO-BENEFITS	Albedo (α)	Emissivity (εs)	Hillshade_building (ψb)	Hillshade_green fraction (ψg)	Run-off coefficient (C)	FUA_tunnel (Ft)	
				NEW DEVELOPMENT	RETROFITTING								
	Constructions on piles	Pluvial Flooding	-	++	€€	N/A	Biodiversity • Multifunctional space usage ••	x	x	x		x	x
	Porous pavements	Flooding	+++	+++	€	€	Biodiversity • Multifunctional space usage •	x	x			x	
	Gutter	Flooding	+++	+++	€	€	Social and economic importance •					x	
	Rainwater retention ponds, with or without infiltration possibilities (precipitation can be used in buildings)	Flooding	+++	-	€€	€€	Biodiversity ••• Air quality • Social and economic importance •• Multifunctional space usage •••	x	x			x	
		Heat Wave	++	-									
	Reduced paved surfaces	Flooding	+++	+++	€€	€€	Biodiversity ••• Air quality • Energy efficiency • Social and economic importance •• Multifunctional space usage ••	x	x		x	x	
		Heat Wave	+++	-									
	Use of groundcover and shrubbery	Flooding	+++	-	€€	€€	Biodiversity ••• Air quality •• Energy efficiency • Social and economic importance ••• Multifunctional space usage •••	x	x		x	x	
		Heat Wave	+++	-									
	Green roofs	Flooding	+++	+++	€€	€€	Biodiversity ••• Air quality • Energy efficiency •• Social and economic importance •• Multifunctional space usage ••	x	x			x	
		Heat Wave	+++	-									
	Green facades	Heat Wave	+++	-	€€	€€	Biodiversity ••• Air quality • Energy efficiency • Social and economic importance •• Multifunctional space usage ••	x	x			x	
	Cool (reflective) roofs	Heat Wave	+++	-	€	€	Multifunctional space usage •	x	x				
	Cool paving and building materials	Heat Wave	+++	-	€	€	Energy efficiency • Multifunctional space usage •	x	x				
	Optimize orientation to wind and sun	Heat Wave	+++	-	€	€	Energy efficiency •• Multifunctional space usage •			x			
	Pergolas and canvas above streets	Heat Wave	++	-	€	€	Social and economic importance ••	x	x	x		x	
	Thermal insulation	Heat Wave	+++	-	€	€	Energy efficiency •• Social and economic importance •	x	x				
	Narrow streets	Heat Wave	+++	-	€€	N/A	Energy efficiency •• Multifunctional space usage •		x	x		x	x
	High-rise buildings (shade)	Heat Wave	++	-	€€	N/A	Energy efficiency • Social and economic importance •		x	x			
	Blinds	Heat Wave	+++	-	€	€	Energy efficiency • Social and economic importance • Multifunctional space usage •	x	x				

ADAPTATION OPTIONS FOR TRANSPORT INFRASTRUCTURE		TOWARDS WHICH HAZARD	VARIATION ON VULNERABILITY OF ELEMENT AT RISK	COST		CO-BENEFITS
				NEW	RETROFITTING	
	Afforestation of slopes with drought-resistant	Falling materials and erosion as a consequence of intense rainfall	++	€	€	Improves stability of slope Biodiversity Air quality
	Implementation of erosion control blankets or other type of protection (drains, berms, anchors, gunite or others)	Falling materials and erosion as a consequence of intense rainfall	++	€€	€€	Improves stability of slope
	Reduce the slope of the cut	Falling materials and erosion as a consequence of intense rainfall	+++	€(Soft soils) €€(Rock soils)	€€ €€€	Improves stability of slope
	Improvement of road maintenance resources	Falling materials and erosion as a consequence of intense rainfall	++		€€	Improves road performance Social and economical importance
	Improve of longitudinal and transversal drainage	Insufficient transversal drainage due to intense rainfall	+++	€€	€€€	Improves drainage
	Alternative mixtures (modified bitumen) for bituminous pavements and surface courses	Formation of pavement rutting as a result of elevated pavement temperatures	++	€€	€€	Improves ride quality for the driver
	Porous pavements	Traffic conditions due to intense rainfall	++	€€	€€	Improves ride quality for the driver (no splash and spray)
	Increase surveillance of the section in case of unfavourable weather conditions	Traffic conditions due to snow	++	€€	€€	Improve road management Social and economical importance
	De-icing agents that cause the least possible damage to pavements and the environment.	Traffic conditions due to snow	++	€	€	Improve road management Social and economical importance Less affection to environment
	Allow alternative routes in case of road closure	Traffic conditions due to snow	++	€	€	Improve road management Social and economical importance

9 Annex III: Adaptation Measures Technical Cards

This annex contains technical cards summarizing the characteristics of some key adaptation options. They are formatted for printing on glossy cards and complement the adaptation options descriptions on the online CLARITY Climate Information Service.

The Technical Cards provide end-users with a synthetic summary of most recurring adaptation measures to be integrated in building/open spaces design. This information is also integrated in the CSIS, and used to test the effect of adaptation strategies by modifying the land use layers in the study area according to the selected strategy, so that when the models are run, the effect of the adaptation option can be seen in the new results.

The scales included in the fact sheets were determined as follows:

- Adaptation target: derived from <https://www.climateapp.nl/> [22]
- Performance parameters: derived by various literature sources and/or calculated and calibrated through validated software tools (e.g. ENVIMET, SOLWEIG), subsequently integrated in the CLARITY WP3 “Hazard - Local Effect” models. These are the main parameters used in the hazard/impact modelling workflow, determining the extent of potential “climate benefits” (as described in the fact sheet box) linked to the implementation of the adaptation measure/strategy. The choice of limiting the factsheets only to the key parameters of Albedo, Emissivity and Runoff is due to the fact that these are the only parameters that can be directly attributed to the land use type, while other key modelling parameters (e.g. SVF, Surface Temperature) strongly depend on further context conditions (e.g. urban morphology, solar radiation, etc.).
- Costs: derived by previous national research project conducted at UNINA (Metropolis -“Integrated and sustainable methods and technologies for resilience and safety in urban systems”) [27]. Originally calculated based on parametric costs for the Italian construction market, they have been extended to other EU countries by CLARITY WP5.
- Co-benefits: derived from diverse sources [23], [52], [53] and connected to each adaptation measure as found in literature, grouped into three main categories (environmental, social, economic) and homogenized into a qualitative scale, with a pure indicative purpose, since the scale is not used in the CSIS calculation. The purpose is mainly to inform end-users about the achievable “co-benefits” (as described in the fact sheet box), linked to each solution.
- The literature review and methodological approach has been developed with the support of A. Eggert (Aalborg University), during her 6 months internship at UNINA-PLINIVS (2019-2020), and included in her Master Degree thesis work [54].

Introduction

CLIMATIC BENEFITS

Climatic benefits concern the following two aspects:

(1) thermal conditions improvement and thermal comfort increase, through a surface temperature decrease and a urban heat island effect reduction, and (2) flood risks adaptation and mitigation, due to the rainfall increased and sea level rise.

CO-BENEFITS

Adaptation measures co-benefits are independent of their climatic benefits.

They can be described as additional effects to the direct reduction of climate impacts (global warming and sea level rise). Co-benefits can appear as relevant from an environmental, social and economic point of view, or as integrated and interdependent co-benefits.

PERFORMANCE PARAMETERS

Albedo

Albedo is the incident solar radiation fraction that is reflected. It therefore indicates the reflective power of a surface. Thus, the higher the albedo factor the more light is reflected.

Emissivity

It defines a material ability to emit thermal radiation. Surfaces with high emissivity factors remain cooler thanks to their rapid heat release ability.

Runoff

It correlates the amount of rain with the amount of surface run-off. This value is higher for low infiltration areas (pavement, steep slope) and lower for permeable and well-vegetated areas (soil, flat terrain).

Transmissivity

It defines the portion of solar radiation transmitted (measured e.g. under the canopy of trees) with respect to the actual values of the global radiation measured at the nearby open site. The value varies from 0 to 1, where the lower the value the higher the shading effect.

URBAN MICROCLIMATE THEORY

Since the temperature of a surface mainly depends on the characteristics of the its own material, indicators such as "albedo" and "emissivity" are of great importance.

Another important performance indicator is the "runoff factor".

Permeable materials, like green areas, increase rainfall infiltration into the substrate, decrease surface runoff, increase evapotranspiration and, therefore, reduce the "urban heat island" effect and the floods risk. In addition to the materials characteristics, shading is essential for increasing thermal comfort and reducing energy loads. This can be optimized through a careful vegetation configuration, in relation to the gray infrastructures like buildings. Vegetation, in particular, plays an important role in cooling surfaces through shading.

Legend

MEASURES CATEGORY (Datasheet colour)

Green infrastructures



Blue infrastructures



Functional-spatial constitution



Construction materials



INFORMATION TYPOLOGIES (Datasheet side)

A TECHNICAL DESCRIPTION

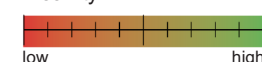
B CO-BENEFITS

PERFORMANCE PARAMETERS

Albedo



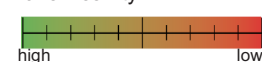
Emissivity



Runoff



Transmissivity



CO-BENEFITS CATEGORIES

Environmental

Air quality



GHG emissions



Water quality



Water recollection and security



Biodiversity



Landslides and Weathering



Social

health impacts



Public space access



Aesthetic value



Community inclusion



Economic

Employment and income generation



Savings



Innovation and investment



Property value



A

Green infrastructures BIOSWALES

A TECHNICAL DESCRIPTION

B CO-BENEFITS

ADAPTATION TARGETS

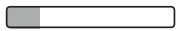
Heat Wave



Pluvial Flooding

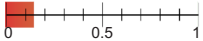


Fluvial Flooding / Storm Surge

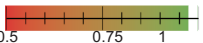


PERFORMANCE PARAMETERS

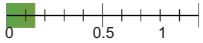
Albedo



Emissivity



Runoff



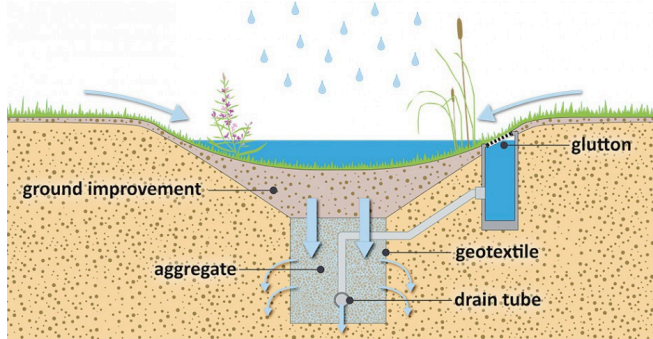
COSTS

Construction

€€€

Maintenance / Management

€€€



DESCRIPTION

A bioswale consists of a shallow trench or a small depression in the ground, with vegetation and porous bottom, made with natural materials such as plants, rocks and soil. In these systems, the water that flows from roofs and streets is not only channeled into the sewers but also conducted in the bioswale through gutters and/or ditches above ground. For most of the year, the bioswale remains dry, filling up with water only during heavy rainfall.

CLIMATE BENEFITS

Bioswales are an efficient instrument to improve the efficacy of waste water disposal in urban systems, by intercepting rainwater, filtering it and allowing its infiltration, thus reducing the overload of the sewage system. A properly designed Bioswale system minimizes overflow, improves the shallow waters and prevents the soil from drying up. Furthermore, Bioswales help to reduce the heat stress: this effect can be boosted by planting some carefully selected species, which help to reduce temperatures and consequently improve thermal comfort.

B

Co-benefits in total

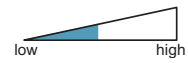
Environmental



Social



Economic



CO-BENEFITS



Bioswales improve rainwater quality by removing heavy metals and other pollutants, and improve air quality through carbon sequestration from green elements. Bioswales can provide a huge variety of flora by creating habitats for wild fauna, like birds and insects, thanks to differentiated types of grasses and vegetation



Bioswales have a positive impact on wellness and human health thanks to the reduction of the "heat island effect"; they can be used also as recreational areas open to public.



Vegetation and water increase the aesthetic and recreational value of urban places, improving life quality for local communities. Bioswales, having a relatively simple and rapid realization, can be considered a low cost technology. They represent a cheaper alternative to conventional rainwater management systems, like drainage basins. The volume reduction of polluted water filtered by bioswale reduces transport and rainwater treatment costs.

A

Green infrastructures GREEN FACADES

A TECHNICAL DESCRIPTION

B CO-BENEFITS

ADAPTATION TARGETS

Heat Wave



Pluvial Flooding



Fluvial Flooding / Storm Surge



PERFORMANCE PARAMETERS

Albedo
N/A

Emissivity
N/A

Run-off
N/A

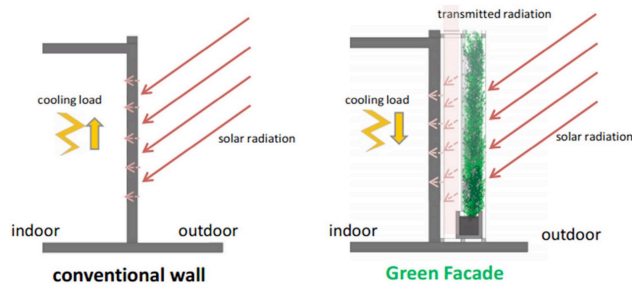
COSTS

Construction

€€€

Maintenance / Management

€€€



DESCRIPTION

The advantage of green façades in dense urban areas is that they occupy a small horizontal surface compared to urban green spaces, giving at the same time a lot of vertical surface of greenery, considering that a generic climbing plant is able to cover the façade of a five storey building in only few years. To properly design green façade systems it is necessary to carefully assess the need for spaces for the root system in relation to the desired extension on the façade, providing enough space to allow the roots growing in a healthy way that guarantee resistance of plants especially in prolonged drought periods, limiting the consumption of water for irrigation. There are several types of green façade depending on plant type and needed support on building façades. It is necessary, to avoid structural damages, to conduct preventive inspections to check eventual problems, as melted grout or cracks, which must be repaired before realizing the green façade system.

CLIMATE BENEFITS

Vertical vegetation protects from direct solar radiation the external façades of buildings, reducing their overheating and facilitating the heat release during the night. Plants produce also water vapour through evapotranspiration, promoting the cooling effect of surrounding areas. Vertical vegetation produces also a mitigating effect on maximum external temperatures, improving both indoor and outdoor thermal perceived comfort.

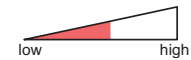
B

Co-benefits in total

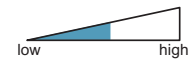
Environmental



Social



Economic



CO-BENEFITS



Green façades, by capturing particulate matter and air pollutants, like CO₂, improve air quality. Green façades can also improve biodiversity, by giving habitat for birds and insects.



By protecting buildings facades by direct solar radiation, green facades give an insulating effect that increases internal thermal comfort and therefore it influences positively human health, reducing heat related disorders. Mitigating temperatures, both in autumn and winter, can help to save on energy costs that came from both heating and cooling. Evergreen climbing plants, like ivy, reduce building thermal dispersion during fall and winter periods. Vertical vegetation reduces also noise emissions and noise reflection from building façades.



Their aesthetic value improves the perceived quality of urban places and can contribute to increase the real estate value. Furthermore, if integrated with solutions for rainwater collection and reuse for irrigating the vegetation on the façade, they contribute to reduce water consumption..

A

Green infrastructures EXTENSIVE GREEN ROOFS

A TECHNICAL DESCRIPTION

B CO-BENEFITS

ADAPTATION TARGETS

Heat Wave



Pluvial Flooding

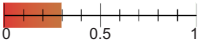


Fluvial Flooding / Storm Surge

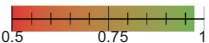


PERFORMANCE PARAMETERS

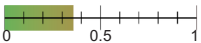
Albedo



Emissivity



Runoff



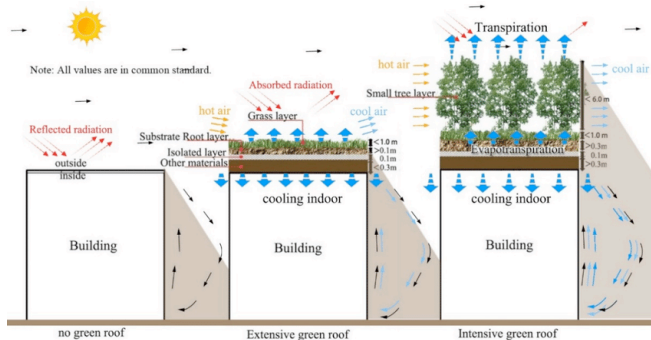
COSTS

Construction

€€€

Maintenance / Management

€€€



DESCRIPTION

Extensive green roofs can be partially or completely covered with vegetation. Usually, paved portions can be integrated to allow maintenance operations or for specific uses. Filtering and waterproofing layers below the terrain substrate should be continuous over the entire surface of the roof, and therefore installed both on green and paved portions. This intervention is ideal both for flat and sloped roofs, and it implies a limited structural overload because its vegetation is superficial, and the required terrain substrate thickness is about 15/20 cm. Extensive roofs are prevalently realized with perennial herbaceous plants and shrubs ground covers (sedum). Musk/sedum plants are very suitable for this purpose, because they have the capacity of storing a high quantity of water and surviving in long drought periods.

CLIMATE BENEFITS

Green roofs help to reduce the surrounding urban air temperature and to mitigate the urban heat island effect. Another advantage consists in rainwater drainage action, which is partially absorbed by the terrain and it is partially returned to natural cycle through evapotranspiration, thus reducing the overload of sewage systems in case of extreme rain events.

B

Co-benefits in total

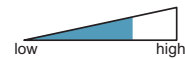
Environmental



Social



Economic



CO-BENEFITS



Extensive green roofs ensure an excellent thermal control of underlying indoor spaces, reducing thermal dispersion in winter and, thanks to their high thermal inertia, improved attenuation and phase shift during summer. This implies a reduction of energy costs (mostly for indoor spaces situated at top floors). In case of partially covered roofs, attention should be given to the thermal properties of both green and paved sections, providing adequate solutions to avoid thermal bridges.



Green roofs improve air quality by capturing particulate matter and air pollutants, like CO₂, with positive impacts on human health, and they also encourage biodiversity, by giving habitat for birds and insects. Furthermore, green roofs have a big aesthetic relevance, because they improve the building appearance, and they contribute to increase the real estate value.



If integrated with solutions for rainwater collection and reuse for irrigating the vegetation on the roof, they contribute to reduce water consumption.

Note: Ecological and environmental benefits are generally increased with a higher depth of terrain substrate. For example, the increase of thermal insulation and rainwater absorption is more relevant in intensive green roofs thanks to the thicker layer of terrain (see "Intensive Green Roofs").

A

Green infrastructures INTENSIVE GREEN ROOF

A TECHNICAL DESCRIPTION

B CO-BENEFITS

ADAPTATION TARGETS

Heat Wave



Pluvial Flooding

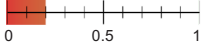


Fluvial Flooding / Storm Surge

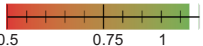


PERFORMANCE PARAMETERS

Albedo



Emissivity



Runoff



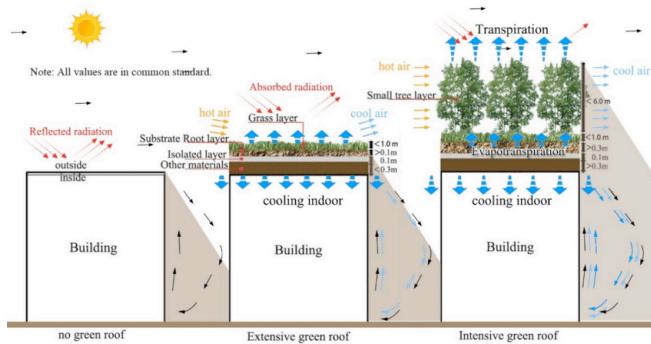
COSTS

Construction

€€€

Maintenance / Management

€€€



DESCRIPTION

Intensive green roofs can be partially or completely covered with vegetation. Usually, paved portions can be integrated to allow maintenance operations or for specific uses. Filtering and waterproofing layers below the terrain substrate should be continuous over the entire surface of the roof, and therefore installed both on green and paved portions. The solution is applicable to flat roofs capable with a load-bearing capacity of more than 150 kg/m², because intensive roofs are characterized by a variety of vegetation, unlike extensive roofs, which may also include little trees and shrubbery which require a thicker terrain substrate. The variety of plants usually require more maintenance compared to extensive roofs, and the integration of an irrigation system, like ordinary gardens, is generally advised.

CLIMATE BENEFITS

Green roofs help to reduce the surrounding urban air temperature and to mitigate the urban heat island effect. Another advantage consists in rainwater drainage action, which is partially absorbed by the terrain and it is partially returned to natural cycle through evapotranspiration, thus reducing the overload of sewage systems in case of extreme rain events.

B

Co-benefits in total

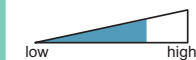
Environmental



Social



Economic



CO-BENEFITS



Intensive green roofs ensure an optimal thermal control of underlying indoor spaces, reducing thermal dispersion in winter and, thanks to their high thermal inertia, improved attenuation and phase shift during summer. This implies a reduction of energy costs (mostly for indoor spaces situated at top floors). In case of partially covered roofs, attention should be given to the thermal properties of both green and paved sections, providing adequate solutions to avoid thermal bridges. Green roofs improve air quality by capturing particulate matter and air pollutants, like CO₂, with positive impacts on human health, and they also encourage biodiversity, by giving habitat for birds and insects.



Intensive green roofs offer also a space for recreational uses, as well as for urban gardening and agriculture, with positive social effects on the neighborhood community.



Green If integrated with solutions for rainwater collection and reuse for irrigating the vegetation on the roof, they contribute to reduce water consumption. Furthermore, green roofs have a big aesthetic relevance, because they improve the building appearance, and they contribute to increase the real estate value. The use of intensive green roofs for urban agriculture can help to develop local green and circular production supply chains. Other impacts on job market linked with intensive green roofs concern the professional sectors linked by their design, realization and maintenance.

A

Green infrastructures

LAWNS AND GREEN AREAS

A TECHNICAL DESCRIPTION

B CO-BENEFITS

ADAPTATION TARGETS

Heat Wave



Pluvial Flooding

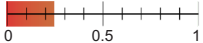


Fluvial Flooding / Storm Surge

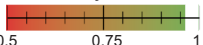


PERFORMANCE PARAMETERS

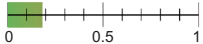
Albedo



Emissivity



Runoff



COSTS

Construction

€€€

Maintenance / Management

€€€



DESCRIPTION

Lawn Lawns and green areas are permeable surfaces that perform some important functions in an urban environment, such as heat and run-off control, space for recreational and sport uses, biodiversity hubs and carbon storage components. There are several typologies of lawn suitable for urban areas, such as: - rustic lawns, which ask for less maintenance and are mainly used for river/canal banks and floodable public places; - ornamental lawn, used in public and private gardens; - sports lawns, formed by species that allow a high trampling; - flowery lawns, formed by a mix of herbaceous flowering plants, annual or perennial.

Depending on the types, they may or not require a regular irrigation and mowing. The use of spontaneous species and the support of symbiotic behaviours (between different plant types and/or fungi), when carefully designed, can greatly enhance the quality of green areas, reducing maintenance and irrigation costs, as well as providing improved resistance during droughts.

CLIMATE BENEFITS

The main advantage of lawns consists in the reduction of surface run-off and the improvement of urban drainage, reducing flooding phenomena related to extreme rainfall. Furthermore, nearby buildings and public places, lawns perform an important role in microclimate thermal regulation. The surface temperature of a lawn can be 5°C lower than bare soil, and up to 15°C lower than asphalt. The efficacy from the thermal point of view of lawn surfaces is strictly linked to the ability to provide adequate evapotranspiration, therefore their use should be limited to urban spaces where irrigation systems are installed. Shrub species and aromatic plants with resistance characteristics suitable for the specific local climate can be integrated into green lawn areas to improve both their thermal regulation and surface drainage capacity, but require careful design that guarantees the suitability of the substrate and minimizes the need for maintenance and irrigation. Perennial urban lawns require only little maintenance throughout the year and are therefore less expensive than manicured parks.

B

Co-benefits in total

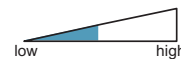
Environmental



Social



Economic



CO-BENEFITS



Like all elements of green infrastructure, green areas also promote CO2 sequestration and improve air quality. Urban lawns could be used in combination with selected flowers and plants in order to improve their appearance and support biodiversity in cities.



Green urban areas have an aesthetic and social value when used as recreational places for residents, encouraging social interactions that strengthen community cohesion. Furthermore, green urban areas have a significant positive impact on human health by fostering physical activities in open spaces.



Green areas, in addition to contributing to the reduction of the surface run-off and to the infiltration of rainwater, improve the quality for the non-drained component, thus reducing the load of the purification systems.

A

Green infrastructures TREES

A TECHNICAL DESCRIPTION

B CO-BENEFITS

ADAPTATION TARGETS

Heat Wave



Pluvial Flooding

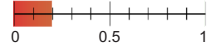


Fluvial Flooding / Storm Surge

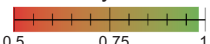


PERFORMANCE PARAMETERS

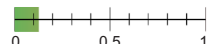
Albedo



Emissivity



Transmissività



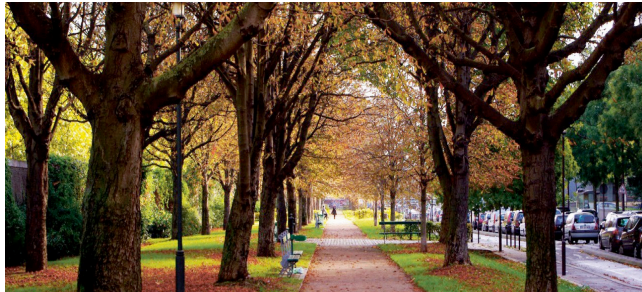
COSTS

Construction

€€€

Maintenance / Management

€€€



DESCRIPTION

The planting of trees within urban areas includes their integration in public parks, along roads, in squares and other open spaces (including private spaces). It is important that the location identified and the space intended for the root system is suitable for the tree to fully develop its crown. In addition, the type of tree should be chosen based on local climate features, taking into account the expected climate projections over a time horizon corresponding to the years needed for the complete maturation of the tree. Although trees improve air quality, dense foliage along busy roads can cause unwanted effects, as vehicle emissions tend to get trapped under the canopies. The right type of tree and the right shape of the crown in relation to the urban canyon geometry (and related wind channeling), road size and expected traffic load can help preventing the accumulation of pollutants. Furthermore, it is essential to provide adequate regular maintenance and protection cycles for the tree in order to guarantee its climatic benefits over time and prevent them from being a risk factor in the event of extreme events such as wind storms, which can cause trees with a weakened or not fully developed root system to collapse.

CLIMATE BENEFITS

The presence of trees in urban spaces reduces the impact of heat waves through shade and high levels of evapotranspiration which guarantee a cooling effect that improves outdoor thermal comfort. Trees are able to absorb and infiltrate a great amount of rainwater thanks to the presence of root systems, limiting the surface runoff in case of heavy rains and contributing to the stabilization of slopes, thus reducing the risk of flash floods and landslides

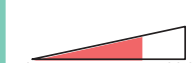
B

Co-benefits in total

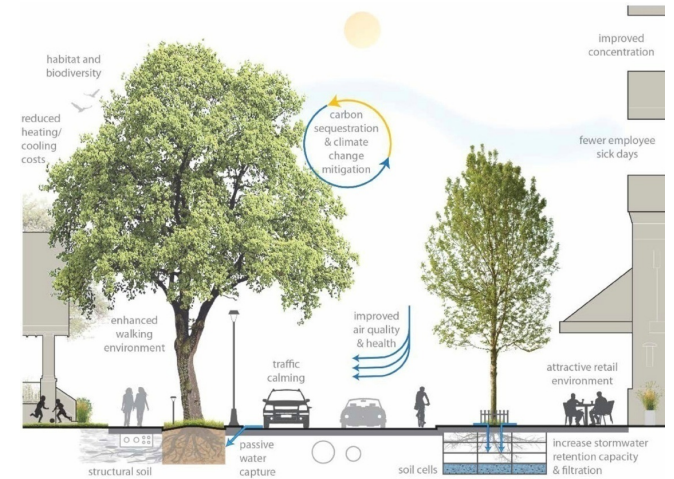
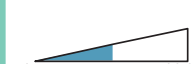
Environmental



Social



Economic



CO-BENEFITS



The filtering of rainwater through the roots system of trees allows to improve the quality of groundwater, acting as as natural water purification systems. The trees also improve air quality by capturing particulate matter and CO2, increase biodiversity by offering living space to many species of birds and insects, reduce noise by creating absorbing barriers.



All these environmental factors, in turn, positively influence human health.



In addition, trees add an aesthetic value to the city. The trees that directly shade the buildings reduce the demand for energy for air conditioning, energy costs and the associated CO2 emissions.

A

Green infrastructures URBAN AGRICULTURE

A TECHNICAL DESCRIPTION

B CO-BENEFITS

ADAPTATION TARGETS

Heat Wave



Pluvial Flooding

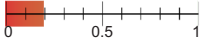


Fluvial Flooding / Storm Surge

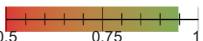


PERFORMANCE PARAMETERS

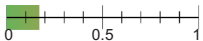
Albedo



Emissività



Runoff



COSTS

Construction

€€€

Maintenance / Management

€€€



DESCRIPTION

Agricultural land differs from natural soil due to repeated tillage and various agronomic interventions. All types of crop, in general, affect the water cycle and promote environmental protection. The increase of agricultural production in cities can be promoted through the cultivation of bare soils and residual areas, as well as outdoor spaces of residential buildings. Crop types are closely related to local climatic conditions and therefore have to be carefully selected. The spatial configuration of urban land for agricultural use must also take into account the impact of urban activities in the surrounding areas (in particular vehicular pollution). Therefore, the cultivation of agricultural products intended for human consumption must be assessed based on the specific location in the city.

CLIMATE BENEFITS

The main advantage of urban agriculture is the reduction of surface run-off, ensuring a reduction in the risk of flooding in case of extreme precipitation events. Depending on the type of vegetation, the performance parameters may vary. The contribution to heat stress reduction can be relevant, but seasonality of cultivation types must be taken into account, preferring those growing during hot seasons.

B

Co-benefits in total

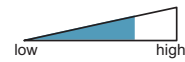
Environmental



Social



Economic



CO-BENEFITS



Urban agriculture offers high quality urban green spaces and preserves biodiversity by attracting birds and insects. Local food production reduces the consumption of fossil fuels and the greenhouse gas emissions associated with the transport, packaging and sale of food, thus contributing to the improvement of air quality in cities.



Agricultural areas integrated in community initiatives increase food awareness and promotes a healthier diets, with potential benefits for human health. In addition, by involving residents and providing a place for cooperation and knowledge sharing, urban agriculture strengthens community cohesion and inclusion, including positively affecting mental health diseases. Finally, urban agriculture fields contribute to the aesthetic value of the city.



Local cultivation allows saving on household expenses for food. The presence of local products and markets bring benefits in terms of job opportunities and stimulus to local circular economy. Specific interactions between urban agricultural systems and their different urban environments create opportunities for technical, social and organizational innovations. Urban agriculture can help increase the values of real estate in the surrounding areas.

A

Construction materials CANOPIES

A TECHNICAL DESCRIPTION

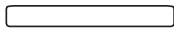
B CO-BENEFITS

ADAPTATION TARGETS

Heat Wave



Pluvial Flooding

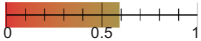


Fluvial Flooding / Storm Surge

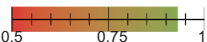


PERFORMANCE PARAMETERS

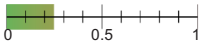
Albedo



Emissivity



Transmissività



COSTS

Construction

€€€

Maintenance / Management

€€€



DESCRIPTION

Shading systems are integral part of physical configuration of many equipped public spaces. They can be installed as fixed or removable elements, designed for protect the underlying space from solar radiation and, if realized as waterproof canopies, from rain. The shadow quality, in terms of quantity of radiation transmitted is determined by the covering typology (e.g. continuous or discontinuos surface) and material. The upper surface should be designed with light color finishings, in order to reach adequate albedo values. The most used material include wood (with waterproof treatment), metals (steel or aluminium), glass (with optional selective treatment) and fabrics (acrylic and high resistance polyester) to meet not only structural but also aesthetic needs. In any case, the materials should preferably meet the requirements of lightness and flexibility. If not properly designed, they can however contribute to the trapping of heat and the overheating of the underlying area.

CLIMATE BENEFITS

The creation of shaded surfaces reduces the overheating of roads, pavements and green spaces, affecting the direct solar radiation, which is the main component of thermal stress conditions. If those surfaces are realized with waterproof materials and equipped with gutters connected to sustainable urban drainage systems, like green infrastructures and storage systems, they can help to reduce flooding phenomena in case of heavy rain.

B

Co-benefits in total

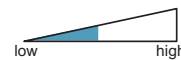
Environmental



Social



Economic



CO-BENEFITS



Shading systems, if integrated in public spaces can attract people, encouraging social interaction, commercial and recreational activities.



Canopies which directly shade buildings can reduce energy demand for cooling and related CO2 emissions, especially for indoor spaces at groundfloor levels. Design innovations and the addition of functions (like recharge of electrical devices and vehicles, information systems and digital services, etc.) can bring economic benefits linked by new green and innovative supply chains.

A

Construction materials GRASSED JOINT FLOORING

A TECHNICAL DESCRIPTION

B CO-BENEFITS

ADAPTATION TARGETS

Heat Wave



Pluvial Flooding

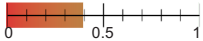


Fluvial Flooding / Storm Surge

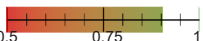


PERFORMANCE PARAMETERS

Albedo



Emissivity



Runoff



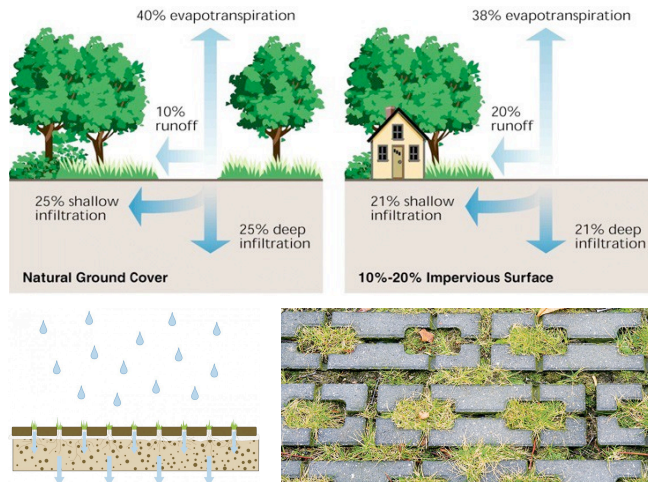
COSTS

Construction

€€€

Maintenance / Management

€€€



DESCRIPTION

Outdoor floors, made with tiles, slabs or blocks of various materials, may include the presence of grassy joints. The filling of the cavities, with openings of different number and size depending on the type, is composed of vegetable soil with spontaneous or cultivated herbaceous species. Depending on the type of substrate present under the pavement, the percentage of infiltration can even reach 100%. This type of flooring cannot support heavy loads, therefore it can only be used for pedestrian areas, parking lots or streets with a limited intensive use.

CLIMATE BENEFITS

The presence of grass increases the surface permeability and the ability to absorb and retain rainwater (this capacity is directly proportional to the percentage of plant surface compared to the total paved surface). Frequent maintenance is required to ensure greater absorption of rainwater. The evapotranspiration and emissivity components reduce the heat island effect, increasing the perceived thermal comfort.

B

Co-benefits in total

Environmental



Social



Economic



CO-BENEFITS



The soil-sealing reduction in urban areas slows down the surface run-off and allows rainwater to infiltrate the soil more easily, thus reducing the overload of sewer systems and the necessity of manholes maintenance.



The presence of green areas in urban paved spaces increases its aesthetic quality compared to asphalt or concrete sidewalks.




The higher initial construction costs of grassy joint pavements, compared to conventional ones, are justified by the potential savings due to the avoided construction of other more expensive rainwater collection/disposal systems.

A


Construction materials REFLECTIVE SURFACES

- A** TECHNICAL DESCRIPTION
- B** CO-BENEFITS

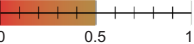
ADAPTATION TARGETS

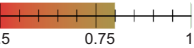
Heat Wave


Pluvial Flooding


Fluvial Flooding / Storm Surge


PERFORMANCE PARAMETERS

Albedo*


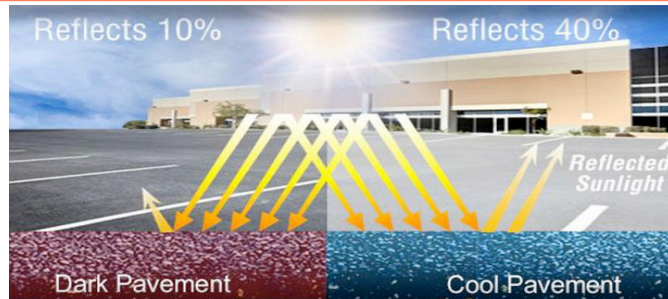
Emissivity*


*dependent on degree of brightness of color

COSTS

Construction
 €€€

Maintenance / Management
 €€€



DESCRIPTION

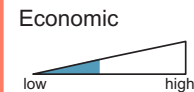
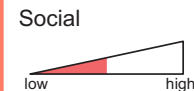
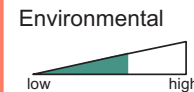
Reflective surfaces are characterized by a high solar reflectance (albedo), obtained by using light colors (typically tending to white) or darker colors treated with special reflective pigments, which limit the increase in surface temperature when they are directly radiated. Furthermore, they are typically characterized by a high emissivity which determines during night a more favorable release of heat stored during the day, with effect on the reduction of the thermal flux release on environment. Reflective materials can be used for various types of external pavements or buildings façades, both as coatings and paints. Horizontal and vertical surfaces must be kept clean so that reflective properties are preserved over time.

CLIMATE BENEFITS

Since pavements occupy 30-40% of the urban area, reflective surfaces can play an important role in reducing heat island effect. These solutions have a positive influence on the surface temperature control, compared to asphalt, dark stone or cementitious materials that can reach surface temperatures up to 70 °C in the summer months. The high albedo can however cause glare phenomena, as well as conditions of thermal discomfort due to the reflection of the solar radiation at human height. The use of reflective pavements or building façades in areas characterized by high direct solar radiation thus must be carefully designed, favouring their use in dense building fabrics or by providing for the integration of appropriate trees and shading elements.

B

Co-benefits in total



CO-BENEFITS



The cooling effect of reflective surfaces slows down surface chemical reactions and the consequent formation of smog on surfaces.



Used as external finishings of buildings, they slightly reduce the energy demand for cooling and the associated greenhouse gas emissions.

A

Construction materials COOL ROOFS

A TECHNICAL DESCRIPTION

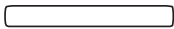
B CO-BENEFITS

ADAPTATION TARGETS

Heat Wave



Pluvial Flooding

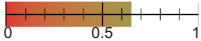


Fluvial Flooding / Storm Surge

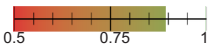


PERFORMANCE PARAMETERS

Albedo*



Emissivity*



*for mineral reflex white

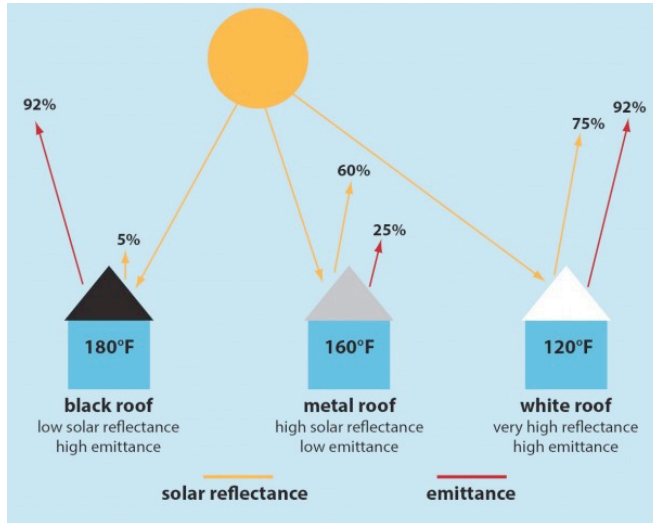
COSTS

Construction

€€€

Maintenance / Management

€€€



DESCRIPTION

The cool roof is a roof characterized by a high ability to reflect the incident solar radiation (solar reflectance or albedo) and, at the same time, to emit thermal energy in the infrared spectrum (thermal emissivity). It is achieved by applying on the external surface of the roof paints or layers of surface coating, generally white or light grey materials.

CLIMATE BENEFITS

Cool roofs allow a reduction of the urban heat island effect, affecting the air temperature at different altitudes. On sunny summer days, traditional roofs can reach surface temperatures of about 80 °C while cool roofs usually do not exceed 50 °C.

B

Co-benefits in total

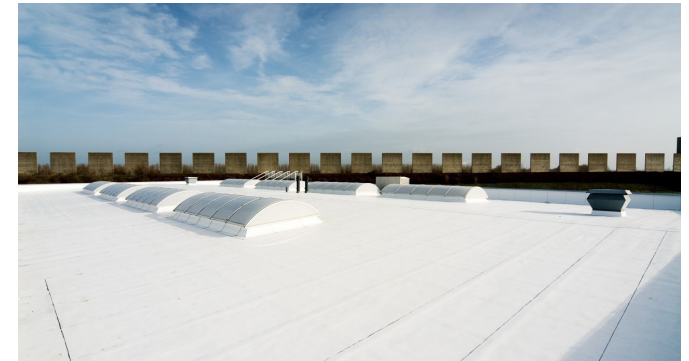
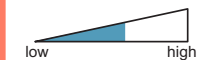
Environmental



Social



Economic



CO-BENEFITS



-



-



-



Construction materials GREEN PERGOLAS

A TECHNICAL DESCRIPTION

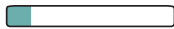
B CO-BENEFITS

ADAPTATION TARGETS

Heat Wave



Pluvial Flooding

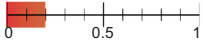


Fluvial Flooding / Storm Surge

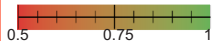


PERFORMANCE PARAMETERS

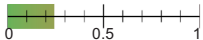
Albedo



Emissivity



Transmissività



COSTS

Construction

€€€

Maintenance / Management

€€€



DESCRIPTION

A green pergola combines the benefits of artificial shading systems, in terms of integration with buildings and urban equipment, with those linked to urban green. Plants must be selected based on the local climate and on the necessity of exposure to sunlight. The pergolas are designed and constructed in such a way as to protect the underlying areas from solar radiation during the central hours of the day, when the sun reaches its maximum height. A vertical wall can be associated with the horizontal green layer, in order to shield also towards morning or afternoon solar radiation (depending on location).

CLIMATE BENEFITS

Green pergolas guarantee excellent shading conditions, alongside the evapotranspiration component of vegetation, although with a lesser extent than trees and urban green areas. Compared to other artificial canopies, pergolas guarantee better conditions of thermal comfort during heat waves.



Co-benefits in total

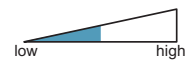
Environmental



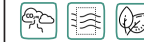
Social



Economic



CO-BENEFITS



Green pergolas, by capturing CO2 and the particulate present in the air, improve their quality. In addition, they can have a positive effect on urban biodiversity by offering living space for birds and insects.



Green pergolas increase the aesthetic value of the city and, consequently, improve the liveability and quality of life of the local communities.



Made in public spaces, they can attract people to gather, promoting social interaction and the development of commercial and recreational activities. The pergolas that directly shade the buildings reduce the demand for energy for cooling and the associated CO2 emissions.

A

Construction materials PERMEABLE CONCRETE

A TECHNICAL DESCRIPTION

B CO-BENEFITS

ADAPTATION TARGETS

Heat Wave



Pluvial Flooding

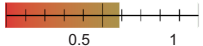


Fluvial Flooding / Storm Surge

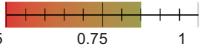


PERFORMANCE PARAMETERS

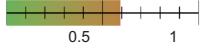
Albedo



Emissivity



Runoff



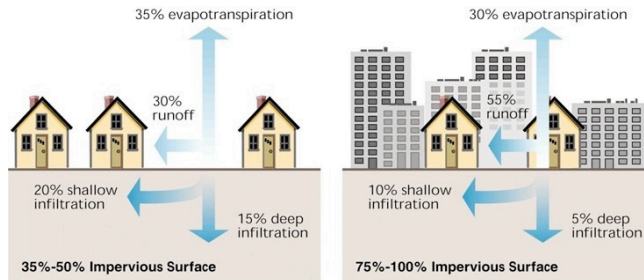
COSTS

Construction

€€€

Maintenance / Management

€€€



DESCRIPTION

External continuous made with porous or permeable material (concrete, stabilized earth or other materials) allow water to infiltrate and can be used for parking lots, pedestrian walkways and cycling paths. However, permeable floors cannot be used for roads or parking areas subject to intensive use as they generally cannot support large loads, but also because of the risk of soil contamination due to the infiltration of particulates and other road pollutants.

CLIMATE BENEFITS

Porous or permeable continuous pavements have a good performance in terms of rainwater absorption, being characterized by low inflow values and, therefore, good water permeability (with percentages varying between 15% and 40%). Consequently, thanks to the high infiltration, they reduce the risk of flooding in case of extreme precipitation events.

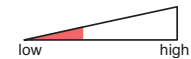
B

Co-benefits in total

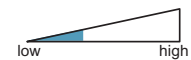
Environmental



Social



Economic



CO-BENEFITS



The improved infiltration over large paved areas, by reducing the overload of sewer systems, contribute to lower their maintenance costs, including manholes. The higher initial construction costs of the permeable floors, compared to conventional ones, are justified by the potential savings due to the avoided construction of other more expensive rainwater collection/disposal systems.

A

Blue infrastructures

GUTTERS AND STORM DRAINS

A TECHNICAL DESCRIPTION

B CO-BENEFITS

ADAPTATION TARGETS

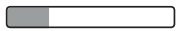
Heat Wave



Pluvial Flooding

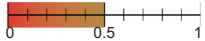


Fluvial Flooding / Storm Surge

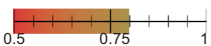


PERFORMANCE PARAMETERS

Albedo



Emissivity



Runoff

N/A

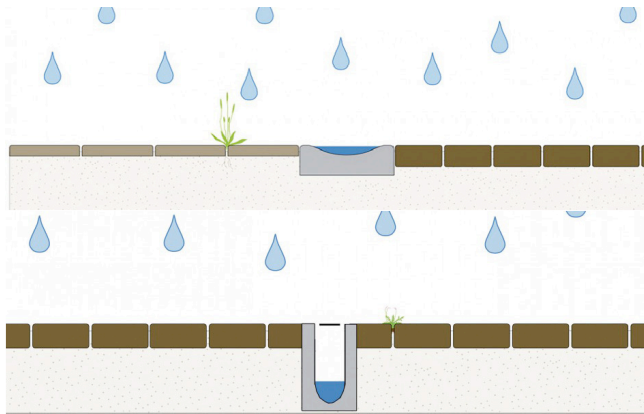
COSTS

Construction

€€€

Maintenance / Management

€€€



DESCRIPTION

Gutters and manholes are important elements of the urban drainage system, having the function of intercepting rainwater that flows on the horizontal surfaces of buildings and open spaces and conveying them into the sewerage network, using special infiltration systems. The main factor that determines surface flooding in case of extreme precipitation events is the obstruction of the manholes, due to lack of maintenance or design mistakes. Open canals connected to disposal systems, green areas, bioswales, flooded squares, rainwater collection systems and retention basins can be integrated into pedestrian areas to reduce the risk of flooding.

CLIMATE BENEFITS

By collecting and conveying rainwater, gutters, ditches and manholes reduce surface run-off, thus mitigating the risk of surface flooding in the surrounding areas. Open gutters/canals, connected to water recirculation systems, can be used during heat wave events to realize a network of small blue infrastructure artificially filled with water, which contributes to reduce outdoor thermal stress

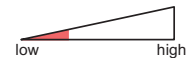
B

Co-benefits in total

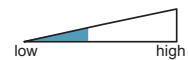
Environmental



Social



Economic



CO-BENEFITS



Through the drainage of surface water in retention areas or collection systems, the gutters facilitate the collection and reuse of rainwater, helping to ensure water safety.



In open canal systems, water can be visible and contribute to the aesthetic value of the neighborhood.



Open surface drainage systems are generally easier to clean and maintain than covered systems with consequent economic savings.

A

Blue infrastructure RAINWATER HARVESTING SYSTEMS

A TECHNICAL DESCRIPTION

B CO-BENEFITS

ADAPTATION TARGETS

Heat Wave



Pluvial Flooding



Fluvial Flooding / Storm Surge



PERFORMANCE PARAMETERS

Albedo
N/A

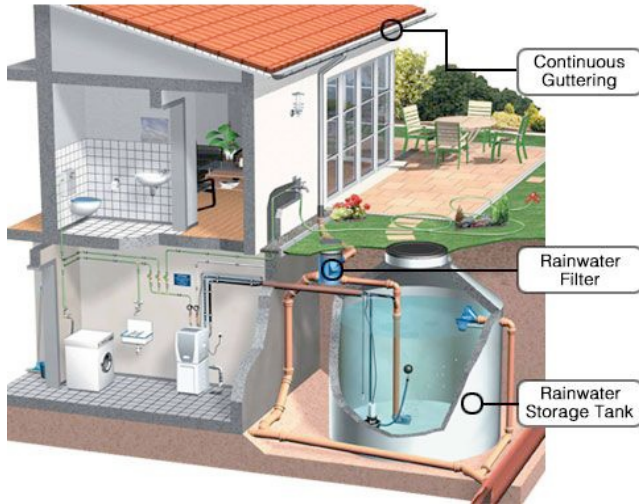
Emissivity
N/A

Runoff
N/A

COSTS

Construction
€€€

Maintenance / Management
€€€



DESCRIPTION

Rainwater collection, filtering, storage and reuse systems can be used for various purposes, including irrigation, cleaning of paved surfaces, toilet flushes and fire prevention systems. The simplest example of a rainwater collection system consists of storage tanks. In areas where dry periods alternate with extreme rainfall, excess water can be stored and used to refill aquifers through artificial techniques.

CLIMATE BENEFITS

The main function of rainwater harvesting system is to contribute to reducing flooding phenomena, limiting the overload of sewer system and increasing their disposal capacity during heavy rain events.

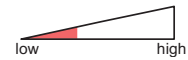
B

Co-benefits in total

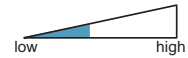
Environmental



Social



Economic



CO-BENEFITS



Recycling and reusing rainwater for domestic or industrial purposes can significantly reduce water consumption, with relevant environmental benefits over large territories, and savings on utility bills.



The collection systems are based on simple and easily maintainable technologies. Installation costs are much lower than those of groundwater treatment (such as pumping and purification).



Blue infrastructure

RETENTION BASINS

A TECHNICAL DESCRIPTION

B CO-BENEFITS

ADAPTATION TARGETS

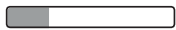
Heat Wave



Pluvial Flooding

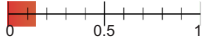


Fluvial Flooding / Storm Surge

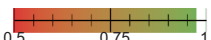


PERFORMANCE PARAMETERS

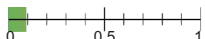
Albedo



Emissivity



Runoff



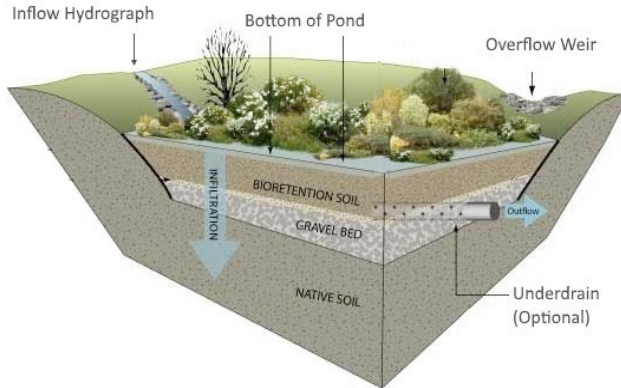
COSTS

Construction

€€€

Maintenance / Management

€€€



DESCRIPTION

Retention basins are water collection and storage areas configured as multifunctional vegetated spaces, created with a dual function: reducing the impact of flood events and conserving water for periods of drought. The accumulated water can be used for non-potable uses, such as irrigation, street cleaning, etc.

CLIMATE BENEFITS

The main function of the retention basins is to reduce the impact of floods in urban areas, collecting and storing rainwater in the event of heavy rains or floods. In the areas surrounding the retention basins, the temperature is significantly lower due to the presence of green areas and water, with a consequent increase in the perceived thermal comfort.



Co-benefits in total

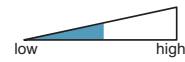
Environmental



Social



Economic



CO-BENEFITS



Retention basins facilitate the collection of water and reduce the overload of sewage systems during extreme precipitation events. They also allow a first purification of the water thanks to natural sedimentation, improving its quality, securing water availability in periods of shortage and seasonal stress, reducing the use of groundwater and limiting its potential depletion in periods of prolonged drought. Retention basins favour the growth of vegetation, absorbing CO2 and humidifying the air, creating habitats for animals, with a positive impact on biodiversity.



Retention basins, thanks also to the presence of vegetation, allow the integration of public recreational functions. In general, blue and green infrastructures in cities increase aesthetic value and encourage citizens to use public space as a recreational area for social gatherings or other purposes, increasing social inclusion and interaction.



Retention basins therefore has potential positive effects on real estate values of the surrounding areas.

Note: For "dry" retention basins see also "Water Squares".

A

Blue infrastructure WATER SQUARES

A TECHNICAL DESCRIPTION

B CO-BENEFITS

TARGETS ADAPTING

Heat Wave



Pluvial Flooding

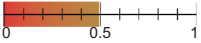


Fluvial Flooding / Storm Surge

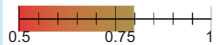


PERFORMANCE PARAMETERS

Albedo



Emissivity



Runoff

N/A

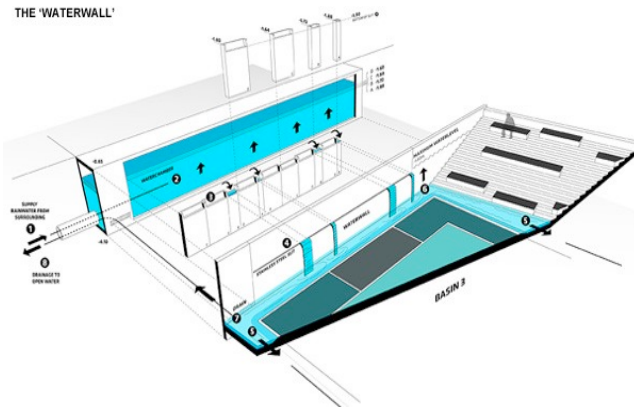
COSTS

Construction

€€€

Maintenance / Management

€€€



DESCRIPTION

In densely built-up urban areas it is often difficult to find a space for the temporary collection of rainwater during extreme events. Water squares can be realized in areas with a high flood risk, and appear as public spaces which in most cases are “dry” and can be used like any other traditional public space, for play and leisure. Carefully designed, in periods of heavy rainfall, the square is flooded by conveying the waters from the surrounding surfaces, limiting the impact of extreme rainfall.

CLIMATE BENEFITS

The flooded squares work as retention and storage basins for rainwater within the city, reducing the impacts of extreme rainfall.

B

Co-benefits in total

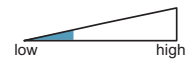
Environmental



Social



Economic



CO-BENEFITS



Depending on the intensity of the rainfall, they can be more or less flooded, up to being used even during flood events.



Due to the need of realizing water squares at a lower level with respect to surrounding urban areas, and generally accessed with steps, they can perfectly host a number of recreational activities, such as theatre, sport and play, strengthening social inclusion and interaction.





Functional-spatial constitution PERMEABLE GROUND-FLOOR

A TECHNICAL DESCRIPTION

B CO-BENEFITS

ADAPTATION TARGETS

Heat Wave



Pluvial Flooding



Fluvial Flooding / Storm Surge



PERFORMANCE PARAMETERS

Albedo
N/A

Emissivity
N/A

Runoff
N/A

COSTS

Construction
€€€

Maintenance Management
/
€€€



DESCRIPTION

Buildings with permeable ground floors allow water to flow along defined paths, possibly connected to collection or drainage systems, also promoting natural ventilation within dense urban areas. If built on pilotis, the buildings must be able to withstand water loads in the event of floods and local seismic risk conditions. The space intended to convey the water must be free of obstacles to avoid damage to the building during extrem precipitation events.

CLIMATE BENEFITS

By making the ground floors permeable, physical damage to buildings (structural or finishing elements) and people during flooding events can be reduced. The improved natural ventilation helps to mitigate the urban heat island effect even in the absence of wind. The presence of green or blue areas, as well as shaded areas carefully designed on the sides of the buildings, allows to promote cross-ventilation air exchanges, improving comfort conditions. If used as public spaces, open ground floors can be used as "cool spots" during heat waves.

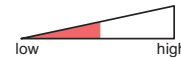


Co-benefits in total

Environmental



Social



Economic



CO-BENEFITS



The openings on the ground floors of the buildings, especially if integrated into a network of pedestrian or cycling paths and green and blue infrastructures, favour the passage of some animals, preserving biodiversity. Furthermore, the improved ventilation reduces the concentration of air pollutants.



The greater pedestrian and cycling permeability increase the quality of public spaces and favours the development of commercial, cultural and recreational activities.

